

MONASH UNIVERSITY
THESIS ACCEPTED IN SATISFACTION OF THE
REQUIREMENTS FOR THE DEGREE OF
DOCTOR OF PHILOSOPHY

ON..... **3 August 2001**.....

Sec. Ph.D. and Scholarships Committee

Under the copyright Act 1968, this thesis must be used only under the normal conditions of scholarly fair dealing for the purposes of research, criticism or review. In particular no results or conclusions should be extracted from it, nor should it be copied or closely paraphrased in whole or in part without the written consent of the author. Proper written acknowledgement should be made for any assistance obtained from this thesis.

ERRATA

p vi, para 3, last sentence: "increasing the charge" for "increasing in the charge"

p 116, para 1, last sentence: "vacancies within these layers" for "vacancies these layers"

p 146, line 4: "as a function of temperature" for "as a function temperature"

*An NMR Diffusion Study of the
Transport Properties in Novel
Electrolytes*

By

Hayley A. Every

BSc. (Hons)

A thesis submitted to the Faculty of Engineering, Monash University, in
fulfilment of the requirements for the degree of *Doctor of Philosophy*.

Department of Materials Engineering

Monash University

Australia

February 2001

For my Grandfather

Table of Contents

<i>Abstract</i>	<i>vi</i>
<i>Declaration</i>	<i>ix</i>
<i>Acknowledgments</i>	<i>x</i>
 <i>Chapter One Introduction</i>	 <i>1</i>
1.1 The Importance of Electrolytes	1
1.2 The Conductivity-Diffusion Relationship	3
1.3 Diffusion Mechanisms	6
1.3.1 Solid State Transport Mechanisms	6
1.3.1.1 Examples of Solid State Ionic Conductors	8
1.3.2 Liquid State Theories	10
1.3.2.1 Ionic Liquid Models	11
1.3.2.2. Examples of Liquid State Ionic Conductors	14
1.4 Specific Aims and Thesis Outline	16
1.5 References	17
 <i>Chapter Two The Theory and Methodology of Nuclear Magnetic Resonance Techniques</i>	 <i>20</i>
2.1 Nuclear Magnetic Resonance Theory	20
2.1.1 The Resonance Phenomenon	20
2.1.2 Spin Manipulation and Signal Acquisition	23
2.1.3 Linewidths and Second Moments	26
2.1.3.1 Factors Influencing Lineshape	26
2.1.3.2 The Linewidth-Mobility Relationship	27
2.1.3.3 Second Moments	29
2.1.4 Relaxation	32
2.1.4.1 Relaxation Mechanisms	34
2.1.4.2 The Linewidth-Transverse Relaxation Relationship	40
2.1.5 Diffusion Measurements	40
2.1.5.1 The Development of Diffusion Techniques	41
2.1.5.2 Fringe Field Gradient Diffusion	45
2.1.5.3 Pulsed Field Gradient Diffusion	50
2.1.5.4 A Comment on Spin Diffusion	51
2.2 Experimental Method	51
2.2.1 Fringe Field Gradient NMR Measurements	51
2.2.1.1 Fringe Field Gradient NMR Probe Holder	51

2.2.1.2 Fringe Field Gradient NMR Methodology	53
2.2.2 Pulsed Field Gradient NMR Measurements	54
2.2.2.1 Measurements at the University of Queensland	54
2.2.2.2 Measurements at Umeå University	56
2.2.3 Error Analysis	57
2.3 References	57
 Chapter Three Imidazolium Salts	 59
3.1 Introduction	59
3.1.1 The Dialkylimidazolium/Aluminium Halide Systems	60
3.1.2 Hydrophobic Imidazolium Salts	63
3.1.2.1 Altering the Anion	63
3.1.2.2 Altering the Cation	64
3.1.2.3 Binary Systems	65
3.1.3 The Research of A. G. Bishop	65
3.1.3.1 The Alkyl Chain Length Effect	66
3.1.3.2 The Anion Effect	67
3.1.3.3 Binary Systems	68
3.2 Research Objective	68
3.3 Results	70
3.4 Discussion	83
3.4.1 The Anion Effect	83
3.4.1.1 The Role of the Medium on the Transport Properties	86
3.4.1.2 The Role of Charge Carrier Concentration on the Transport Properties	94
3.4.1.3 Summary	99
3.4.2 MeEtImTf and MeEtImNTf ₂ Binary System	100
3.4.3 The Alkyl Chain Length Effect	104
3.4.4 Solid State Diffusion	113
3.5 References	124
 Chapter Four Pyrrolidinium Salts	 128
4.1 Introduction	128
4.1.1 Orientational Disorder in Molecular Crystals	128
4.1.2 Orientational Disorder in Ionic Crystals	134
4.1.2.1 Inorganic Plastic Crystals	134
4.1.2.2 Organic Plastic Crystals	137
4.1.2.3 Inorganic-Organic Plastic Crystals Combinations	140
4.2 Research Objective	144

4.3	Results	145
4.3.1	Pyrrolidinium Salt Systems	145
4.3.2	Diffusion in LiNTf ₂ /P ₁₂ NTf ₂ Mixtures	146
4.4	Discussion	152
4.4.1	Characterisation of the Diffusion Mechanisms	152
4.4.2	Analysis of the Charge Carrier Concentration	162
4.4.3	Modelling Conductivity from Diffusion	167
4.4.4	The Nature of Ion Transport	181
4.5	References	182
<i>Chapter Five</i>	<i>A Comparison of the Imidazolium and Pyrrolidinium Salt Systems</i>	<i>187</i>
5.1	Comparing the Salts	187
5.2	References	196
<i>Chapter Six</i>	<i>Conclusions and Future Work</i>	<i>197</i>
6.1	Imidazolium Salts	197
6.1.1	The Anion Effect	197
6.1.2	MeEtImTf and MeEtImNTf ₂ Binary System	198
6.1.3	The Alkyl Chain Length Effect	198
6.1.4	Solid State Diffusion	199
6.1.5	Future Work	200
6.2	Pyrrolidinium Salts	201
6.2.1	Diffusion Mechanisms	201
6.2.2	Future Work	203
6.3	A Comparison of Imidazolium and Pyrrolidinium Salts	204
6.4	The Merits of NMR Diffusion Techniques	205
<i>Appendix</i>		<i>207</i>

Abstract

1,3-methylalkylimidazolium and N,N-methylethylpyrrolidinium salts are two organic electrolyte systems based on cyclic ammonium structures. These salts have been found to exhibit exceptional ionic conductivities in both the solid and liquid states, making them possible electrolytes for alternative energy sources. In this work, ionic diffusion coefficients have been measured using the Fringe Field Gradient (FFG) and Pulsed Field Gradient (PFG) techniques in order to establish an ionic transport mechanism for these systems. In particular, the effect of chemical structure, as well as binary formation, on the transport properties was investigated.

The effect of the anion on the diffusion behaviour was examined for 1,3-methylethylimidazolium salts with bromide, iodide, trifluoromethanesulfonate (triflate) and bis(trifluoromethanesulfonyl)amide (amide) anions. Cation diffusion coefficients for the halide salts were significantly lower than those for the fluorinated salts, which was attributed to the higher halide salt viscosities. Despite the differences in the diffusion coefficients, the melt conductivities were very similar for all four electrolytes. The halide salts have a greater charge carrier concentration per unit volume, as determined by the density. Therefore, the combination of more ions with lower diffusion coefficients for the halide salts results in the same conductivity as the more diffusive but less concentrated fluorinated salts.

Combining the imidazolium triflate and amide salts to form binary mixtures resulted in enhanced conductivities compared to the pure components. By contrast, no appreciable differences in ionic diffusion coefficients were observed for the binaries. Formation of a binary was thought to promote the dissociation of ion aggregates, thereby increasing in the charge carrier concentration and the conductivity accordingly.

The imidazolium bromide and iodide salts are both solids at room temperature with melting points of 352 and 351K respectively. Diffusion was measured in the solid state and found to be considerably higher than diffusion in the supercooled liquid. A difference in the diffusion mechanism accounts for this behaviour; diffusion in the solid is likely to occur via a vacancy mechanism while liquid state diffusion involves cooperative rearrangements of small sections of the material. Conductivity in the solid is lower than that in the liquid due to fewer mobile charge carriers, as confirmed by the NMR signal intensities. Conductivities were calculated from the diffusion coefficients and NMR signal intensities using the Nernst-Einstein equation. Reasonable agreement between the calculated and measured values was obtained if it was assumed that only the cations contribute to the conduction mechanism.

Ionic transport in the imidazolium salts was also affected by the substitution of different alkyl groups onto the imidazolium ring. Increasing the length of the alkyl group was found to decrease the conductivity. Similar behaviour was also observed for the cation diffusion coefficients at 298K. At a higher temperature however, a maximum diffusion coefficient was obtained when the alkyl group consisted of three carbons. This maximum corresponds to the salt with the lowest viscosity. The subsequent decrease in both conductivity and diffusion was attributed to the size of the cation, with the larger ions experiencing slower diffusion.

For N,N-methylethylpyrrolidinium bis(trifluoromethanesulfonyl)amide, the addition of a small amount of the analogous lithium salt (lithium amide) forms a solid solution such that the lithium salt is incorporated into the pyrrolidinium salt lattice. Both the pyrrolidinium and amide diffusion coefficients were found to increase with increasing lithium salt content up to 4.8mol%. Higher lithium amide concentrations resulted in a decrease in the melting point and the detection of lower diffusion coefficients. The differences in diffusion behaviour were again attributed to different transport mechanisms. Vacancy diffusion was assumed to occur in the solid materials while

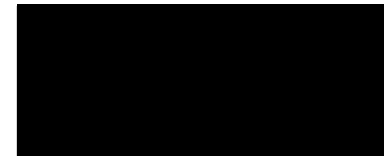
liquid state diffusion was thought to involve the cooperative rearrangements within the material.

In contrast to this diffusion behaviour, an increase in the lithium salt content, up to 33mol%, resulted in a steady increase in conductivity. A difference in the concentration of available charge carriers was again thought to be responsible for the observed conductivity behaviour. It was proposed that the addition of small amounts of lithium amide distorts the crystal lattice, thus creating vacancies. The higher vacancy concentration enables more ions to move, resulting in an increase in conductivity. More lithium amide results in the formation of a liquid phase. Although diffusion is slower in this phase, the concentration of mobile ions is considerably greater, resulting in a further increase in conductivity.

Despite the similarity in structure, the properties of the imidazolium and pyrrolidinium salts are remarkably different. Although similar diffusion coefficients were measured for these salts in the melt, overall the imidazolium salts displayed lower melting points, higher conductivities, higher ionic diffusion coefficients and higher charge carrier concentrations. This contrasting behaviour was related to the ionic interaction strength. The imidazolium salt is aromatic and the charge is therefore delocalised between the nitrogen atoms within the ring. This distribution of charge weakens the ionic interactions, thus resulting in a more mobile system.

Declaration

This thesis contains no material which has been accepted for the award of any degree or diploma at any university and, to the best of the author's knowledge and belief, contains no material previously published or written by another person, except where due reference has been made in the text.

A solid black rectangular box used to redact the author's signature.

Hayley A. Every

Acknowledgments

Despite only my name on the title page, there are many others that have played an integral part in the completion of this thesis. First and foremost, I am indebted to my supervisors, Dr. Maria Forsyth and Prof. Doug MacFarlane for their continual inspiration, encouragement and support. They have provided me with so many wonderful opportunities from which I have learnt so much. This gratitude is also extended to the "Electrolyte Group" members (past and present) who have made research a most enjoyable experience. Of this group, I would particularly like to acknowledge Dr. Andrea Bishop and Jewel Huang for collaborating with me in this research, and Dr. Alice Voelkel and Dr. Jacob Golding for providing me with my materials.

Many thanks to Dr. Andrew Whittaker, Queensland University, Australia, for allowing me to use his spectrometer. Also, to Dr. Greger Orädd, Umeå University, Sweden - for his willingness to assist me with some of the diffusion measurements. To Denis Bell, Geoff Mead and Bill Keane - your involvement in the maintenance of the spectrometer has been most appreciated. I would have been lost without the help from you all.

My sincere gratitude to Dr. Mark Smith (formerly of the University of Kent, United Kingdom) for inviting me to work with him at UKC, and Dr. Maria Garcia for her kindness, generosity and friendship. Also to Dr. Jörgen Tegenfeldt, Uppsala University, Sweden, for teaching me the fundamentals of fringe field gradient diffusion, and Dr. Sabina Abbrent and Dr. Helena Berg for making Sweden my second home. Tusen tack!

Thanks to the residents of Siberia for providing a lighter side of life, and in particular Karen, Ellen, Astrid, Simon, Kate and Scott for keeping me sane(?). Last, but not least, a BIG thank you to my family for their constant support and belief in me over the last five years.

Chapter One

Introduction

1.1 The Importance of Electrolytes

We are at the mercy of technology; reliant on cars, computers, mobile phones and the like for our everyday needs. This lifestyle however, necessitates energy, with impending technological advances likely to utilise more energy. Can the current energy sources cope with such demands? Our main energy supply is from fossil fuels. Although currently in plentiful supply, fossil fuels are a finite resource. Furthermore, environmental concerns over greenhouse gas emissions have imposed restrictions on fossil fuels consumption. Consequently, if we are to maintain our current standard of living, alternative energy sources need to be investigated.

A number of possible energy sources have been considered in recent years, including batteries, fuel cells and photoelectrochemical cells. Each of these devices is based on an electrochemical cell, consisting of two electrodes separated by an ionically conducting electrolyte (Figure 1-1). The cell functions by transporting ions from one electrode to the other across the electrolyte while electrons are transported through the external circuit. The overall cell efficiency is largely governed by the rate of ion transport through the electrolyte; thus it is important that these materials exhibit excellent ionic conductivities.

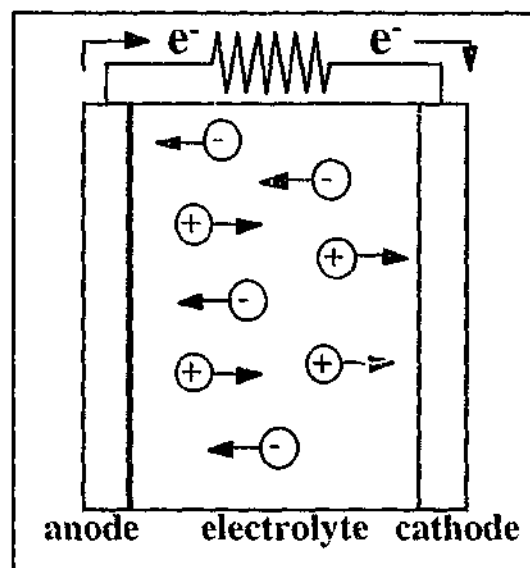


Figure 1-1 A schematic of an electrochemical cell.

In the simplest sense, ionic conductivity, σ , is dependent on the concentration of ions, n , with a given charge, q , and mobility, μ , as shown by the following equation:¹

$$\sigma = \sum_i n_i q_i \mu_i$$

Equation 1-1

An appropriate electrolyte will, therefore, consist of a large number of active charge carriers (those involved in the cell reactions) with high mobilities. There are a range of different electrolyte materials that have been considered for electrochemical cells.² Some glasses and ceramics have been found to be excellent solid state ionic conductors. The high conductivity observed in these materials is a result of a high concentration of mobile ions and a low activation energy for ion motion.² The brittle nature of these materials however, is often detrimental to their implementation in electrochemical cells. Liquid electrolytes exhibit high ionic mobilities, but can be volatile and corrosive. Polymer electrolytes have generated considerable interest in recent years as they are flexible materials with liquid-like conduction mechanisms. The conductivity, however, is limited by low salt solubilities and restricted ion

motion. The desired physical properties of an electrolyte will depend on the type of application. Therefore, there is an on-going need for novel ion conducting materials.

The systems that are the focus of this thesis have evolved from this search for new electrolytes for electrochemical devices. The materials are based on simple organic salts that have been found to be conductive in both the solid and liquid states.³⁻⁶ The major aim of this research was to characterise the nature of the ion transport mechanism in such organic salts. An understanding of these conduction mechanisms will assist in the development of more efficient electrochemical cells.

1.2 The Conductivity-Diffusion Relationship

The nature of the charge carriers within an electrolyte is largely determined upon synthesis of the material. The mechanism by which the ions move throughout the electrolyte, however, can not be controlled so easily. In order to characterise ionic conduction mechanisms, a number of experiments can be employed. Ionic conductivities are typically measured by alternating current (AC) impedance methods. Although one may gauge the overall mobility of a system from such measurements, it is difficult to elucidate the individual contribution from each ionic component. Such information can be obtained more readily by measuring the mobility of each ionic species independently via Nuclear Magnetic Resonance (NMR) methods.

Fifty-five years ago, two independent teams, led by Professor F. Bloch and Professor E. M. Purcell, detected proton magnetic resonance absorption signals in bulk materials.⁷ For this discovery, they were jointly awarded the Nobel Prize in 1952. Since these first NMR experiments, both the instrumentation and methodology have advanced significantly. The advent of pulsed Fourier transform experiments provided an efficient means for spectral acquisition. Moreover, chemical structure

and molecular motions can be monitored independently through manipulation of the pulse sequences. As a consequence, NMR spectroscopy has become one of the most important analytical techniques for material characterisation.

NMR has shown particular prominence in the study of material dynamics, offering a number of experimental methods for the detection of atomic mobility. Linewidth and relaxation measurements can reveal information about the local motions within a material, but are not always indicative of the translational motions related to conduction. Nevertheless, diffusion, which is closely associated with ionic conductivity, can be measured directly by the Fringe Field Gradient (FFG) and Pulsed Field Gradient (PFG) NMR techniques. These techniques provide a relatively simple, non-destructive method (compared to radiotracer methods) for obtaining diffusion coefficients for individual species.⁸ In this research, NMR diffusion techniques were employed to study ion diffusion within electrolytes. The experimental details of these NMR techniques can be found in Chapter 2.

The relationship between conductivity and diffusion is apparent when Equation 1-1 is expressed using the more detailed Nernst-Einstein equation:⁹

$$\sigma = \frac{Dq^2c}{kT}$$

Equation 1-2

where D is the diffusion coefficient of the solute (the sum of the cation and anion diffusion coefficients, D_+ and D_-), q is the charge on each carrier, c is the concentration of ions, k is the Boltzmann constant, and T is temperature. It can be seen that an increase in the ionic diffusion coefficient results in an increase in conductivity.

For an electrolyte of known concentration, it is possible to model the conduction mechanisms from the measured diffusion coefficients with the help of Equation 1-2. The Nernst-Einstein equation, however, was originally developed in the context of dilute solutions where ionic interactions were expected to be minimal.⁹ Consequently, the conductivities predicted by this equation for concentrated liquid electrolytes and solids are often higher than the measured values. There are three factors that may account for this discrepancy: drag effects, correlated motions (in the case of tracer measurements) and uncharged species. A drag effect results if the ions experience friction as they move past one another. Such interference effects are well recognised in gas phase diffusion, but the consequence of such effects on diffusion in a liquid phase has yet to be identified.^{9,10} In many cases, interference effects are probably overshadowed by the other limiting factors. It has been proposed that tracer diffusion in the solid state is not a random process, but that the ion mobility is correlated to the previous position.¹⁰ Consequently, the ion would experience a more direct path through the material rather than a random walk process. The result of this correlated motion, however, would actually result in a lower calculated conductivity value than the measured value, contrary to what is commonly observed.

The final factor which can influence the validity of the Nernst-Einstein equation is the concentration effect. In using Equation 1-2, it is assumed that there is complete ion dissociation in the electrolyte and that all the ions will be available for conduction. This will be the case in dilute solutions where ion interactions are limited, but, for more concentrated electrolytes, ion pairs and larger aggregates may form. While the diffusion measurements do not discriminate between charged and uncharged species in the electrolyte, it is only the charged species that will contribute to the conductivity. Therefore, the calculated conductivity from the diffusion coefficients is often significantly higher than the measured value. Moreover, this concentration term does not take into consideration any temperature dependence. For example, the decrease in density of a molten salt with increasing temperature will result in a reduction in the number of charge carriers per unit volume. Similarly, ion association

tends to occur to a greater extent as the temperature increases, which would again alter the number of available charge carriers.¹¹

As the nature of the transport mechanisms within an electrolyte is dependent on the chemistry and morphology of the system, one would expect the conduction in a solid electrolyte to differ considerably from that in a liquid. A number of possible transport mechanisms have already been identified and are summarised below with reference to relevant examples.

1.3 Diffusion Mechanisms

1.3.1 Solid State Transport Mechanisms

In crystalline solids there are a number of possible ion transport mechanisms. Conduction which involves self-diffusion of the host material will generally occur via a vacancy mechanism.^{12,13} In a crystal lattice, vacancies are the sites where an atom or ion is absent. Vacancy diffusion therefore occurs via the migration of an atom from its own lattice site to an adjacent vacant lattice site (Figure 1-2). The formation of vacancies is a thermally activated process described by the following equation:¹

$$N_v = N \exp\left(\frac{-Q_v}{RT}\right)$$

Equation 1-3

where N_v is the number of vacancies, N is the total number of atomic sites, Q_v is the activation energy (vibrational energy) for vacancy formation, R is the gas constant and T is temperature. In the presence of a large quantity of vacancies, self-diffusion should occur readily.

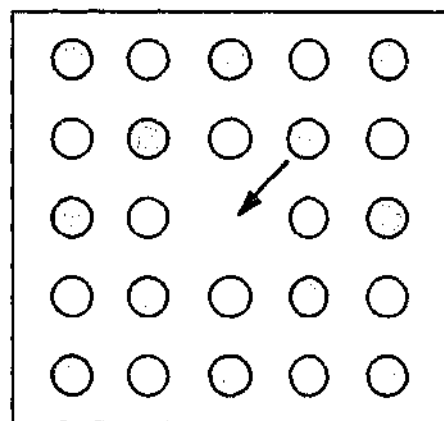


Figure 1-2 Vacancy diffusion.

Ion transport in the solid state can also involve an interstitial diffusion process.^{12,13} Interstitial sites are the voids that are not normally occupied in the crystal lattice and diffusion therefore occurs when ions migrate from one interstitial site to another available site (Figure 1-3). In some materials, the interstitials can form 1-, 2- or 3-dimensional channels through which ion transport occurs.² This diffusion mechanism usually involves small atoms or molecules, as they are able to fit easily into these voids. Larger atoms, including the host atoms, are unlikely to undergo such diffusion as they are not normally found at interstitial sites. Interstitial diffusion should be more rapid than vacancy diffusion since the diffusing particles are smaller and there are more available interstitial sites than vacancies. The preferred mechanism - vacancy or interstitial - will depend on the structure and chemical nature of the electrolyte.

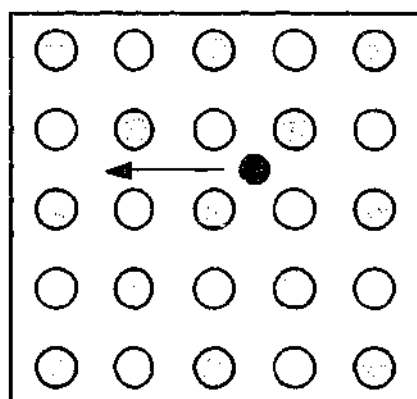


Figure 1-3 Interstitial diffusion.

A variation on the interstitial diffusion process is the interstitialcy mechanism.^{12,13} An interstitial atom moves to a normal lattice site, displacing the atom that was there by pushing it into a neighbouring interstitial site. The transport of atoms in this diffusion process is by $a/2$ jumps (Figure 1-4). However, for each diffusive jump the charge is displaced by a . The conductivity calculated from the diffusion coefficients measured for this process will therefore be underestimated by a factor of 2.¹³

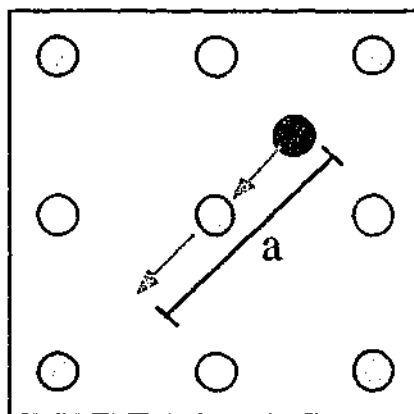


Figure 1-4 Interstitialcy diffusion.

1.3.1.1 Examples of Solid State Ionic Conductors

Two of the more common solid state ionic conductors are sodium β -alumina and NASICON ceramics. β -alumina exists as two polymorphs, β and β' , of which β' is a metastable material and the better conductor.^{2,8,14} Sodium ion transport occurs within 2-dimensional "conduction planes" that separate the spinel layers. The conduction mechanism has been described by Ingram¹⁵ as a "concerted migration of 'interstitial pairs'", a claim supported by conductivity and dielectric measurements. NMR spin-lattice relaxation has been studied for ^{27}Al and ^{23}Na in this material^{16,17} (for experimental details, see Chapter 2). T_1 for ^{27}Al is sensitive to the diffusion of the sodium cations whereas electric field gradient inhomogeneities are responsible for ^{23}Na T_1 relaxation. For both materials, asymmetric T_1 versus $1/T$ curves were observed and adequately modelled assuming the conduction mechanism mentioned above, thus providing further evidence for such ion transport.

The NASICON family of ceramics are based on non-stoichiometric zirconophosphosilicate materials, which consist of a 3-dimensional network structure through which the conducting ions can move.² The conductivity, however, is very sensitive to the chemical composition. Sodium magic angle spinning (MAS) NMR spectra for the analogous $\text{Na}_{1.4}\text{M}_{1.6}\text{In}_{0.4}(\text{PO}_4)_3$ ceramics, where M is either Ti, Sn, Hf or Zr, display a difference in sodium mobility.¹⁸ Broad signals were detected for Ti and Sn containing compounds, whereas the spectra for the Hf and Zr materials were much narrower. The differences in spectral linewidth suggest that sodium diffusion occurs more readily in the Hf and Zr ceramics, which is also supported by the conductivities and activation energies for these materials. The sodium mobility is dependent on the structure of the ceramic. The radii of the metallic ions increases according to:

$$\text{Ti} < \text{Sn} < \text{Hf} < \text{Zr}$$

with the unit cell for these NASICON compounds increasing in a similar manner. In the case of these materials, increasing the unit cell opens up the pathways for diffusion, which therefore increases the sodium ion mobility.¹⁸

The effect of chemical composition is apparent in the analogous LISICON materials, consisting of Li_4SiO_4 and $\text{Li}_5\text{GaSi}_2\text{O}_8$ solid solutions.¹⁴ A 50:50 solid solution of these two materials has a conductivity that is four orders of magnitude greater than for the pure ceramics. The conduction mechanisms in these materials are thought to involve the interstitial sites, which provide a 3-dimensional pathway for lithium ion transport.^{2,14}

These transport mechanisms are not only limited to crystalline materials. There is some evidence that similar mechanisms occur in glasses despite the irregularity of the structure.¹⁹ In alkali silicate glasses, the silicate network forms channels through which ion transport is thought to occur.²⁰ A similar mechanism has also been

observed in alkali aluminosilicate glasses.²¹ The actual nature of the conduction mechanism in such materials, however, is still a point of contention.

A novel group of materials, referred to as plastic crystals, have been found to exhibit high conductivities in the solid state. The soft, "plastic" nature of these materials is the result of ion reorientation in the solid, which is also thought to facilitate ion diffusion. Sodium orthophosphate exhibits dynamic rotational disorder of the anion along with significant cation diffusion.²² It has been proposed that the cation transport is associated with the anion rotation via a mechanism reminiscent of a "paddle-wheel" motion. It is not certain, however, whether this mechanism is typical for all plastic crystals. More information on the properties of plastic crystals can be found in Chapter 4.

1.3.2 Liquid State Theories

In a suitable solvent, a solute will dissociate into ionic constituents that are then capable of carrying charge throughout the electrolyte. In the most dilute solutions, the ions are completely solvated by the solvent molecules and are therefore electrically isolated from one another. The Debye-Hückel model, which proposes that ions are discrete particles that move in a dielectric continuum, is appropriate for modelling the behaviour of dilute solutions up to concentrations of $1 \times 10^{-3} \text{ mol.dm}^{-3}$.²³ In this case, ion mobility is facilitated by Brownian motions that are biased in the direction of an applied field.²⁴

As the solute concentration increases, however, two interionic effects begin to hinder ion transport: the electrophoretic effect and the relaxation effect.^{23,24} The electrophoretic effect occurs when ions, moving under an applied electric field, drag solvent molecules along in the same direction. Counter ions diffusing in the opposite direction will therefore be moving against the stream of solvent molecules. The result

is a reduction in the ionic mobility and hence the overall conductivity. The relaxation effect is the result of unbalanced charge distribution. In the absence of an electric field, the ions are positioned symmetrically in solution in order to maintain the charge balance. Upon the application of an electric field, the ions will be attracted towards the appropriate electrode, resulting in a distortion of this ionic equilibrium. To counteract this effect, a small restoring force occurs in the opposite direction, which again retards the ionic mobility.

Further increases in solute concentration result in a breakdown of the solvation sheath, allowing ionic interactions to occur. The behaviour can no longer be adequately modelled by the Debye-Hückel theory as the ion interactions form uncharged pairs and larger complex ions, reducing the overall number of charge carriers and therefore the conductivity. A slight modification of this theory, by means of an ionic association parameter, can extend the model to concentrations of 1mol.cm^{-3} . However, the validity of this modified model is dependent on the electrolyte.²⁵

In the absence of any solvent, as is the case for ionic liquids (*aka* molten salts), a whole new approach is required to formulate an appropriate theory. Ion motion in these materials is not facilitated by any solvent motion and does not involve individual ion migration. Instead, it is thought that ion motion occurs via the cooperative motion of volume elements within the liquid.²⁶ A number of models have been proposed to describe the properties of ionic liquids, as summarised below.

1.3.2.1 Ionic Liquid Models

The simplest model to describe the transport mechanism in ionic liquids is the Quasilattice or Vacancy model developed by Frenkel²⁷ and Bresler.²⁸ This model assumes that a crystal lattice structure is maintained in the liquid state, but with an

excess of vacancies to account for the absence of long range order. The vacancies may form tunnels through which the ions can be transported. There are two main criticisms of this model with respect to ion transport. The activation volume (the volume for forming a hole and for making the jump⁹) for diffusion in liquids is small compared to solids, and therefore holes that are the size of ions are incapable of diffusing. Also, this model can not describe the deviations from linearity often observed in the diffusion data near a thermal transition.⁹ Similar behaviour is predicted by the Transition State theory,^{29,30} where the liquid forms a regular structure and the particles oscillate in a cage formed by the neighbouring atoms. A particle can jump from one equilibrium site to another once a minimum energy of activation is exceeded. The theory predicts that each individual jump should be distinguishable from the particle oscillations and occur through a relatively static matrix. Fluid, high temperature ionic liquids are unlikely to exhibit these characteristics, precluding the use of this theory for such materials.²³

The Hole model, from the work of Altar³¹ and Fürth,³² also proposes the existence of unoccupied cavities in the liquid state, but unlike vacancy defects (as in the quasilattice model), these unoccupied cavities are randomly distributed throughout the material.⁹ These 'holes' are able to conglomerate to form larger holes via behaviour reminiscent of Brownian motion.³² Ionic mobility is therefore facilitated by jumping to adjacent holes. According to Fürth³², the average hole volume, v , is dependent on temperature as described by the following equation:

$$v = \frac{4}{3}\pi r^3 = 0.68 \left(\frac{kT}{\gamma_L} \right)^{3/2}$$

Equation 1-4

where r is the hole radius, k is the Boltzmann constant, T is temperature and γ_L is the surface tension of the liquid. In ionic liquids, however, the activation volumes for

conduction do not concur with this equation.²³ Also, this model assumes that the energy to form holes is much larger than the energy associated with the jump, which is often contrary to what is actually observed.²³

The Crystallite model³³ is based on the presence of defects in solids. Schottky-type defects diffuse to the dislocation lines forming sheets of vacancies. As the temperature increases, these sheets are the first to melt, thus creating a liquid with "islands" of solid particles. Such behaviour has been used to explain the iceberg phenomenon observed by Bockris³⁴ in liquid silicate systems. However, the Stokes-Einstein equation, which relates diffusion to the viscosity and has been found to be applicable in many ionic liquids, is not supported by this model.⁹

The Significant Structure model³⁵ is related to the vacancy and crystallite models. It implies that a liquid consists of regions of holes or vacancies that exhibit gas-like behaviour, interspersed amongst regular close-packed solid-like particles. It is therefore the motion of the vacancies in these materials that gives the material fluidity. The Polyhedra model^{36,37} suggests that molecular rearrangement is irregular in the liquid. The particles aggregate to form polyhedra with anomalous symmetry, which are incapable of forming a close-packed structure, thus creating holes. The structure is, of course, dynamic and is therefore constantly changing, enabling diffusion to occur.

The Free Volume model comes in two forms: the Cell Free Volume model³⁸ and the Liquid Free Volume model.³⁹ In the Cell Free Volume model, molecules are considered to reside in cells that exhibit a certain free volume, taken to be the difference between the size of the cell and the volume of the particle it contains. In this case, the free volume is not dynamic but confined to each individual cell. The Liquid Free Volume model, however, suggests that the free volume is not associated

with individual cells but is randomly dispersed throughout the liquid. Therefore, the free volume can be easily redistributed in the liquid, giving rise to ion mobility.

The Configurational Entropy theory of Adam and Gibbs⁴⁰ suggests that motions in a material are governed by collective rearrangements of small sections of the liquid. The extent of these rearrangements is dependent upon the amount of material involved and the accompanying configurational entropy. This theory also predicts a decrease in the transport properties as the configurational entropy approaches zero. Adam and Gibbs⁴⁰ found that this theory adequately models the behaviour of a number of glass forming liquids. It has since been applied to many liquid electrolytes.

1.3.2.2 Examples of Liquid State Ionic Conductors

Liquid electrolytes are simply formed upon the dissolution of a salt within a solvent, which can be achieved readily for a wide range of materials. As mentioned above, the Debye-Hückel model can adequately describe the behaviour of dilute solutions, while deviations are observed as the salt concentration increases. Examples of liquid electrolyte behaviour can be found in the book by Stuart I. Smedley.²³

The conduction mechanisms in ionic liquids are far more complicated. Angell and Moynihan⁴¹ have studied the transport processes in molten salts and suggested that mass transport is dependent on the Coulombic potential. As the absolute glass transition temperature, T_0 , is approached (upon cooling the sample), the attractive and repulsive forces between ions become stronger. The result is a non-linear temperature dependence for the transport properties. This departure from linearity can be modelled with the Vogel-Tammann-Fulcher (VTF) equation:

$$\sigma = \sigma_0 \exp\left(\frac{-k}{T - T_0}\right)$$

Equation 1-5

where σ is the conductivity, σ_0 is the limiting conductivity, k is a pseudo activation energy and T is the temperature. Although this is an empirical equation, it has also been derived from both the free volume model and configurational entropy theory. Angell and Moynihan showed that the conductivity behaviour of some metal nitrate melts supported this proposal. A detailed discussion of other ionic liquids can be found in Chapter 3.

Polymer electrolytes, although inherently solid, actually exhibit a conduction mechanism that is reminiscent of liquid-like behaviour. Despite almost 30 years of research, however, the nature of ion transport in polymer electrolytes is still a contentious issue. The most common polymer electrolytes are based on poly(ethylene oxide) (PEO), which is a semi-crystalline material with melting and glass transition temperatures of 338 and 213K respectively.² Ionic conductivity in these electrolytes was originally thought to involve ion hopping through tunnels created by the crystalline helices.² However, an NMR study by Berthier *et al.*⁴² indicated higher conductivity in the elastomeric amorphous phase. It has since been conceded that the segmental motions of the polymer are largely responsible for ion transport, analogous to a localised liquid-like environment.² However, the conduction mechanism is further complicated by ion-ion interactions resulting in ion pair and/or aggregate formation.² It is most likely that the reorientation of the polymer chains enables the ions to transfer from one suitable site to another, whether such a site exists on the polymer chain or on an ionic cluster.

1.4 Specific Aims and Thesis Outline

In the field of electrolytes, organic salts, with melting points ranging from 200 to 450K, have occasioned considerable interest. With evidence of conduction in both the solid and liquid states, these materials are favourable candidates for electrochemical cells, in particular solar cells. In the absence of any solvent, these salts form concentrated ionic liquids that, when coupled with significant ion mobility, form a highly conductive material. Good conduction in the solid state suggests a fast ion conduction mechanism, where a proportion of the ions are mobile in what is a largely immobile crystal lattice. The precise mechanism of ion transport in these materials has not been revealed, hence a study of diffusion in these systems is warranted.

The aim of this research was to investigate the ionic transport mechanisms in two organic salt systems based on 1,3-dialkylimidazolium salts and N,N-dialkylpyrrolidinium salts. In the case of the imidazolium salts, the effect of the chemical structure on the diffusion characteristics was examined with particular reference to the role of the anion and the effect of alkyl chain length. For the pyrrolidinium salts, the effect of adding an analogous lithium salt in quantities ranging from 0.9mol% to 50mol% was investigated. NMR diffusion measurements were conducted in order to characterise the transport properties in these systems. Where possible, the fringe field gradient (FFG) and pulsed field gradient (PFG) diffusion methods were employed to measure the anion and cation diffusion coefficients. Through independent characterisation of the anion and cation diffusion in each system, in conjunction with previously reported conductivities, an appropriate model for conduction was proposed.

This dissertation is comprised of two major chapters (Chapters 3 and 4), one each on the imidazolium and pyrrolidinium salts. Each chapter provides a brief account of the appropriate literature, followed by a detailed analysis and discussion of the

diffusion and related conductivity behaviour of the salt. Chapter 5 then compares and contrasts the two salt systems before the main findings are summarised in Chapter 6. Possible avenues for future research are also outlined in this chapter. A detailed discussion of NMR theory associated with these measurements, along with a description of the diffusion methodology, can be found in Chapter 2. Although diffusion in organic salts was the focus of this thesis, another electrolyte system based on polyvinyl alcohol (PVA) was also considered. A preliminary investigation of the transport mechanisms in PVA electrolytes involved NMR linewidth and relaxation measurements. However, equipment limitations impeded the study of diffusion. The publications associated with this work and the research presented in this dissertation can be found in Appendix 1.

1.5 References

1. W. D. Callister, *Materials Science and Engineering, An Introduction*, (John Wiley and Sons, Inc., 1991).
2. F. M. Gray, *Polymer Electrolytes*, (Royal Society of Chemistry, Cambridge, 1997).
3. A. G. Bishop, Ph.D Thesis, Monash University, Melbourne, Australia, 1999.
4. M. Forsyth, J. Huang and D. R. MacFarlane, *J. Mater. Chem.* **10**, 2259-2265 (2000).
5. D. R. MacFarlane, J. Huang and M. Forsyth, *Nature* **402**, 792-794 (1999).
6. J. Huang, M. Forsyth and D. R. MacFarlane, *Solid State Ionics* **136**, 447-452 (2000).
7. D. Shaw, *Fourier Transform N.M.R. Spectroscopy*, 2nd ed. (Elsevier Science Publishers B.V., Amsterdam, 1984).
8. A. V. Chadwick, in *Diffusion in Solids: Unsolved Problems*, Vol. 83, edited by G. E. Murch (Trans Tech Publications Ltd, 1992), pp. 235-258.

9. H. Bloom and J. O. M. Bockris, in *Fused Salts*, 1st ed., edited by B. R. Sundheim (McGraw-Hill Book Company, New York, 1964), pp. 1-62.
10. J. O. M. Bockris and G. W. Hooper, *Discussions Faraday Soc.* **32**, 218-236 (1961).
11. R. Frech and W. Huang, *Solid State Ionics* **72**, 103-107 (1994).
12. L. A. Girifalco, *Atomic Migration in Crystals*, (Blaisdell Publishing Company, New York, 1964).
13. R. J. Borg and G. J. Diets, *An Introduction to Solid State Diffusion*, (Academic Press, Inc., San Diego, 1988).
14. A. R. West, *Ber. Bunsenges. Phys. Chem.* **93**, 1235-1241 (1989).
15. M. D. Ingram, *J. Am. Ceram. Soc.* **63**, 248-253 (1980).
16. J. L. Bjorkstam and M. Villa, *Mag. Res. Rev.* **6**, 1-57 (1980).
17. J. L. Bjorkstam and M. Villa, *J. Phys.* **42**, 345-351 (1981).
18. E. R. Losilla, M. A. G. Aranda and S. Bruque, *Chem. Mater.* **10**, 665-673 (1998).
19. A. Bunde, K. Funke and M. D. Ingram, *Solid State Ionics* **86-88**, 1311-1317 (1996).
20. A. Bunde, K. Funke and M. D. Ingram, *Solid State Ionics* **105**, 1-13 (1998).
21. G. N. Greaves and K. L. Ngai, *Phys. Rev. B* **52**, 6358-6380 (1995).
22. M. Witschas, H. Eckert, D. Wilmer, R. D. Banhatti, K. Funke, J. Fitter, R. E. Lechner, G. Korus and M. Jansen, *Z. Phys. Chem.* **214**, 643-673 (2000).
23. S. I. Smedley, *The Interpretation of Ionic Conductivity in Liquids*, (Plenum Press, New York, 1980).
24. R. A. Robinson and R. H. Stokes, *Electrolyte Solutions*, 2nd ed. (Butterworths Publications Ltd., London, 1959).

25. M. Spiro and F. King, in *Ionic Liquids*, edited by D. Inman and D. G. Lovering (Plenum Press, New York, 1981), pp. 57-77.
26. J. Richter, in *Ionic Liquids*, edited by D. Inman and D. G. Lovering (Plenum Press, New York, 1981), pp. 145-164.
27. Y. I. Frenkel, *Acta Physicochim. URSS* **3**, 913 (1935).
28. S. E. Bresler, *Acta Physicochim. URSS* **10**, 491 (1939).
29. S. Glasstone, K. J. Laidler, and H. Eyring, *The Theory of Rate Processes*, (McGraw Hill, New York, 1941).
30. J. O. M. Bockris, J. A. Kitchener, S. Ignatowicz and J. W. Tomlinson, *Trans. Faraday Soc.* **48**, 75-91 (1952).
31. W. Altar, *J. Chem. Phys.* **5**, 577-586 (1937).
32. R. Fürth, *Proc. Cambridge Phil. Soc.* **37**, 252-275 (1941).
33. J. Rothstein, *J. Chem. Phys.* **23**, 218-219 (1955).
34. J. O. M. Bockris, J. W. Tomlinson, and J. L. White *Trans. Faraday. Soc.* **52**, 299-310 (1956).
35. H. Eyring, T. Ree and N. Hirai, *Proc. Natl. Acad. Sci.* **44**, 683 (1958).
36. J. D. Bernal, *Sci. Am.* 124-134 (1960).
37. J. D. Bernal, *Nature* **185**, 68-70 (1960).
38. H. Eyring and J. Hirschfelder, *J. Phys. Chem.* **41**, 249-257 (1937).
39. M. H. Cohen and D. Turnbull, *J. Chem. Phys.* **31**, 1164-1169 (1959).
40. G. Adam and J. H. Gibbs, *J. Chem. Phys.* **43**, 139-146 (1965).
41. C. A. Angell and C. T. Moynihan, in *Molten Salts*, edited by G. Mamantov (Marcel Dekker Inc., New York, 1969), pp. 315-375.
42. C. Berthier, W. Gorecki, M. Minier, M. B. Armand, J. M. Chabagno and P. Rigaud, *Solid State Ionics* **11**, 91-95 (1983).

Chapter Two

The Theory and Methodology of Nuclear Magnetic Resonance Techniques

2.1 Nuclear Magnetic Resonance Theory

Over 75% of the elements in the periodic table have a Nuclear Magnetic Resonance (NMR) active isotope, making NMR spectroscopy a valuable technique for analysing a multitude of materials. The versatility of this technique enables structural and dynamic properties to be analysed and makes NMR particularly advantageous for the study of electrolytes, where transport mechanisms are of interest. However, the concept of NMR, is not trivial and an explanation of the fundamental principles is best done using an approach that combines classical and quantum mechanical perspectives. The theory of NMR has been thoroughly discussed in many excellent texts,¹⁻⁷ and these references have been used in this chapter to provide a summary of the experiments employed in the characterisation of mobility in electrolyte systems.

2.1.1 The Resonance Phenomenon

Nucleons (protons and neutrons) possess an intrinsic rotation known as spin.⁸ Within a nucleus, spins of opposite sign but of the same nucleon are paired (protons will not pair with neutrons). If all the nucleons are paired, the overall nucleus will have no spin ($I=0$ where I is the spin quantum number). However, the presence of any unpaired spins will result in a net nuclear spin ($I \neq 0$) or angular momentum, J ($J=I\hbar$ where \hbar is the reduced Planck's constant $h/2\pi$).² Associated with the angular momentum is a magnetic moment, μ :

$$\mu = \gamma J$$

Equation 2-1

where the proportionality constant, γ , known as the gyromagnetic ratio, is an inherent property of the nucleus of a particular isotope. In the absence of any appreciable magnetic field, there will be a random orientation of these magnetic moments. However, upon applying a large magnetic field, B_0 , to the system, the nuclei will adopt a particular orientation and precess around the direction of the applied magnetic field (often defined as the z-direction) (Figure 2-1). The rate of precession is related to the field strength and is defined as the Larmor frequency, ω_L :

$$\omega_L = \gamma B_0$$

Equation 2-2

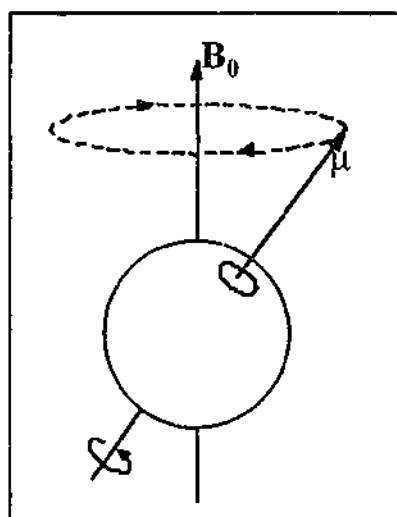


Figure 2-1 Precession of a nucleus around a magnetic field, B_0 , at the Larmor frequency.⁶

The orientation of the spins in a magnetic field is limited to a particular number of possible configurations or energy states. The energy states available result from a

discrete set of integer or half-integer possibilities as given by $2I+1$ ($I, I-1, \dots, -I+1, -I$).³ For example, ^1H and ^{19}F have a spin number of $1/2$ and therefore two possible energy states ($1/2, -1/2$), whereas ^7Li has a spin number of $3/2$ and consequently four possible energy states ($3/2, 1/2, -1/2, -3/2$) (Figure 2-2). The terminology is such that $1/2$ is the lower energy state corresponding to spin orientation parallel to the applied magnetic field and $-1/2$ is the higher energy state or antiparallel orientation. The formation of discrete energy states in the presence of a magnetic field is known as Zeeman splitting.

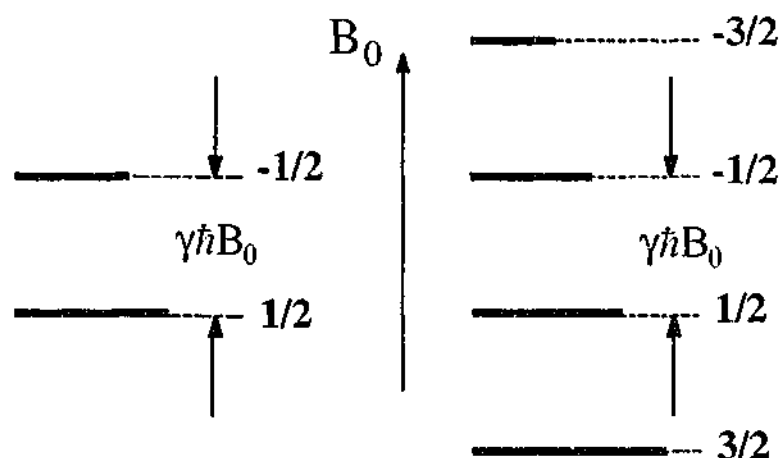


Figure 2-2 Spin distribution (as indicated by the heavy lines) in discrete energy levels.³

The distribution of spins between the energy levels is given by the Boltzmann function² (Equation 2-3 shown for $I=1/2$):

$$N_{-1/2} = N_{1/2} \exp\left(\frac{-\Delta E}{kT}\right)$$

Equation 2-3

where $N_{1/2}$ and $N_{-1/2}$ are the populations of the lower and upper levels respectively, ΔE is the energy difference between the two levels, k is the Boltzmann constant and T is temperature. There is a slight excess of spins in the lower energy state that

results in a net positive angular momentum or magnetisation in the z-direction of the applied magnetic field. The separation of the energy levels, ΔE , is given by:

$$\Delta E = \gamma \hbar B_0 = \hbar \omega_L$$

Equation 2-4

Therefore, promotion of spins from the lower to the higher energy state requires a photon with an energy proportional to the Larmor frequency, ω_L . Photons in the radiofrequency (*rf*) range possess the correct energy for such excitation to occur and this is exploited in NMR experiments.

2.1.2 Spin Manipulation and Signal Acquisition

As mentioned above, the disparity in spin population results in a net magnetisation in the direction of the applied magnetic field, B_0 . Applying an *rf* pulse can alter this population distribution and therefore affect the net magnetisation. From a classical perspective, the *rf* pulse generates a magnetic field, B_1 , perpendicular to B_0 that perturbs the magnetisation from the z-direction (Figure 2-3). The effect is to tip the magnetisation through an angle, θ , given by the angular frequency, ω_1 (equal to γB_1) and duration of the pulse, t (Equation 2-5).³

$$\theta = \omega_1 t$$

Equation 2-5

Rotation of the magnetisation through any angle can be achieved by altering the length of the *rf* pulse. A 90° ($\pi/2$) pulse will result in a net maximum magnetisation in the x-y plane whereas a 180° (π) pulse will invert the magnetisation.

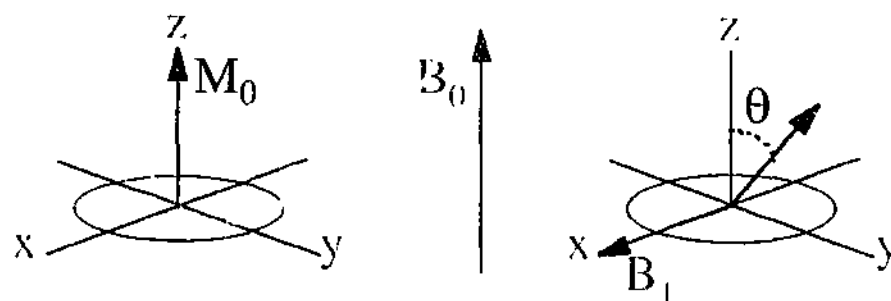


Figure 2-3 Perturbation of magnetisation.³

It is necessary to digress for a moment and introduce the frame of reference concept. There are two frames of reference that are used to describe the spin behaviour during an NMR experiment. The laboratory frame is a stationary frame of reference where the axes, x , y and z , are fixed and the applied magnetic field, B_0 , is in the z -direction. The magnetisation in this frame would be seen to be precessing around the z -axis at the Larmor frequency, ω_L . In the rotating frame, the x - y plane is now also rotating around the z -axis at the Larmor frequency. From the point of view of this rotating x - y plane, the precessing magnetisation appears stationary. To distinguish the rotating frame from the laboratory frame, the notation x' , y' and z' is used for the axes in the rotating frame.⁶ The magnetisation perturbation shown in Figure 2-3 has been reproduced in Figure 2-4 to highlight the difference between the laboratory and rotating frames. Nutation of the magnetisation is observed in the laboratory frame as the magnetisation precesses around not only the applied magnetic field, B_0 , but the rf field, B_1 . In the rotating frame, however, this appears as a simple tipping of the magnetisation around the B_1 field. Typically, the magnetisation diagrams are presented in the rotating frame, although it is common practice to interchange between the two frames of reference.

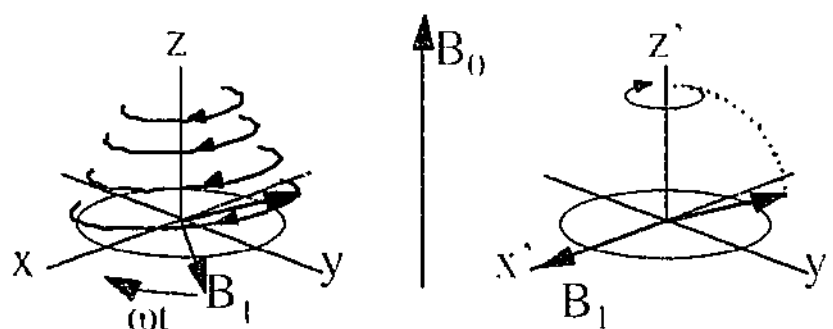


Figure 2-4 Magnetisation behaviour in the laboratory and rotating frames.³

A receiver coil in the x-y plane is used to detect the NMR signal. Immediately after an *rf* pulse, any magnetisation in the x-y plane will induce a current in the coil. The strength of this current is dependent on the magnitude of the magnetisation. As the magnetisation returns to equilibrium (the z-direction), the x-y component will exponentially decay away to zero with a time constant characteristic of the material (further discussion in section 2.1.4). The detected signal is known as a free induction decay (FID) and is a measure of the magnetisation (current) as a function of time. Via a Fourier Transform (FT), the same data can be converted to the frequency domain where the signal appears as a peak. Converting the data from the time domain to the frequency domain allows individual peak positions and intensities to be observed, hence the frequency domain is the common domain for signal analysis.

Numerous sequences of *rf* pulses have been developed to study the structure and dynamics of materials (see Fukushima and Roeder,⁵ Shaw⁶ and Callaghan³ for example) and the following is a discussion of some of the more common NMR experiments used in studying nuclear mobility.

2.1.3 Linewidths and Second Moments

2.1.3.1 Factors Influencing Lineshape

The interactions experienced by nuclei within a material can be very simply characterised by studying the NMR linewidth. If all the nuclei behaved in an identical fashion and experienced exactly the same environment, then a single narrow peak would be observed. In an actual NMR experiment, the observed peaks are of finite widths ranging from a few hertz to megahertz.

The shape of NMR spectra is governed by magnetic field inhomogeneities and the generation of local magnetic fields within the sample through dipolar and quadrupolar interactions, chemical shift anisotropy, spin rotation and scalar coupling.^{3,6} The field inhomogeneities are a characteristic of the magnet and therefore an intrinsic limitation of the apparatus. The result of this inhomogeneity is a slight broadening of the NMR linewidth. In the case of large NMR linewidths, the source of the broadening is the nuclear interactions. Dipolar interactions occurring between neighbouring nuclei generate a local dipolar magnetic field of the order of:⁷

$$B_{\text{loc}} = \frac{\mu}{r^3}$$

Equation 2-6

Quadrupolar interactions are experienced by non-spherical nuclei ($I > 1/2$) that possess a quadrupolar moment. The quadrupolar moment interacts with electric field gradients that are generated by electrons and surrounding nuclei. Depending on the strength of these interactions, different nuclei will experience slightly different magnetic fields, resulting in a distribution of precession frequencies and a broadening of the NMR line. However, motion in the material will modulate these interactions, resulting in motional narrowing of the NMR linewidths.⁷

2.1.3.2 The Linewidth-Mobility Relationship

Strong internuclear interactions are observed in solid materials with limited internal mobility, and the measured linewidth (at full width half maximum, FWHM, of the peak) can range from kilohertz to megahertz. Such behaviour is observed at low temperatures and is often defined as the rigid lattice due to the relative immobility of the nuclei. As the nuclei begin to move within the material, some of the interactions are averaged and the line begins to narrow. This occurs upon heating of a material, with further heating resulting in further narrowing. Ultimately, the spectral line will narrow to a finite width determined by the limitations of the spectrometer (magnetic field inhomogeneities). The temperature dependence is sigmoidal in shape and an example is shown in Figure 2-5. Narrowing of the linewidth will only occur when the frequency of motion is greater than the internuclear interactions (defined by the linewidth) at the rigid lattice limit. The onset of narrowing can be obtained from an extrapolation of the linear region of the sigmoidal plot to the rigid lattice limit (see Figure 2-5).

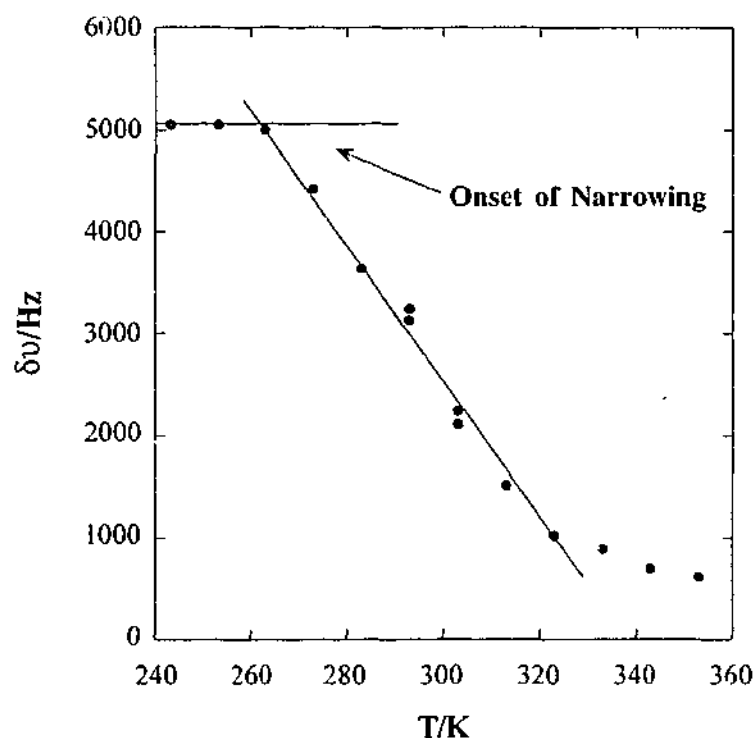


Figure 2-5 A typical linewidth versus temperature plot.

The temperature dependence of narrowing can be modelled with the following formula:^{1,9}

$$\delta v^2 = \delta v_0^2 \frac{2}{\pi} \tan^{-1}[\alpha \delta v \tau_c]$$

Equation 2-7

where δv and δv_0 are the narrowed and rigid lattice linewidths respectively, α is a constant approximately equal to unity and τ_c is the correlation time, which can be assumed to have an Arrhenius temperature dependence (Equation 2-8):¹

$$\tau_c = \tau_\infty \exp\left[\frac{-E_a}{RT}\right]$$

Equation 2-8

In this equation, τ_∞ is the limiting correlation time, E_a is the activation energy, R is the gas constant and T is temperature. The correlation time, τ_c , is a common parameter found in many NMR experiments and has a number of definitions. In essence, it is the time taken for a nucleus to have no memory of its previous environment.³ Therefore, it can also be known as the time taken to move from one site to another or the time a nucleus resides in one position. The correlation time characterises the mobility in the system, whether it be rotation or translation.

Temperature dependent linewidth analysis does have some limitations. In mobile systems, it is almost impossible to isolate the motion of particular nuclei. A nucleus moving through an immobile substrate will have the same effect as a mobile substrate around a stationary nucleus. In either case, the interactions between the nuclei of interest and the surroundings are averaged by the motion and line narrowing occurs. Only by performing other experiments, such as diffusion measurements, can the

absolute mobility of the specific nuclei be characterised. Moreover, while Equation 2-7 is a valid model for the temperature dependence of the linewidth, it fails to indicate the interactions involved and the shape of the peak. Such information can be obtained from second moment (as discussed below) and relaxation experiments (see section 2.1.4).

2.1.3.3 Second Moments

Moments can be used to approximate the lineshape of an NMR spectrum without having to find the eigenstates of the dipolar Hamiltonian.¹ The n th moment, M_n , of an NMR line can be calculated from the normalised shape function, $f(\omega)$, with a maximum frequency of ω_0 , using the following equation:

$$M_n = \int (\omega - \omega_0)^n f(\omega) d\omega$$

Equation 2-9

In the case of a Gaussian curve, the normalised shaped function is given by:^{1,10}

$$f(\omega) = \frac{1}{\Delta\sqrt{2\pi}} \exp\left(\frac{-(\omega - \omega_0)^2}{2\Delta^2}\right)$$

Equation 2-10

where Δ is the mean deviation of the frequency from the Larmor value. For a Lorentzian curve, however, the shape function is given by:¹

$$f(\omega) = \frac{\delta}{\pi} \frac{1}{\delta^2 + (\omega - \omega_0)^2}$$

Equation 2-11

where δ is the half width at half maximum intensity. If $f(\omega)$ is symmetric with respect to ω_0 , then all the odd moments (n is odd) are equal to zero, leaving only the even moments. The second moment for a Gaussian line can be calculated by substituting Equation 2-10 into Equation 2-9, which results in the following:

$$M_2 = \Delta^2$$

Equation 2-12

The half width at half maximum intensity, δ , which can also be determined from the shape factor, is given by:

$$\delta = \Delta \sqrt{2 \log 2} = 1.18 \Delta$$

Equation 2-13

which indicates that M_2 can be approximated by the linewidth. For Lorentzian lines, the second moment cannot be calculated from the shape factor as the integrals diverge.¹ If the extremities of the Lorentzian line are excluded such that the shape factor is calculated within the interval $|\omega - \omega_0| \leq \alpha$ with $\alpha \gg \delta$, the second moment can be approximated to:

$$M_2 = \Delta^2 = \frac{2\alpha\delta}{\pi}$$

Equation 2-14

hence M_2 can be estimated from the Lorentzian linewidth.

Van Vleck^{1,10} used a quantum mechanical approach to calculate the second moment, which resulted in the following equation for homonuclear interactions:

$$M_2 = \frac{3}{4} \gamma^4 \hbar^2 I(I+1) \sum_k \frac{(1 - 3 \cos^2 \theta_{jk})^2}{r_{jk}^6}$$

Equation 2-15

where γ is the gyromagnetic ratio, I is the spin number and r is the distance between the interacting nuclei. If the nuclei are randomly oriented in the material, the term $(1 - 3 \cos^2 \theta_{jk})^2$ is averaged over all directions such that M_2 becomes:

$$M_2 = \frac{3}{5} \gamma^4 \hbar^2 I(I+1) \sum_k \frac{1}{r_{jk}^6}$$

Equation 2-16

For heteronuclear interactions, the second moment is given by:

$$M_2 = \frac{1}{3} \gamma_I^2 \gamma_S^2 \hbar^2 S(S+1) \sum_{k'} \frac{(1 - 3 \cos^2 \theta_{jk'})^2}{r_{jk'}^6}$$

Equation 2-17

where I and S refer to the interacting heteronuclei. This equation also reduces to:

$$M_2 = \frac{4}{15} \gamma_I^2 \gamma_S^2 \hbar^2 S(S+1) \sum_{k'} \frac{1}{r_{jk'}^6}$$

Equation 2-18

when the spins are randomly oriented. Through the measurement of second moments and implementation of these equations, it is therefore possible to determine the nature of the interactions that are responsible for the broadening of the NMR line.

2.1.4 Relaxation

The equilibrium condition in an NMR magnet is one of a net non-zero magnetisation in the z-direction and a net zero magnetisation in the x-y plane. In performing an NMR experiment, the magnetisation is perturbed from this equilibrium, changing both the z and x-y components. Before the experiment can be repeated, equilibrium must once again be achieved and the return to equilibrium occurs via processes known as relaxation.

Restoration of the net magnetisation in the z-direction (along the direction of the applied field) is known as longitudinal relaxation and is defined by a characteristic time constant T_1 . As energy is transferred from the spins to the surroundings during longitudinal relaxation, this relaxation process is also often referred to as spin-lattice relaxation. The transverse relaxation process restores equilibrium in the x-y plane (zero net magnetisation) and is defined by the characteristic time constant T_2 . In this case, the relaxation process involves a transfer of energy from one spin to another, hence the alternative name, spin-spin relaxation. Longitudinal relaxation is also possible in the rotating frame. The magnetisation is "locked" in the x-y plane such that the magnetisation and the applied field, B_1 , rotate together. In the rotating frame, the B_1 field is fixed and therefore analogous to the B_0 field in the laboratory frame.

The relaxation process occurs in the direction of B_I , (hence the name spin-lattice relaxation in the rotating frame), and is characterised by the time constant $T_{1\rho}$.

The transfer of energy involved in these relaxation processes is stimulated by fluctuations in the local magnetic field generated by dipolar and quadrupolar interactions, chemical shift anisotropy, spin rotation and scalar coupling. Efficient relaxation occurs when there are many local magnetic fields (spectral density, $J(\omega)$) fluctuating at the Larmor frequency, ω_L , for the observed nuclei as represented by the equation shown below.

$$J(\omega) = \frac{\tau_c}{1 + \omega^2 \tau_c^2}$$

Equation 2-19

This equation suggests that the spectral density at a given Larmor frequency, ω_L , is dependent upon the correlation time, τ_c , which is assumed to exhibit an Arrhenius temperature dependence (see Equation 2-8). Figure 2-6 shows the spectral densities for short, intermediate and long τ_c values. A short correlation time results in a large distribution of fluctuating fields, albeit limited in abundance. In contrast, a high probability of low frequency motions will occur when τ_c is long, with the higher frequency motions essentially non-existent. In the case of intermediate τ_c values, a maximum in the spectral density occurs when $\omega_L \tau_c \sim 1$ thus providing the most efficient means for relaxation.

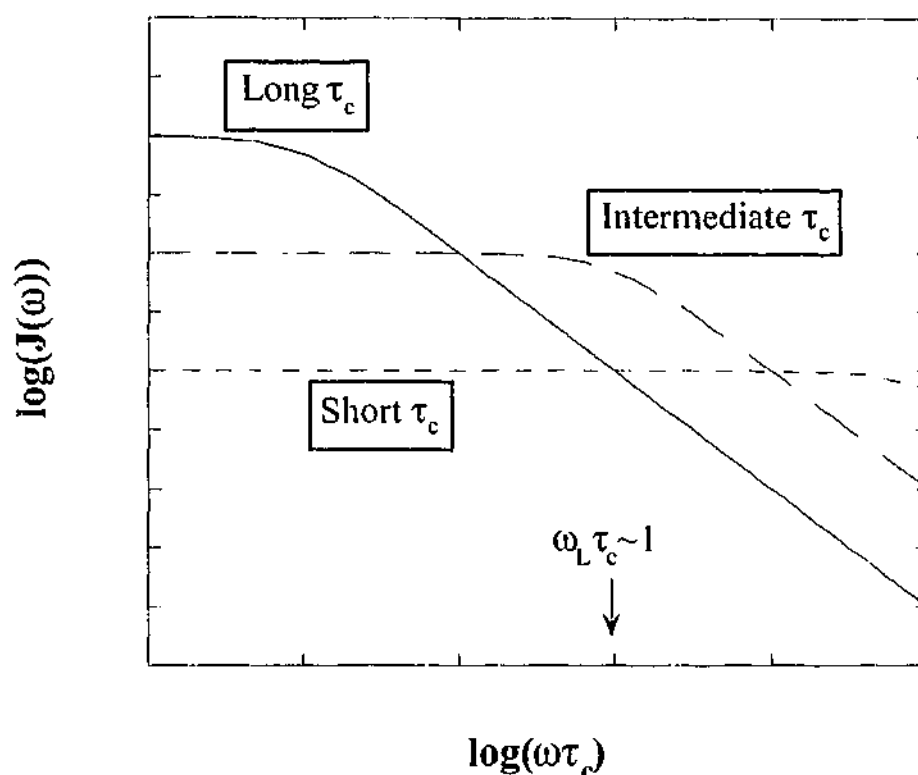


Figure 2-6 Spectral density as a function of frequency.

2.1.4.1 Relaxation Mechanisms

As mentioned above, the fluctuations in local magnetic field that facilitate relaxation are generated by dipolar and quadrupolar interactions, chemical shift anisotropy, spin rotation and scalar coupling. Relaxation in most materials is caused predominantly by the dipolar and/or quadrupolar mechanisms. The following is a discussion of these relaxation mechanisms.

Dipolar Relaxation

Dipolar interactions are the result of a nucleus experiencing the local magnetic fields of neighbouring nuclei. The strength of the interaction is dependent upon the nature

of the interacting nuclei (as given by the gyromagnetic ratios, γ), the distance separating them, r , and the relative orientation. Any motion within the system will alter these factors and consequently the strength of the dipolar interaction, thereby causing relaxation. The manner and rate of the fluctuations in the dipolar interaction are given by the spectral density equation (Equation 2-19). Assuming the theory of Bloembergen, Purcell and Pound (BPP theory),^{4,9} the T_1 , T_2 and $T_{1\rho}$ relaxation times for nuclei experiencing homonuclear dipolar interactions are given by Equation 2-20, Equation 2-21 and Equation 2-22 respectively:

$$\left(\frac{1}{T_1}\right)_{\text{hom}} = \left(\frac{\mu_0}{4\pi}\right)^2 \frac{2\gamma^4 \hbar^2 I(I+1)}{5r^6} \{J(\omega_L) + 4J(2\omega_L)\}$$

Equation 2-20

$$\left(\frac{1}{T_2}\right)_{\text{hom}} = \left(\frac{\mu_0}{4\pi}\right)^2 \frac{\gamma^4 \hbar^2 I(I+1)}{5r^6} \{3J(0) + 5J(\omega_L) + 2J(2\omega_L)\}$$

Equation 2-21

$$\left(\frac{1}{T_{1\rho}}\right)_{\text{hom}} = \left(\frac{\mu_0}{4\pi}\right)^2 \frac{\gamma^4 \hbar^2 I(I+1)}{5r^6} \{3J(\omega_1) + 5J(\omega_L) + 2J(2\omega_L)\}$$

Equation 2-22

where μ_0 is the permeability of a vacuum, \hbar is the reduced Planck's constant and I is the spin number of the nuclei of interest. While all three relaxation processes are dependent on local magnetic field fluctuations (as given by the spectral densities, $J(\omega_L)$), T_2 is also sensitive to static fields. $T_{1\rho}$ is also dependent on motions occurring

at the rotational frequency, ω_I , in the B_I field. However, as ω_I tends to zero, then $T_{I\rho}$ will approach T_2 .

A plot of these relaxation times as a function of correlation time is shown in Figure 2-7. A similar plot is expected if the relaxation times are plotted as a function of temperature. At short correlation times, when the material is extremely mobile, all three relaxation times are the same. As the correlation time increases, T_I and $T_{I\rho}$ both go through a minimum while T_2 steadily decreases. At the T_I and $T_{I\rho}$ minima, $\omega\tau_c$ is approximately equal to one and relaxation is most efficient. The position of the minima are different as T_I is dependent on fluctuations at the Larmor frequency, ω_L , whereas $T_{I\rho}$ is sensitive to fluctuations at the precession frequency in the B_I field, ω_I . From this plot, it can be seen that T_I relaxation probes fast motions, as expected from molecular rotations, while T_2 relaxation detects slower motions, which are often associated with translational motions such as diffusion. The behaviour of $T_{I\rho}$ is somewhere in between T_I and T_2 . The mobility of a material can be fully characterised through the measurement of these relaxation processes.

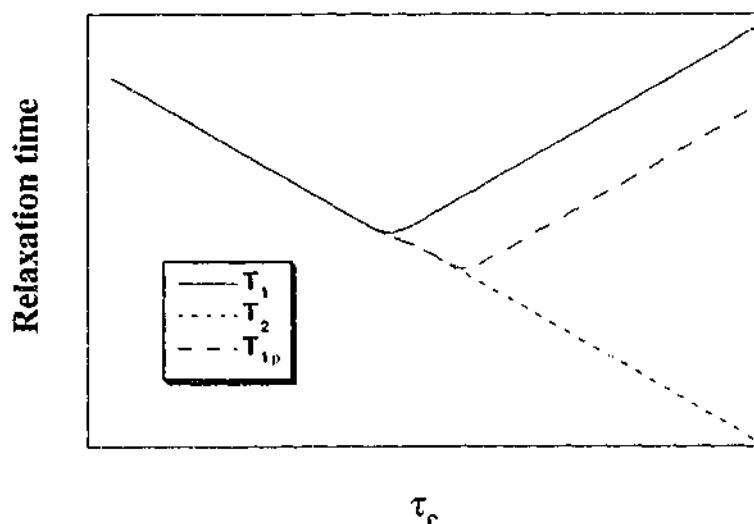


Figure 2-7 T_I , T_2 and $T_{I\rho}$ homonuclear dipolar relaxation as a function of correlation time.

Equation 2-20, Equation 2-21 and Equation 2-22 are applicable for modelling relaxation via homonuclear interactions. However, relaxation may also involve heteronuclear interactions, for which another set of equations exist. Equation 2-23 and Equation 2-24 show the T_1 and T_2 relaxation times for nuclei experiencing heteronuclear dipolar interactions.

$$\left(\frac{1}{T_1}\right)_{\text{het}} = 2C\{J(\omega_I - \omega_S) + 3J(\omega_I) + 6J(\omega_I + \omega_S)\}$$

Equation 2-23

$$\left(\frac{1}{T_2}\right)_{\text{het}} = C\{4J(0) + J(\omega_I - \omega_S) + 3J(\omega_I) + 6J(\omega_S) + 6J(\omega_I + \omega_S)\}$$

Equation 2-24

The notation I and S refer to the observed nuclei and the relaxing nuclei respectively. The constant C is the same in each case and consists of the gyromagnetic ratios, γ_I and γ_S , the separation distance, r , for the interacting nuclei and the spin number of the relaxing nucleus, S , as shown in Equation 2-25.

$$C = \left(\frac{\mu_0}{4\pi}\right)^2 \frac{\gamma_I^2 \gamma_S^2 \hbar S(S+1)}{15r^6}$$

Equation 2-25

Figure 2-8 shows the T_1 and T_2 heteronuclear dipolar relaxation times as a function of correlation time. The relaxation behaviour calculated from the heteronuclear equations is similar to what was observed in the homonuclear case (Figure 2-7). In a material, a nucleus can experience both homo- and heteronuclear interactions. The more effective relaxation mechanism will depend somewhat on the nature of the

interacting nuclei and the distance between them. Figure 2-9 compares the T_1 relaxation mechanisms for carbon equidistant from three nuclei: another carbon atom, a hydrogen atom and a silicon atom. In this case, the heteronuclear interactions dominate the relaxation mechanism. However, the nature of the relaxation mechanisms will vary for different materials.

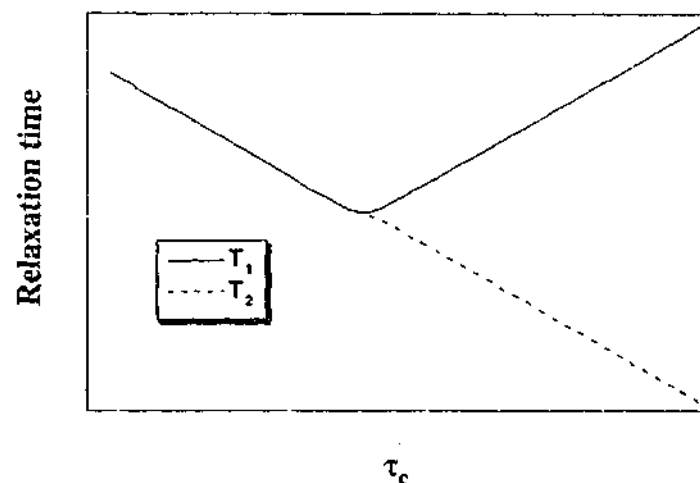


Figure 2-8 T_1 and T_2 heteronuclear dipolar relaxation as a function of correlation time.

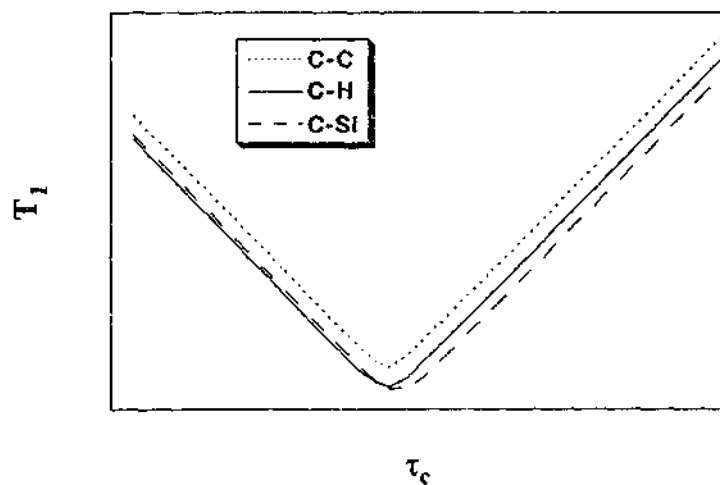


Figure 2-9 T_1 relaxation behaviour for homonuclear C-C interactions and heteronuclear C-H and C-Si interactions.

In using the BPP theory, a number of limitations need to be considered.¹¹ For T_1 relaxation, the theory predicts a symmetric curve with a single correlation time over the entire temperature range and the same activation energy on either side of the minimum. For a number of materials, in particular electrolytes, asymmetry has been observed and has been attributed to a distribution of correlation times.¹¹ Furthermore, the values obtained for the inverse of the limiting correlation time, $1/\tau_\infty$, may be invalid.¹¹ Activation energies obtained from relaxation measurements also tend to disagree with other mobility measurements, such as conductivity.¹¹ This discrepancy has been attributed to a difference in the motion being detected, with relaxation measuring more localised motions.¹¹ Such anomalies may lead to ambiguous interpretation of the data.

Quadrupolar Relaxation

Non-spherical nuclei ($I > 1/2$) possess a quadrupolar moment that can interact with electric field gradients, thereby undergoing relaxation. Relaxation dominated by quadrupolar interactions can be modelled by equations similar to those shown above (but with the addition of a quadrupolar coupling constant). For example, Equation 2-26 shows the T_1 behaviour for quadrupolar relaxation.¹

$$\left(\frac{1}{T_1} \right)_{\text{quad}} = \frac{3}{40} \frac{2I+3}{I^2(2I-1)} \left(1 + \frac{\eta^2}{3} \right) \left(\frac{eQ}{\hbar} \frac{\partial^2 V}{\partial z'^2} \right)^2 \{ J(\omega_L) + 4J(2\omega_L) \}$$

Equation 2-26

In this equation, η is an asymmetry factor, Q is the quadrupole moment and $\partial^2 V / \partial z'^2$ is a component of the electric field gradient tensor.² A similar equation also exists for T_2 quadrupolar relaxation. The quadrupolar relaxation mechanism is more effective when the electric field gradient is large or as the quadrupolar moment increases. As many energy levels exist for quadrupolar nuclei (as given by $2I+1$), a number of

relaxation processes can occur between the different levels for the same nucleus.⁵ Consequently, relaxation via a quadrupolar mechanism may yield multiple T_1 and T_2 relaxation times, depending upon the nature of the system.

2.1.4.2 The Linewidth-Transverse Relaxation Relationship

There is some correlation between the T_2 relaxation time and the NMR linewidth, $\delta\omega$ (angular frequency). The same nuclear interactions are responsible for both and a reciprocal relationship exists between them, as shown in Equation 2-27.⁵

$$\delta\omega = \frac{1}{T_2^*} = \frac{1}{T_2} + \frac{\gamma\Delta B_0}{2}$$

Equation 2-27

A broad NMR line that results from strong nuclear interactions corresponds to a short T_2 relaxation time. Since the linewidth measurement is also sensitive to magnetic field inhomogeneities, inverting the measured linewidth will actually underestimate the value of T_2 , referred to as T_2^* . A linewidth measurement, however, can still be used to approximate T_2 .

2.1.5 Diffusion Measurements

Diffusion coefficients, D , can be indirectly obtained from the correlation time, τ_c , determined from relaxation experiments such that:¹

$$D = \frac{r^2}{2\tau_c}$$

Equation 2-28

where r is the jump distance of the diffusing nuclei. However, this method assumes that the relaxation process is related to translational motion, which may not be the case.¹² More direct methods for measuring diffusion involve monitoring the dephasing of nuclear spins as the nuclei undergo translational motion in the presence of a magnetic field gradient. Such behaviour forms the basis of the Fringe Field Gradient (FFG) and Pulsed Field Gradient (PFG) methods employed in this study. The following is a brief account of the development of these diffusion techniques.

2.1.5.1 The Development of Diffusion Techniques

In a study of spin-echo formation, E. L. Hahn¹³ concluded that the signal was not only dependent on T_1 and T_2 but also affected by the self-diffusion of molecules experiencing magnetic field inhomogeneities. This theory was further developed by Carr and Purcell,¹⁴ who also provided appropriate pulse sequences in order to measure diffusion coefficients. Based on these seminal papers, McCall, Douglass and Anderson¹⁵ studied self-diffusion with a steady-gradient method in a number of organic materials. In a concluding statement, they commented that the decay time in the presence of the steady field gradient must be shorter than the decay time in a uniform field, $2\gamma^2 G^2 D t^3 \geq t/T_2$, in order to study diffusion by this method. Therefore, in the presence of a short T_2 and small D , the field gradient, G , must be increased, necessitating larger rf pulses. They proposed, however, that this limitation could be overcome through the use of alternating field gradients where the gradient is small during the rf pulse. The mathematical analysis of such pulsed gradient experiments was provided by Stejskal and Tanner,¹⁶ and subsequently formed the basis of the

pulsed field gradient technique. The theory behind NMR diffusion experiments is discussed below.

In an homogenous field, B_0 , nuclei with a given gyromagnetic ratio, γ , will precess at the Larmor frequency, ω_L (as given by Equation 2-2). The application of a magnetic field gradient, g , however, results in a spatial dependence of ω as shown below:¹²

$$\omega_{\text{eff}}(n, r) = n(\omega_0 + \gamma(g \cdot r))$$

Equation 2-29

where g is given by:

$$g = \nabla B_0 = \frac{\partial B_z}{\partial x} i + \frac{\partial B_z}{\partial y} j + \frac{\partial B_z}{\partial z} k$$

Equation 2-30

with i, j and k the unit vectors of the laboratory frame of reference. In the case of imaging experiments, the gradient is applied along the x, y and z directions.¹² For diffusion measurements, however, the gradient is generally oriented along the z -axis, parallel to B_0 . Thus the magnitude of the gradient in the z -direction, G , is a function of the position, k , such that $G = g \cdot k$. The position of a spin within a sample is therefore labelled by the magnetic field gradient.

The diffusion experiment monitors the change in precession frequency, and the resulting phase shift, of a nucleus as it moves from an original position to one where the field is slightly different.¹⁴ In a steady gradient experiment, the magnetic field gradient is "on" throughout the entire measurement and a spin-echo sequence is commonly employed (Figure 2-10). A 90° pulse tips the magnetisation onto the x - y

plane. A waiting period, referred to as a variable delay time, τ , follows. If diffusion occurs during this time, the nuclei will experience a phase shift that is given by the following equation:

$$\phi(t) = \gamma B_0 t + \gamma \int_0^t G(t') z(t') dt'$$

Equation 2-31

where t is the duration of the gradient (which in this case is the same as τ). The first term corresponds to the phase shift due to the static field while the second term relates to the applied gradient. The phase shift is seen as a spreading of the signal (defocussing), the extent of which is dependent upon the nature of the nucleus, γ , the strength of the gradient, G , the duration of the gradient, t , and the displacement of the spin along the direction of the gradient.¹² A 180° pulse is then applied, keeping the magnetisation in the x-y plane but reversing the precession frequency. After a second equivalent variable delay time period, nuclei that have not experienced any diffusion will refocus and the resultant signal may be detected. The signal intensity is therefore the average of the phase shifts resulting from diffusion for all the nuclei. The result is an attenuated signal compared to that which would be obtained in the absence of diffusion. For small magnetic field gradients, the change in magnetic environment experienced by a diffusing nucleus is relatively small, thereby causing only limited signal attenuation. For larger gradients, the change will be significantly greater, resulting in a greater phase shift and reduced signal intensity. The same effect will also result if diffusion is faster.¹²

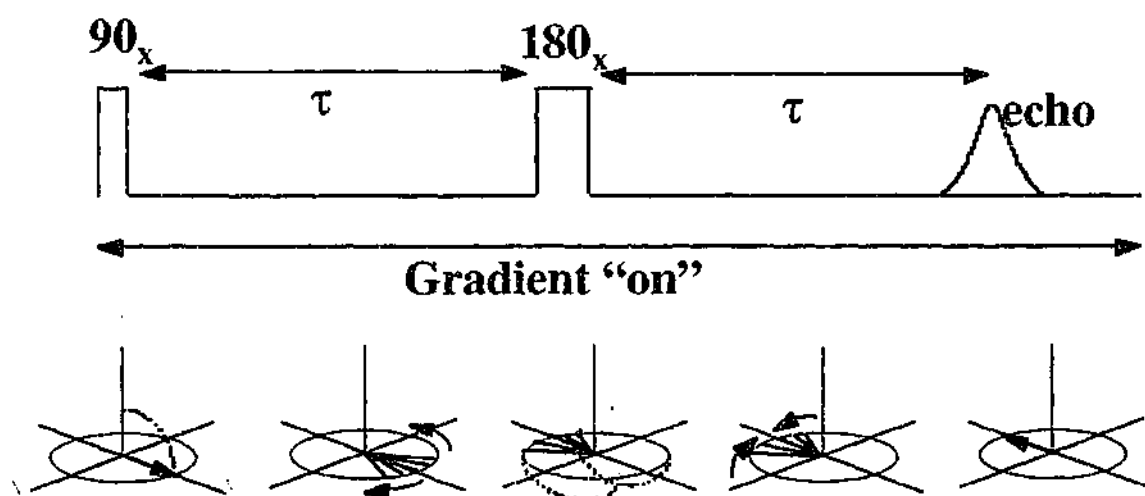


Figure 2-10 The steady-gradient spin-echo diffusion experiment.

For a steady-gradient experiment, the echo attenuation as a function of τ is modelled with the following equation:¹⁵

$$A(2\tau) = A(0) \exp\left(\frac{-2\tau}{T_2}\right) \exp\left(-\frac{2}{3} \gamma^2 G^2 D \tau^3\right)$$

Equation 2-32

where $A(0)$ and $A(2\tau)$ are the echo amplitudes initially and after 2τ respectively, T_2 is the spin-spin relaxation time, γ is the gyromagnetic ratio, G is the field gradient strength and D is the diffusion coefficient. This equation indicates that the echo amplitude attenuation is dependent on both the diffusion process and T_2 relaxation. In order to keep the T_2 contribution constant, the pulsed field gradient method can be employed. As the name suggests, the field gradients are applied as pulses after the 90° and 180° rf pulses (Figure 2-11). There are three possible variables with this experiment: the time between the gradient pulses, Δ , the gradient strength, G , and the gradient pulse length, δ . By varying either the strength or duration of the gradient pulse, the effect of T_2 relaxation is kept constant throughout the entire experiment

and the observed echo attenuation is solely due to diffusion. In this case, the signal intensity can be modelled with the following equation:¹⁶

$$A(G) = A(0) \exp \left[-\gamma^2 G^2 D \delta^2 \left(\Delta - \frac{\delta}{3} \right) \right]$$

Equation 2-33

where $A(0)$ and $A(G)$ are the initial and attenuated echo amplitudes respectively, γ is the gyromagnetic ratio, G is the maximum gradient strength, D is the diffusion coefficient, δ is the gradient pulse length and Δ is the time between the gradient pulses. Both steady gradient (fringe field gradient) and pulsed field gradient methods have been employed in this work as each has advantages, as outlined below.

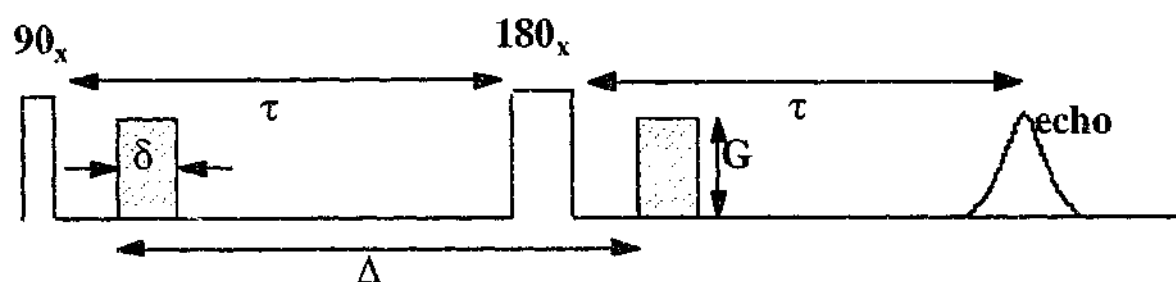


Figure 2-11 The pulsed field gradient spin-echo diffusion experiment.

2.1.5.2 Fringe Field Gradient Diffusion

The fringe field gradient (FFG) diffusion technique takes advantage of the large static gradient associated with an NMR superconducting magnet. The NMR probe is positioned a certain distance from the centre of the magnet where the field strength is no longer constant, but the change in the field, ie. the gradient, is constant. The fringe field technique has several advantages over other NMR diffusion methods.¹⁷⁻¹⁹ The gradient is very stable, avoiding the problems associated with imbalanced gradient pulses, eddy currents and mechanical shocks. The gradient strength is extremely large

and greater than any of the other techniques, allowing diffusion coefficients as low as $10^{-16} \text{m}^2 \cdot \text{s}^{-1}$ to be observed. The purchase of other accessories is not necessary and only minor modification of the existing equipment is required in order to fix the probe in the field gradient. Calibration of the gradient is simply performed on a sample of known diffusion coefficient.

The disadvantages of this technique are as follows. The poor sensitivity associated with the lower magnetic field strength results in a reduced signal intensity. This is of particular concern for nuclei with low gyromagnetic ratios and/or low abundance. Since only a thin section of the sample will be excited by the *rf* pulse, there will be a further reduction in sensitivity. The inhomogeneity of the field results in an extremely broad signal, requiring a spectrometer with a suitably large sweepwidth for signal observation. The broad peak also eliminates the possibility of any chemical shift analysis, making it impossible to observe different diffusion processes for individual species. Consequently, the diffusion coefficients measured are an average of all possible moving nuclei of a particular isotope. Possibly the greatest limitation of the fringe field gradient technique is the inability to measure diffusion independent of the T_2 relaxation time. The effect of T_2 on the diffusion measurement is discussed below.

The Effect of T_2 on the Fringe Field Gradient Experiment

Equation 2-32 consists of a transverse relaxation (T_2) component and a diffusion component. The decay in signal intensity measured in a diffusion experiment may depend on one or both components. If T_2 is large with respect to the τ values used in the experiment, the T_2 component can be ignored and the signal will be solely representative of the diffusion behaviour. However, as T_2 relaxation decreases, it will begin to encroach on the signal intensity. To demonstrate this effect, some theoretical simulations have been performed using Equation 2-32.

For a typical proton diffusion measurement, τ ranges from 1×10^{-5} to 1×10^{-3} s, the gradient strength is 46.8 T.m^{-1} and the gyromagnetic ratio for protons is $26.752 \times 10^7 \text{ rad.T}^{-1}.\text{s}^{-1}$. Figure 2-12 shows the effect of five T_2 values (1×10^{-4} s, 1×10^{-3} s, 0.01 s, 0.1 s and 1 s) on the signal intensity for a constant proton diffusion coefficient of $1 \times 10^{-10} \text{ m}^2.\text{s}^{-1}$. This diffusion coefficient value was chosen as it is a typical room temperature value for the materials in this study. For comparison, the signal intensity for an infinitely large T_2 has also been calculated. The two largest T_2 values (0.1 s and 1 s) have almost identical behaviour to the infinite T_2 data and only a slight decrease in signal intensity is observed for a T_2 of 0.01 s. For the other two T_2 values, there is a significant decrease in signal intensity resulting from T_2 relaxation, and this could be misconstrued as a larger diffusion coefficient. Therefore, as long as T_2 exceeds the largest tau value by at least an order of magnitude, the signal observed will be characteristic of diffusion.

What is obvious from these simulations is that the data that is relatively unaffected by the T_2 relaxation time exhibits an "S" shaped curve when plotted as shown in Figure 2-12. Consequently, the T_2 affected data was identified by the absence of the "S" shaped curve. In this work, a number of diffusion measurements were affected by the T_2 relaxation time, particularly for some of the solid samples where diffusion was assumed to be limited. An example of a T_2 affected diffusion curve for a proton measurement is shown in Figure 2-13. For comparison, a diffusion measurement where T_2 had no influence is also shown. There is a very distinct difference between the two sets of data, thus enabling the T_2 affected data to be easily differentiated from the unaffected measurements.

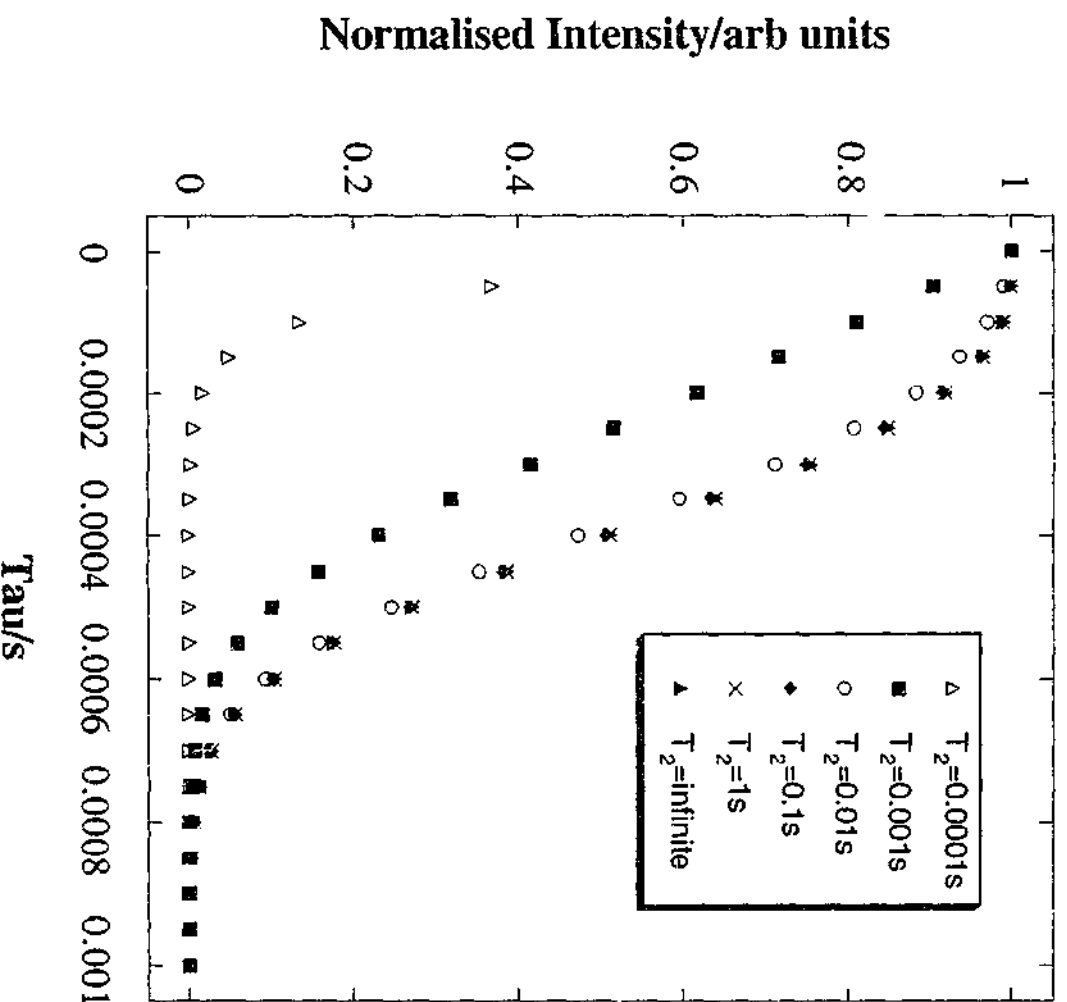


Figure 2-12 The effect of different T_2 values in the fringe field gradient equation.

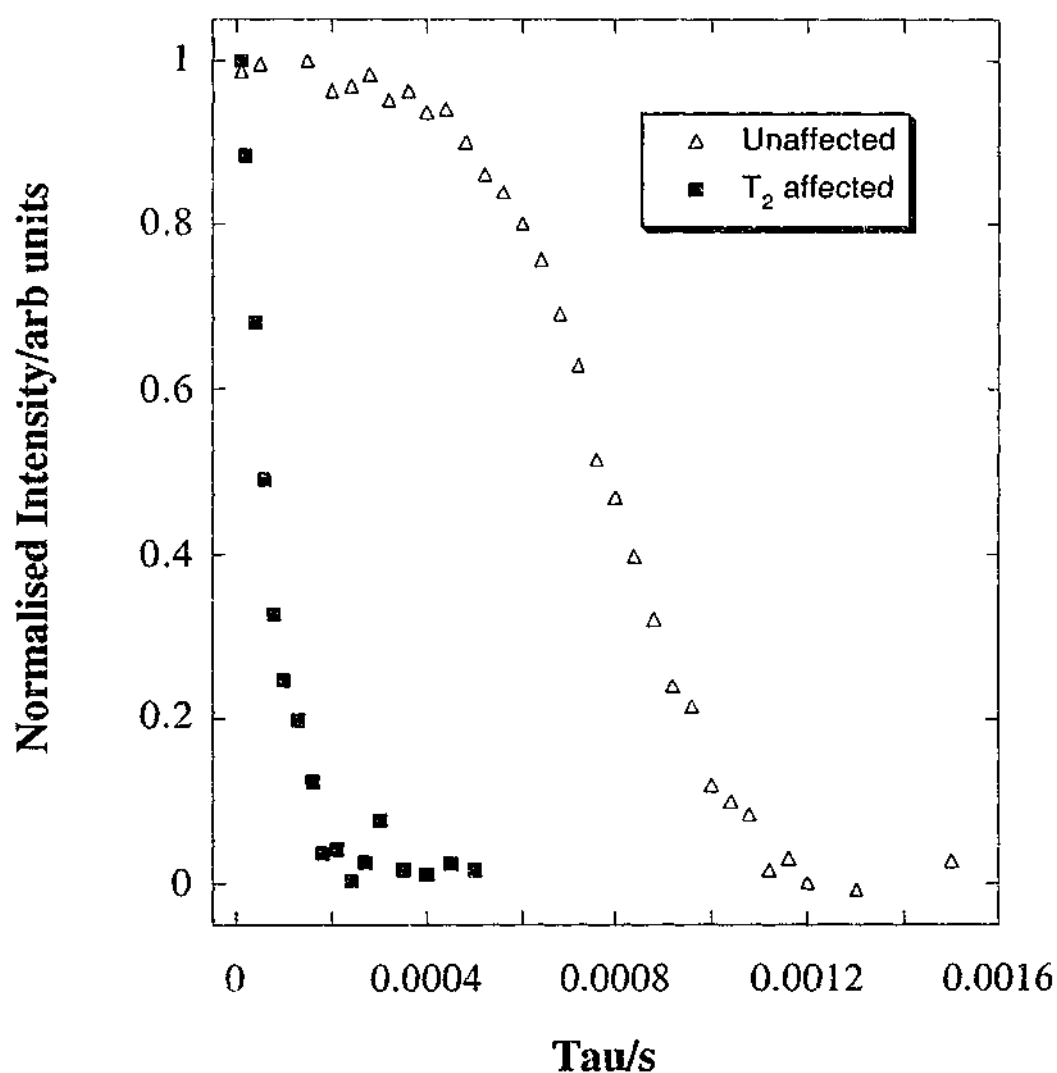


Figure 2-13 Actual proton diffusion measurements highlighting the effect of T_2 relaxation on the signal intensity versus tau.

Demco¹⁷ has recognised this problem and has developed a method for measuring diffusion where T_2 has no contribution to the signal attenuation. Two stimulated-echo experiments are conducted and the intensities are multiplied together. By doing this, the T_2 contribution is kept constant and the diffusion process is responsible for the echo attenuation. The specific details of the experimental procedure can be found

elsewhere.¹⁷ If the T_2 relaxation time is not an issue, the spin-echo method is preferred as it is less time consuming.

2.1.5.3 Pulsed Field Gradient Diffusion

The pulsed field gradient (PFG) method for measuring diffusion utilises a separate coil (positioned around the *rf* coil) in which the gradient pulses are generated by a power supply. As mentioned earlier, the gradients are pulsed with finite lengths and it is the ability to switch the pulses that gives this technique some advantages over the fringe field method.^{12,17-19} With three possible variables - the time between the gradient pulses, Δ , the gradient strength, G , and the gradient pulse length, δ - it is possible to conduct a measurement that keeps the effect of T_2 constant. The PFG experiment is also performed in the homogeneous field and therefore the problems with the fringe field experiment (poor sensitivity and broad signal) are also no longer an issue. Moreover, it is possible to observe chemical shift behaviour with the PFG technique and analyse the diffusion coefficients for nuclei in different environments (different species).

The PFG method does have its limitations.¹⁷⁻¹⁹ The technique requires a suitable probe and gradient power supply that must be purchased or constructed. The gradient strength is also lower than that of the fringe field gradient method (2 to 5 T.m⁻¹), although gradients as large as 20 T.m⁻¹ can be achieved.¹² Lower gradients mean that measurable diffusion coefficients are limited to values greater than 10⁻¹⁴ m².s⁻¹. Problems can also arise if the pulses are not perfectly square or are improperly balanced, with both conditions leading to faster echo attenuation. The switching of the gradients can also cause mechanical shocks that may result in movement of the sample. Eddy currents and localised heating will also have detrimental effects on the observed signal.

2.1.5.4 A Comment on Spin Diffusion

Through dipolar interactions, two like spins can undergo a "flip-flop" transition such that the direction of each spin is reversed simultaneously while the energy is conserved.⁷ In the case of a collection of dipolarly coupled spins, a succession of spin flips may occur which is referred to as spin diffusion.²⁰ The "flip-flop" process results in a loss of phase coherence, analogous to the phase shifts observed during the self-diffusion measurements mentioned above. Spin diffusion can therefore be detected by a similar measurement and for many systems,²⁰ the spin diffusion coefficients are of the order of 10^{-16} to $10^{-15} \text{ m}^2 \cdot \text{s}^{-1}$. As the diffusion coefficients reported in this thesis are considerably higher (the smallest being 10^{-13} to $10^{-12} \text{ m}^2 \cdot \text{s}^{-1}$), it would seem that these coefficients reflect a self-diffusion process and not spin diffusion.

2.2 Experimental Method

2.2.1 Fringe Field Gradient NMR Measurements

2.2.1.1 Fringe Field Gradient NMR Probe Holder

In order to conduct fringe field gradient NMR experiments, a suitable method is necessary for positioning the probe at the desired location in the magnet. The holder should accurately fix the probe in the same position for every experiment, but enable fine adjustments for the measurement of samples of different sizes or different observed nuclei. The probe should also be securely held in position so that it is not susceptible to vibrations or motion. A specific holder was designed so that all these criteria could be accommodated. A diagram of the device is shown in Figure 2-14. The holder is permanently attached to one leg of the magnet at approximately the right height, but has a winding mechanism that allows for fine adjustment of the probe position. The swinging arm allows for easy installation and removal of the

probe and two screws hold the probe securely in place. The coil within the probe is positioned in the field gradient at a distance of 24.5cm from the centre of the magnet.

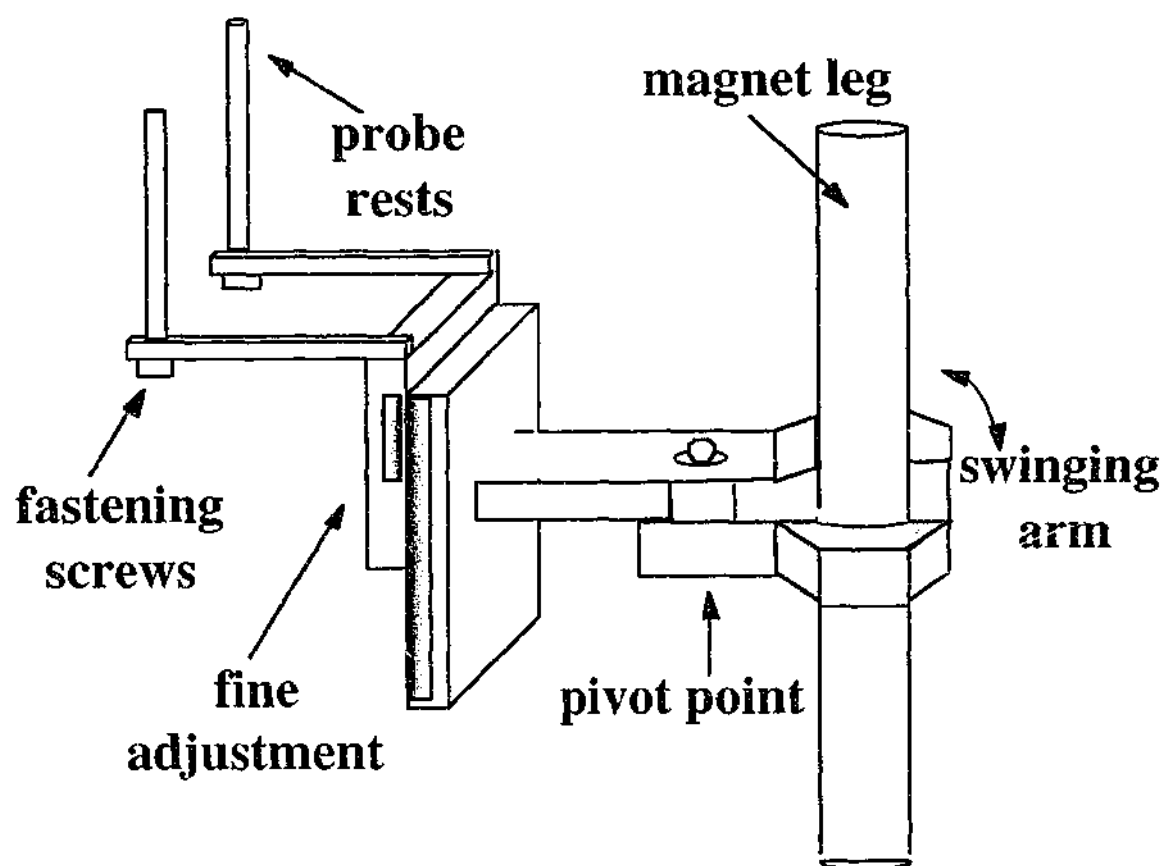


Figure 2-14 Fringe field gradient probe holder

2.2.1.2 Fringe Field Gradient NMR Methodology

Proton and fluorine fringe field diffusion experiments were performed on a modified Bruker CXP300 with a 7T Oxford superconducting magnet. The field gradient was mapped using a Bell 610 Gaussmeter with a 10T axial probe, with the results of shown in Figure 2-15. The probe was positioned in a region of constant field gradient (24.5cm from the centre of the magnet) at a field strength of 2.7T. The gradient was calibrated with water (diffusion coefficient of $2.299 \times 10^{-9} \text{m}^2 \cdot \text{s}^{-1}$ at 298K^{21}), and was found to be $46.8 \text{T} \cdot \text{m}^{-1}$. The ^1H resonance frequency at this field is 116MHz. Fluorine resonates at the same frequency when the sample is moved a further 4mm towards the centre of the magnet when compared with the positioning for the proton measurements.

Diffusion coefficients were measured using the spin-echo sequence (Figure 2-10) in a probe with a 5mm coil that had a 90° pulse length of $2.1 \mu\text{s}$. As the NMR line is broadened by the inhomogeneous field, these finite pulse lengths will only excite some fraction of the nuclei. To ensure that there is sufficient excitation, the pulse lengths were kept to a minimum and combined with a fast digitizer over a sweep width of $\pm 500,000 \text{Hz}$ and a filter width of $1,000,000 \text{Hz}$. The sample size was also kept small to minimise the resultant NMR linewidth. The echo attenuation as a function of τ was fitted with Equation 2-32. The samples were sealed in capillary tubes in order to prevent uptake of water. Measurements were made over the temperature range 273 to 403K. Subambient temperatures were achieved with liquid nitrogen, while heated dry air was used for measurements above room temperature. Samples were left to equilibrate at a given temperature for at least 30 minutes.

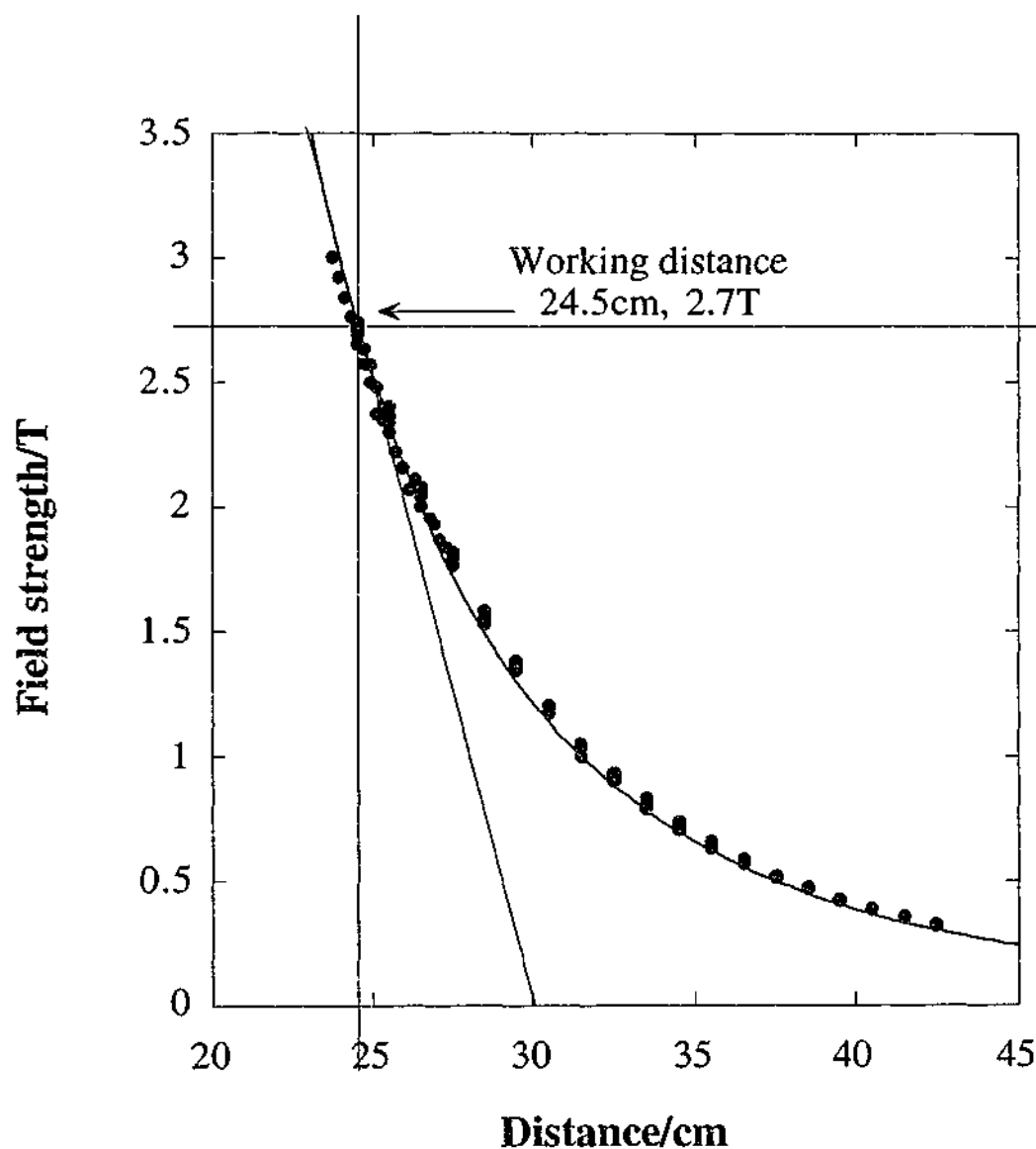


Figure 2-15 Mapping of the fringe field.

2.2.2 Pulsed Field Gradient NMR Measurements

2.2.2.1 Measurements at the University of Queensland

Proton diffusion coefficients were measured using the z-gradient of a microimaging set on a Bruker AMX300 spectrometer with a 7T magnet. The gradient was

calibrated with water and found to have a maximum strength of 1.66T.m^{-1} . Measurements were made using a stimulated-echo pulse sequence (Figure 2-16) with a 5mm probe that had a 90° pulse length of $7.5\mu\text{s}$. The first *rf* pulse tips the magnetisation through 90° , after which the first gradient pulse is applied. A second 90° *rf* pulse tips the magnetisation to the negative *z*-direction, where it is "stored" for a defined duration (τ_2). A third and final 90° pulse followed by the second gradient pulse refocusses the magnetisation and the resultant signal is detected. For materials in which T_2 is very short, the stimulated-echo experiment is particularly advantageous as it is limited by the length of T_1 instead of T_2 (contrary to the case in the spin-echo experiment).

In this experiment, a 2ms gradient pulse was applied after the first and third *rf* pulses and the echo attenuation was measured as a function of gradient strength, G . The time between the second and third *rf* pulses (storage time, τ_2) was adjusted for each temperature while all other delay times were kept constant. The signal intensity was modelled using Equation 2-33. To limit exposure of the sample to the atmosphere, the samples were sealed in 5mm tubes. Measurements were conducted as a function of temperature from 278 to 373K in a similar routine to the fringe field experiments.

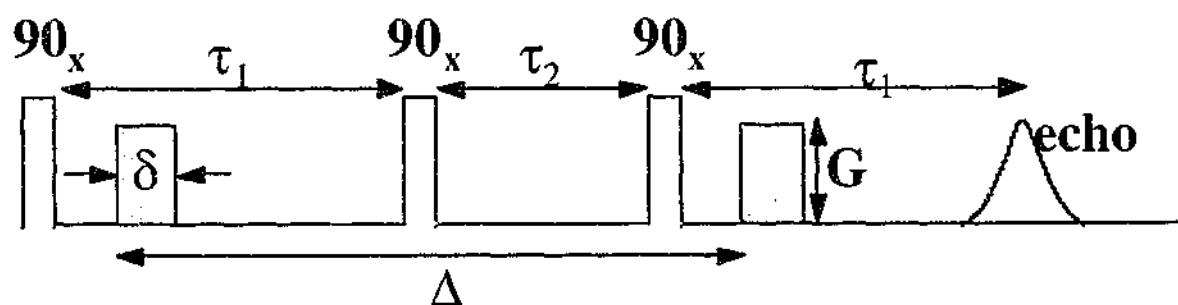


Figure 2-16 Stimulated-echo pulse sequence.

2.2.2.2 Measurements at Umeå University

Pulsed field gradient proton diffusion coefficients were also measured at Umeå University on two Varian CMX Infinity spectrometers (100 and 400MHz) equipped with a 2.3 and 9.4T magnet respectively. Measurements were again made using a stimulated-echo pulse sequence (Figure 2-16), the details of which are provided in Table 2.2-1. During each measurement, either the gradient strength or duration was varied while the other parameters were kept constant. The signal attenuation was once again modelled with Equation 2-33. Diffusion coefficients were studied for temperatures ranging from 293 to 353K. The temperature was controlled to within $\pm 0.5\text{K}$ by a heated airstream passing over the sample.

Table 2.2-1 Experimental parameters for the stimulated-echo diffusion experiments conducted at Umeå University.

Spectrometer	τ_1/ms	δ/ms	$G/\text{T.m}^{-1}$	τ_2/ms	Δ/ms	$90^\circ/\mu\text{s}$
CMX100	20	0.5-10 or	0.477 or	20	40	5
		0.5-15 or	0.954	50	70	
		0.3-9		100	120	
		(temperature dependent)		500	520	
CMX400	2.5	2	0.28-11.3	2.5	5	6.5
	2.5	2	0.113-3.39	47.5	50	
	10	2	0.113-3.39	40	50	
	10	2	0.028-1.13	490	500	

2.2.3 Error Analysis

In order to ensure reproducibility of the diffusion coefficients, at least two measurements were made at each temperature. Experiments were also conducted on multiple samples to limit any effect of material inhomogeneity. The errors quoted for the diffusion coefficients are taken from the least-squares fitting of appropriate equations (Equation 2-32 or Equation 2-33) for each measurement using the program KaleidaGraphTM. It is assumed that these errors provide a reasonable estimate of the uncertainties apparent in each experiment. Errors for other fitted parameters were obtained in a similar manner. The temperatures for each measurement are assumed accurate to within ± 1 K.

2.3 References

1. A. Abragam, *Principles of Nuclear Magnetism*, (Oxford University Press Inc., New York, 1961).
2. J. W. Akitt, *NMR and Chemistry: An Introduction to Modern NMR Spectroscopy*, 3rd ed. (Chapman & Hall, London, 1992).
3. P. T. Callaghan, *Principles of Nuclear Magnetic Resonance Microscopy*, (Oxford University Press, 1995).
4. T. C. Farrar and E. D. Becker, *Pulse and Fourier Transform NMR: Introduction to Theory and Methods*, (Academic Press, Inc., New York, 1971).
5. E. Fukushima and S. B. W. Roeder, *Experimental Pulse NMR: A Nuts and Bolts Approach* (Addison-Wesley Publishing Company, Inc., Reading, 1981).
6. D. Shaw, *Fourier Transform N.M.R. Spectroscopy*, 2nd ed. (Elsevier Science Publishers B.V., Amsterdam, 1984).
7. C. P. Slichter, *Principles of Magnetic Resonance*, 2nd ed. (Springer-Verlag, New York, 1978).

8. *Physical Principles and Instrumentation*, Vol. 2, edited by C. L. Partain, R. R. Price, J. A. Patton, M. V. Kulkarni and J. A. E. James (W. B. Saunders Company, Philadelphia, 1988).
9. N. Bloembergen, E. M. Purcell and R. V. Pound, *Phys. Rev.* **73**, 679-712 (1948).
10. J. H. van Vleck, *Phys. Rev.* **74**, 1168-1183 (1948).
11. D. Brinkmann, *Prog. NMR. Spect.* **24**, 527-552 (1992).
12. W. S. Price, *Concepts Magn. Reson.* **9**, 299-336 (1997).
13. E. L. Hahn, *Phys. Rev.* **80**, 580-594 (1950).
14. H. Y. Carr and E. M. Purcell, *Phys. Rev.* **94**, 630-638 (1954).
15. D. W. McCall, D. C. Douglass and E. W. Anderson, *Ber. Bunsenges. Phys. Chem.* **67**, 336-341 (1963).
16. E. O. Stejskal and J. E. Tanner, *J. Chem. Phys.* **42**, 288-292 (1965).
17. D. E. Demco, A. Johansson and J. Tegenfeldt, *J. Mag. Res.* **110**, 183-193 (1994).
18. E. D. von Meerwall, *Rubber Chem. Technol.* **58**, 527-560 (1985).
19. P. Stilbs, *Prog. NMR Spec.* **19**, 1-45 (1987).
20. W. S. Veeman and W. E. J. R. Maas, in *Solid-state NMR III: Organic Matter*, Vol. 32, edited by B. Blümich (Springer-Verlag, Berlin, 1994), pp. 127-162.
21. R. Mills, *J. Phys. Chem.* **77**, 685-688 (1973).

Chapter Three

Imidazolium Salts

3.1 Introduction

Ionic liquids, or molten salts, are extremely versatile solvents for clean synthesis and catalytic processes.¹ Being the most concentrated of all electrolytes, they also have potential in many electrolytic applications, particularly solar cells.² The dialkylimidazolium series of salts have generated much interest due to their impressive electrochemical and physical properties.²⁻²⁸ All of these materials have a common structure based on the imidazolium ring, shown in Figure 3-1, with different alkyl substituents and anions used to alter the material properties. The names of these imidazolium salts are often long and complex, hence, for simplicity, the salts will be abbreviated according to the main components of the salt, eg. 1-methyl-3-butylimidazolium iodide is referred to as MeBuImI. The following is an historical account of the research into dialkylimidazolium salts as novel ionic liquids.

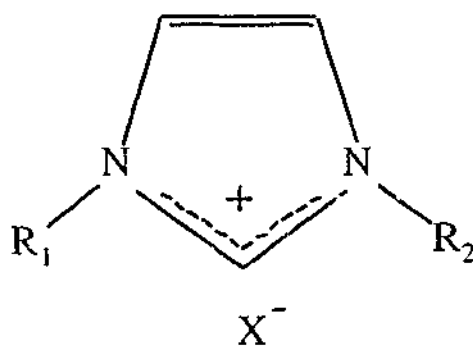


Figure 3-1 The structure of 1,3-dialkylimidazolium salts.

3.1.1 The Dialkylimidazolium/Aluminium Halide Systems

In 1982, the synthesis route and properties of a new family of ionic liquids were published by John S. Wilkes *et al.*⁷ When dialkylimidazolium chlorides were mixed with aluminium chloride, the compound was found to be liquid at room temperature and to have improved electrochemical and physical properties over other salts. This revelation prompted exhaustive investigations of such systems by Wilkes and coworkers³⁻⁷ and Hussey⁸⁻¹⁶ among others.¹⁷⁻²²

Of the 1-methyl-3-ethylimidazolium halide/aluminium halide systems (MeEtImX/AlX₃), the chloride and bromide are the most commonly studied.^{5,7,13,14} The pure imidazolium salts melt around 353K, although the chloride salt has a higher melting point than the bromide salt as the result of stronger ionic interactions.^{5,13} Addition of the corresponding aluminium halide (AlX₃) to form a binary system lowers the melting point and at certain compositions suppresses it completely.^{5,13,14} The binary is neutral at an aluminium halide mole fraction of 0.5, while lower AlX₃ mole fractions are basic and higher AlX₃ mole fractions are acidic.⁶ The nature of the anions in the melt depends on the binary composition. The addition of the aluminium halide results in a decrease in free halide ion concentration and an accompanying formation of AlX₄⁻. Upon exceeding an aluminium halide mole fraction of 0.5, there are no free halide ions and Al₂X₇⁻ forms at the expense of AlX₄⁻. The ionic complexes as a function of AlX₃ concentration are shown in Figure 3-2.⁶ Structural analysis from x-ray²⁰ and NMR^{6,29} measurements reveals extensive hydrogen bonding in the basic binary systems, which is reduced as the amount of the aluminium halide increases. In the basic melts, modelling of the proton chemical shifts as a function of AlCl₃ mole fraction suggests that the cation interacts with two or more anions to form oligomeric chains.⁶ ¹H NMR relaxation in the ternary 0.35AlCl₃/0.4MeEtImCl/0.25EtAlCl₂ melt also supports the notion of ionic interaction between the imidazolium cation and AlCl₄⁻.²¹

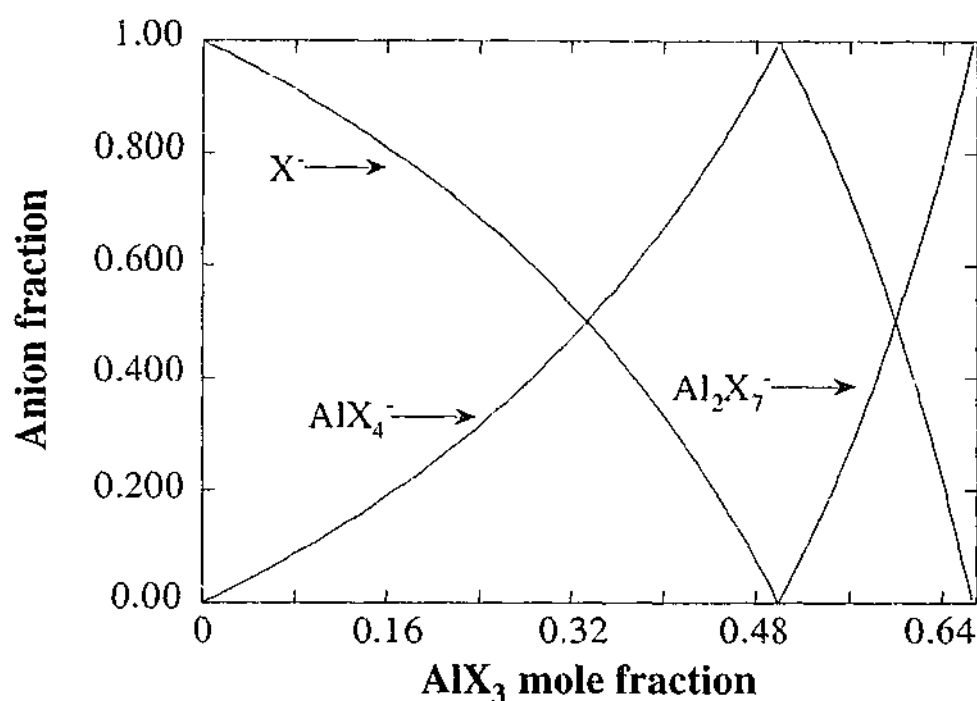


Figure 3-2 Anion mole fraction as a function of AlX₃ mole fraction (from Fannin⁶).

Despite a local maximum in melting point, the neutral melt exhibits the highest conductivity.^{5,13} The temperature dependence for conductivity and viscosity does not show Arrhenius behaviour, but is adequately modelled by the VTF equation. To understand the conduction mechanism, external and internal transport numbers were calculated for these binary melts.^{4,9-11} The difference between these two transport numbers is the frame of reference used for the calculation. External transport numbers are a measure of ion transport with respect to a fixed component (for example, the porous membrane used in the cell), whereas internal transport numbers indicate ion transport relative to another component of the electrolyte (typically the bromide or chloride ions). The experimental method, similar to the Hittorf process,⁹ involves passing a known charge through a cell divided by a porous membrane, and measuring the change in concentration and weight in each compartment. The results suggest that the transport number for the cation is largely independent of the binary

composition over the range of aluminium halide mole fractions from 0.33 to 0.67. The external transport numbers for the cation were 0.71 and 0.76 for the chloride and bromide systems respectively. The slightly higher value for the bromide system may be the result of weaker ionic interactions. The average internal cationic transport numbers were 1 for both salts, which suggests that the cation is the dominant charge carrier. However, some small deviations from a transport number of 1 were observed for the bromide salt, which may indicate an association between the cation and the bromide ions. The internal transport number of 0 for the aluminium ions confirms that they are coordinated to the halide ions and move as complex anions.

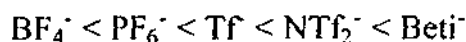
An NMR relaxation and diffusion study of acidic chloroaluminate melts by Carper and co-workers¹⁹ compared the cation diffusion coefficients and correlation times with the viscosities and conductivities. At 303K, cation diffusion in the neutral melt was found to be $1.27 \times 10^{-10} \text{ m}^2 \cdot \text{s}^{-1}$, whereas the acidic melt (2:1 AlCl_3 - MeEtImCl) had a slightly higher diffusion coefficient of $1.44 \times 10^{-10} \text{ m}^2 \cdot \text{s}^{-1}$. In accordance with this behaviour, the viscosity and the correlation time for the neutral melt were both higher than the acidic melt. It was stated earlier, however, that the neutral melt exhibited the highest conductivity of all the binary compositions.⁵ This disparity between the transport properties suggests that the mechanism governing diffusion and viscosity may not be that governing the conductivity. Carper¹⁹ concluded that either the molar mass or molar volume of the salt - not the structure of the ions - influences the transport mechanisms in these materials. Similar behaviour has been observed in an analogous system where the AlCl_3 is replaced by ethylaluminium dichloride (EtAlCl_2)²² and also in binary tetraalkylammonium-tetraalkylboride salts.³⁰

3.1.2 Hydrophobic Imidazolium Salts

3.1.2.1 Altering the Anion

The 1-methyl-3-ethylimidazolium/aluminium halide binary systems consist of extremely basic anions with a strong affinity to water. In an attempt to resolve this problem, considerable research has been focussed into finding alternative hydrophobic forms of the imidazolium salts. Larger ions, where the charge is delocalised, are weak bases or neutral and are less likely to undergo hydrogen bonding. Substituting the halide ions for tetrafluoroborate (BF_4^-),^{24,26} hexafluorophosphate (PF_6^-),^{23,26} trifluoromethanesulfonate (also referred to as triflate, CF_3SO_3^- , Tf),^{2,25} bis(trifluoromethanesulfonyl)amide (also referred to as amide, $(\text{CF}_3\text{SO}_2)_2\text{N}^-$, NTf_2^-)²⁵⁻²⁷ or bis(perfluoroethylsulfonyl)amide ($(\text{C}_2\text{F}_5\text{SO}_2)_2\text{N}^-$, Beti)²⁶ anions results in relatively hydrophobic salts. Crystal structure analysis of 1-methyl-3-ethylimidazolium hexafluorophosphate²³ and 1-ethyl-2-methyl-3-benzylimidazolium amide²⁷ confirmed that only weak interactions exist in these materials. The anion-cation attraction is responsible for maintaining the crystal structures with hydrogen bonding absent in both cases. The extent of hydrogen bonding has also been examined through ^1H NMR chemical shift analysis.²⁵ The chemical shift is anion dependent and an increase in anion basicity results in a greater shift in the signal for the protons on the imidazolium ring. In other words, the NTf_2^- salt effectively produces no change to the proton chemical shift in contrast to the effect of a water soluble acetate anion.

The ionic volume for these anions increases according to:²⁶



and it is expected that the decrease in the ionic strength follows the same order. Not all the properties of these salts, however, appear to correlate with this series,^{25,26} as shown in Table 3-1. MeEtIm PF_6 salt has the highest melting point at 335K, whereas the MeEtIm NTf_2 salt has the lowest melting point at 258K. MeEtIm BF_4 and

MeEtImBetl exhibit the highest and lowest conductivities respectively. MeEtImPF₆, however, has a very low conductivity, which is probably due, in part, to the higher melting point of the material. A slight curvature was observed in the conductivity and viscosity data when plotted as a function of temperature, indicative of VTF behaviour. Ignoring MeEtImPF₆, the conductivity decreases with increasing ionic size, while the viscosity reflects the behaviour observed for the melting points. In the case of the aluminium halide binary salts, the conductivity and viscosity behaviours reported are thought to be dependent on the molar mass or molar volume and not due to the nature of the ions. Perhaps the same applies for the hydrophobic systems.

Table 3-1 Properties of imidazolium salts.^{25,26}

MeEtImX	BF ₄	PF ₆	Tf	NTf ₂	Betl
MW/g.mol ⁻¹	198	256	260	391	491
Anion volume/Å ³	48	68	80	143	189
Concentration/M	6.5	5.7	5.3	3.9	3.2
T _m /K	284	335	264	258	272
σ/mS.cm ⁻¹ at 299K	13	5.2	9.2	8.4	3.4
η/cP at 299K	43	15†	38	28	61

†This value at 353K.

3.1.2.2 Altering the Cation

Both McEwen²⁶ and Bonhôte²⁵ have examined the effect of ion size on the viscosity of these salts. In keeping the anion the same, but increasing the size of the cation (from 1-methyl-3-ethylimidazolium amide, MeEtImNTf₂ to 1,2-dimethyl-3-n-propylimidazolium amide, MeMePrImNTf₂) the viscosity doubles.²⁶ Bonhôte²⁵ has observed a similar effect upon increasing the length of the alkyl substituents, and also

when changing the conformation of the chain from linear to branched (butyl to isobutyl). Increased Van der Waals interactions as well as decreased rotational freedom are thought to be responsible for such behaviour. While these effects are observed upon altering the cation, the same behaviour was also seen when the anion is changed from NTf_2^- to Bet^- .²⁶ Although there is a strong correlation between viscosity and conductivity, the viscosity alone does not always account for the conductivity behaviour. For example, MeEtImTf and BuEtImNTf_2 have similar viscosities and densities, but the former salt is twice as conductive.²⁵ To quote P. Bonhôte:²⁵ "In the search for highly conducting ionic liquids, one must not focus on viscosity only, but keep in mind the importance of ionic size."

3.1.2.3 Binary Systems

Mixing the salts to form binary systems has a pronounced effect on the resultant material properties. MeHxImI has a reasonably high viscosity and a correspondingly low conductivity.² However, adding MeHxImI to MeBuImTf to form a binary results in an increase in conductivity relative to the pure MeHxImI . Diffusion measurements as a function of MeHxImI show an initial sudden decrease upon adding 25wt% MeHxImI , after which adding more MeHxImI only results in a small change in the diffusion coefficients. The viscosity measurements tend to reflect the diffusion data, although there is a steady increase in viscosity upon further addition of MeHxImI (>25wt%). The reason for the increase in conductivity in the binary system is unclear, although it is thought to be the result of either changing the ion solvation or changing the transport mechanism.

3.1.3 The Research of A. G. Bishop

A comprehensive study of the dialkylimidazolium salt family was also conducted by a colleague, Dr. Andrea Bishop, in the Department of Chemistry at Monash University as a part of her doctoral thesis.²⁸ The emphasis of Bishop's work was

the characterisation of the pure dialkylimidazolium salts. A series of iodide salts was synthesised with different alkyl chains increasing in length from methyl through to a linear heptyl chain. Anion exchange was also possible, allowing bromide, trifluoromethanesulfonate (referred to as triflate) and bis(trifluoromethanesulfonyl) amide (referred to as amide) salts to be studied. The effect of combining these pure salts to form binary systems was also analysed. The research for this thesis was conducted in conjunction with Dr. Bishop and, in many cases, her data will be reproduced to support the observations in this work. The following is a summary of the main findings.

3.1.3.1 The Alkyl Chain Length Effect

MeMeImI and MeEtImI are both solids at room temperature, melting at 368K and 351K respectively. No glass transition is observed upon quenching these materials from the melt and conducting thermal analysis from 153K. Increasing the length of the alkyl substituent, from propyl through to heptyl, results in glass forming materials with glass transitions around 203K. No crystallisation could be induced in these glasses. ^1H NMR in solution and infrared analysis both suggest that the longer alkyl chains increase the aromaticity of the imidazolium ring. This has been attributed to the inductive effects of the chains. There was evidence of hydrogen bonding in both measurements and it appears to occur more readily in the salts with longer alkyl chains. Bishop has suggested that this behaviour may be due to intramolecular interactions between the alkyl chain and the imidazolium ring.

MeMeImI and MeEtImI display solid state conductivity which were slightly lower than the liquid state conductivity for these salts. A discontinuity accompanies the transition from solid to liquid state conductivity and occurs close to the melting point in each case. Only liquid state conductivity was measured for the other salts in this series. The nature of the conduction mechanism also appears to change with alkyl

substituent; MeMeImI and MeEtImI displayed Arrhenius behaviour, while the other salts exhibited a slight curvature in their temperature dependence, implying VTF behaviour. Upon measuring the conductivity as a function of alkyl chain length, MeMeImI and MeEtImI had the highest conductivities for this series of salts and increasing the length of the alkyl chain results in a decrease in the conductivity. Complementary to this behaviour, the activation energies for conduction in MeMeImI and MeEtImI were also the same and an increase in the alkyl chain length increased the activation energy.

3.1.3.2 The Anion Effect

Four salts with the same cation but different anions were also studied. MeEtImBr and MeEtImI have similar melting points, well above room temperature, whereas MeEtImNTf₂ and MeEtImTf salts are colourless liquids with subambient melting points. While IR analysis indicated extensive hydrogen bonding for the iodide salt, MeEtImTf showed a weaker interaction and hydrogen bonding was absent in MeEtImNTf₂. Both solid and liquid state conductivities were observed for MeEtImBr and MeEtImI and the data was adequately modelled with the Arrhenius equation. An interesting observation is the apparent ease with which ion transport occurs in the crystalline materials, as indicated by very high solid state conductivity and low activation energy. Conductivities for MeEtImTf and MeEtImNTf₂ are remarkably similar, with only slight deviations occurring at lower temperatures. There is an obvious curvature to the MeEtImNTf₂ data, which could imply VTF conductivity behaviour. The same curvature is not as obvious in the MeEtImTf data, but there does seem to be a slight deviation from linearity. At high temperatures, all four salts show remarkably similar conductivities, which may suggest a similar conduction mechanism in the melts.

3.1.3.3 Binary Systems

A number of binary systems were formed by combining the pure salts (Table 3-2). These binary combinations enabled the effect of like anions and like cations, as well as mixed ion systems, to be analysed. In most cases, the binary mixtures exhibited a lower melting point, or one that was often suppressed altogether. Moreover, the binary system conductivities were often greater than expected from a simple rule of mixtures. This was attributed to a combination of factors: an increase in the number of charge carriers available for conduction because of a reduction in the degree of ionic association; an increase in ion mobility as a result of an increase in the free volume of the material; or both. Where binary formation lowers the melting point, one might expect the increase in conductivity to be attributed to an increase in the ion mobility. However, if the pure materials are already fluid liquids, the enhanced conductivity upon forming the binary is probably the result of decreased ionic interactions.

Table 3-2 Binary systems.

	MeMeImI	MeEtImI	MePrImI	MeEtImTf	MeEtImNTf ₂
MeEtImI	√	-	√	√	√
MeEtImTf	√	√	√	-	√
MeEtImNTf ₂	-	√	√	√	-

3.2 Research Objective

The dialkylimidazolium/aluminium halide systems have been well characterised using thermal analysis, conductivity, viscosity and electrochemical techniques. The main limitation of these materials is their affinity for water, particularly at low AlX_3 contents where the salts are very basic. More recently however, a range of dialkylimidazolium salts, in which the anion is larger and the charge is delocalised,

have been synthesised. This anion substitution has been found to produce hydrophobic salts that are also liquids at room temperature, offering promising materials for electrolytic applications. Characterisation of these materials has included structural analysis, thermal analysis, conductivity, viscosity and electrochemical measurements. However, the nature of the ion transport mechanism in these hydrophobic salts is a contentious issue. There does not appear to be any obvious correlation between the structure of the salt and the resultant conductivity. In an attempt to resolve this conundrum, Bishop conducted a methodical and thorough investigation of the dialkylimidazolium salt family. The main factors explored were the effects of alkyl chain length and anion substitution, as well as the combination of two pure salts to form a binary system. It was shown that increasing the alkyl chain length decreases the melting point, but also the conductivity. In keeping the cation structure constant, but substituting the anion, the melting point also decreases but the conductivity in the melt is remarkably similar. The conductivity was also found to be greater than expected from a simple law of mixing in the binary systems. From these observations, one can speculate as to the conduction mechanisms in these materials and several hypotheses can be proposed to explain this behaviour:

1. The decrease in conductivity, which accompanies the increase in alkyl chain length, is due to limited mobility of the larger cation;
2. Anion substitution does not effect cation mobility in the melt; and
3. Ion mobility in the MeEtImTf/MeEtImNTf₂ binary is constant and the enhanced conductivity is the result of a decrease in the ionic association.

The objective of the research presented here was to test these hypotheses by measuring the ionic diffusion coefficients for the 1,3-methylalkylimidazolium salts using NMR techniques. The effect of the salt structure on the diffusion properties was examined by altering the anion or the length of the alkyl chain. The ion diffusion in the MeEtImTf/MeEtImNTf₂ binary system was also studied. The measurements were correlated with the conductivity data in order to elucidate the conduction

mechanisms in these materials. Cation diffusion was studied as a function of alkyl chain length using the pulsed field gradient method. The anion substitution and the binary systems were studied using the fringe field gradient technique. The results will be discussed in the context of the previous work performed on these materials, in particular with reference to the work of Bishop.

3.3 Results

Imidazolium Salt Systems

Preparation of the 1,3-methylalkylimidazolium ionic liquid family involves reacting 1-methylimidazole with an appropriate alkyl halide (for example, ethyl iodide) as described elsewhere.^{7,13,28} For this thesis, the iodide salts were prepared first, mainly due to the ease of synthesis.²⁸ From the iodides, an appropriate acid and Ag_2O were used to form bromide (Br^-), trifluoromethanesulfonate (CF_3SO_3^- , also known as triflate or Tf) and bis(trifluoromethanesulfonyl)amide ($\text{N}(\text{CF}_3\text{SO}_2)_2^-$, also known as amide or NTf_2^-) salts.²⁸ The imidazolium ring consists of two alkyl substituents; a constant methyl group and a variable alkyl substituent. Different alkyl chains were substituted onto the imidazolium ring by altering the alkyl halide used in the reaction. As discussed earlier, the complex chemical nomenclature has been simplified according to the main components of the salt, eg. 1-methyl-3-ethylimidazolium bromide is referred to as MeEtImBr. Occasionally, a collective term, namely the halide salts (MeEtImBr and MeEtImI) or the fluorinated salts (MeEtImTf and MeEtImNTf₂) will also be used when discussing a group of similar salts. MeEtImBr, MeEtImI, MeEtImTf and MeEtImNTf₂ were employed to analyse the effect of the anion on transport properties. The effect of the alkyl chain length (methyl through to heptyl) on the transport properties was studied with a series of iodide salts. Mixtures of MeEtImTf and MeEtImNTf₂ were also prepared in order to study the ion transport in a binary system.

The Anion Effect

The role of the anion in the imidazolium salt transport mechanisms was investigated for MeEtImI, MeEtImBr, MeEtImTf and MeEtImNTf₂ using the fringe field diffusion technique. Cation diffusion coefficients were obtained for all four salts from proton fringe field measurements, while the anion diffusion coefficients for MeEtImTf and MeEtImNTf₂ were obtained from fluorine fringe field measurements. The cation diffusion coefficients, D , as a function of reciprocal temperature, $1/T$, are shown for all four salts in Figure 3-3, Figure 3-4, Figure 3-5 and Figure 3-6. MeEtImI and MeEtImBr cation diffusion coefficients exhibit two diffusion processes that are dependent on the thermal history of the sample. Measurements made upon cooling the salt showed a steady decrease in diffusion with decreasing temperature, even below the DSC melting point of the material. Such behaviour is indicative of supercooling, and this was confirmed by inspection of the quenched material. Measurements made during heating from room temperature resulted initially in higher diffusion coefficients than those observed in the supercooled state. The DSC melting point corresponds to a change in the transport mechanism. Close inspection of the supercooled halide salts and the fluorinated salts reveals a slight curvature in the data, implying a deviation from simple Arrhenius behaviour. Anion diffusion coefficients were measured for MeEtImTf and MeEtImNTf₂ and are shown in Figure 3-7 and Figure 3-8. The anion and cation diffusion coefficients of each fluorinated salt are compared in Figure 3-9 and Figure 3-10. In general, the diffusion coefficients of the anion are slightly lower than those of the cation.

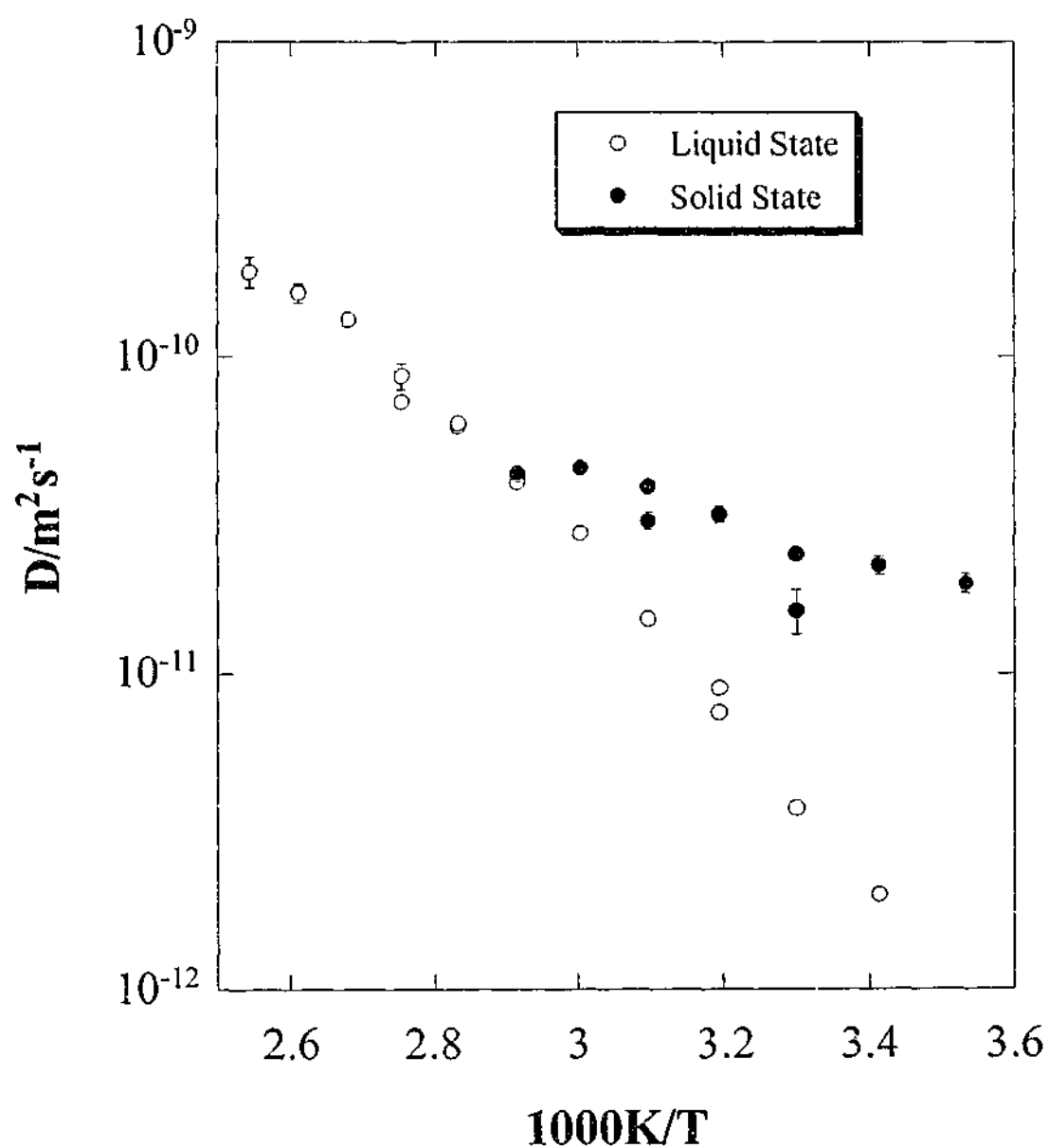


Figure 3-3 Cation diffusion coefficients as a function of temperature for MeEtImBr.

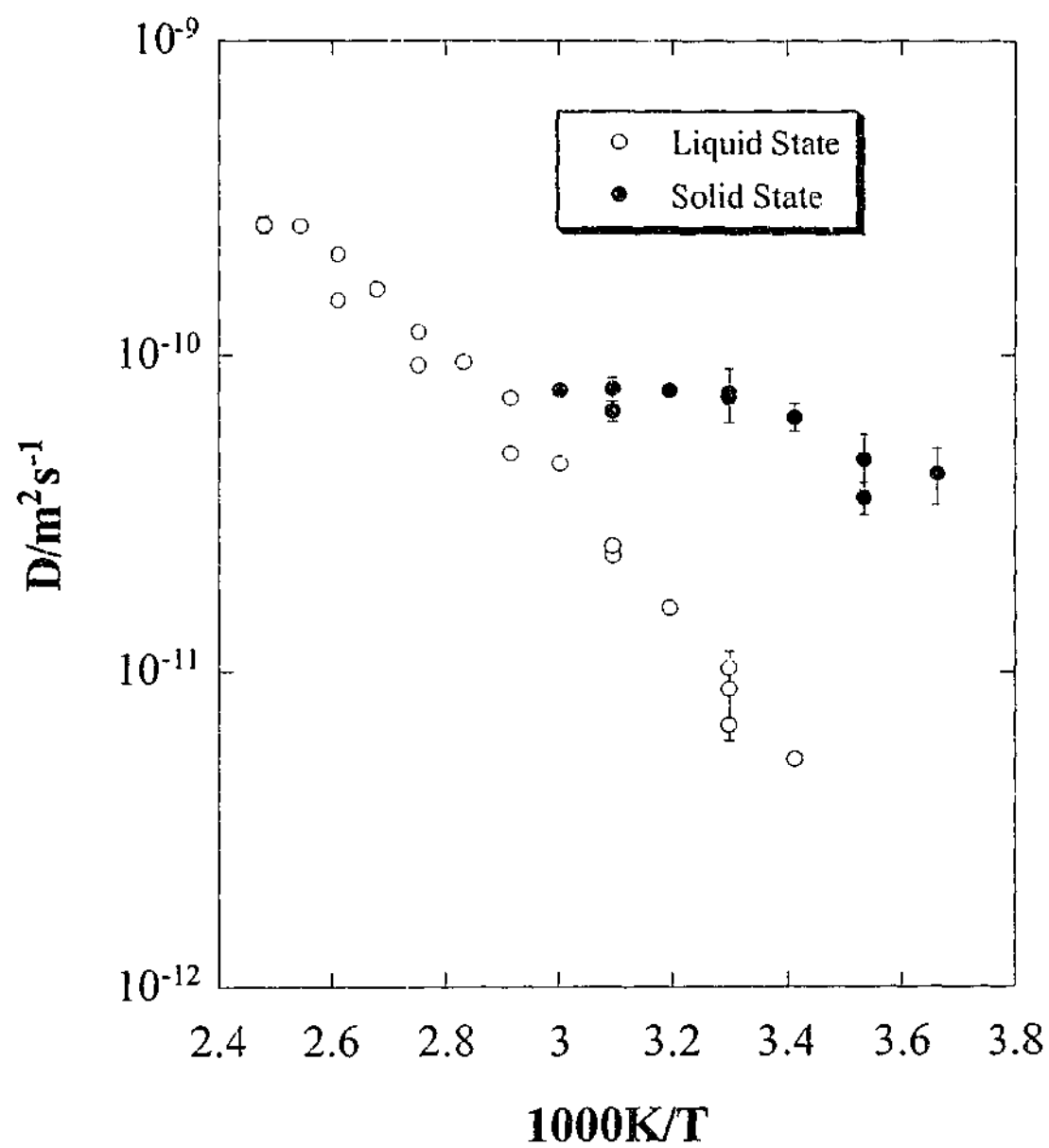


Figure 3-4 Cation diffusion coefficients as a function of temperature for MeEtImL.

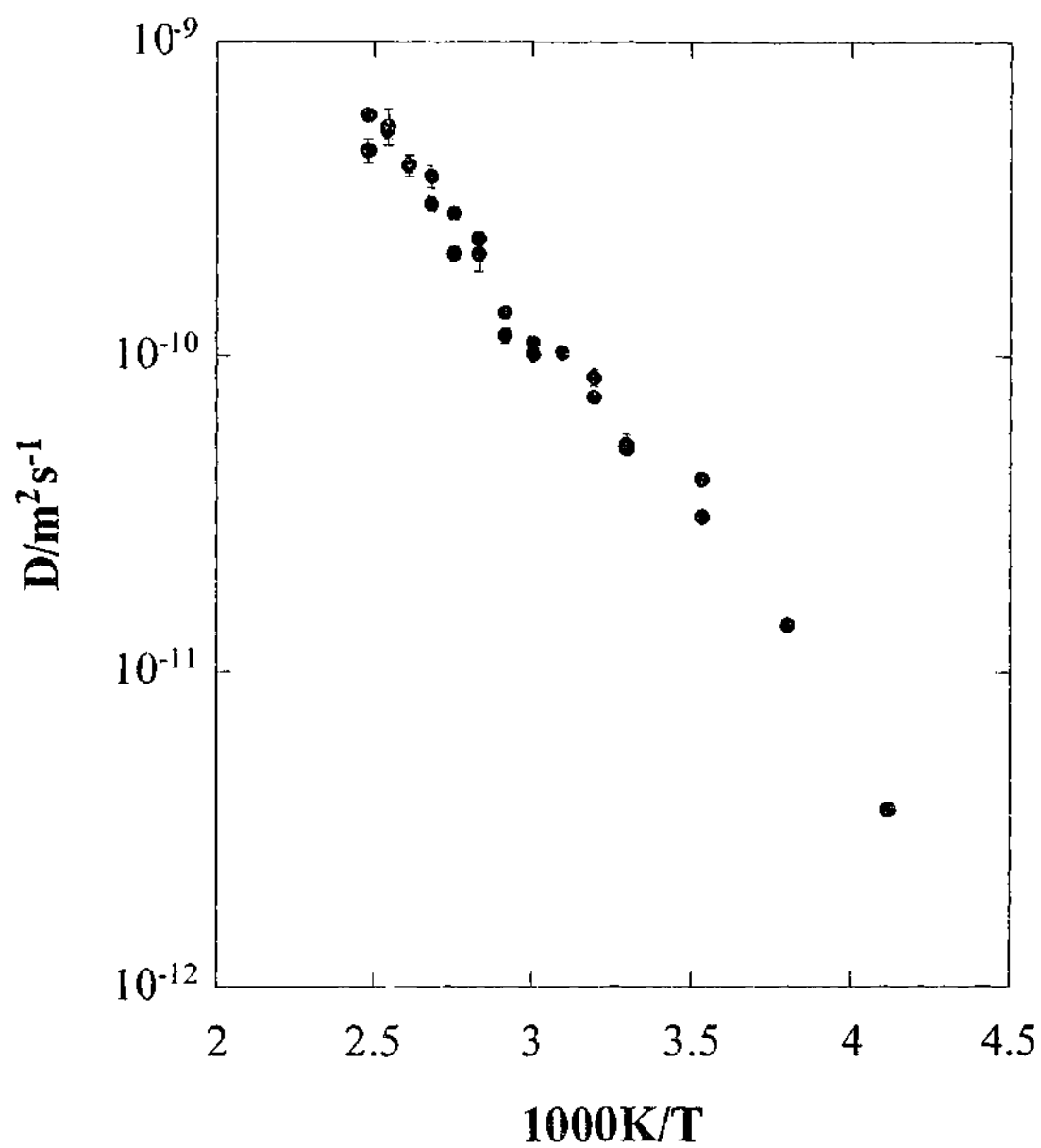


Figure 3-5 Cation diffusion coefficients as a function of temperature for MeEtImTf.

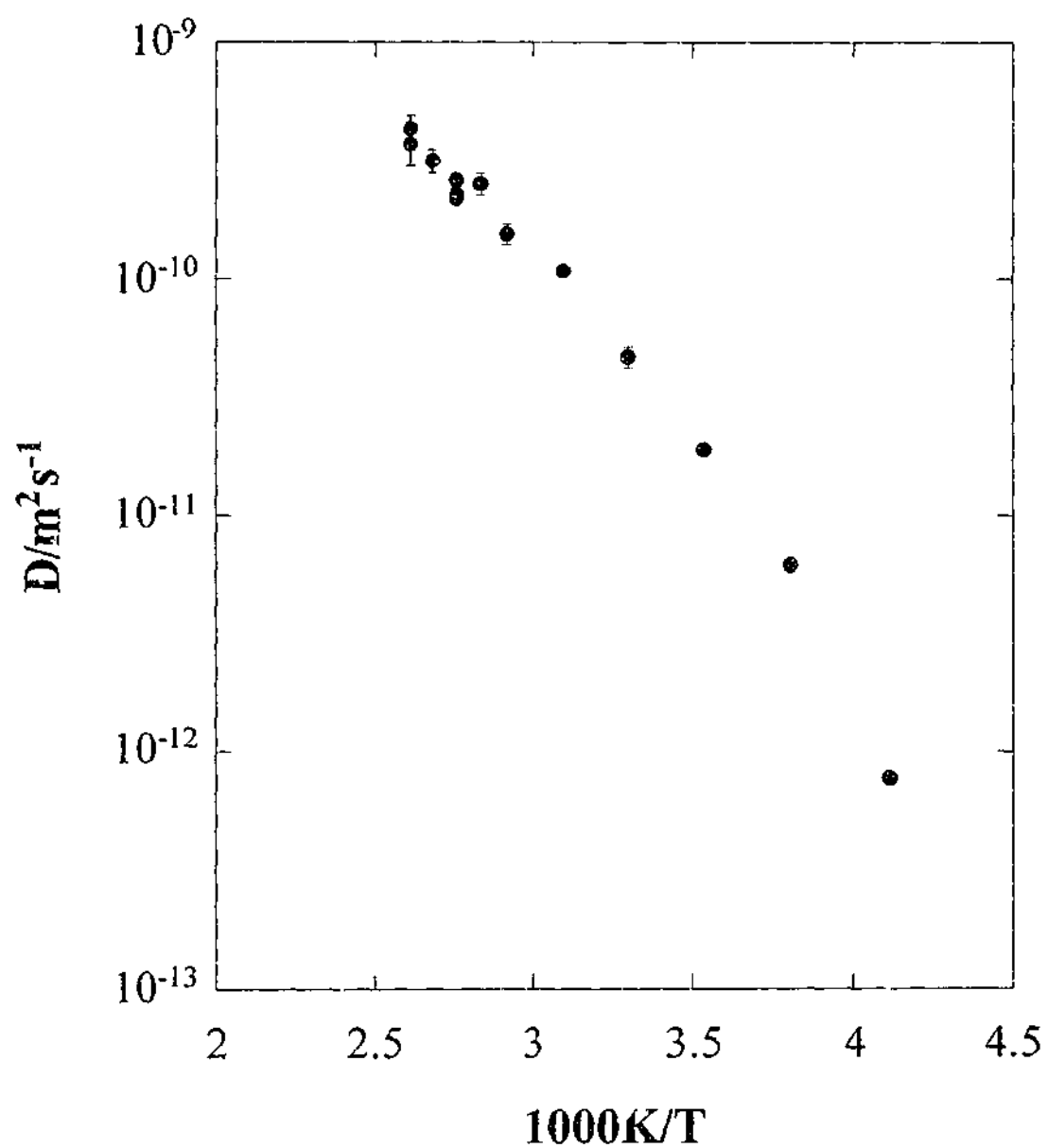


Figure 3-6 Cation diffusion coefficients as a function of temperature for $MeEtImNTf_2$.

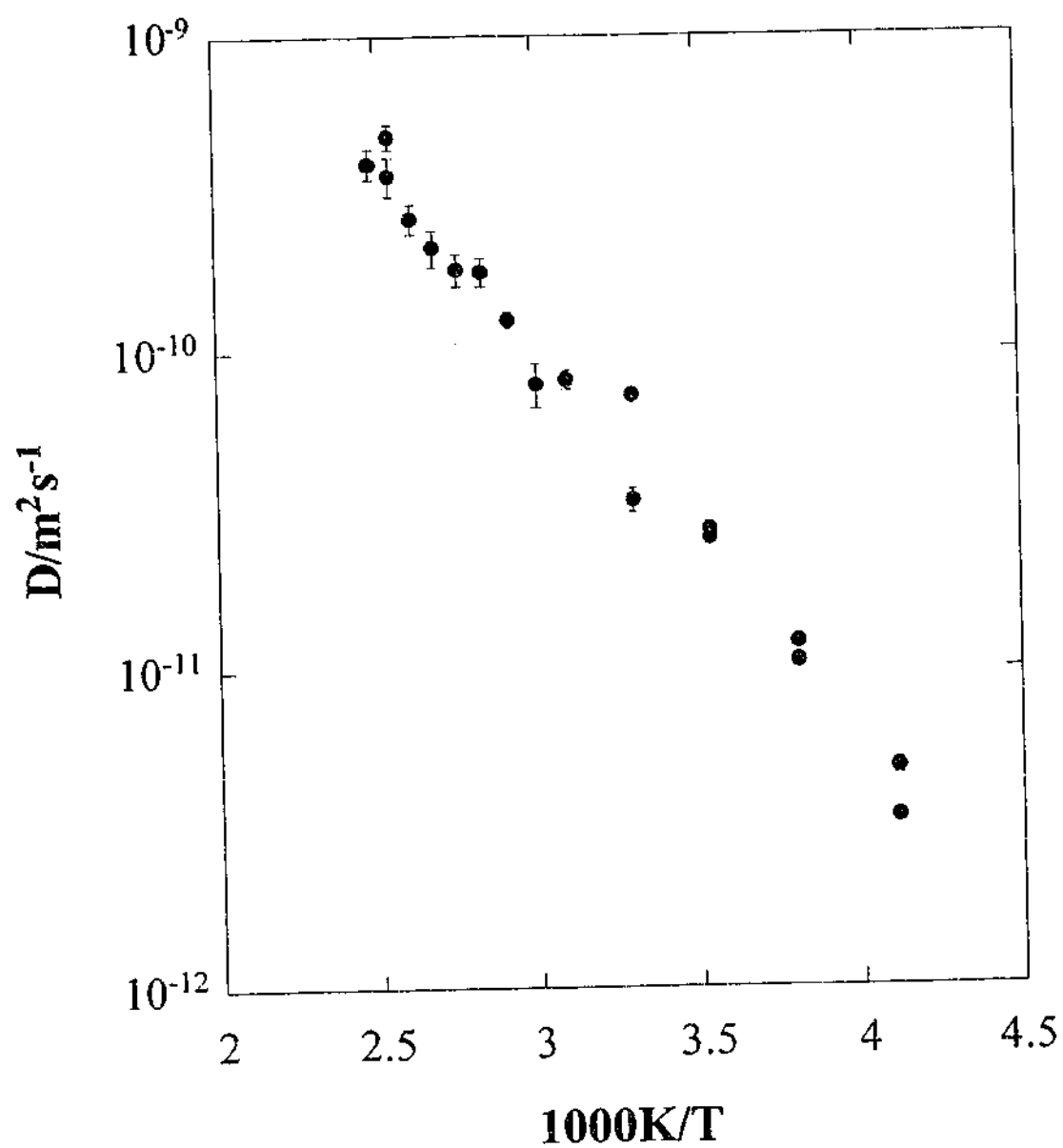


Figure 3-7 Anion diffusion coefficients as a function of temperature for MeEtImTf.

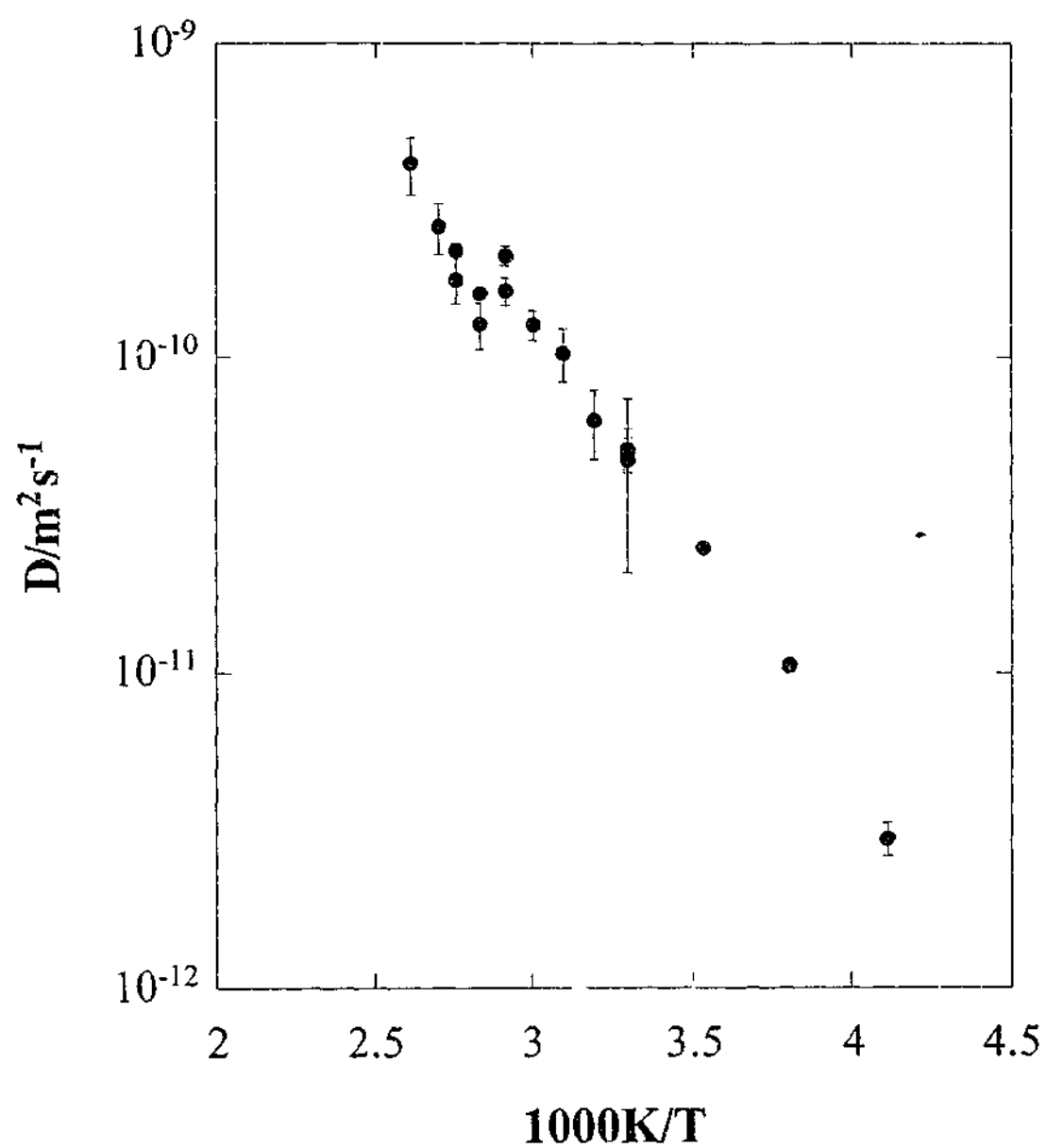


Figure 3-8 Anion diffusion coefficients as a function of temperature for MeEtImNTf₂.

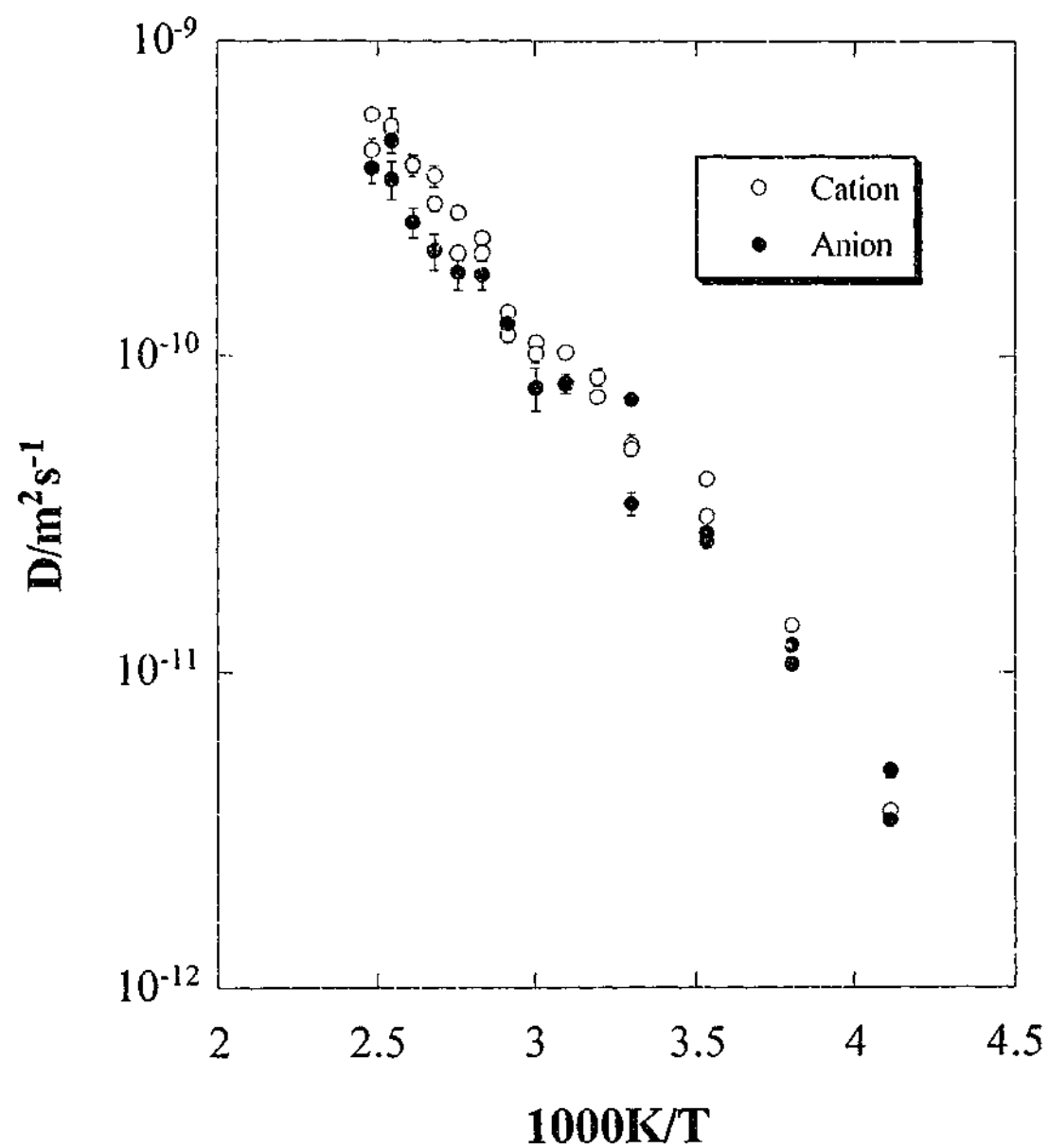


Figure 3-9 A comparison of the ionic diffusion coefficients for MeEtImTf.

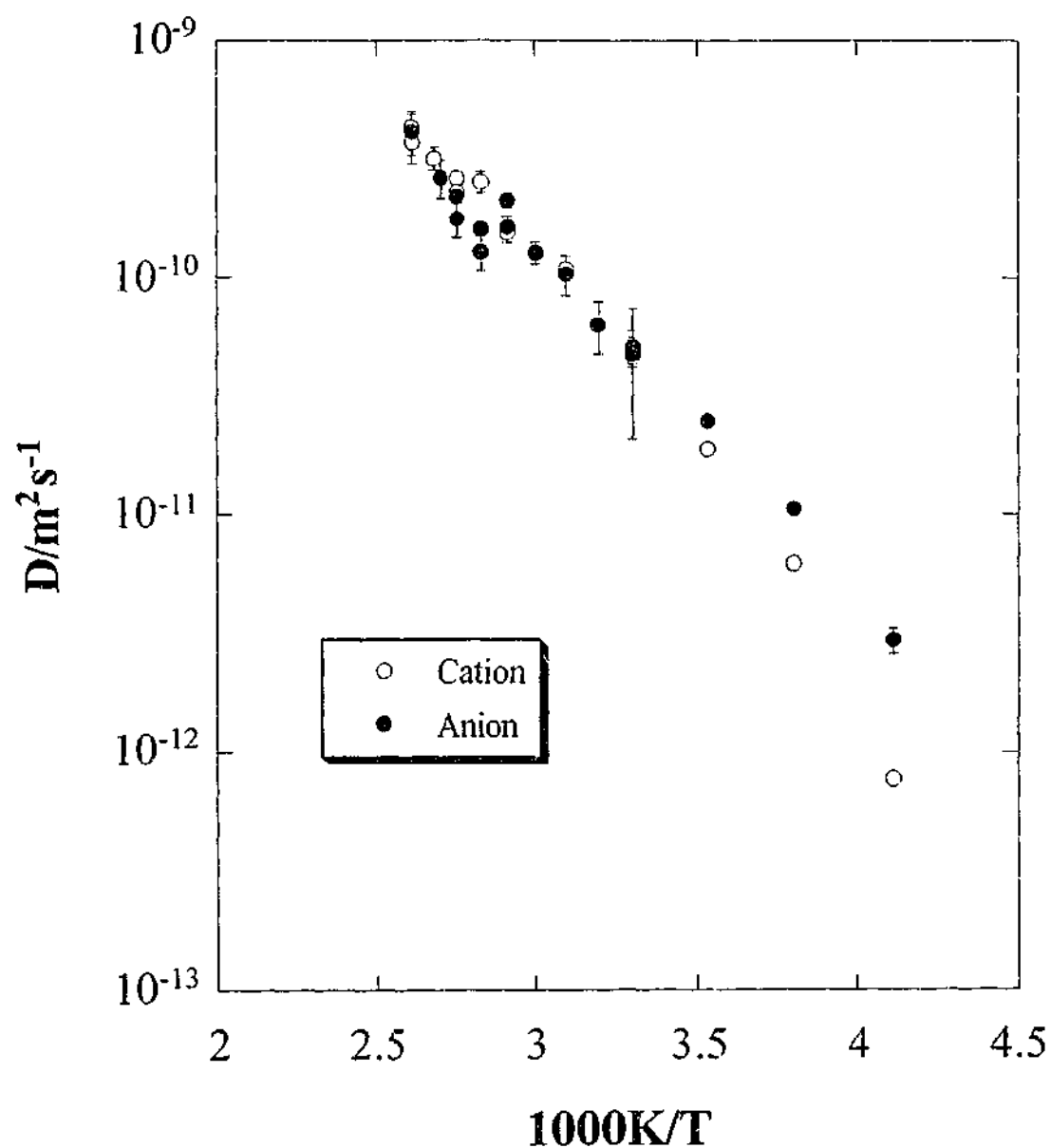


Figure 3-10 A comparison of the ionic diffusion coefficients for MeEtImNTf₂.

The Alkyl Chain Length Effect

The effect of the alkyl substituent on the imidazolium ring was studied with the iodide series of salts using the proton pulsed field gradient NMR method. Only cation diffusion coefficients were measured as there was no equipment available to study the iodide behaviour. MeMeImI and MeEtImI are both solids and melt at 368K and 351K respectively. MePrImI, MeBuImI, MePtImI, MeHxImI and

MeHpImI could not be crystallised but form glasses around 203K. The proton diffusion coefficients for all seven salts, shown in Figure 3-11, indicate that there is a decrease in diffusion coefficient as the length of the alkyl chain increases. The slight curvature in the diffusion data for the glass forming salts is once again suggestive of a deviation from simple Arrhenius behaviour.

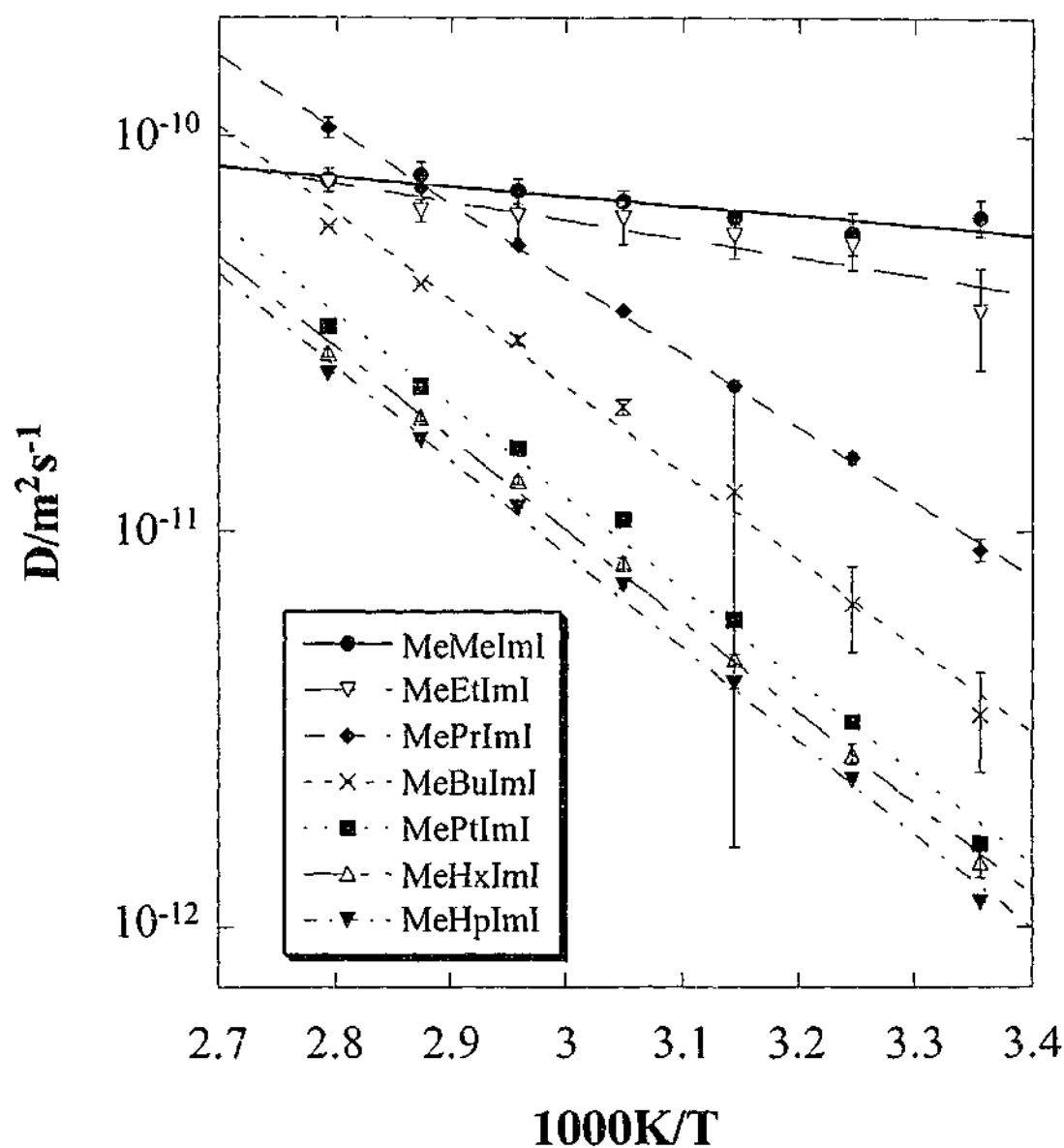


Figure 3-11 A comparison of the proton diffusion coefficients for MeRImI. Lines are to guide the eye.

Binary Mixtures of MeEtImTf and MeEtImNTf₂

In the work of Bishop,^{28,31} the conductivity of a binary mixture of MeEtImTf and MeEtImNTf₂ was greater than for either of the pure components. In order to understand this binary behaviour, the cation and anion diffusion coefficients were measured as a function of MeEtImTf mole fraction at 293K (Figure 3-12) and 363K (Figure 3-13). In both cases, the cation diffusion coefficients are greater than those for the anion and the behaviour seems to follow a simple law of mixtures.

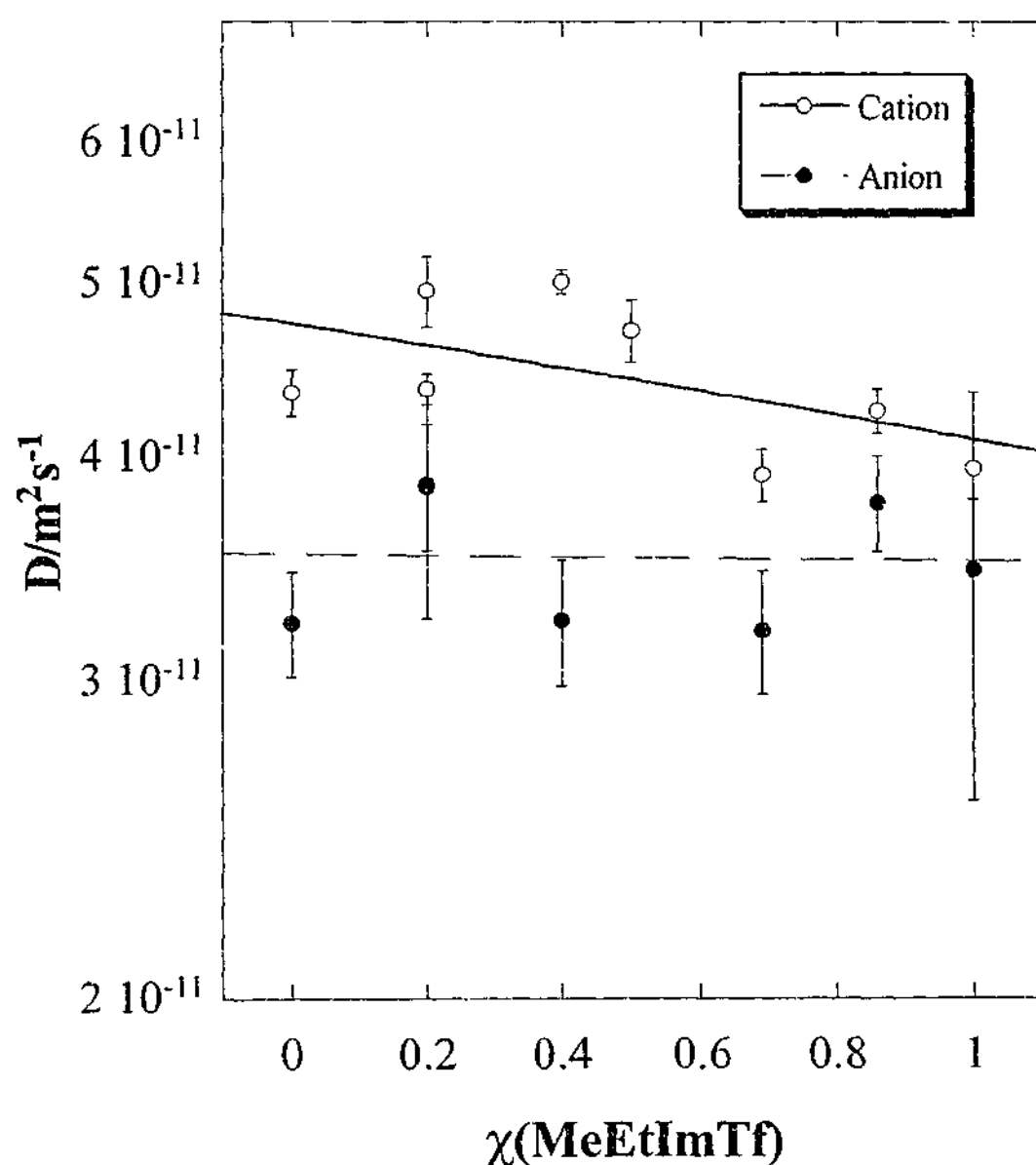


Figure 3-12 Proton and fluorine diffusion coefficients in MeEtImTf/MeEtImNTf₂ binary at 293K. Lines are to guide the eye.

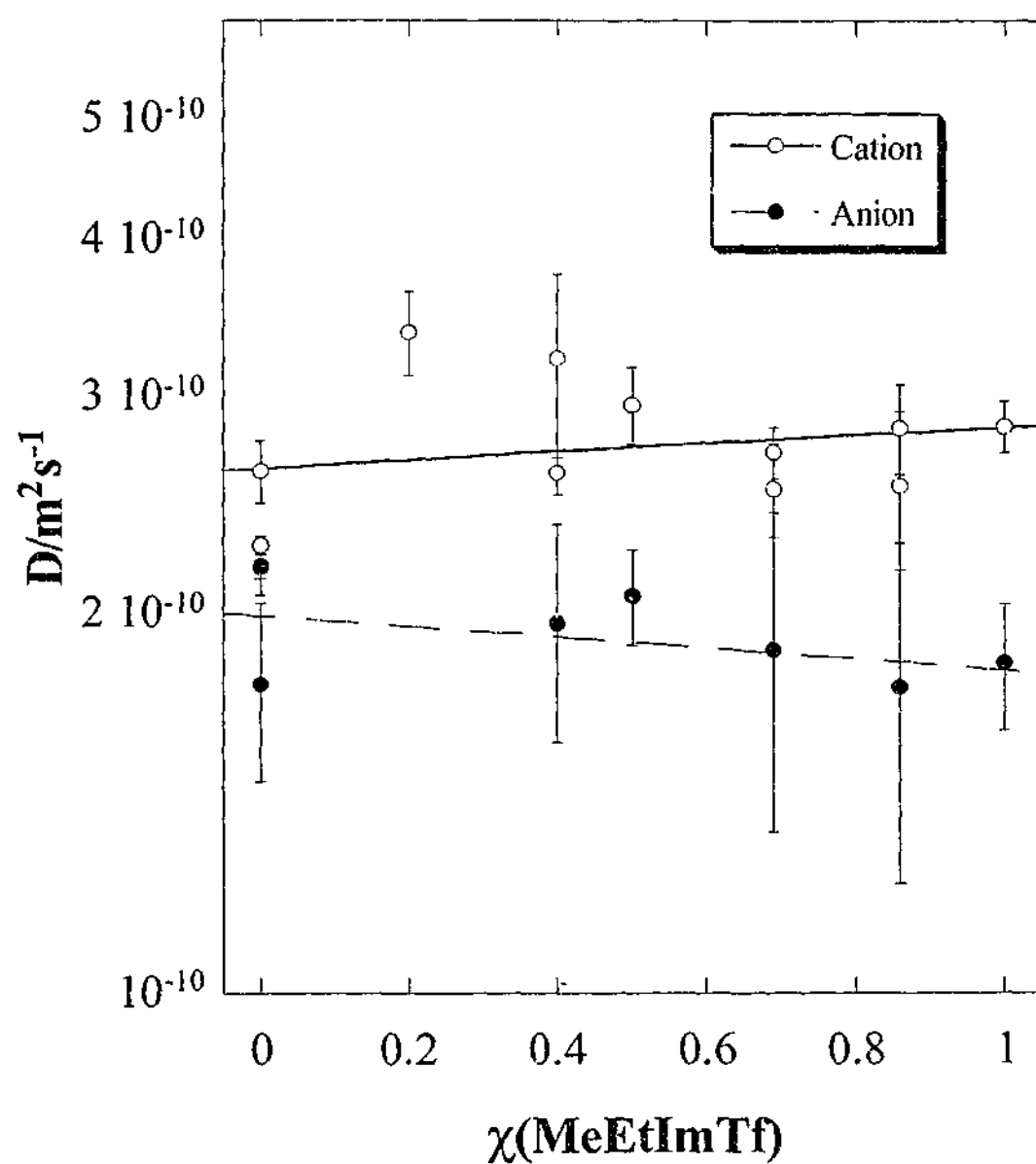


Figure 3-13 Proton and fluorine diffusion coefficients in MeEtImTf/MeEtImNTf₂ binary at 363K. Lines are to guide the eye.

In the following sections, the differences in diffusion behaviour in these salts are discussed in an attempt to reveal the transport mechanisms involved in the diffusion and conduction processes.

3.4 Discussion

3.4.1 The Anion Effect

The diffusion coefficients for the halide salts have been measured in both the liquid (supercooled) and solid states, but the initial discussion will be limited to the liquids so that comparisons can be drawn between all four salts. Analysis of the solid state behaviour can be found in section 3.4.4.

The proton diffusion coefficients for all four salts are compared in Figure 3-14. Although MeEtImBr has slightly lower diffusion coefficients than MeEtImI, the temperature dependence is similar. At higher temperatures, the proton diffusion coefficients for the fluorinated salts are almost identical but MeEtImNTf₂ shows a greater decrease in diffusivity at the lowest temperatures. The proton diffusion coefficients for the fluorinated salts are over two times greater than those of the halide salts. The fluorine diffusion coefficients have also been compared for the fluorinated salts, as shown in Figure 3-15. In accordance with the proton diffusion data, the fluorine diffusion coefficients are also remarkably similar for these salts, albeit slightly lower than the cation diffusion coefficients (Figure 3-9 and Figure 3-10). On the basis of this diffusion behaviour, the conductivities for the fluorinated salts would be expected to be greater than the halide salts (reproduced from Bishop²⁸ and shown in Figure 3-16). Although the conductivity behaviour does show a slight variation between the different anions, it does not reflect the disparity seen in the diffusion data. In particular at the high temperatures, where there was an obvious difference in the diffusion data, all four salts exhibit the same conductivity. Although the conductivity is directly related to the diffusion coefficients, it is also dependent on the concentration of the charge carriers. The disparity in the diffusion coefficients will be addressed initially, followed by an examination of the effect of charge carrier concentration on the transport properties.

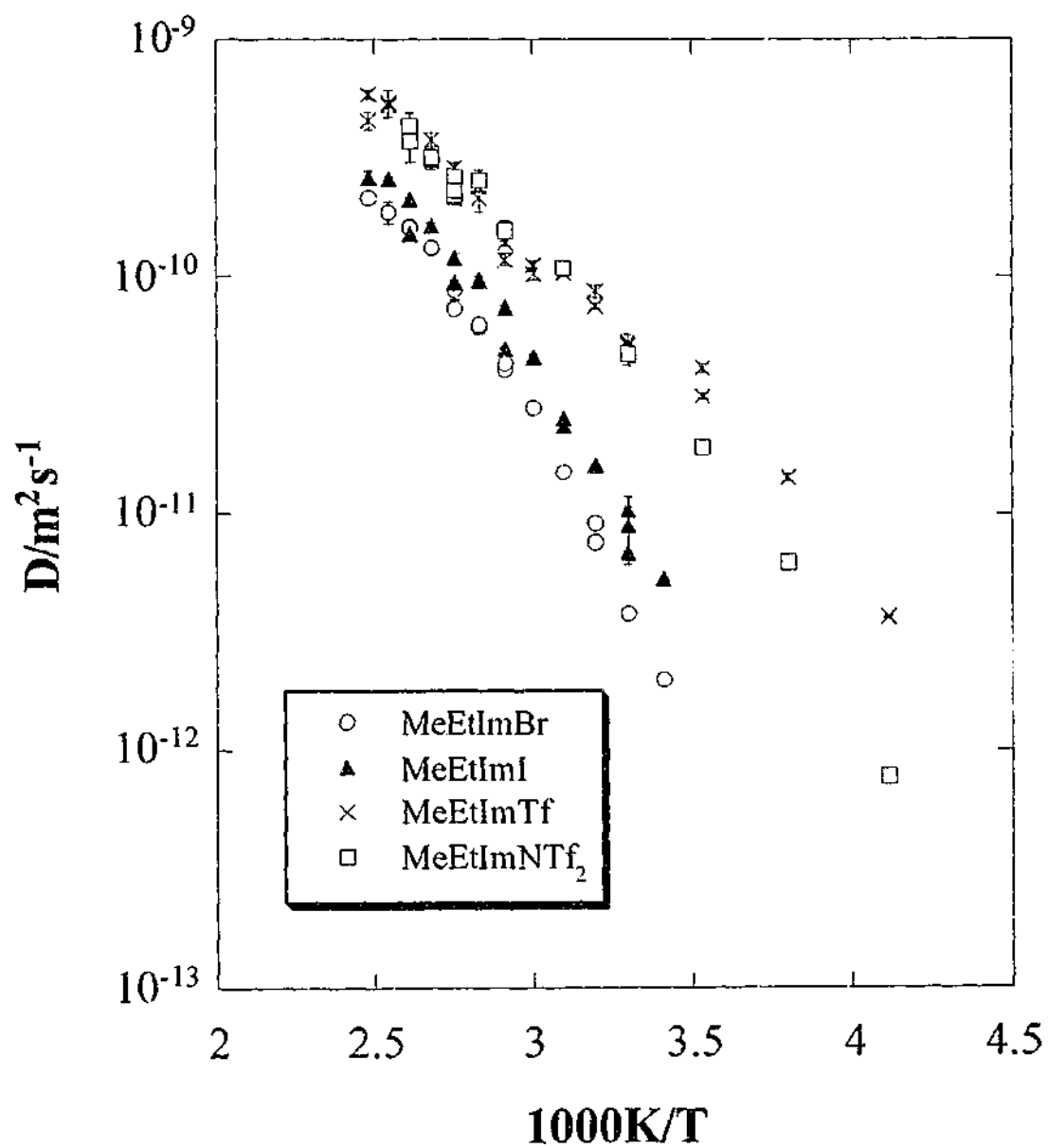


Figure 3-14 A comparison of proton diffusion coefficients for MeEtImX.

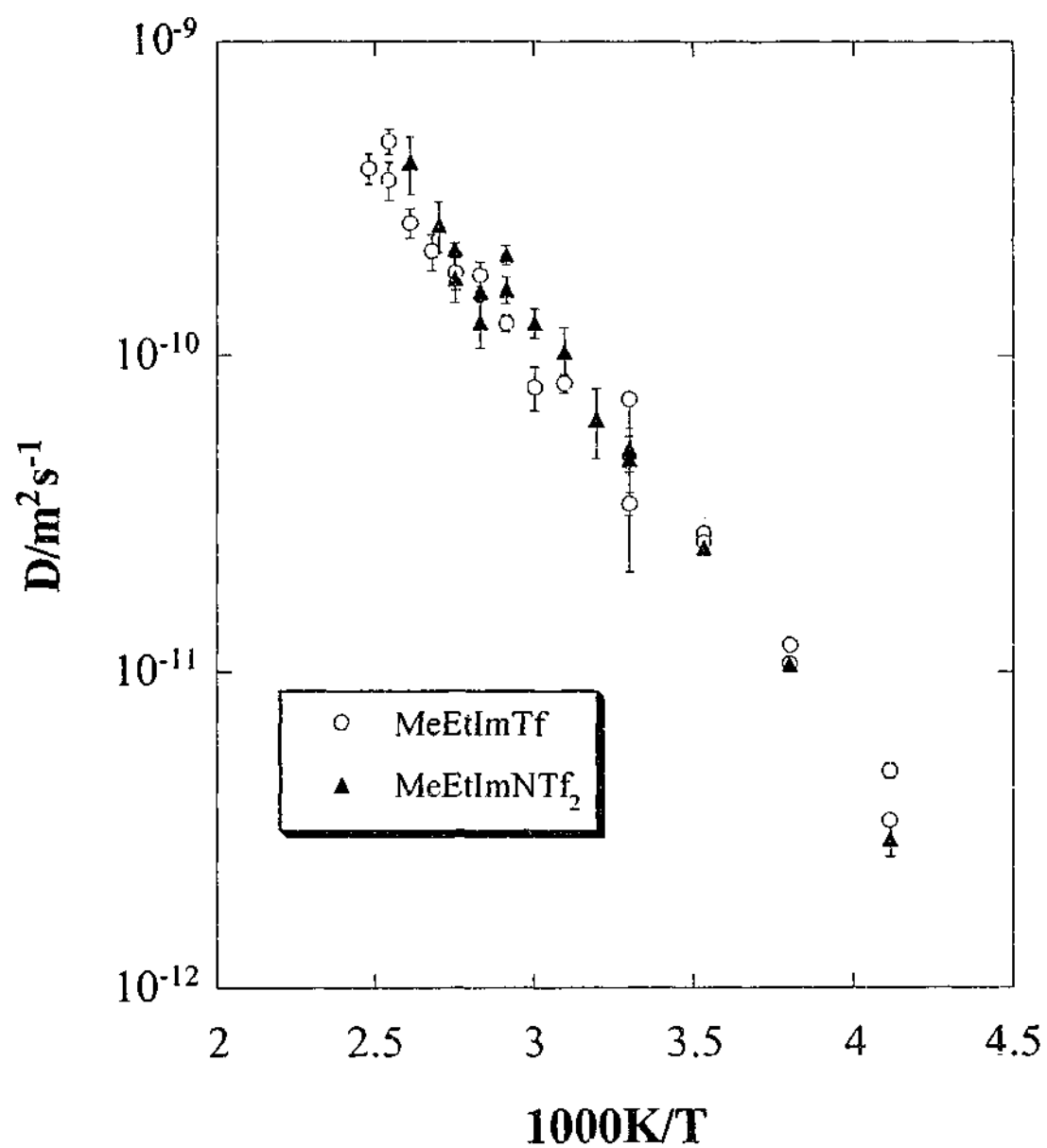


Figure 3-15 A comparison of fluorine diffusion coefficients for MeEtImTf and MeEtImNTf₂.

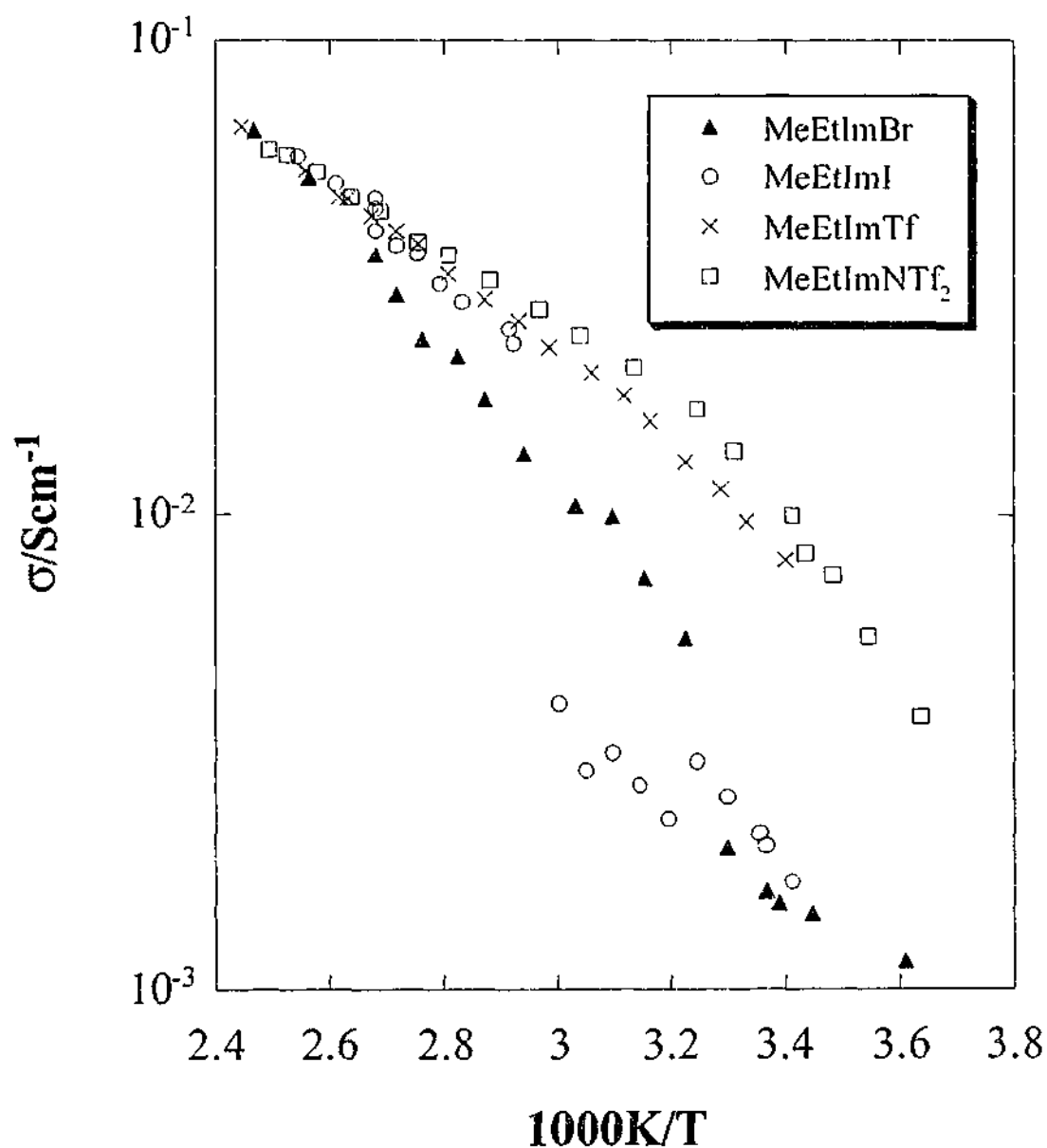


Figure 3-16 Temperature dependent conductivity data for MeEtImX (reproduced from Bishop²⁸).

3.4.1.1 The Role of the Medium on the Transport Properties

Diffusion will be hindered if the size of the diffusing species increases, the pathways for diffusion are restricted, or where both of these factors combine.³² Given that MeEtImI, MeEtImBr, MeEtImTf and MeEtImNTf₂ have the same cation, the disparity in the cation diffusion coefficients between the halide and the fluorinated

salts must therefore reflect a difference in the diffusion pathways. That is, the diffusion pathways in the halide salts are more restricted than in the fluorinated salts. Since all four salts are in the liquid state, this difference is possibly due to differing viscosities. According to the Stokes-Einstein equation,³³ diffusion is inversely proportional to the viscosity, η , of the medium:

$$D = \frac{kT}{F\pi\eta a}$$

Equation 3-1

In this equation, k is the Boltzmann constant, T is temperature and a is the radius of the diffusing element. The factor, F , varies from 3 to 6 depending on the nature of the system and the interactions experienced by the solute.^{19,34} The viscosities of the fluorinated salts have been measured at 348K^{25,26} and were reported to be approximately 11cP and 7 to 9cP for MeEtImTf and MeEtImNTf₂ respectively. The viscosity of MeEtImBr at the same temperature has been obtained from extrapolation of the data for a MeEtImBr/AlBr₃ binary system to zero AlBr₃ content¹³ and was found to be 93cP, considerably higher than the values obtained for the fluorinated salts. Since MeEtImBr is actually a solid at this temperature, this viscosity would only be expected under supercooled conditions. Although no viscosity measurements have been made for MeEtImI, it was assumed that the viscosity would be similar to MeEtImBr. From these values and the assumption that F and a are the same for all four salts, the following behaviour is predicted: the diffusion coefficients for the cation in the two fluorinated salts should be almost the same, while the cation diffusion coefficients for the halide salts should be considerably lower. This agrees with the experimental diffusion data and consequently, the differences in the cation diffusion coefficients may be related to the differences in viscosity.

This conclusion is fairly rudimentary as it only involves a qualitative analysis. There are a number of theories, however, that relate the viscosity of a material to the free volume.^{33,35,36} The Batschinski theory³⁵ suggests that the fluidity, ϕ , (which is the reciprocal of the viscosity) is directly proportional to the free volume as given by the following equation:

$$\phi = \frac{1}{\eta} = A(v - v_0)$$

Equation 3-2

where v is the molar volume of a liquid and v_0 is the limiting volume at zero fluidity such that the free volume, v_f , is equal to $v - v_0$. Doolittle,³⁶ however, proposed a different theory:

$$\phi = A \exp\left(\frac{-bv_0}{v_f}\right)$$

Equation 3-3

where b is a constant approximately equal to 1. This equation predicts a sudden decrease in fluidity upon approaching a small free volume. Williams, Landel and Ferry³⁷ have related the free volume to the glass transition temperature such that:

$$v_f = v_g \left[0.025 + \alpha(T - T_g) \right]$$

Equation 3-4

where v_g is the volume at the glass transition temperature, T_g , and α is the difference between the thermal expansion coefficients of the liquid and the glass. Cohen and

Turnbull³³ have highlighted the relationship between diffusion and free volume as described by the following equation:

$$D = g(a^*)u \exp \left[\frac{-\gamma v^*}{\bar{v}_m \alpha (T - T_0)} \right]$$

Equation 3-5

where g is a geometric factor, a^* is approximately the molecular diameter, u is the gas kinetic velocity, γ is a numerical factor introduced to correct for overlap of free volume, v^* is the critical volume for diffusion, \bar{v}_m is the average molecular volume, α is the average thermal expansion coefficient, T is temperature and T_0 is the ideal glass transition temperature (taken to be $T_g - 50K$). Free volume theory has been criticised due to the ambiguous definition of free volume and the inability to adequately model experimental data.^{38,39} Adam and Gibbs⁴⁰ have derived an analogous equation based on the configurational entropy theory, where small sections of the material undergo cooperative rearrangements. In either case, these equations highlight the relationship between transport properties, such as viscosity or diffusion, and the absolute glass transition temperature, T_0 . Consequently, a plot of diffusion versus $1/(T - T_0)$ should normalise the data to a constant mobility (viscosity), thereby confirming the relationship between diffusion and viscosity.

The manipulated data is shown in Figure 3-17. For the fluorinated salts, the T_0 values were obtained from a simple calculation as the glass transition temperatures have been measured for these materials. For the halide salts, however, T_g was estimated from a known theory in which the glass transition temperature is 2/3 of the melting temperature.⁴¹ A comparison of the actual glass transition temperatures and the estimated values for MeEtImTf and MeEtImNTf₂ showed reasonable agreement (Table 3-3), thereby suggesting that this assumption is valid for these systems.

Table 3-3 Experimental and calculated glass transition temperatures.

Salt/MeEtImX	DSC T_m /K	DSC T_g /K	Calculated T_g /K
MeEtImBr	352	-	235
MeEtImI	351	-	234
MeEtImTf	258	175	172
MeEtImNTf ₂	255	180	170

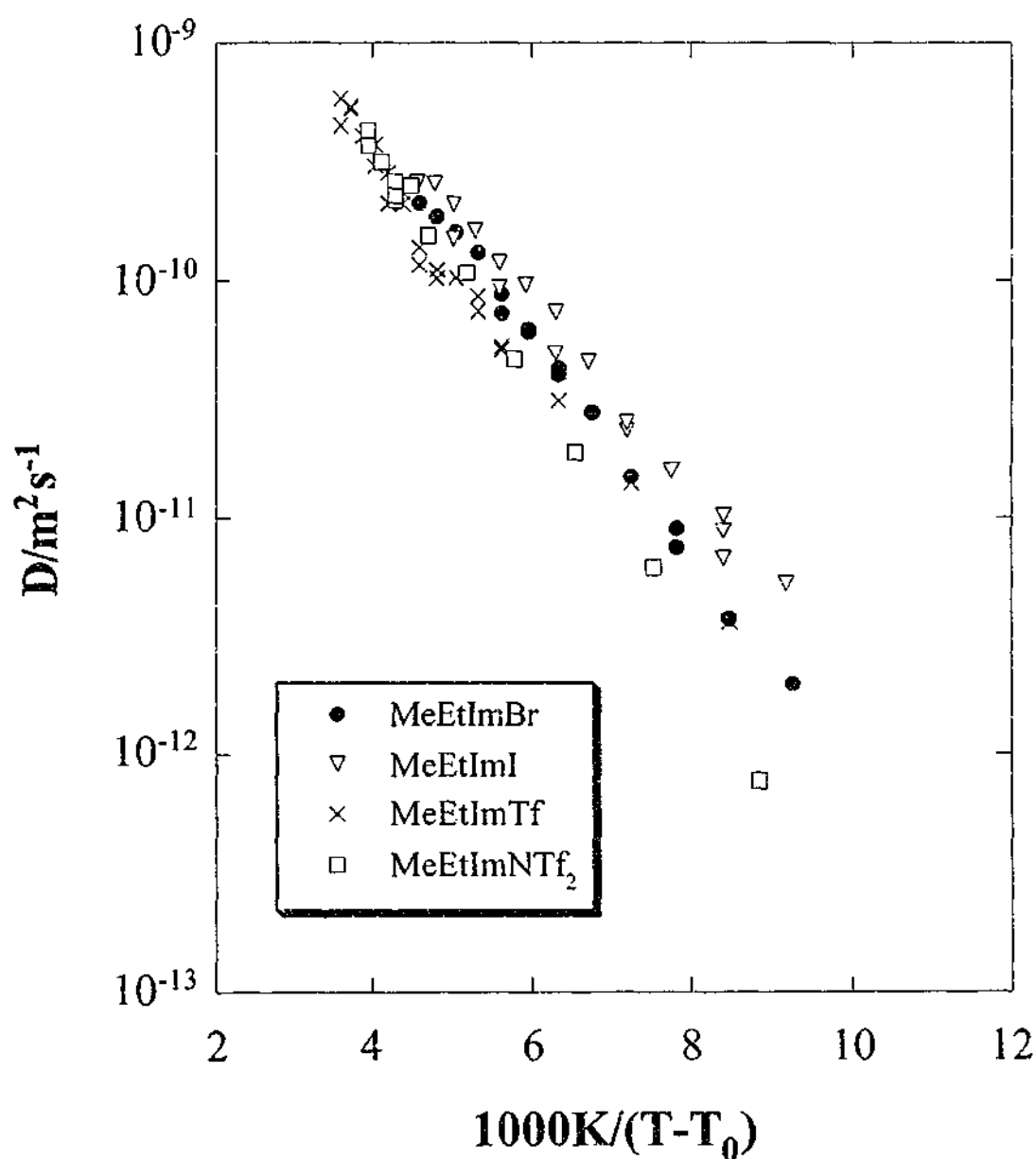


Figure 3-17 Diffusion data for MeEtImX as a function of $1/(T-T_0)$.

Given the errors in the data and the assumptions regarding the glass transition temperatures, this form of normalisation results in a reasonable concordance between the data, particularly at the higher temperatures. The curves are also reasonably linear, supporting the choice of T_0 values. Consequently, there appears to be a correlation between diffusion and viscosity for these materials.

Is the same effect responsible for the variations in conductivity among these materials? Conductivity is dependent on both the number of ions, n , with a charge, q , as well as their mobility, μ , summed over all ions, i , and can be simply represented with the following equation.⁴²

$$\sigma = \sum_i n_i q_i \mu_i$$

Equation 3-6

If it is assumed that there is complete ion dissociation and that the ionic charge is constant over the entire temperature range studied, the conductivity should be directly proportional to the mobility of the ions. If the mechanisms governing diffusion and conductivity are the same, a similar normalisation of the conductivity data with respect to T_0 should be observed. The results of this data manipulation are shown in Figure 3-18. All of the salts, except MeEtImNTf₂, are linear in this form, but unlike the diffusion data, the conductivity curves are not superimposed. It was implied in the diffusion analysis that if the viscosity and diffusion are related phenomena, then this normalisation should shift the data so that the curves would coincide with one another at the same $1/(T-T_0)$ value. The lack of coincidence observed in the conductivity data is probably indicative of differences in the charge carrier concentrations for each salt. This will be discussed in the next section (section 3.4.1.2).

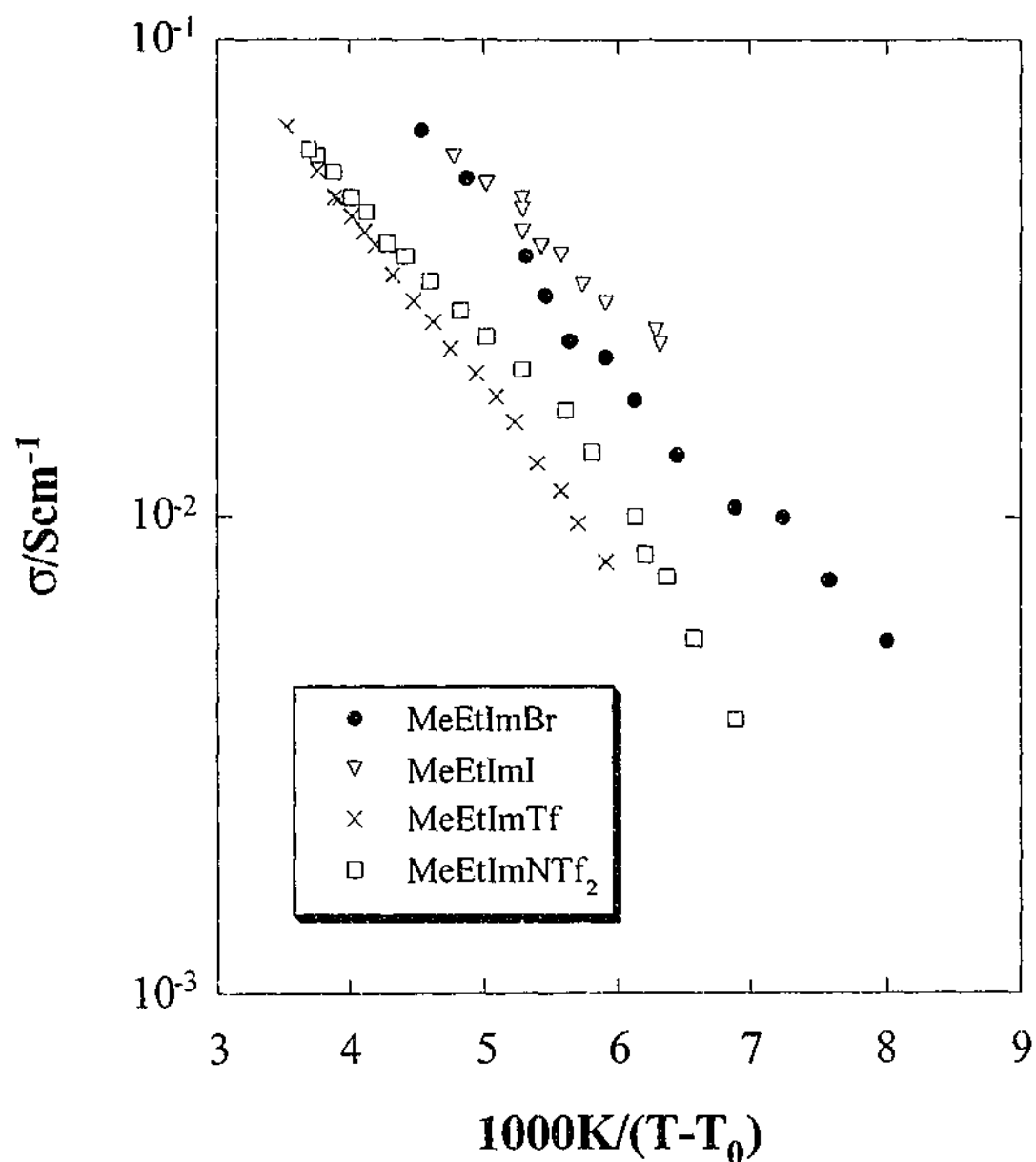


Figure 3-18 Conductivity data for MeEtImX as a function of $1/(T-T_0)$.

If the same transport mechanism is responsible for both diffusion and conduction, a similar temperature dependence would also be expected. This can be obtained by calculating a pseudo activation energy, B , for the diffusion and conductivity data shown in Figure 3-17 and Figure 3-18 by fitting a linear form of the VTF equation:

$$\ln Y = A + \frac{B}{T - T_0}$$

Equation 3-7

where Y is either the diffusion coefficient or conductivity, and A is a constant. The calculated B values for diffusion and conductivity are shown in Table 3-4.

Table 3-4 B values for diffusion and conductivity calculated from Equation 3-7.

Salt/MeEtImX	B/K for diffusion	B/K for conductivity
MeEtImBr	1046 ± 17	699 ± 28
	$R=0.9981$	$R=0.9923$
MeEtImI	897 ± 26	592 ± 33
	$R=0.9933$	$R=0.9863$
MeEtImTf	1018 ± 33	857 ± 9
	$R=0.9880$	$R=0.9992$
MeEtImNTf ₂	1225 ± 29	800 ± 23
	$R=0.9969$	$R=0.9914$

In all cases, the conductivity data have slightly lower B values than the diffusion coefficients for the same salt, suggesting that the diffusion process has a higher energy barrier than the conductivity process. McEwen²⁶ reported higher activation energies for the viscosity measurements compared to the conductivity measurements for a range of imidazolium salts. Since it has been suggested that the viscosity and diffusion measurements are dependent on the same process, the observations made by McEwen are consistent with the values presented here. Therefore, it appears that

the conductivity is not solely governed by the diffusion in these salts. With regard to Equation 3-6, it was initially assumed that these salts were completely dissociated and that the concentration of charge carriers was a constant over the entire temperature range studied. Since the variations in conductivity can not be explained by changes in diffusion, this assumption must not be valid, and there must be a temperature dependence of the number of available charge carriers. The role of charge carrier concentration on the transport properties is discussed in the following section.

3.4.1.2 The Role of Charge Carrier Concentration on the Transport Properties

Equation 3-6 is expressed in more detail by the Nernst-Einstein equation:

$$\sigma = \frac{Dq^2c}{kT}$$

Equation 3-8

where q is the ionic charge, c is the concentration of charge carriers, k is the Boltzmann constant and T is temperature. The diffusion coefficient used in this equation is calculated from the sum of the cation (D_+) and the anion (D_-) diffusion coefficients. In the case of an ionic liquid, the concentration can be calculated from the density, ρ , of the material through the use of the following equation:

$$c = \frac{N_A \rho}{MW}$$

Equation 3-9

where N_A is Avogadro's number and MW is the molecular weight of the salt. The densities for MeEtImTf and MeEtImNTf₂ were determined by weighing 0.5mL

aliquots at room temperature²⁸ and are in reasonable agreement with the values reported elsewhere.²⁵ The density of MeEtImBr was obtained by extrapolating the density data at 353K for a binary mixture of MeEtImBr and AlBr₃ to zero AlBr₃ content.¹³ The density for MeEtImBr²⁰ in the solid state has been quoted as 1.52g.cm⁻³ and therefore the liquid density value of 1.48g.cm⁻³ is consistent with the volume expansion experienced upon melting. Based on the behaviour of this binary salt and a solid state density²⁰ of 1.73g.cm⁻³, the density for MeEtImI was estimated to be 1.69g.cm⁻³ at 353K. The densities of all four salts are shown in Table 3-5.

Table 3-5 Densities and molar volumes for MeEtImX.

Salt/MeEtImX	MW/g.mol ⁻¹	ρ /g.cm ⁻³
MeEtImBr	191.07	1.48 at 353K ¹³
MeEtImI	238.08	1.69 at 353K†
MeEtImNTf ₂	260.23	1.36 at 295K ²⁸
		1.39 at 295K ²⁵
		1.55 at 295K ²⁸
MeEtImNTf ₂	391.20	1.52 at 295K ²⁵

† Estimated value.

A number of ionic liquid materials⁴³ show a 2 to 3% decrease in density over a 100K temperature range. It was therefore assumed that the density of these salts would also decrease by 3% over a similar temperature range. Using this temperature dependence, the theoretical concentrations for each salt (Figure 3-19) indicate that the halide salts are far more concentrated than the fluorinated salts. Consequently, the combination of higher ion concentration with the lower diffusion coefficients for the

halide salts results in the same conductivity as the more diffusive but less concentrated fluorinated salts.

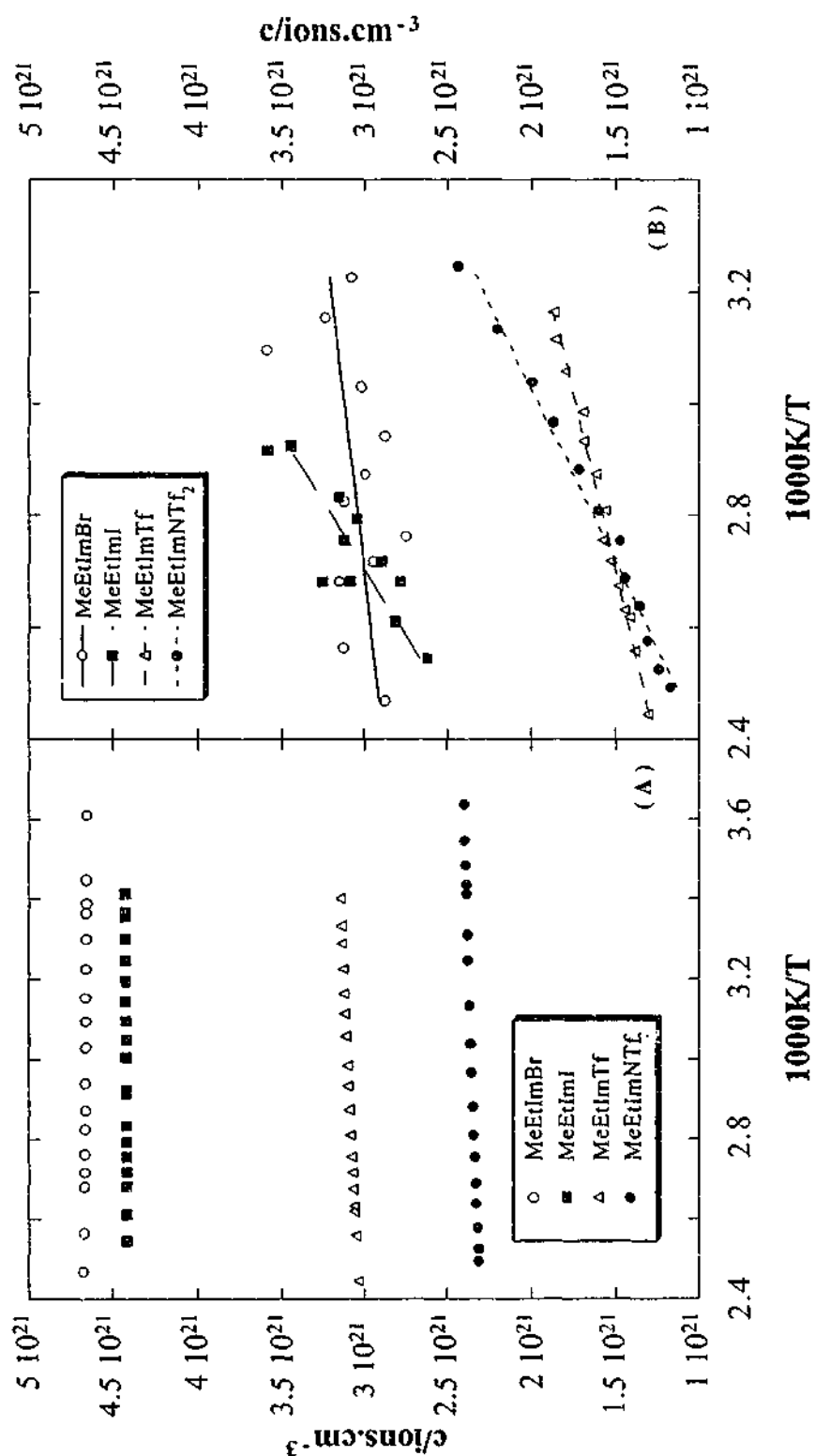


Figure 3-19 Theoretical (A) and actual (B) ion concentrations for MeEtImX. Lines are to guide the eye.

Since the liquid state conductivities and diffusion coefficients are known for these salts, the Nernst-Einstein equation (Equation 3-9) can be used to calculate the actual concentration of charge carriers available for conduction (also shown in Figure 3-19). For the halide salts, it was assumed that the diffusion coefficients of the anions (bromide or iodide ions) are the same as the cation diffusion coefficients. This would seem to be an acceptable assumption due to the similarity between the anionic and cationic diffusion coefficients in the fluorinated salts (Figure 3-9 and Figure 3-10). From Figure 3-19, it appears that not all the charge carriers are available for conduction in these salts and that ionic association occurs, forming pairs or higher aggregates. The extent of aggregation in these systems can be calculated using the following equation.

$$f = 1 - \left(\frac{c_{\text{theo}} - c_{\text{act}}}{c_{\text{theo}}} \right)$$

Equation 3-10

In this equation, f is the fraction of ions available for conduction, c_{theo} is the theoretical concentration if there is complete dissociation and c_{act} is the actual concentration determined from the Nernst-Einstein equation. The fraction of ions available for conduction in the liquid state is shown in Figure 3-20. MeEtImTf has the least number of charge carriers over the entire temperature range. While MeEtImI shows a substantial decrease in concentration with increasing temperature, MeEtImBr shows very little variation in charge carrier concentration. Despite the apparent complete dissociation of MeEtImNTf₂ at room temperature, this salt has the greatest decrease in charge carrier concentration over the temperature range, approaching a similar value to the MeEtImTf at 403K. It is interesting to compare this behaviour with the infrared analysis performed by Bishop.²⁸ MeEtImI was found to experience the strongest ionic interactions, while MeEtImNTf₂ showed the weakest in the spectroscopic measurements. Consequently, one might expect MeEtImI to have fewer ions available for conduction. The calculation performed

here, however, does not take into consideration the strength of the interactions nor the lifetime of the associated species. Although MeEtImI experiences stronger ionic interactions, the associated species may only exist for a limited lifetime before dissociating to form different aggregates. On the time scale of the infrared experiment, the salt will appear associated, but on the time scale of the conductivity and diffusion experiments, these aggregates are capable of dissociating and therefore contributing to the conduction mechanism. The main conclusion drawn from this information is that the halide salts have more charge carriers per unit volume available for conduction.

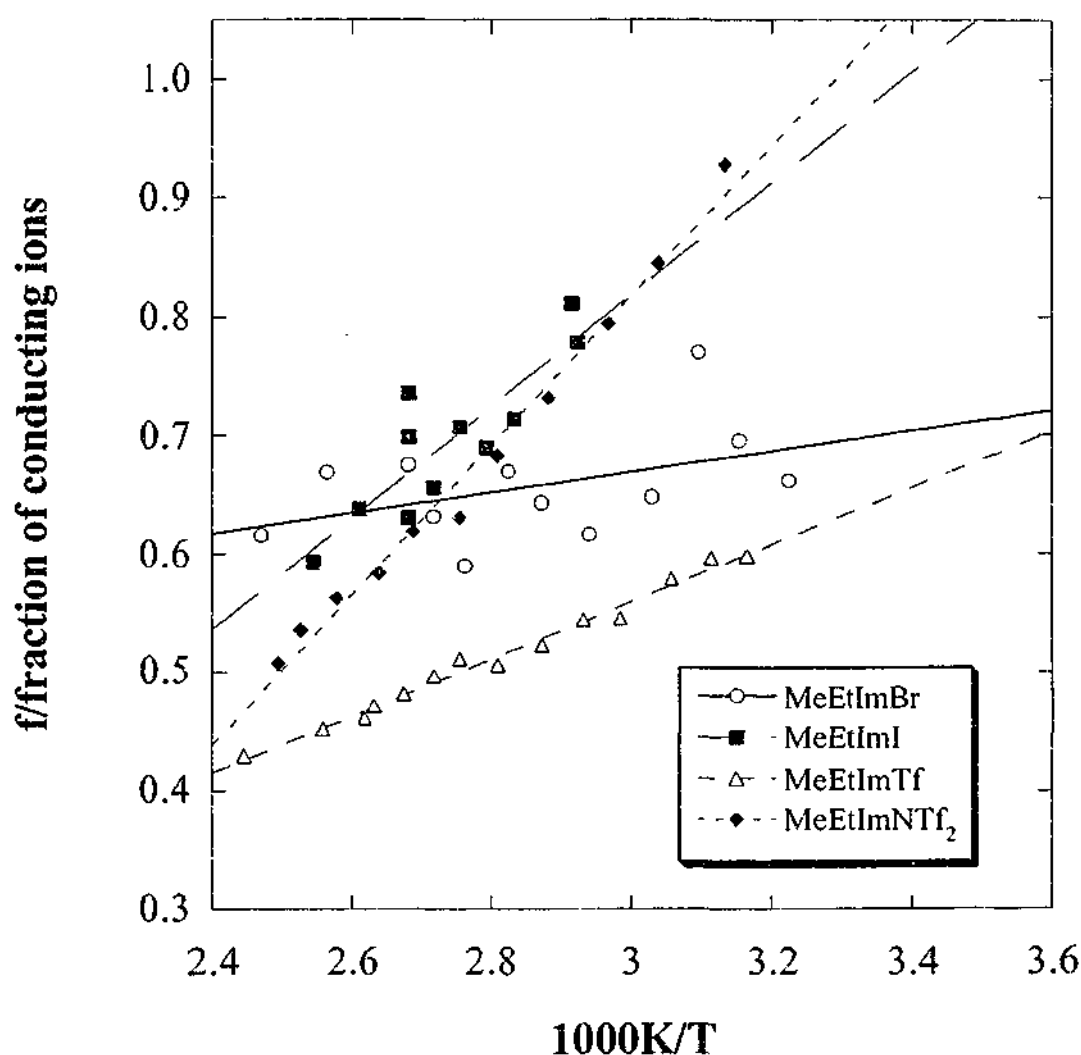


Figure 3-20 Fraction of ions available for conduction. Lines are to guide the eye.

In using the Stokes-Einstein equation (Equation 3-1), it was assumed that the factor, F , and the radius of the diffusing element, a , were constant and hence the diffusion coefficient was directly proportional to the inverse of the viscosity. Both of these "constants", however, are sensitive to ionic association, such that F ranges from 3 to 6 for a material exhibiting perfect slip and perfect stick respectively. From the calculations of the fraction of ions available for conduction, significant ionic association was observed for these materials, with MeEtImTf exhibiting the greatest degree of ionic association, while the halide salts were reasonably dissociated. If F and a are sensitive to ionic association, MeEtImTf should have a much lower diffusion coefficient than MeEtImNTf₂ for the given viscosities. As this is not the case, the ionic association observed in these materials would appear to have very little impact on the mechanism of diffusion.

3.4.1.3 Summary

Imidazolium salts with different anions displayed different diffusion behaviours. Slightly faster diffusion was observed for MeEtImI compared to MeEtImBr, although the temperature dependence was the same. The fluorinated salts exhibit similar diffusion coefficients, which were double the cation diffusion coefficients of the halide salts. This disparity was thought to be due to the difference in viscosities. Normalisation of the diffusion data with respect to T_g results in concordant mobilities for all four salts. The same behaviour is not true of the conductivity data, suggesting that the conductivity is not solely dependent on the ionic mobility. Analysis of the charge carrier concentration indicates that all four salts experience some degree of ionic association, but the halides have more charge carriers per unit volume available for conduction. Combining the higher charge carrier concentration with the lower diffusion coefficients for the halide salts results in the same conductivity as the more diffusive but less concentrated fluorinated salts.

3.4.2 MeEtImTf and MeEtImNTf₂ Binary System

The conductivity data at 293K and 363K for the MeEtImTf/MeEtImNTf₂ binary system are shown in Figure 3-21. In comparison to the pure components, the binary mixtures show a significantly higher conductivity that deviates considerably from what would be expected according to the law of mixtures. The deviation appears to be most significant for the MeEtImTf rich compositions, particularly at 293K. As implied by Equation 3-6, conductivity enhancement will only occur if there is an increase in the ion mobility and/or the number of charge carriers. Analysis of the diffusion coefficients in these binary systems (Figure 3-12 and Figure 3-13) shows a consistently higher cation diffusion coefficient when compared to the anion. However, no appreciable deviation from a simple law of mixing was observed for all binary compositions taking the errors into consideration. Consequently, it would appear that enhancement of ionic mobility is not responsible for the increase in conductivity observed for the binary systems.

The enhanced conductivity must therefore be due to an increase in the charge carrier concentration, which can only be achieved by one of two possible methods: through volume contraction upon mixing or through decreasing the degree of ionic association. An increase in the density of the material should be observed if there is a volume contraction upon combining the salts to form a binary. Density measurements performed by Bishop²⁸ showed no evidence of any increase in density, with a linear relationship due to additivity being observed. A change in the extent of ionic association would appear to be responsible for the increase in conductivity.

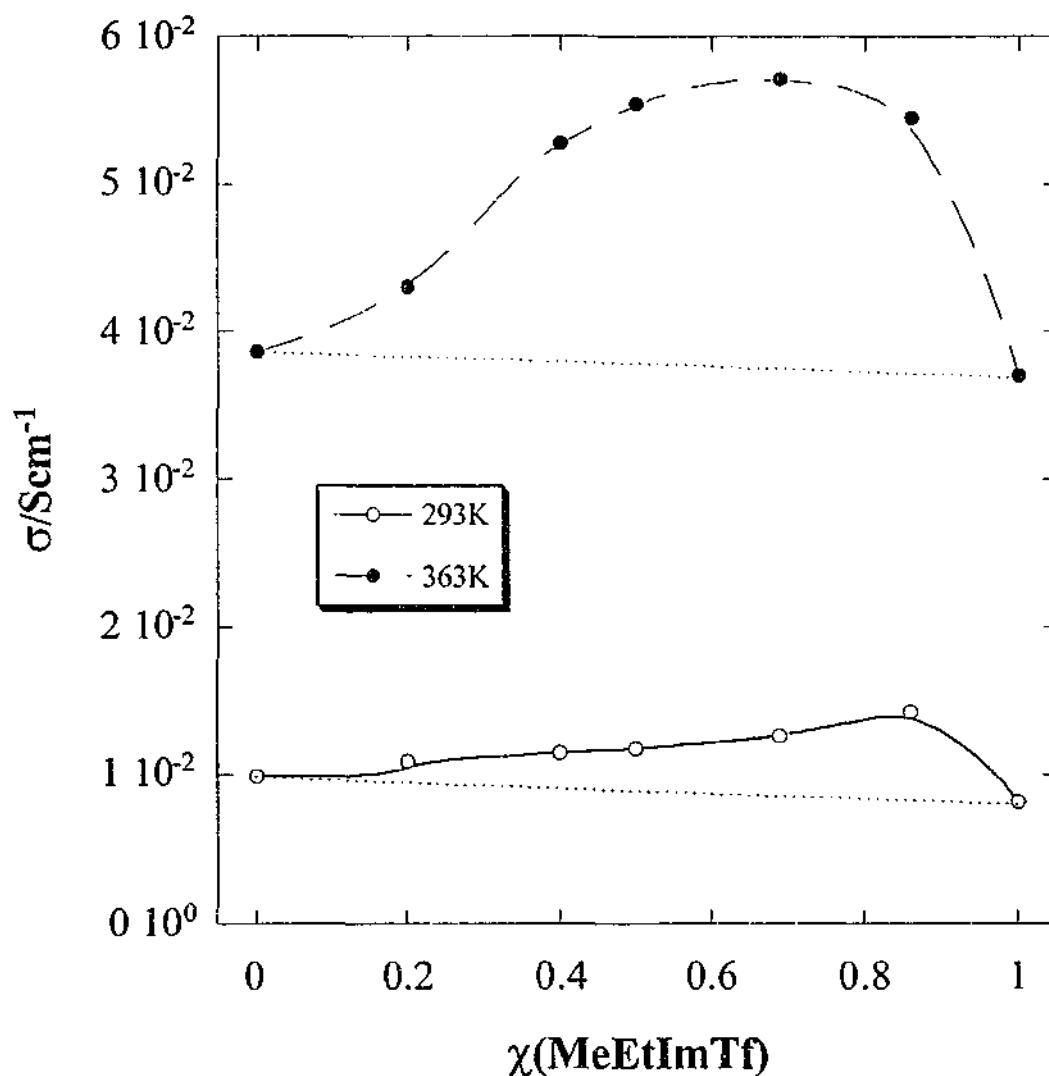


Figure 3-21 Conductivity in the MeEtImTf/MeEtImNTf₂ binary system at 293K and 363K (reproduced from Bishop²⁸). Solid lines are to guide the eye. Dashed lines represent the conductivity from additivity.

A comparison of the calculated ion concentration with the theoretical ion concentration allowed the fraction of ions available for conduction to be determined for the imidazolium salts with different anions (see section 3.4.1.2). A similar calculation can be performed for this binary system, the results of which are shown in Figure 3-22. The relationship between the fraction of ions for conduction and the composition indicates that association in the binary systems has been suppressed relative to the pure components. Notably, the highest aggregation occurs in pure

MeEtImTf but the addition of even a small mole fraction of MeEtImNTf₂ results in a marked decrease in ion association.

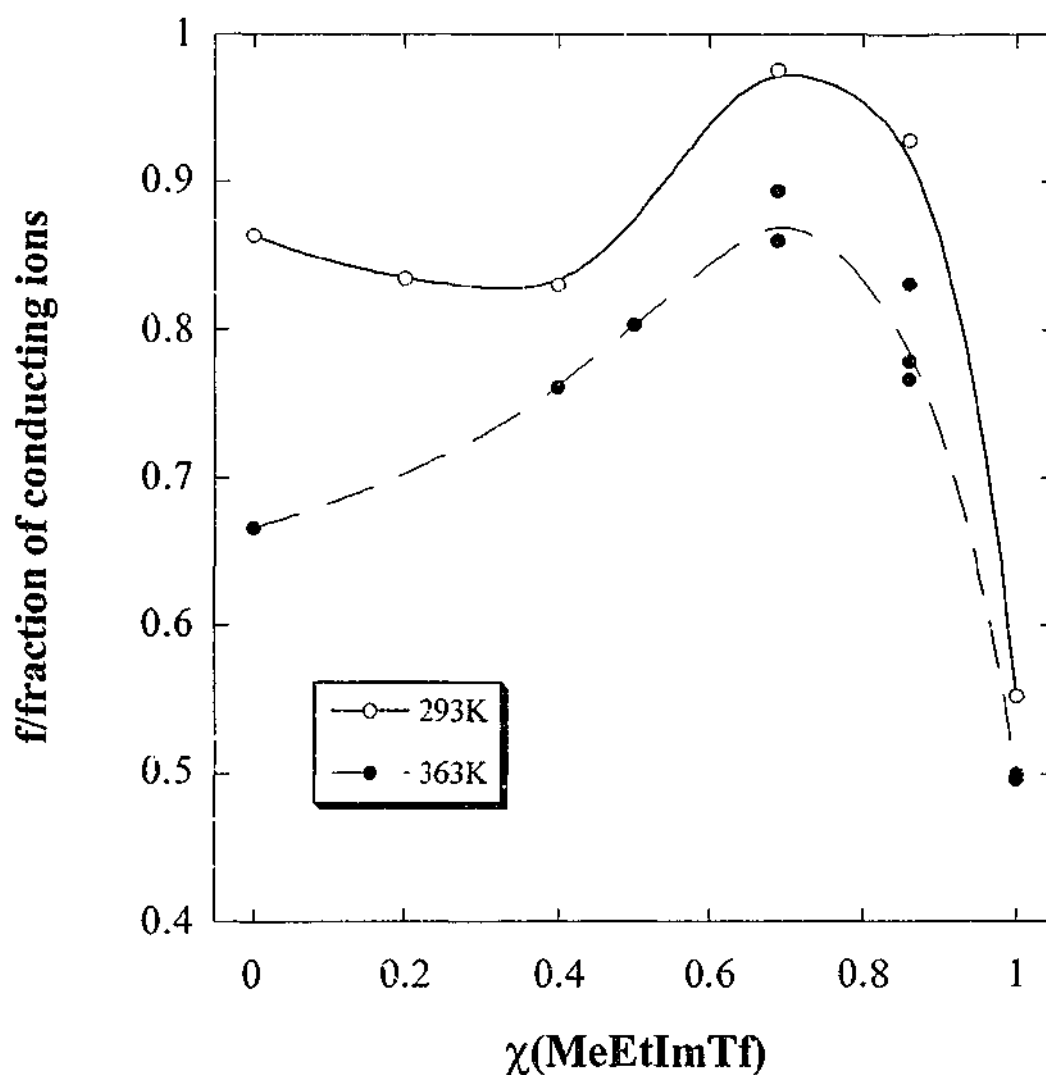
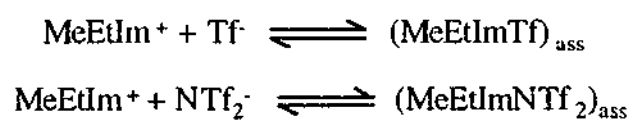


Figure 3-22 Fraction of ions available for conduction in the MeEtImTf/MeEtImNTf₂ binary. Lines are to guide the eye.

This change in ionic association can be explain when the association equilibria are considered^{28,31}



where $(\text{MeEtImTf})_{\text{ass}}$ indicates an associated species in the mixture. In the case of a binary where $\chi(\text{MeEtImTf})=0.5$, the cation concentration is unchanged upon binary mixing, while the concentration of each anion is halved. This decrease in anion concentration will shift the equilibria from association towards dissociation, thereby increasing the overall number of ions within the system. It is evident that this increase in the number of conductive species accounts for the rise in conductivity observed in the binary systems.

The effect of temperature on the binary compositions has also been examined. Previously, it was reported that MeEtImNTf_2 had very little ionic association at low temperatures compared to MeEtImTf (see section 3.4.1.2). In this case, adding a small amount of MeEtImTf to MeEtImNTf_2 would not have much effect on the association equilibria shown above and, therefore, one would expect only a small conductivity enhancement. Conversely, adding a small amount of MeEtImNTf_2 to MeEtImTf should result in an increase in conductivity since MeEtImTf showed some degree of association at the lower temperatures. At the higher temperature, however, both MeEtImTf and MeEtImNTf_2 experience some degree of ionic association. Addition of the second component should therefore result in enhanced conductivity for the entire range of binary compositions. The diffusion and conductivity results at these two temperatures appear to support this theory.

The observations made for this binary system may not be indicative of other binary systems formed from different combinations of imidazolium salts. MeEtImTf and MeEtImNTf_2 have remarkably similar melting and glass transition temperatures, conductivities, diffusivities and viscosities. Mixing these salts to form a binary has been shown to have very little impact on the glass transition temperature²⁸, diffusivities and presumably the viscosities. Therefore, it can be concluded that the enhanced conductivity in this system does not result from any change to these properties. However, the same can not be said for other binary systems. Bishop²⁸

has studied a number of imidazolium binary systems and has concluded that there a number of factors responsible for the increased binary conductivities. Ion size, changes in viscosity and mobility and ionic association are all factors that may influence the transport mechanisms, with the extent of each factor dependent upon the system. Take, for example, the MeBuImTf/MeHxImI system studied by Papageorgiou and co-workers.² MeBuImTf has a much higher conductivity and considerably lower viscosity than MeHxImI. Adding MeBuImTf to MeHxImI increases the conductivity relative to pure MeHxImI, although the conductivity never exceeds that of MeBuImTf. Triiodide diffusion coefficients show very little variation up to approximately 80wt% MeBuImTf, after which there is a rapid increase. Analogous behaviour is observed for the viscosities in this binary. Consequently, viscosity and diffusion are related properties in this system. Similar behaviour has also been observed in other systems by Bishop.²⁸ It must therefore be noted that the simple analysis applied here to the MeEtImTf/MeEtImNTf₂ binary system should not be generalised to other binary systems.

In summary, a binary system formed from mixing MeEtImTf and MeEtImNTf₂ shows enhanced conductivities compared to the pure components. The same trend is not observed for the diffusion coefficients, however, which showed no appreciable deviation from a simple law of mixtures. Combining the pure salts alters the extent of ionic association, with the resultant increase in charge carrier concentration leading to increased conductivity.

3.4.3 The Alkyl Chain Length Effect

Different length alkyl chains have been substituted onto the 3 position of the imidazolium ring and the cation diffusion coefficients measured in each case. Figure 3-11, which compares the diffusion coefficients for all the salts, reveals a decrease in diffusion with increasing alkyl chain length. The same trend is also reflected in the

conductivity data²⁸ (Figure 3-23). The decrease in transport properties with increasing alkyl chain length is highlighted in isothermal conductivity (Figure 3-24) and diffusion (Figure 3-25) plots at 298K and 358K. At both temperatures, a steady decrease in conductivity is observed. It should be noted, however, that MeMeImI and MeEtImI are both solids at this 298K and MeMeImI is still solid at 358K. Under such conditions, ion transport is therefore in the solid state. It is interesting that the solid state conductivities and diffusivities for these two salts are higher than the liquid state transport properties for the other salts. At 298K, the diffusion coefficients show a decreases with increasing alkyl chain length. At 358K, however, proton diffusion shows a slight increase with alkyl chain length up to MePrImI, after which the longer alkyl chain lengths result in slower diffusion processes.

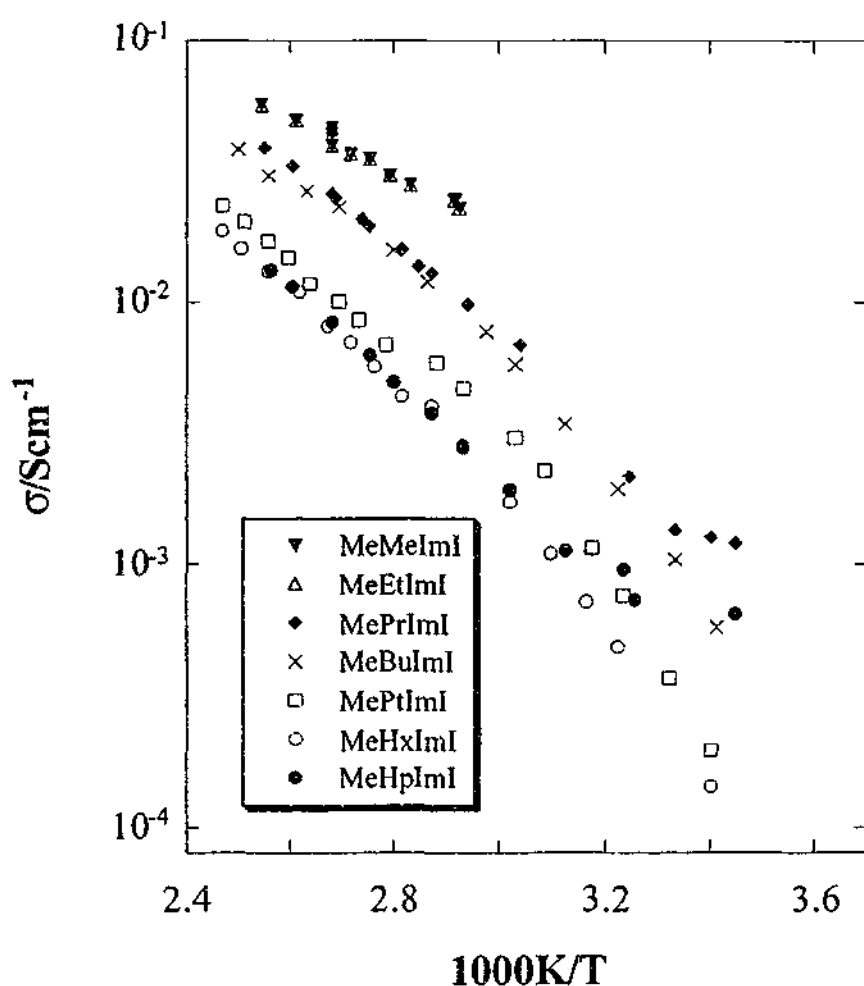


Figure 3-23 Conductivity as a function of temperature for the imidazolium salts with different alkyl substituents (reproduced from Bishop²⁸).

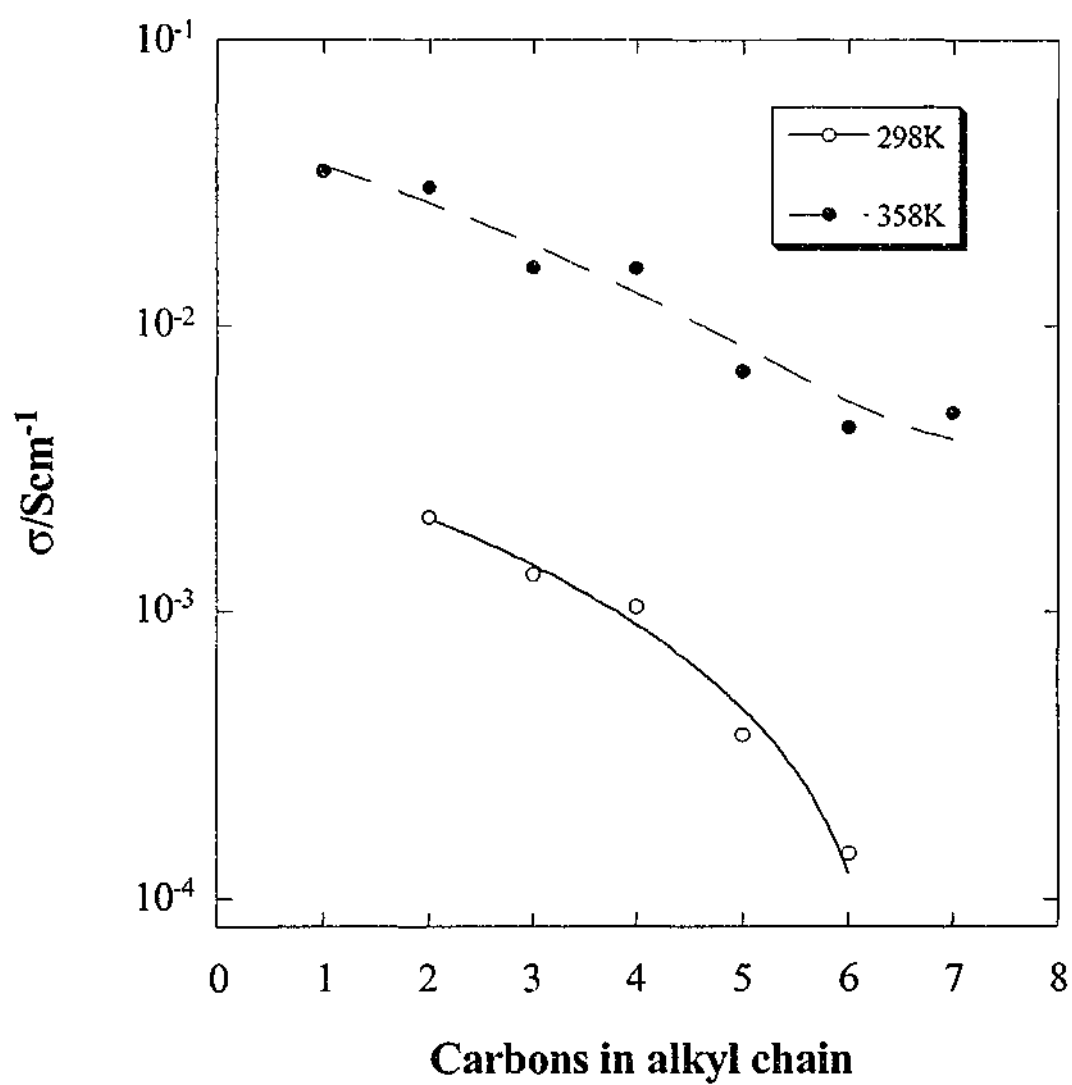


Figure 3-24 Isothermal conductivity plots for MeRImI (reproduced from Bishop²⁸). Lines are to guide the eye.

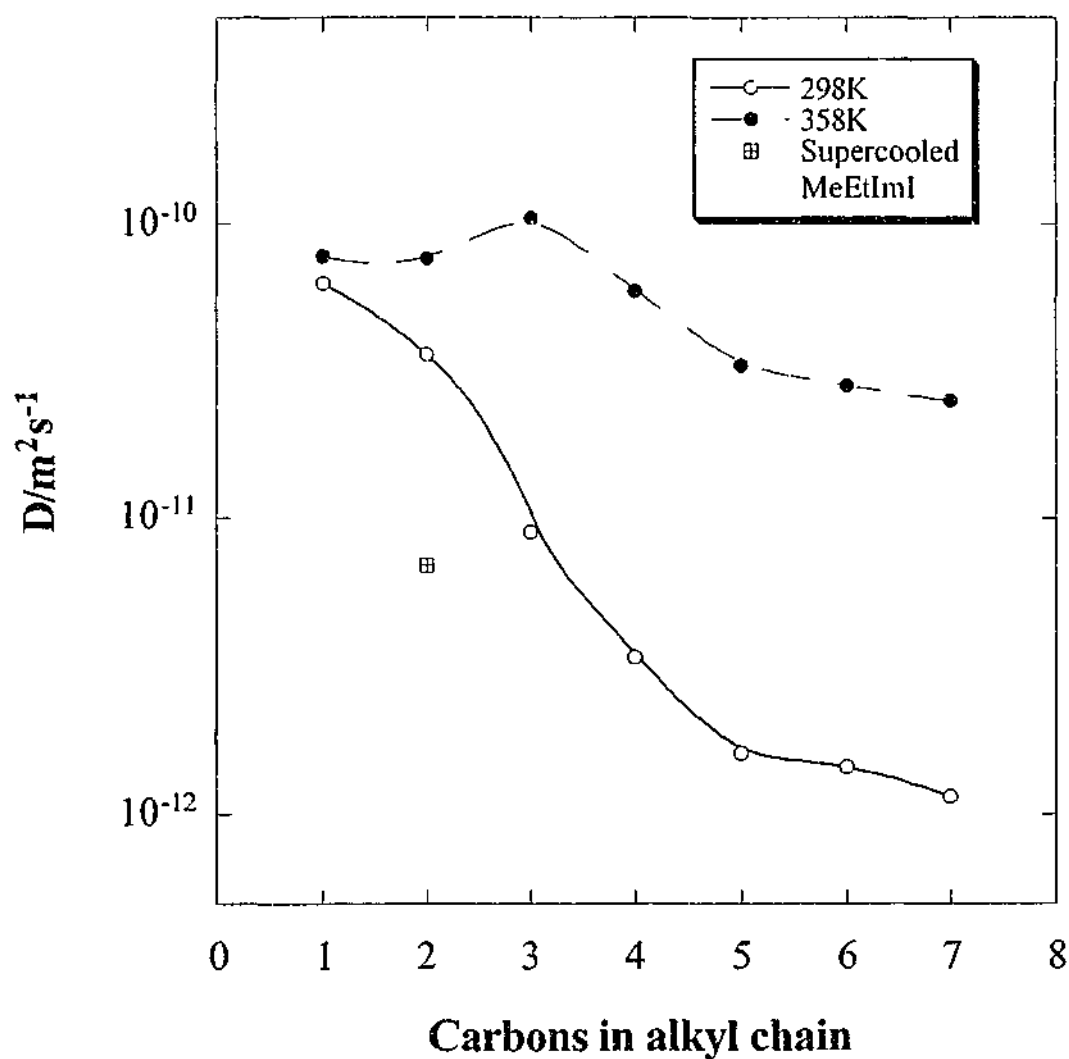


Figure 3-25 Isothermal diffusion plots for MeRImI. Lines are to guide the eye.

In section 3.4.1, the effect of the anion on the diffusion process was analysed. Despite a common cation, there were differences in the cation diffusion coefficients. Although varying degrees of ion association were observed, this did not appear to contribute to the resultant diffusion behaviour. The main conclusion drawn from this analysis was that diffusion is related to viscosity. With this iodide series of salts, however, the imidazolium ring has been altered by changing the length of the alkyl substituents. In this case, diffusion will possibly be sensitive to both viscosity and

cation size (see Equation 3-1 in section 3.4.1.1). The following is an analysis of the diffusion mechanism in these salts.

Analysing the effect of viscosity on the transport properties is limited to the liquid state. However, the diffusion coefficients for MeMeI and MeEtI at 298K are in the solid state and at 358K, MeEtI has only just melted while MeMeI is still solid. The conductivities in the solid state for these salts are much higher than for the other iodide salts in the liquid state, which is probably due to the difference in transport mechanism. The solid state transport process will most likely involve discrete jumps of individual ions. The liquid state diffusion mechanism, however, probably involves the cooperative motion of large amounts of the material.³⁹ It is, therefore, inappropriate to compare these two transport mechanisms, and consequently, the isothermal diffusion plot at 298K is misleading. The liquid state diffusion coefficients for supercooled MeEtI have been measured, however, using the fringe field diffusion method. In comparing this value to the other liquid state values (Figure 3-25), MeEtI has a lower diffusion coefficient than MePrI, reflecting the trend observed at 358K. The effect of viscosity on the diffusion properties for the salts in the liquid state will now be considered.

Due to the high melting points for MeMeI and MeEtI, one would expect the viscosities to be consistently higher than for the other salts. The viscosity for MeEtI was extrapolated to be 93cP at 348K,¹³ while Papageorgiou *et al.*² have reported a viscosity of 75cP for MeHxI at the same temperature. It must be noted that the value quoted for MeEtI at this temperature is the predicted value for the supercooled state. Although no viscosities have been measured for the other salts in this series, the viscosity of MePrI was found to be much lower than MeHxI upon handling the materials. The initial increase in diffusion coefficient that accompanied the change in cation from MeEtI⁺ to MePrI⁺ is thus probably due to

a decrease in viscosity. The subsequent decrease in diffusion coefficient with increasing alkyl chain length is likely to be related to the increasing viscosity.

If the transport properties were solely dependent on the viscosity of the salt, one would expect MeHxImI to have a larger diffusion coefficient than MeEtImI. In studying the anion effect (see section 3.4.1), this was found to be the case where cation diffusion correlated to the viscosity. The data in Figure 3-25, however, actually shows faster diffusion for MeEtImI than MeHxImI. Therefore, the size of the cation would also appear to have some influence on the diffusion properties. MeEtIm⁺ is a much smaller cation and would be expected to diffuse more readily throughout the material. MeHxIm⁺ is a much larger cation with a long alkyl substituent, which should limit its mobility.

Angell and Moynihan³⁹ have pursued further the relationship between diffusivity and the size of the diffusing entity. According to configurational entropy theory, the following equation can be used to model the diffusion data.

$$D = AT^{1/2} \exp\left(\frac{-k}{T - T_0}\right)$$

Equation 3-11

In this equation, T is temperature, k is a pseudo activation energy and T_0 is the ideal glass transition temperature. The pre-exponential term, A , is considered to be proportional to the radius, r , and the mass, m , of the diffusing species as follows.

$$A \propto \frac{r}{m^{1/2}}$$

Equation 3-12

By plotting $D/T^{1/2}$ versus $1/T-T_0$ (Figure 3-26) and fitting the above equation, the constant A can be determined for each salt. The T_g values for these salts are listed in Table 3-6 and T_0 was taken to be T_g-50K . The calculation was not performed for MeMeImI as only solid state diffusion coefficients were measured for this salt. From the calculated A values and the molecular weights of each cation (also shown in Table 3-6), Equation 3-12 can be rearranged to examine the effect of cationic radius on the diffusion properties. $A.m^{1/2}$ will be the same for all the salts if the diffusion coefficients are independent of the cation size. This product as a function of alkyl chain length is shown in Figure 3-27.

Table 3-6 Molecular weights and densities for MeRImI.

Salt/MeEtImX	T_g/K	MeRIm ⁺ MW/g.mol ⁻¹
MeEtImI	234†	111.17
MePrImI	203	125.20
MeBuImI	202	139.22
MePtImI	204	153.25
MeHxImI	203	167.28
MeHpImI	205	181.3

† Calculated from the melting point (see section 3.4.1.1)

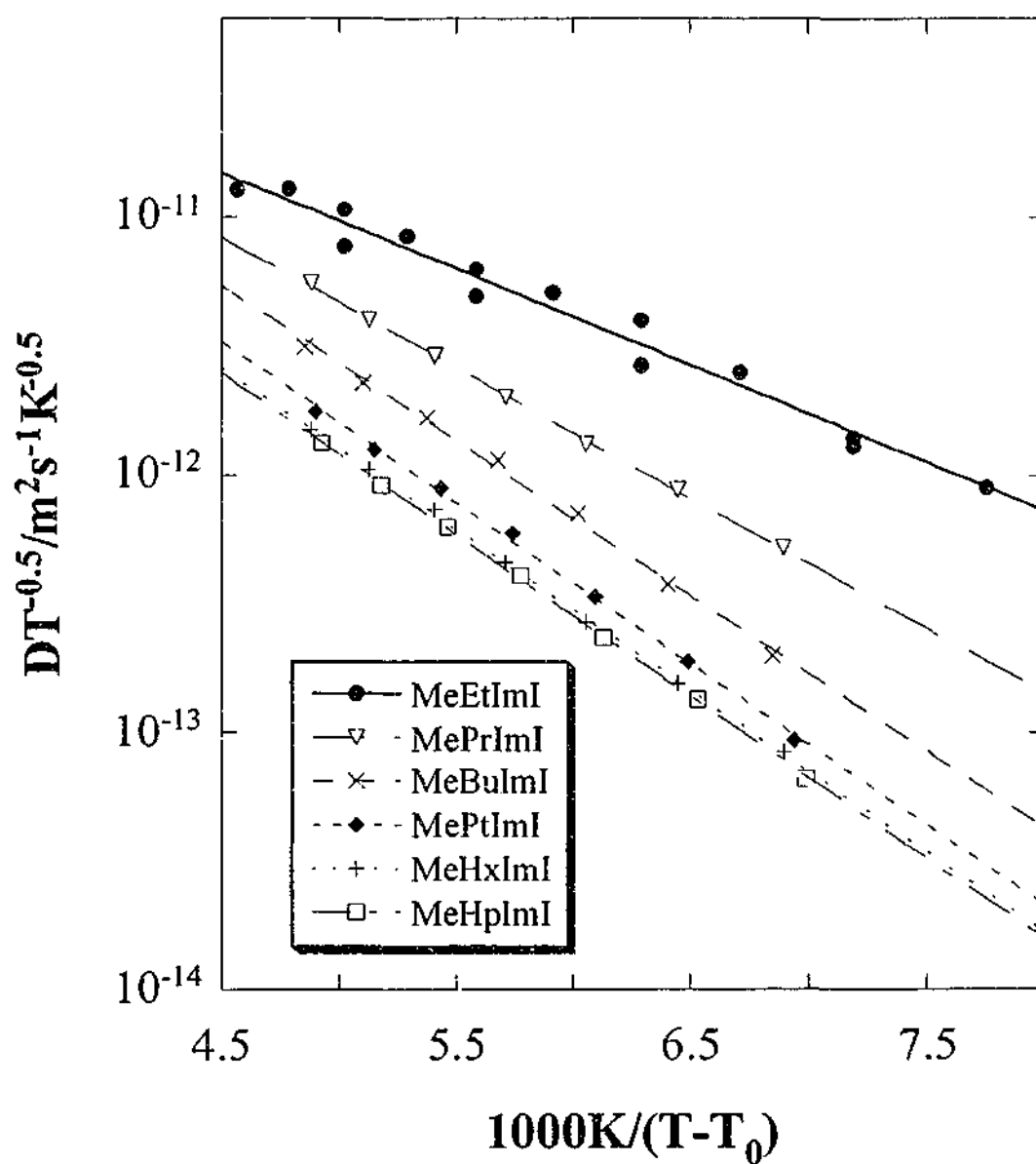


Figure 3-26 $DT^{-1/2}$ versus $1/T-T_0$ for the MeRIml salts. Data fitted with Equation 3-11.

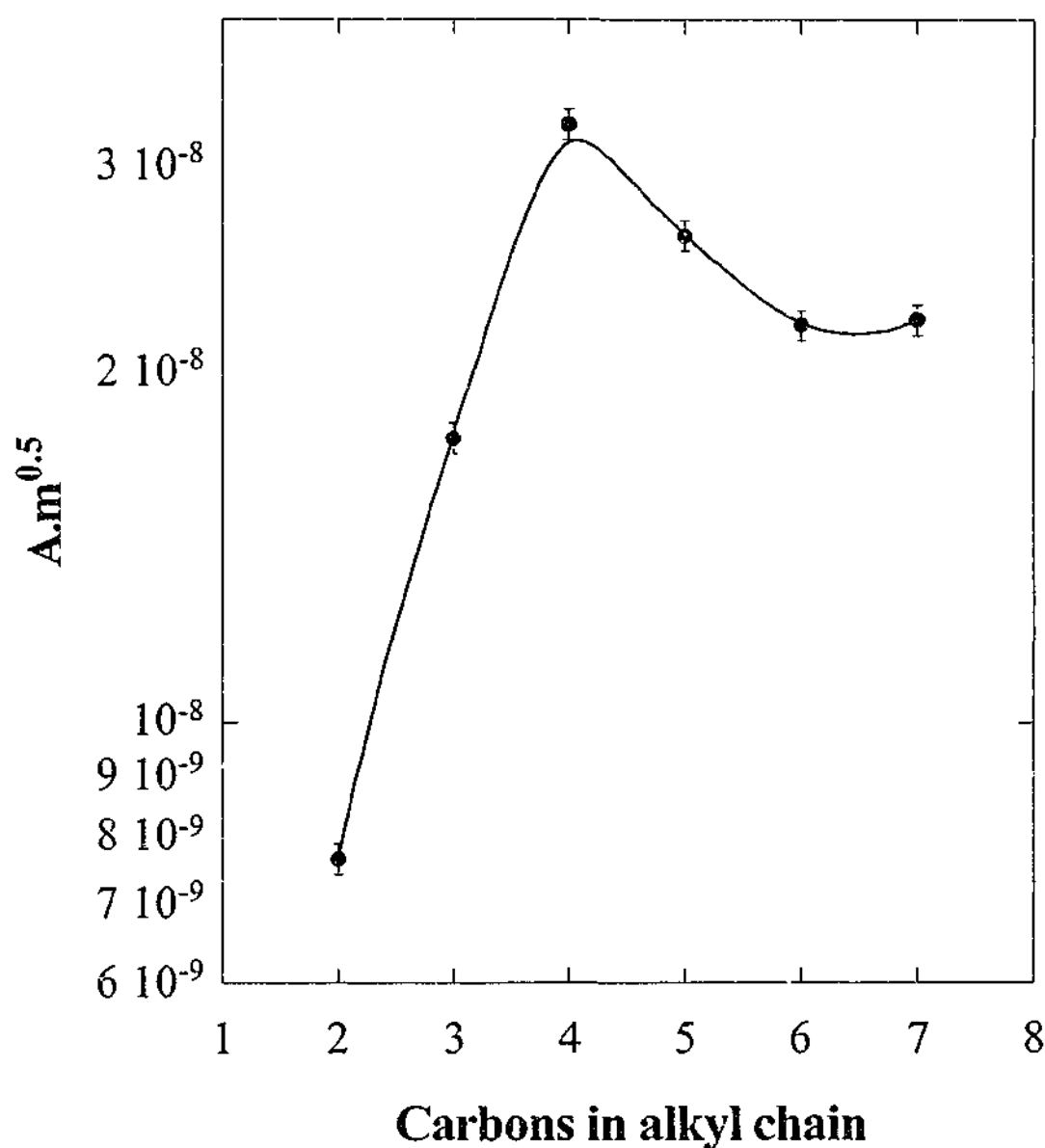


Figure 3-27 The calculated ionic radius as a function of alkyl chain length. The line is to guide the eye.

The results imply that the cation radius initially increases with increasing alkyl chain until MeBuImI. A further increase in alkyl chain length results in a decrease in ionic radius before reaching a plateau at MeHxImI and MeHpImI. Initially, these results may appear to be impossible, as one would intuitively expect the larger cations to occupy more volume. However, infrared analysis by Bishop²⁸ did imply that intramolecular interactions are possible between the imidazolium ring and the alkyl

chain if the alkyl chain is capable of folding back over the ring. The size of the cation would therefore be smaller than expected. Such an analysis should be performed with caution, however, as the constant A is particularly sensitive to the choice of T_0 .³⁹ The qualitative conclusion that can be drawn from this analysis is that the diffusion in these systems is dependent on the size of the cation.

The same trends were observed in comparing the diffusion coefficients to the conductivities of these salts. An increase in the alkyl chain resulted in a decrease in both the diffusivity and conductivity data. Despite the absence of iodide diffusion data, it would appear that the cation dominates the ionic transport mechanism in these salts. In accordance with the anion effect behaviour, the diffusion coefficients in this series of salts are related to the viscosity. Furthermore, the size of the cation is also a factor contributing to the diffusion mechanism.

3.4.4 Solid State Diffusion

Although most of the interest in these materials has been with the molten state, there was also evidence of good conduction in the solid state for MeEtImBr and MeEtImI. Therefore, some attempt has been made to understand the conduction mechanism in this state, as the salts could be of interest for solid state devices.

The two salts that showed diffusion in the solid state were MeEtImBr and MeEtImI, which have melting points at 352K and 351K respectively. The conductivities for these salts have been reproduced from the work of Bishop²⁸ and are shown in Figure 3-16. The solid state conductivity is of the order of 10^{-3}S.cm^{-1} , which is comparable to some of the liquid state conductivities observed for other dialkylimidazolium salts.²⁸ An obvious discontinuity is observed in this conductivity data where the conduction mechanism appears to change from a solid state diffusion process to a liquid state process. For both salts, however, this transition occurs at a temperature

slightly lower than the melting point and could be due to supercooling, a phenomenon observed in the diffusion measurements (as discussed in section 3.3).

The proton diffusion coefficients for these salts are shown in Figure 3-3 and Figure 3-4. These results show a change in behaviour around the melting point of the salt, indicating a change in the diffusion mechanism. Unlike for the conductivity data, however, the change is not accompanied by a step increase in the diffusion coefficient but only by a change in the activation energy for the transport mechanism. The diffusion coefficients in the solid state are therefore almost the same as those observed above the melting point and actually greater than those observed in the supercooled state.

It was initially suspected that these diffusion coefficients were affected by the T_2 behaviour in these materials (see section 2.1.5.2 in Chapter 2). In measuring diffusion coefficients with the fringe field method, both diffusion and spin-spin (T_2) relaxation can contribute to the signal attenuation, particularly if T_2 is shorter than the tau values used in the experiment. Since T_2 in solids is often quite short, one might expect that these materials will also have small T_2 values. The pulsed field gradient method for measuring diffusion coefficients, however, does not suffer from the same T_2 interference and signal attenuation is solely due to diffusion. Diffusion in MeEtImI has also been studied using the PFG method and a comparison of these two diffusion techniques is shown in Figure 3-28. The diffusion results are very similar in the solid state, confirming that the measurements from the fringe field method are valid.

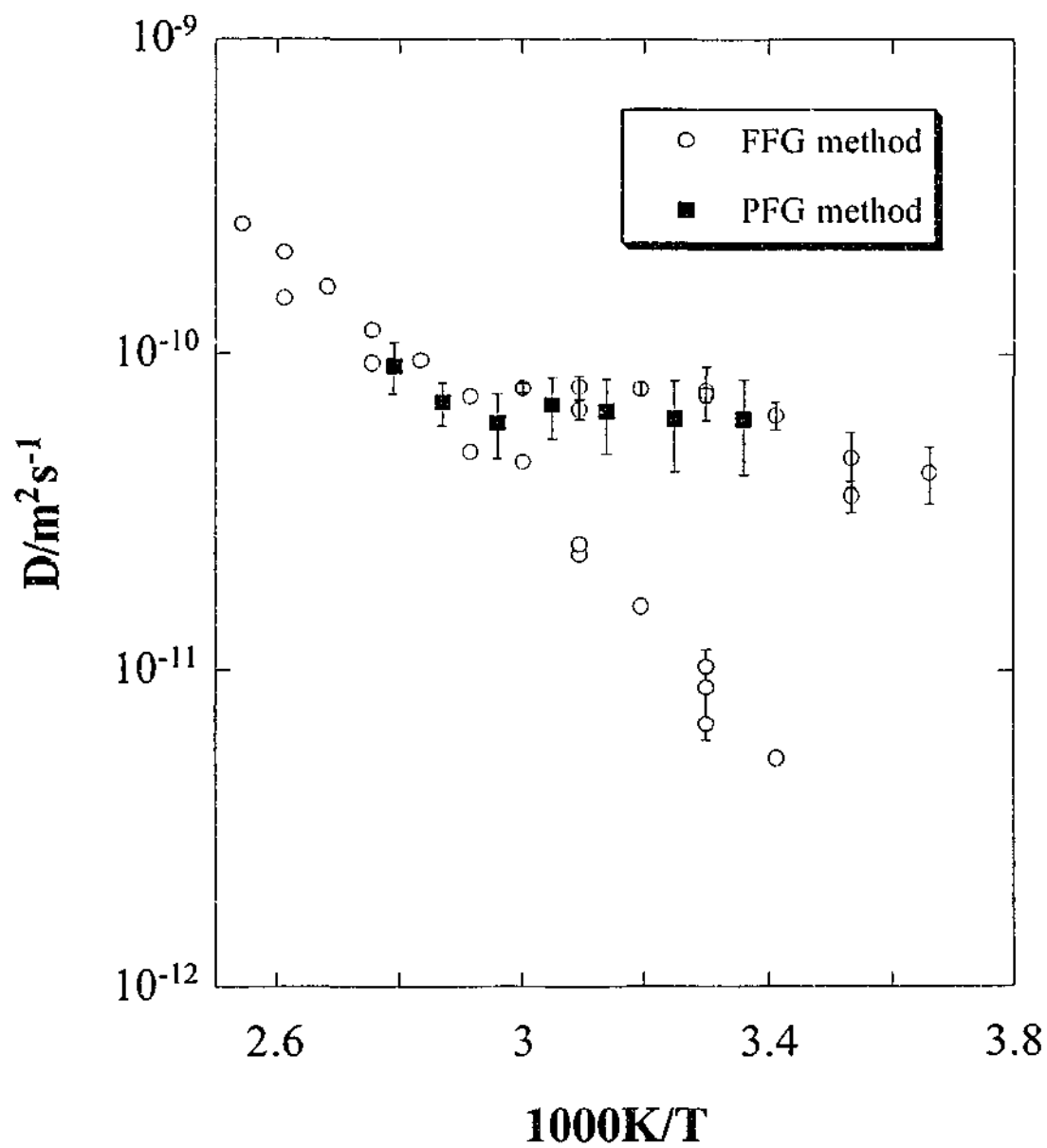


Figure 3-28 Comparison of fringe field and pulsed field gradient NMR techniques for MeEtImI.

As outlined in Chapter 1, the most common transport mechanisms in solids are associated with interstitial and vacancy diffusion. Interstitial sites are voids, or empty space, that are not normally occupied in a crystal lattice, whereas the vacancies are lattice sites where the atom is absent. Interstitial diffusion involves migration from one interstitial site to another available interstitial site. Small atoms or molecules undergo interstitial diffusion because they are able to fit easily into these voids. Larger atoms and even the host atoms are unlikely to undergo interstitial diffusion because they are not normally found at interstitial sites. Since interstitial atoms are rather small, this mode of diffusion is normally quite rapid and will generally occur in preference to a vacancy mechanism. Vacancy diffusion involves the migration of an atom from one lattice site to another vacant, lattice site. This mechanism is more likely to occur in a self-diffusion process whereby the host material diffuses to these vacancies. The formation of vacancies is a temperature dependent process and can be calculated using the following equation:

$$N_v = N \exp\left(\frac{-Q_v}{RT}\right)$$

Equation 3-13

where N_v is the number of vacancies, N is the total number of atomic sites, Q_v is the activation energy (vibrational energy) for vacancy formation, R is the gas constant and T is temperature. MeEtImBr and MeEtImI are isomorphous and their crystal structures have been reported by Elaiwi *et al.*²⁰ The cations and anions appear to form alternate layers held together by intermolecular hydrogen bonding. One can envisage that the presence of vacancies these layers would provide a suitable 2-dimensional pathway for ion diffusion.

The solid state diffusion results presented herein predict a change in the conduction mechanism near the melting points for these salts, as indicated by a change in

activation energy. However, the diffusion data fails to explain why the change in ion transport is accompanied by a jump in conductivity of almost an order of magnitude as the materials go from solid to liquid. Recall from the Nernst-Einstein equation (Equation 3-8) that conductivity is not only dependent on the diffusion coefficients but also on the number of charge carriers involved in the conduction process (see section 3.4.1.2). Therefore, the lower absolute conductivity in the solid state must be the result of fewer mobile charge carriers.

The number of charge carriers available for conduction can be analysed by monitoring the NMR signal intensity. The signal intensity is typically governed by the Boltzmann distribution (Equation 2-3 in section 2.1.1), which predicts that an increase in the temperature would produce a slight decrease in signal intensity. In performing a fringe field NMR diffusion experiment, however, only nuclei moving on the time scale of the experiment will be detected. Any nuclei that are effectively immobile will not be observed and thus have no contribution to the signal intensity. Therefore, if there is a change in the number of mobile charge carriers as the temperature increases, one would expect to observe a change in the signal intensity. The signal intensities for these two salts were obtained from the diffusion measurements by measuring the echo intensity at an echo time of 100 μ s. Shorter echo times were not chosen as they are often susceptible to errors in the diffusion measurement. Although these intensities may not reflect the absolute number of nuclei in the sample, they are valid in a comparative sense. The intensities were measured upon heating and cooling of the samples, and the results are shown in Figure 3-29 and Figure 3-30.

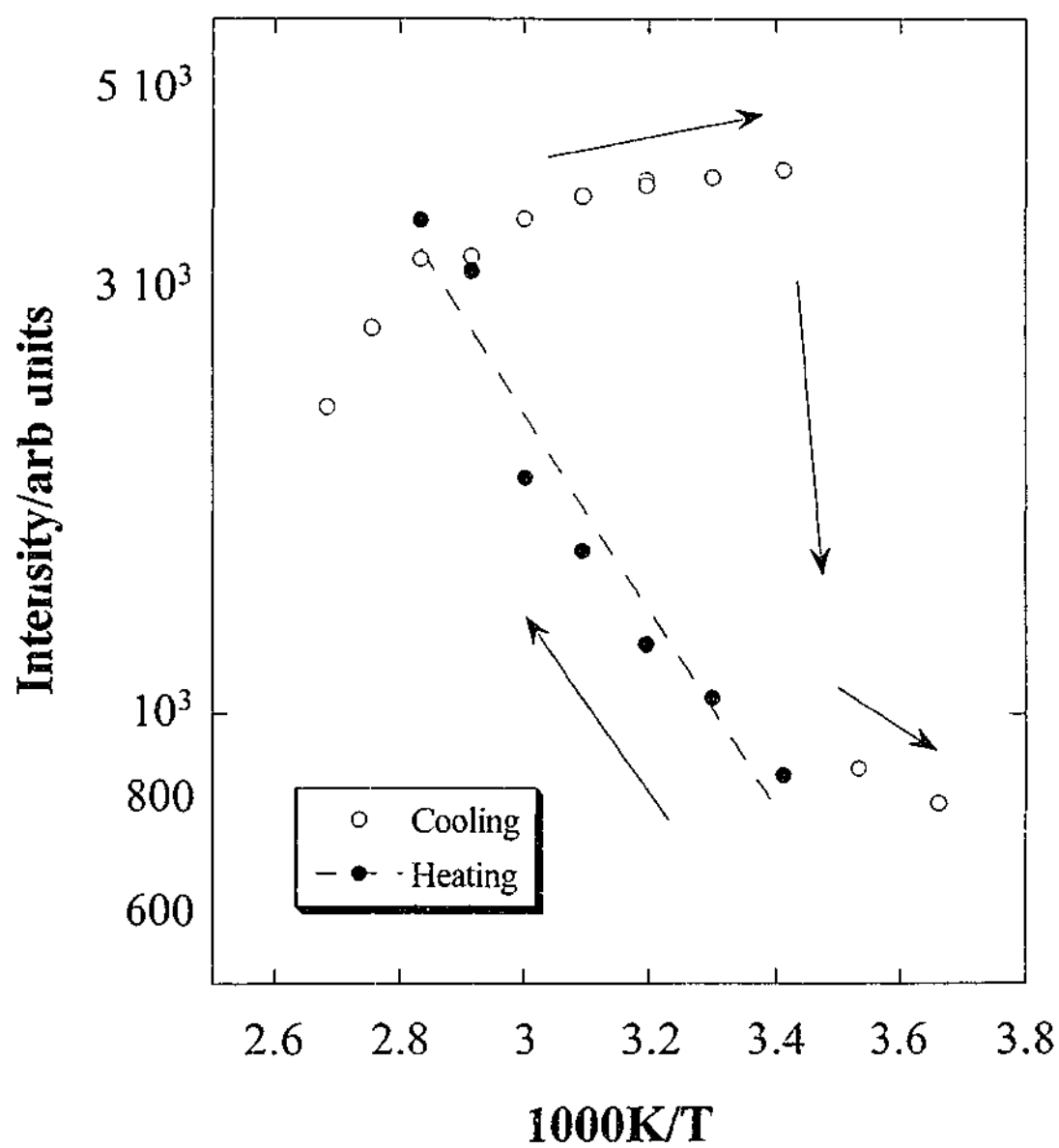


Figure 3-29 NMR signal intensity as a function of temperature for MeEtImBr. Data fitted with Equation 3-13.

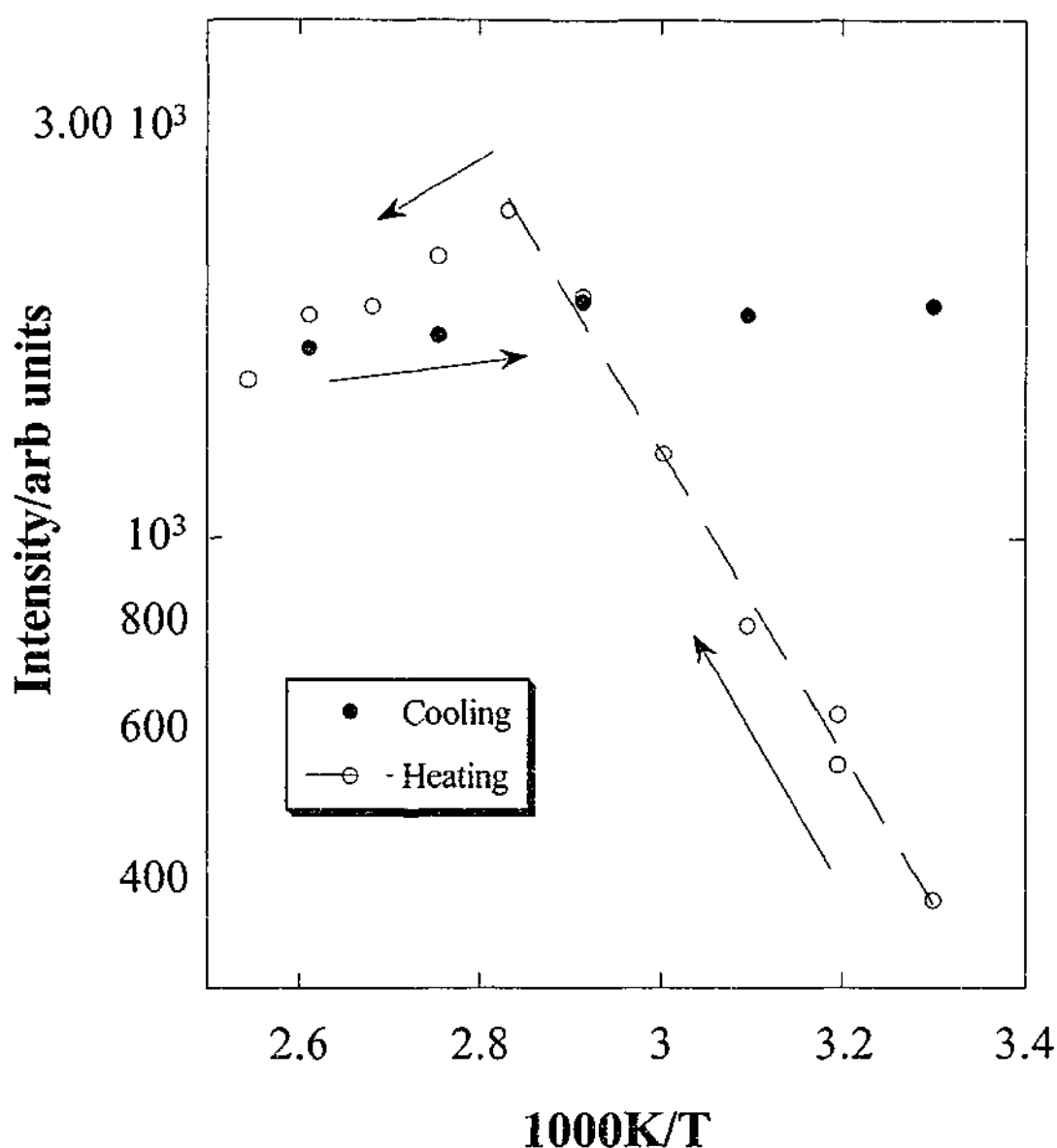


Figure 3-30 NMR signal intensity as a function of temperature for MeEtImL. Data fitted with Equation 3-13.

Upon cooling the samples from 403K down to room temperature, the signal intensity showed very little change with temperature, even below the expected melting point of the material. Such behaviour is expected from the Boltzmann distribution. The diffusion coefficients measured under the same conditions also showed no abrupt change around the melting point but rather a continual steady decrease with decreasing temperature (Figure 3-3 and Figure 3-4). Consequently, it would seem

that, upon cooling these salts, supercooling of the liquid state occurs and the diffusion coefficient continues to exhibit a liquid-like mechanism. At a suitable level of undercooling, the crystallisation process was observed, highlighted by the sudden decrease in signal intensity. This transition temperature occurred between 283 and 293K, about 70K below the DSC melting points of the materials. The signal intensities were then observed as the measurements were made upon heating. The initial intensities were low, as the materials were crystalline, but increasing the temperature resulted in a steady increase in signal intensity. Once the temperature had exceeded the melting point, the intensity then began to decrease slightly as expected from the Boltzmann behaviour. The increase in signal intensity in the solid state as the temperature increases suggests that more charge carriers are becoming available. Earlier, it was proposed that diffusion occurs via a vacancy mechanism and that vacancy formation can be modelled using Equation 3-13. The temperature dependence for the signal intensity showed a linear relationship when plotted as $\log(\text{Intensity})$ versus $1/T$ (Figure 3-29 and Figure 3-30), implying that this equation may be appropriate for modelling the increase in signal intensity.

Closer examination of the signal intensity for these salts indicates that there is a steady increase in the number of mobile ions with heating up to the melting point. Therefore, the change in charge carrier concentration does not appear to adequately explain the jump in the conductivity data. In the solid state, however, it is possible that the anion may be immobile and since no diffusion coefficients have been measured for the bromide nor the iodide anions, it is difficult to predict their behaviour. The Nernst-Einstein equation has been used to calculate the solid state conductivity based on each of two assumptions: that both ions are diffusing, or that only the cation (MeEtIm^+) is mobile. For the calculation where both ions are mobile, the anion was assumed to have the same diffusion coefficient as the cation. The concentration of mobile ions in the solid state was taken from fitting the NMR signal intensity data with the vacancy formation equation (Equation 3-13, the parameters of which are shown in Table 3-7). Above the melting points, the concentration of

mobile species was determined from the densities of the materials and the diffusion coefficients were taken to be the liquid state values.

Table 3-7 Parameters for calculating ion concentration from Equation 3-13.

Salt/MeEtImX	N/ions.cm ⁻³	Q _v /kJ.mol ⁻¹
MeEtImBr	5.88x10 ²⁴	21.0 ± 2.2
MeEtImI	5.11x10 ²⁶	34.2 ± 1.9

A comparison of the calculated conductivities and the measured conductivities reveals some interesting results (Figure 3-31 and Figure 3-32). The calculation assuming that both ions are mobile in the solid state generally overestimates the conductivity. However, if it is assumed that only the cation is mobile, the results are consistent with the measured conductivities. There is some discrepancy in the absolute calculated and measured conductivities for MeEtImI, which is possibly due to the errors in the data and the assumptions made in performing this calculation. However, the trends quite clearly show that the conductivity in the solid state is the result of cation diffusion and that the charge carrier concentration can be adequately estimated from the signal intensity in the fringe field NMR diffusion experiments. The anions in this case would seem to be relatively immobile and are therefore probably involved in maintaining the crystal lattice through which the cations are diffusing. The differences in conductivity above the melting point have been discussed earlier (section 3.4.1.2) and are most likely the result of ionic associations in the salt.

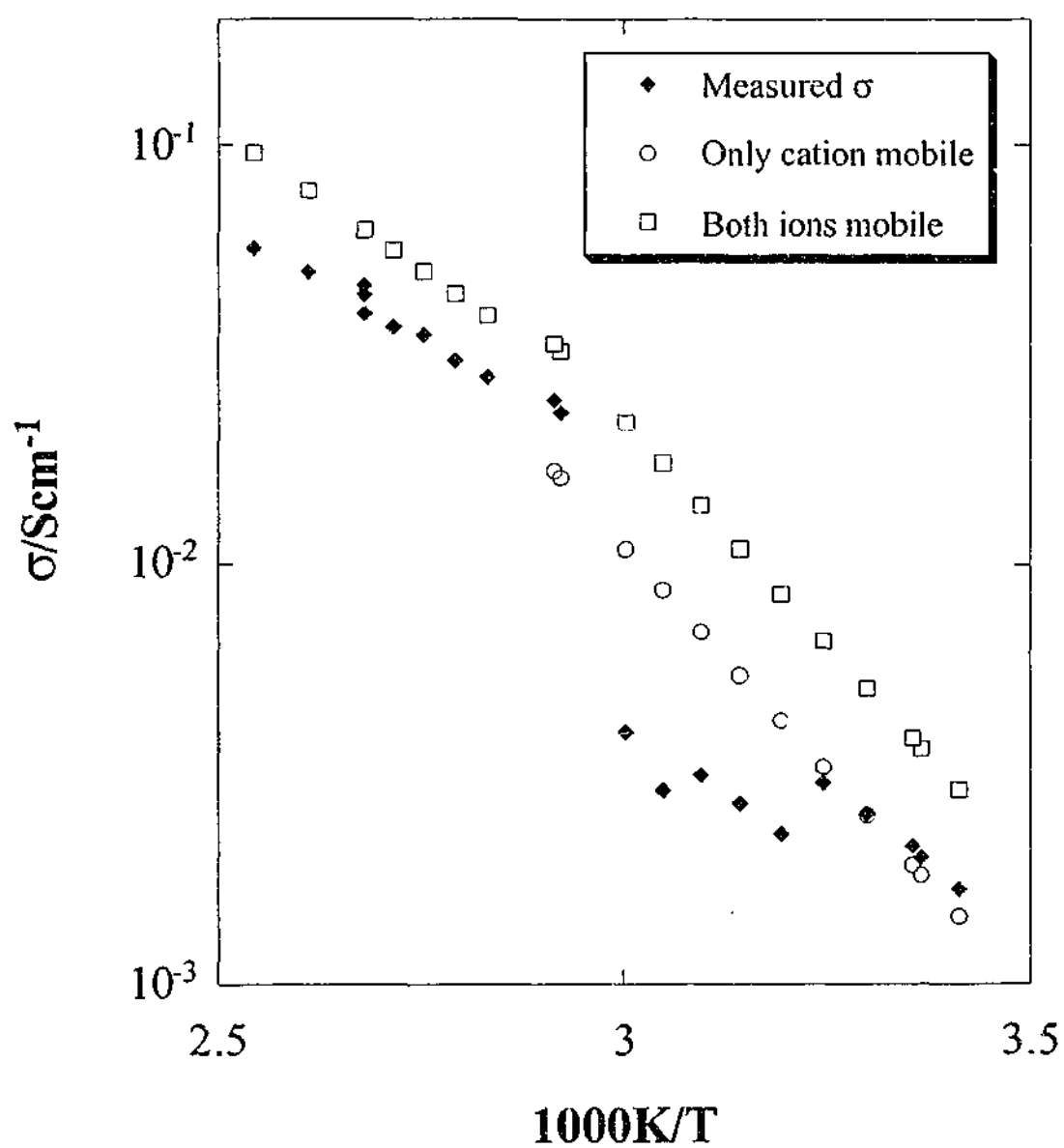


Figure 3-31 A comparison of the measured and calculated conductivities for MeEtImI.

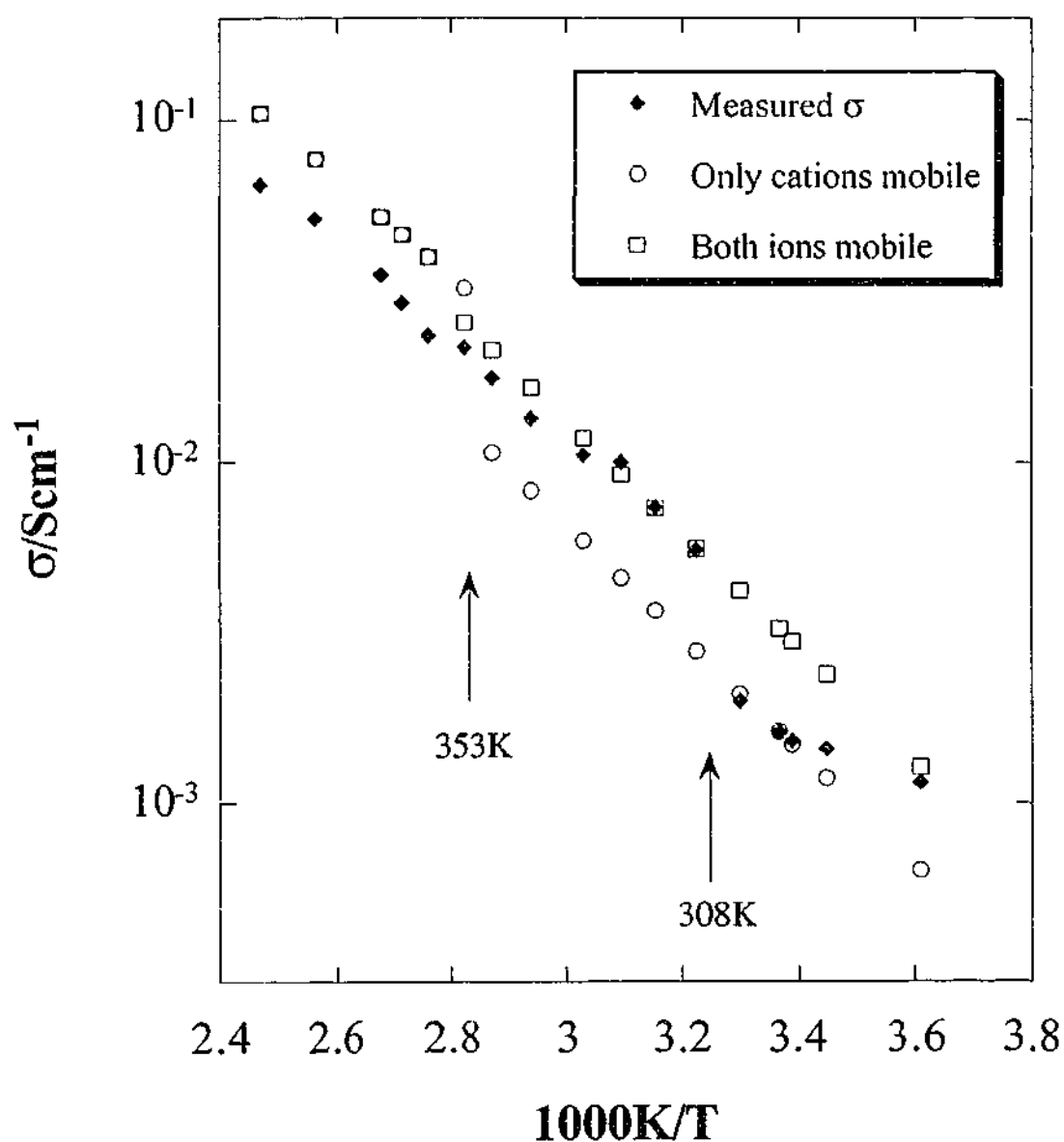


Figure 3-32 A Comparison of the measured and calculated conductivities for MeEtImBr.

For MeEtImBr, the diffusion process changes from a solid state to liquid state mechanism at approximately 353K. The jump in conductivity, however, is observed at a much lower temperature, approximately 308K. This difference is possibly due to supercooling in the conductivity measurement, which was also found to occur under certain conditions in the diffusion measurements. What is interesting though, is the similarity between the measured conductivities and the calculated solid state

conductivities when it is assumed that both ions are mobile (Figure 3-32). It is possible that over a certain temperature range, both ions exhibit some mobility in the solid state. In the absence of any anion diffusion data for this salt, and given the assumptions made during the calculations, it is difficult to draw firm conclusions from this analysis.

To summarise, high solid state conductivities have been observed in these imidazolium salts, with values of the order of 10^{-3}S.cm^{-1} . Near the melting point, there is an abrupt change in the conduction mechanism and an associated sudden increase in conductivity. Cation diffusion in the solid state was found to occur readily, and was faster than the diffusion observed in the supercooled liquid. This behaviour in the solid state suggests that these salts are fast ion conductors, probably belonging to the family of plastic crystals, and that a vacancy process is responsible for ion transport. A change in the diffusion mechanism was also observed near the melting point, but this was not accompanied by a sudden increase in the cation diffusion coefficients. Through the use of the Nernst-Einstein equation, the conductivity was modelled from the diffusion coefficients. Although no anion diffusion coefficients were measured, the conductivity was adequately predicted by assuming that only the cation is mobile and that the charge carrier concentration increases with temperature due to vacancy formation.

3.5 References

1. K. R. Seddon, *J. Chem. Tech. Biotechnol.* **68**, 351-356 (1997).
2. N. Papageorgiou, Y. Athanassov, M. Armand, P. Bonhôte, H. Pettersson, A. Azam and M. Grätzel, *J. Electrochem. Soc.* **143**, 3009-3108 (1996).
3. J. A. Boon, J. S. Wilkes and J. A. Lanning, *J. Electrochem. Soc.* **138**, 465-469 (1991).

4. C. J. Dymek and L. A. King, *J. Electrochem. Soc.* **132**, 1375-1380 (1985).
5. A. A. Fannin, D. A. Floreani, L. A. King, J. S. Landers, B. J. Piersma, D. J. Stech, R. L. Vaughn, J. S. Wilkes and J. L. Williams, *J. Phys. Chem.* **88**, 2614-2624 (1984).
6. A. A. Fannin, L. A. King, J. A. Levisky and J. S. Wilkes, *J. Phys. Chem.* **88**, 2609-2614 (1984).
7. J. S. Wilkes, J. A. Levisky, R. A. Wilson and C. L. Hussey, *Inorg. Chem.* **21**, 1263-1264 (1982).
8. C. L. Hussey, *Pure Appl. Chem.* **60**, 1763-1772 (1988).
9. C. L. Hussey and H. A. Øye, *J. Electrochem. Soc.* **131**, 1621-1625 (1984).
10. C. L. Hussey and J. R. Sanders, *J. Electrochem. Soc.* **134**, 1977-1980 (1987).
11. C. L. Hussey, J. R. Sanders and H. A. Øye, *J. Electrochem. Soc.* **132**, 2156-2158 (1985).
12. C. L. Hussey, I.-W. Sun, S. K. D. Strubinger and P. A. Barnard, *J. Electrochem. Soc.* **137**, 2515-2516 (1990).
13. J. R. Sanders, E. H. Ward and C. L. Hussey, *J. Electrochem. Soc.* **133**, 325-330 (1986).
14. J. R. Sanders, E. H. Ward and C. L. Hussey, *Electrochem. Soc. Ext. Abs.* **85-2**, 726 (1987).
15. X.-H. Xu and C. L. Hussey, *J. Electrochem. Soc.* **140**, 1226-1233 (1993).
16. F.-M. Lin and C. L. Hussey, *J. Electrochem. Soc.* **140**, 3093-3096 (1993).
17. S. A. Bolkan and J. T. Yoke, *J. Chem. Eng. Data* **31**, 194-197 (1986).
18. J. L. E. Campbell, K. E. Johnson and J. R. Torkelson, *Inorg. Chem.* **33**, 3340-3345 (1994).
19. W. R. Carper, G. J. Mains, B. J. Piersma, S. L. Mansfield and C. K. Larive, *J. Phys. Chem.* **100**, 4724-4728 (1996).

20. A. Elaiwi, P. B. Hitchcock, K. R. Seddon, N. Srinivasan, Y.-M. Tan, T. Welton and J. A. Zora, *J. Chem. Soc. Dalton Trans.* **21**, 3467-3472 (1995).
21. C. E. Keller and W. R. Carper, *Inorg. Chim. Acta* **238**, 115-120 (1995).
22. C. K. Larive, M. Lin, B. S. Kinnear, B. J. Piersma, C. E. Keller and W. R. Carper, *J. Phys. Chem. B* **102**, 1717-1723 (1998).
23. J. Fuller, R. T. Carlin, H. C. D. Long and D. Haworth, *J. Chem. Soc., Chem. Commun.* **3**, 299-300 (1994).
24. J. Fuller, R. T. Carlin and R. A. Osteryoung, *J. Electrochem. Soc.* **144**, 3881-3886 (1997).
25. P. Bonhôte, A.-P. Dias, N. Papageorgiou, K. Kalyanasundaram and M. Grätzel, *Inorg. Chem.* **35**, 1168-1178 (1996).
26. A. B. McEwen, H. L. Ngo, K. LeCompte and J. L. Goldman, *J. Electrochem. Soc.* **146**, 1687-1695 (1999).
27. J. J. Golding, D. R. MacFarlane, L. Spiccia, M. Forsyth, B. W. Skelton and A. H. White, *Chem. Commun.* **15**, 1593-1594 (1998).
28. A. G. Bishop, Ph.D Thesis, Monash University, Melbourne, Australia 1999.
29. W. R. Carper, J. L. Pflug, A. M. Elias and J. S. Wilkes, *J. Phys. Chem.* **96**, 3829-3833 (1992).
30. N. Weiden, B. Wittekopf and K. G. Weil, *Ber. Bunsenges. Phys. Chem.* **94**, 353-358 (1990).
31. H. Every, A. G. Bishop, M. Forsyth and D. R. MacFarlane, *Electrochim. Acta* **45**, 1279-1284 (2000).
32. A. Einstein, *Investigations on the Theory of the Brownian Movement* (Methuen and Co. Ltd., London, 1926).
33. M. H. Cohen and D. Turnbull, *J. Chem. Phys.* **31**, 1164-1169 (1959).
34. M. Ue, *J. Electrochem. Soc.* **141**, 3336-3342 (1994).

35. A. J. Batschinski, *Z. Phys. Chem.* **84**, 644 (1913).
36. A. K. Doolittle, *J. Appl. Phys.* **22**, 1471-1475 (1951).
37. M. L. Williams, R. F. Landel and J. D. Ferry, *J. Am. Chem. Soc.* **77**, 3701-3707 (1955).
38. G. Tarjus and D. Kivelson, *Los Alamos Natl. Lab. Prepr. Arch. Condens. Matter*, 1-34 (2000).
39. C. A. Angell and C. T. Moynihan, in *Molten Salts*, edited by G. Mamantov (Marcel Dekker Inc., New York, 1969), pp. 315-375.
40. G. Adam and J. H. Gibbs, *J. Chem. Phys.* **43**, 139-146 (1965).
41. F. W. Billmeyer, Jr., *Textbook of Polymer Science*, 3rd ed. (John Wiley and Sons, Inc., New York, 1984).
42. W. D. Callister, *Materials Science and Engineering, an Introduction* (John Wiley and Sons, Inc., 1991).
43. A. Klemm, in *Molten Salt Chemistry*, edited by M. Blander (Interscience Publishers, John Wiley and Sons, Inc., New York, 1964), pp. 535-606.

Chapter Four

Pyrrolidinium Salts

4.1 Introduction

Some of the fastest ion conduction has been observed in solids such as sodium β -alumina and NASICON ceramics.¹ However, the brittle nature of these electrolytes precludes them from many battery applications, except where the electrodes themselves are flexible (eg. Na-S battery). A family of softer ionically conducting crystalline materials, known as plastic crystals, has shown some promise as a possible alternative solid ionic conductor. The soft, "plastic" nature exhibited by these materials is the result of orientational disorder in the crystal lattice as the molecules or ions undergo rotation around one or more of their axes.² The self-diffusion coefficients for these materials have also been reported to be much higher than those for brittle solids.³ Therefore, these plastic crystals show evidence of fast ion conduction - ionic transport occurs through a largely immobile lattice - but have the advantage of lacking the rigidity seen in ceramics and glasses. Plastic crystal behaviour has been reported for many molecular crystals,³⁻¹⁶ and also more recently for several ionic materials.¹⁷⁻⁵² The following is a brief history of such materials.

4.1.1 Orientational Disorder in Molecular Crystals

Although molecular crystals are neutral solids and thus unable to conduct, an initial discussion of the plastic crystal behaviour observed in these materials is necessary in order to introduce the phenomenon. The idea that molecules can be rotating in a crystal was proposed initially by Simon and von Simson⁴ in their study of hydrogen chloride. The same concept was also suggested by Müller,⁵ who reported the

presence of a "rotator phase" in n-paraffins. Over the last 80 years, numerous molecular crystals have been found to exhibit plastic crystal behaviour, with a number of books and review articles devoted to the subject.^{3,8,12} In the following discussion, the main features of plastic crystal behaviour will be addressed. Cyclohexane will be used as an example where appropriate.

An interesting characteristic of plastic crystals is the presence of one or more sub-melting solid-solid transitions coinciding with the transformation from a brittle solid to the plastic crystal. A relatively large entropy change accompanies this solid-solid transition, thereby signifying the onset of molecular motions (molecular rotations and/or diffusion). As a consequence of this behaviour, the melting entropies are considerably lower than non-plastic crystal solids and are often less than $2.5R$ (approximately $20\text{J.mol}^{-1}\text{.K}^{-1}$, where R is the gas constant).³ A change in crystal structure is also often observed at these solid-solid transitions. The plastic crystal phase has high lattice symmetry, typically cubic in nature, compared to the lower symmetry of the brittle solid phase.² Molecules that display plastic crystal behaviour have been described as "globular" in shape, often exhibiting spherical or ellipsoidal configurations.⁸ Cyclohexane, which is one such example, has a solid-solid transition at 186K followed by a melting transition at 279K, with transition enthalpies of 35.9 and $9.4\text{J.mol}^{-1}\text{.K}^{-1}$ respectively.³ In the plastic crystal phase of cyclohexane, the structure is thought to be face-centred cubic with a lattice parameter of 0.876nm and four molecules per unit cell.² Such features are typical for molecular plastic crystals.

As the molecules undergo rotations and diffusion in these materials, there has been considerable emphasis on characterising these motions. Nuclear magnetic resonance has been particularly useful for such characterisation due to the diversity of experiments that can be performed with this technique. Relaxation measurements probe the rotations in the plastic phase, whereas diffusion measurements study

molecular translations. The simplest NMR experiment, however, involves measuring the linewidth or second moment of a material. In the absence of any molecular motion, the linewidth is a maximum because strong interactions are experienced by the nuclei in the material. As the molecules begin to move, however, some of these interactions are averaged and the line starts to narrow. Significant reductions in linewidth are observed around the solid-solid transition in plastic crystal materials, indicating the onset of rotational motion.^{3,7,53} Further narrowing is often observed at higher temperatures as the molecules start to diffuse. Theoretical second moments can be calculated and subsequently compared to the experimental values, enabling the molecular motions to be identified.⁵³ In the case of cyclohexane (Figure 4-1), molecular motion is limited below 150K resulting in a rigid lattice linewidth of 16G and a second moment of approximately 26G^2 .⁶ Between 150K and 175K, a substantial decrease in the linewidth and second moment is observed as the molecules begin to reorient about the triad axes. At the transition temperature (186K), the second moment drops suddenly to 1.4G^2 as a result of isotropic reorientation of the molecules. This finite value for the second moment suggests that while the intramolecular interactions are averaged to zero, some intermolecular interactions still exist. Upon exceeding a temperature of 220K, however, these intermolecular interactions are also averaged to zero as a result of self-diffusion in the solid state.

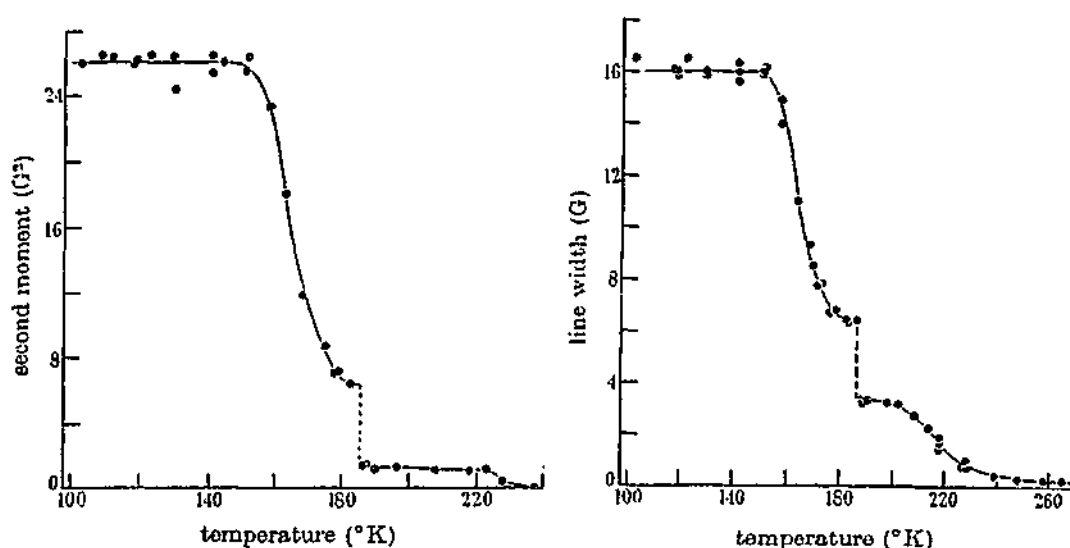


Figure 4-1 NMR second moments and linewidths as a function of temperature for cyclohexane (from Andrew⁶).

Rotational and translational motions are typically observed through the measurement of the spin-lattice relaxation times, T_1 and $T_{1\rho}$, or the spin-spin relaxation time, T_2 . A T_1 measurement is sensitive to molecular motions with frequencies of the order of 10^7 to 10^9 Hz, which are often associated with molecular rotations. $T_{1\rho}$ and T_2 , however, probe motions at much lower frequencies (10^4 to 10^6 Hz) and are therefore often governed by molecular translations. A detailed discussion of relaxation theory can be found in section 2.1.4 of Chapter 2 where the temperature dependence of these relaxation times is shown in Figure 2-7. Deviations from this classical behaviour are common for plastic crystalline materials.^{3,53} Limited motion occurs in the brittle phases of these materials and the relaxation behaviour is similar to that shown in Figure 2-7. However, the onset of molecular motion often results in a discontinuity in the relaxation times due to a change in the relaxation mechanism. The spin-lattice relaxation time, T_1 , for cyclohexane is shown in Figure 4-2.⁶ Below 160 K, the relaxation process is governed by molecular oscillations or lattice vibrations. The decrease in T_1 between 160 K and 186 K is the result of increased molecular

reorientations. At the solid-solid transition temperature, 186K, a discontinuous increase is observed as the reorientation rate of the molecules exceeds the proton Larmor frequency. Finally, a slight decrease in T_1 occurs just before the melting point, which is related to the onset of diffusion and correlates with the absence of any significant change in T_1 after melting.

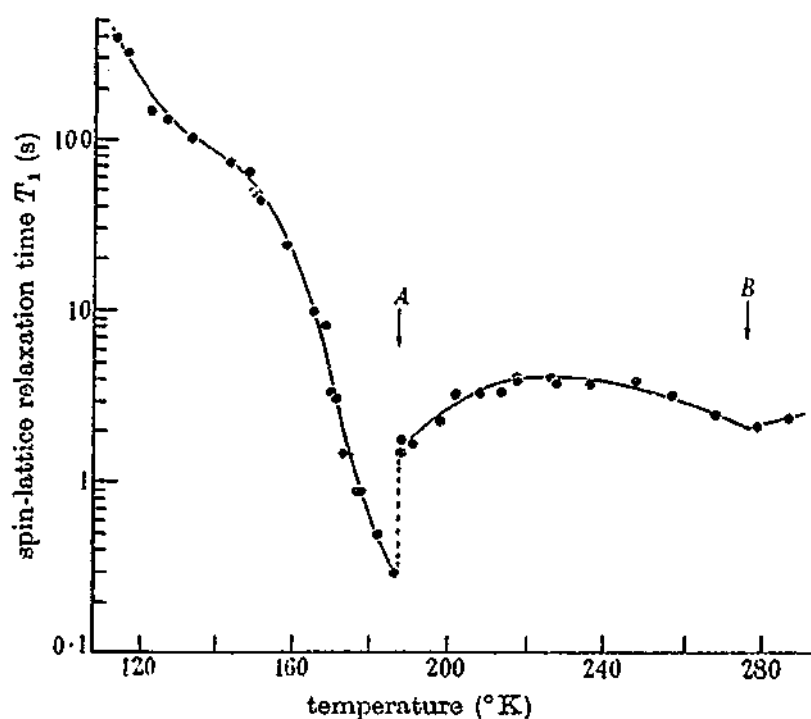


Figure 4-2 The spin-lattice relaxation time as a function of temperature for cyclohexane where *A* is the solid-solid transition and *B* is the melting point (from Andrew⁶).

Both the second moment and relaxation experiments show evidence of molecular diffusion in the plastic crystal phase. The correlation time, τ , obtained from these measurements, in conjunction with a suitable mean square jump distance, $\langle r^2 \rangle$, can be used to calculate a diffusion coefficient from the Einstein relationship.⁵³

$$D = \frac{\langle r^2 \rangle}{6\tau}$$

Equation 4-1

However, absolute diffusion coefficients can also be measured via direct diffusion experiments such as radiotracer or NMR measurements. The self-diffusion coefficients for the plastic phase are typically $10^{-13} \text{m}^2 \cdot \text{s}^{-1}$, substantially higher than the coefficients obtained for the brittle phase ($10^{-15} \text{m}^2 \cdot \text{s}^{-1}$ or less).³ Mechanistic studies of the diffusion in these systems suggest that self-diffusion is dominated by a vacancy mechanism, and is aided by the rotational motion.^{3,11} Divacancies or associated motions may also contribute to the transport mechanism. Plastic deformation, which occurs far more readily in plastic crystalline materials than the brittle solids, also seems to be largely diffusion controlled.¹¹ Self-diffusion of cyclohexane, just below the melting point, was measured by Tanner using pulsed field gradient NMR.¹⁰ There was evidence of both a liquid and solid phase in these measurements, thought to have been brought about by impurities or inhomogeneities in the samples. The diffusion coefficients just below melting were 2.4×10^{-13} and $5.1 \times 10^{-10} \text{m}^2 \cdot \text{s}^{-1}$ for the solid and liquid phases respectively. In comparison, the self-diffusion coefficient just above the melting point was $7.9 \times 10^{-10} \text{m}^2 \cdot \text{s}^{-1}$. Therefore, diffusion in the solid state is several orders of magnitude lower than diffusion in the melt. The difference between the liquid phase diffusion above and below the melting temperature was thought to be the result of restricted diffusion in the presence of the solid. Although there is reasonable agreement between the measured diffusion coefficients and coefficients calculated from NMR relaxation measurements ($1.4 \times 10^{-13} \text{m}^2 \cdot \text{s}^{-1}$), the diffusion coefficients obtained from radiotracer experiments are very different ($10^{-11} \text{m}^2 \cdot \text{s}^{-1}$). There is no obvious explanation for this discrepancy, but it is thought that pipe diffusion may have been measured by the radiotracer technique. Interestingly, the NMR measurement yields a diffusion coefficient for

cyclohexane that is consistent with the diffusion coefficients obtained for other plastic crystals.³

In summary, there are certain features that distinguish plastic crystal materials from brittle solids. Plastic crystal materials often exhibit one or more solid-solid transformations, which tend to have higher transition entropies than the melting transition. For such large entropy changes to occur, this transformation must signify the onset of motion in the solid phase. These motions consist of both rotations and diffusion, as revealed by NMR experiments. The soft, plastic nature of these materials is believed to be the result of motion in the solid phase.

4.1.2 Orientational Disorder in Ionic Crystals

4.1.2.1 Inorganic Plastic Crystals

Although plastic crystal behaviour was initially observed in molecular crystals, it is by no means limited to such materials and has been observed in a number of ionic solids. There is evidence of such behaviour in inorganic salts, such as metal nitrites, MNO_2 ,^{29,36,37} and alkali phosphates or sulphonates, M_3PO_4 or M_2SO_4 (M is Li or Na)^{54,55} among others.^{18,34,35} Due to the high melting temperatures of these solids, the plastic crystal phase is often well above room temperature.

Metal Nitrite Systems

The metal nitrite systems (MNO_2 where M is K, Rb, Cs or Tl) have been extensively studied by Ikeda and co-workers.^{29,36,37} These materials exhibit either two or three solid phases, where the highest temperature phase is the plastic crystal phase. Either NaCl or CsCl type crystal structures are observed for the plastic phases, whereas the lower temperature phases are of lower crystal symmetry. NMR relaxation measurements (T_1 and T_2) have been used to characterise the ionic mobility in each

phase. ^{15}N relaxation is dominated by chemical shift anisotropy whereas ^{39}K and ^{87}Rb relax via a quadrupolar mechanism. ^{205}Tl , which has a spin of $1/2$, is sensitive to both chemical shift anisotropy and dipolar interactions. The relaxation behaviour can be modelled using the BPP equation assuming these relaxation mechanisms. Although limited motion is observed in the brittle solid phases, as confirmed by ^{15}N lineshapes, the NO_2^- ions are thought to undergo 180° flips. As the temperature increases, however, anionic reorientation becomes possible. In the plastic phase, the ^{15}N lineshape shows a single narrow line, which indicates isotropic anionic rotation. As the melting point is approached, a decrease in the T_1 is observed, which is attributed to cation self-diffusion in these materials. This is further confirmed by the measurement of ionic conductivity, which increases from 10^{-6} to $10^{-2}\text{S.m}^{-1}\text{.K}$ over the same temperature range.

LiNO_2 and NaNO_2 show no evidence of a plastic phase, but mobility in the solid state has still been observed.⁵⁰ They have much higher melting entropies than the other alkali salts (36.2 and $29.6\text{J.K}^{-1}\text{.mol}^{-1}$ for LiNO_2 and NaNO_2 respectively compared to less than $20\text{J.K}^{-1}\text{.mol}^{-1}$ for the other salts), which precludes them from the plastic crystal class described for the molecular crystals (see section 4.1.1). In accordance with the other nitrite salts, 180° flipping of the NO_2^- anion was observed in the solid state, but the anion reorientation was not detected. At temperatures close to the melting point, lithium self-diffusion was also evident from the relaxation and conductivity measurements. The absence of anion reorientation was attributed to the energy required to make space for the motion. Less energy is required in the plastic materials than the brittle solids, so the onset of anion reorientation in the brittle solids becomes coincident with the material melting.

Alkali Phosphate Systems

Ion mobility in the plastic crystal α -sodium orthophosphate has been studied by K. Funke and co-workers^{54,55} through the use of neutron scattering, conductivity and

NMR techniques. The transition from the brittle to the plastic crystal phase occurs at 598K, with the latter exhibiting a cubic Li_3B type structure. The tetrahedral PO_4^{3-} ions form an FCC lattice with the sodium ions occupying the tetrahedral and octahedral interstices. Four models for ionic motion in these materials have been proposed: the anions are randomly oriented and experience isotropic rotational diffusion about a fixed point; the P-O bonds in the phosphate units are oriented along the $[111]$ directions such that the anions are able to undergo 90° jumps between two configurations around their C_2 -axes; one of the P-O bonds is fixed, around which the other oxygen atoms rotate through N possible positions; a similar arrangement to the previous model except that the jump angles are smaller and N is much larger. Good agreement was obtained between the neutron scattering results and the latter two models, while the former two were not consistent with the data. Based on this observation, it would appear that only three of four oxygen atoms in the phosphate anions are involved in the reorientational process. There was also some evidence to suggest that the sodium ions may be involved in this reorientation.

Conductivity was measured as a function of frequency from 4MHz to 3THz and was found to be constant up to microwave frequencies. A simple conduction mechanism involving independent hops cannot account for this frequency independence. Consequently, a correlated motion for conduction must exist in Na_3PO_4 . Funke and co-workers⁵⁴ have compared this motion to ion transport in AgBr, which occurs via an interstitialcy mechanism (see section 1.3.1 of Chapter 1). The diffusion coefficient of the sodium ions was calculated from the conductivity data using the Nernst-Einstein equation and found to be $4.4 \times 10^{-10} \text{m}^2 \cdot \text{s}^{-1}$. This value is comparable to the localised diffusion coefficient for the oxygen atoms ($8 \times 10^{-10} \text{m}^2 \cdot \text{s}^{-1}$), as determined by neutron scattering experiments. The agreement between the two values is further evidence for a coupled motion between the rotating anions and the sodium cations.

The notion that sodium ion motion is coupled to the rotation of the anions is further supported by NMR measurements. The T_1 relaxation of ^{17}O was found to involve two processes: the C_3 rotation of the phosphate ion and reorientational jumps of the threefold axis. The T_1 relaxation of ^{23}Na was also dependent on the latter process, in addition to a process that is related to the defect concentration in the material. ^{31}P , which is a spin 1/2 nucleus, will relax via all three processes. Remarkably similar activation energies and correlation times were obtained for all three nuclei, which is further evidence for strong interactions between the cations and anions.

A "paddle-wheel" mechanism has been proposed to describe the ionic motions in such plastic crystal materials. In this mechanism, the rotation of the anions assists the transport of cations in the solid. While there have been a number of arguments for such a mechanism,^{27,54} Secco²⁵ believes that a percolation model is more appropriate. The percolation-type mechanism is largely free volume dependent, more free volume resulting in greater ion mobility. For the Na_3PO_4 systems, however, the results seem to support the paddle-wheel mechanism. Funke and co-workers⁵⁴ have also ruled out a percolation mechanism in this salt, as all the interstices are occupied. This is not to say, though, that a paddle-wheel mechanism is appropriate for all plastic crystalline solids.

4.1.2.2 Organic Plastic Crystals

Plastic crystalline behaviour has also been found in a number of organic solids. Substituted ammonium salts^{17,21-24,31-33,38-41,44,45} and heterocyclic salts^{42,43,46-48} seem to have generated the most interest. Unlike the inorganic salts, however, these materials often exhibit lower solid-solid and melting transitions in a temperature range perhaps more suited to room temperature applications.

Substituted Ammonium Salts

Ammonium halide salts with one,^{17,21-23,44} two,⁴⁵ three^{31-33,38} or four^{24,39-41} alkyl substituents have all shown evidence of plastic crystal behaviour. The thermal analysis of these salts indicates multiple solid phases, with the solid phase just prior to melting being the plastic phase. The structure of this phase is either tetragonal or cubic, with the cubic structures being either NaCl- or CsCl-types. For the materials to display a cubic structure, the cations and anions must behave as spherical ions implying disordered orientations. Ion mobility has been studied in these systems through analysis of the NMR second moments and relaxation times. Most studies have focussed on the behaviour of the cation, although some have also examined the mobility of the anion.³⁸⁻⁴⁰ In most cases, the thermal transitions correlate to changes in ion mobility. Even in the orientationally ordered phases, at temperatures below the plastic phase there exists limited ion motion. At the lowest temperatures, the terminal methyl groups on the ammonium cations are able to rotate around their three fold axes (C_3) and, as the temperature increases, other groups undergo similar C_3 reorientation. In the second highest temperature phase, the cations experience uniaxial rotation that is normally around the long axis (in the case of straight chain substituents). Finally, ion motion in the plastic phase involves isotropic cation rotation as well as diffusion. Depending on the nature of the cation, other motions, such as cation flipping through certain angles, may also occur.

The diffusion mechanism in these salts is also material dependent. Diffusion coefficients in the plastic phase are typically 10^{-14} to $10^{-12} \text{ m}^2 \cdot \text{s}^{-1}$.^{21,22} The smaller, more spherical ions are able to diffuse in three dimensions²⁴ whereas cations with long alkyl chain substituents are often limited to 2D diffusion, perpendicular to the long axis of the cation.^{22,23,44,45} When 2D diffusion occurs, the salts are said to be low-dimensional plastic crystals. Although the motion of the anion was often not directly studied, it was inferred from the motions of the cation and conductivity measurements that the anion could also be diffusing. Ono *et al.*^{38,40} have made an

interesting correlation between the diffusion behaviour and the crystal structure of the salts. They have suggested that diffusion of bulky cations only occurs in CsCl-type cubic structures whereas the anions, which are typically smaller than the cations, can diffuse in any cubic structure. They have attributed this to the size of the openings through which the ions must diffuse. These openings are much larger in CsCl-type structures, compared to the NaCl-type, thereby enabling diffusion to occur more readily.

The conductivity in these salts is limited to approximately 10^{-8} to 10^{-7}S.cm^{-1} in the lower temperature phases, but increases significantly at the transformation temperature to values of approximately 10^{-4} to 10^{-3}S.cm^{-1} . This is in agreement with the NMR measurements, which indicate the presence of ion diffusion in the plastic phase. The mechanism for conduction is largely dependent on the structure of the material. For materials with smaller spherical ions, both ions are likely to be involved in the conduction mechanism. However, the ammonium salts with long alkyl substituents will exhibit an anisotropic conduction mechanism with higher conductivities occurring perpendicular to the long axis of the ion. Consequently, the cation will be the dominant charge carrier in these materials.

Heterocyclic Salts

Plastic crystal behaviour is not only limited to linear ammonium salts, but has been found to occur in cyclic ammonium systems also.^{42,43,46-48} Multiple solid phases also exist in these materials, and are similarly associated with the onset of ionic motions. For pyridinium chlorochromate,⁴³ in-plane reorientation of the pyridinium cation was observed in the lowest temperature phase. The onset of isotropic rotation occurs in the second highest solid phase and continues in the plastic phase along with cation diffusion. Similar behaviour was observed for piperidinium^{42,46} and pyrrolidinium salts.⁴⁷ The plastic crystal phase typically exhibits a CsCl-type crystal structure, except for piperidinium nitrate, which is a NaCl-type crystal.

Consequently, anion and cation diffusion in the plastic phase was reported for all the salts except piperidinium nitrate, where only isotropic rotations were detected. For pyrrolidinium perchlorate and hexafluorophosphate, the diffusion coefficients were found to be of the order of $10^{-13} \text{m}^2 \cdot \text{s}^{-1}$ at the melting point. It has been proposed that the conduction mechanism in these materials involves a correlated vacancy formation, either as a cation-anion vacancy pair and/or a Schottky defect.⁴⁷

Plastic crystal behaviour is also thought to occur in pyrrolidinium amides as suggested by MacFarlane *et al.*⁴⁸ Although the initial focus of this study was on the liquid state behaviour of the materials, there was evidence for plastic crystal behaviour in the solid state. Multiple solid-solid transitions were detected, but the entropy of melting exceeded the plastic crystal limit of $20 \text{J} \cdot \text{mol}^{-1} \cdot \text{K}^{-1}$. Conductivities in the molten state were found to be 10^{-3} to $10^{-2} \text{S} \cdot \text{cm}^{-1}$, comparable to other ionic liquids (see Chapter 3). In the solid state, remarkably high conductivities were also observed, ranging from 10^{-8} to $10^{-4} \text{S} \cdot \text{cm}^{-1}$. Since plastic crystal behaviour has been observed in other pyrrolidinium salts,⁴⁷ it is possible that these materials are also plastic crystalline solids.

4.1.2.3 Inorganic-Organic Plastic Crystals Combinations

Ion diffusion occurs readily in both inorganic and organic plastic crystals. The lithium based plastic crystals, which are appropriate for lithium based batteries, are only conductive at high temperatures. On the other hand, the organic salts, which are mobile at lower temperatures, are not lithium conductors. By combining the two types of salts, one might expect a fast lithium ion conductor at reasonable working temperatures. A similar hypothesis was proposed by Cooper and Angell in 1986¹⁹ in a study where they combined various lithium salts with a number of quaternary ammonium analogues. The melting temperatures of the combined systems were typically around 373K, with a number of solid-solid transitions observed at lower temperatures. The binary consisting of methoxyethyldimethylethylammonium

tetrafluoroborate ($\text{MeOCH}_2\text{CH}_2\text{N}^+\text{EtMe}_2\text{BF}_4^-$) and LiBF_4 had a conductivity of approximately 10^{-5}S.cm^{-1} at room temperature, which is consistent with other ionic conductors and only surpassed by a couple of polyethyleneoxide based polymer electrolytes. The activation energies for this combined plastic crystal system were also comparable to those of other electrolytes. Cooper and Angell believe that the paddle-wheel mechanism controls conductivity in this system. They have also assumed that the anions will be relatively fixed in such a material, making the lithium ions the dominant charge carriers.

More recently, similar work has been pursued in our laboratories.^{49,51,52} Lithium bis(trifluoromethanesulfonyl)amide (LiNTf_2) has been added in various quantities to N,N-dimethyl- and N,N-methylethylpyrrolidinium bis(trifluoromethanesulfonyl)amide. The resultant ion mobility was studied through measurement of the ionic conductivity and NMR linewidths. The addition of small amounts of LiNTf_2 (approximately 1mol%) resulted in over an order of magnitude increase in conductivity in both pyrrolidinium salts.⁴⁹ Further addition of LiNTf_2 up to a concentration of 33mol% saw continued conductivity increases, but exceeding this concentration resulted in a decrease in conductivity. The conductivities for the N,N-methylethylpyrrolidinium mixtures as a function of temperature are shown in Figure 4-3.

These binary salts also show interesting phase behaviour, as outlined in Table 4-1. Below the melting point of pure N,N-methylethylpyrrolidinium amide, a number of solid-solid phase transformations were observed. The same transitions were also seen in the doped systems. Apart from these solid-solid transformations, there was also evidence of a eutectic transformation for the materials with LiNTf_2 concentrations of 9mol% and greater. This eutectic transition occurs at 308K with a composition of 33mol% LiNTf_2 . Based on this information, the solid solubility limit for LiNTf_2 appears to be somewhere between 5 and 9mol%. A phase diagram

highlighting the various phase transformations occurring in these materials is shown in Figure 4-4.

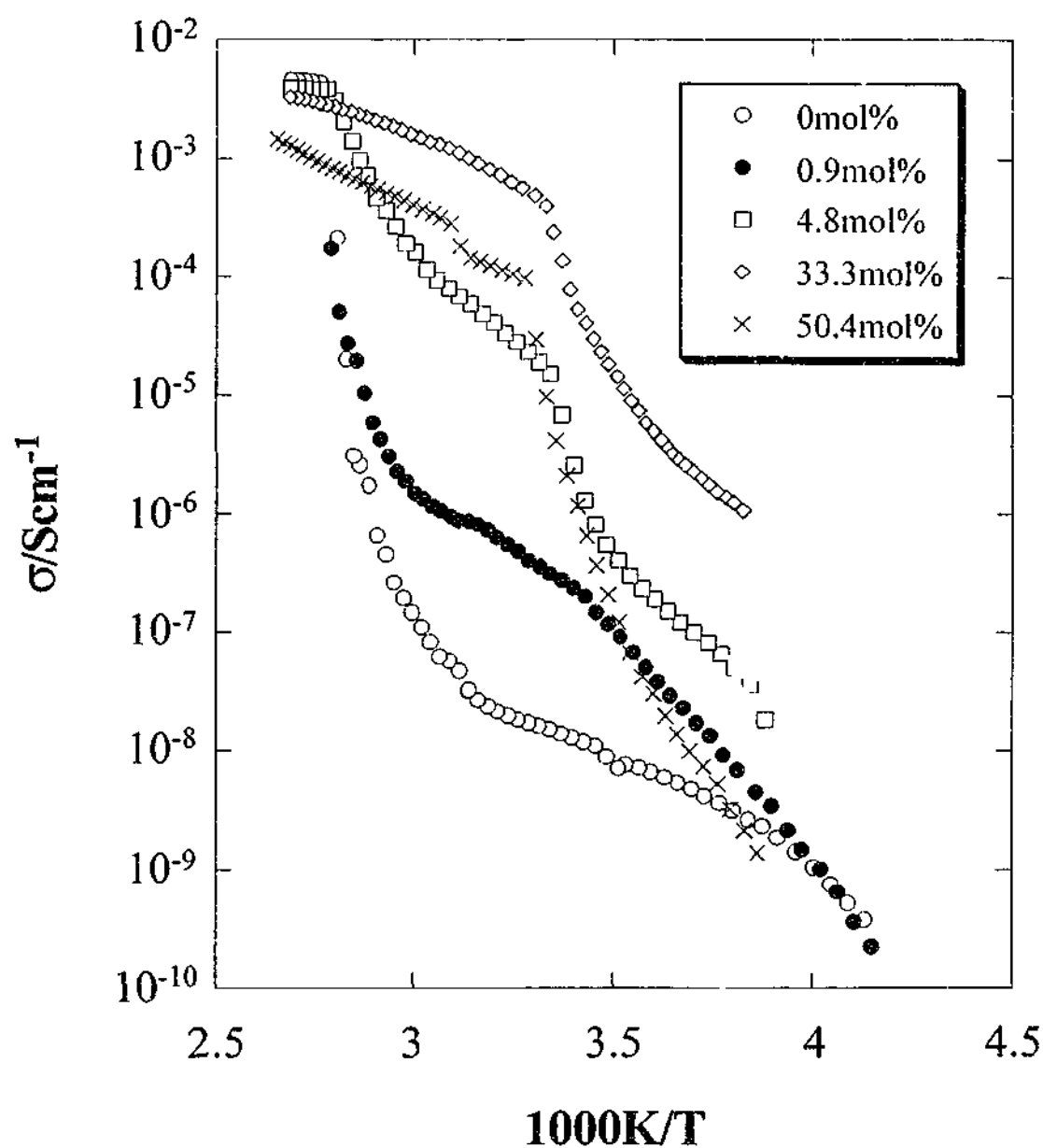


Figure 4-3 Conductivity as a function of temperature for the LiNTf₂/N,N-methylethylpyrrolidinium amide mixtures (reproduced from Forsyth⁵¹).

Table 4-1 Phase transformations in LiNTf₂/N,N-methylethylpyrrolidinium amide binary systems.⁵¹

Li mol%	T _L /K	T _{II-I} /K	Eutectic/K	T _{III-II} /K	T _{IV-III} /K
0	363	314	-	283-289	181
0.6	360	314	-	283	181
4.6	353	314	-	283	-
9.3	343	314	308	286	181
33	308	-	308	286	181
50.4	363	330†	308	286	-

†A new transition, which is not necessarily the same as the T_{II-I} transition.

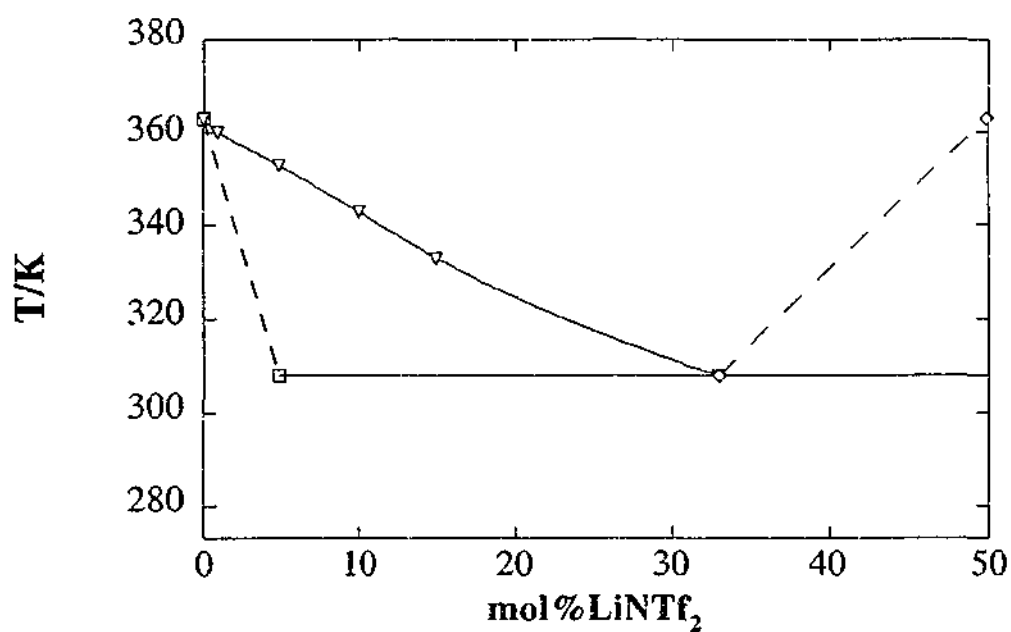


Figure 4-4 A partial binary phase diagram for the LiNTf₂/N,N-methylethylpyrrolidinium amide system.

In order to understand the conduction mechanism in these doped systems, and in particular the factors responsible for the significant increases in conductivity observed upon the addition of small amounts of LiNTf_2 , NMR measurements have been conducted. ^7Li NMR linewidths were measured as a function of temperature for 5mol%, 9.3mol% and 33mol% LiNTf_2 in order to characterise the lithium mobility in these materials. At 160K, when the salts are in Phase IV, the linewidths are very broad (approximately 4000Hz), indicative of very little ion motion. As the material changes from Phase IV to Phase III, a second narrow line is observed. Upon heating through the various phases, the mobility of the system increases and both peaks narrow. Although one cannot say with certainty that the lithium ions are definitely diffusing in this system (see section 2.1.3.2 of Chapter 2), the linewidth measurements do suggest the presence of some lithium motion in these materials.

4.2 Research Objective

The conductivity and thermal behaviour of a new family of salts based on the pyrrolidinium ring displayed some interesting characteristics. Several sub-melting solid-solid phase transformations and solid state conductivities of the order of 10^{-8}Scm^{-1} seem to suggest that these materials exhibit plastic crystalline properties. The addition of small amounts of LiNTf_2 (>1mol%) to the substituted pyrrolidinium salt, N,N-methylethylpyrrolidinium bis(trifluoromethanesulfonyl)amide, resulted in an increase in conductivity of several orders of magnitude. Further increases in conductivity were observed up to a lithium salt concentration of 33mol%, after which more lithium salt actually decreased the conductivity. The thermal analysis of these LiNTf_2 systems suggests that a eutectic transition occurs for greater than 5mol% LiNTf_2 . What was most astounding about these materials is how such a small amount of LiNTf_2 can have such a pronounced effect on the ionic mobility. The measurement of ^7Li linewidths indicated significant mobility in the system, which was consistent with the conductivity data. Based on these observations, a number of hypotheses can be made regarding the conduction mechanism in these materials:

1. In the pure material, the conduction involves a vacancy mechanism and the cation is the dominant charge carrier;
2. The addition of a small amount of lithium salt creates more vacancies enabling more ions to diffuse; and
3. At higher lithium concentrations, the presence of a eutectic liquid phase is responsible for the increased conductivity.

In order to test these hypotheses, NMR diffusion measurements were made as a function of temperature for the pure N,N-methylethylpyrrolidinium salt and the doped systems. Both the pulsed field and fringe field gradient techniques were employed, with proton and fluorine measurements used to study the pyrrolidinium cation and the amide anion respectively. Measurements were made as a function of temperature and LiNTf₂ content. The results obtained from these experiments will be discussed in the context of previous work, with particular reference to the work conducted by the Electrolytes group at Monash University.

4.3 Results

4.3.1 Pyrrolidinium Salt Systems

Preparation of the pyrrolidinium salt involved a two step synthesis.⁴⁸ 1-methylpyrrolidine was reacted with ethyl iodide to form N,N-methylethylpyrrolidinium iodide. The amide salt was then prepared by reacting this iodide salt with lithium bis(trifluoromethanesulfonyl)amide (LiTFSA, LiNTf₂). The structure of N,N-methylethylpyrrolidinium amide is shown in Figure 4-5. The nomenclature used for this family of salts is P₁₂NTf₂ where *P* refers to the pyrrolidinium ring, with the subscripts, *1* and *2*, referring to the methyl and ethyl substituents on the nitrogen of the pyrrolidinium ring. P₁₂NTf₂ was also doped with LiNTf₂ (0.9mol%, 4.8mol%, 33mol% and 49.9mol%) and the diffusion coefficients were measured in these systems as a function of temperature. The experimental details for the diffusion measurements are outlined in Chapter 2.

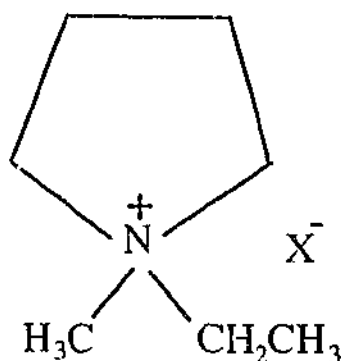


Figure 4-5 The structure of N,N-methylethylpyrrolidinium amide ($P_{12}NTf_2$).

4.3.2 Diffusion in $LiNTf_2/P_{12}NTf_2$ Mixtures

The $LiNTf_2/P_{12}NTf_2$ mixtures showed considerably higher conductivities in comparison to pure $P_{12}NTf_2$.⁵¹ To understand the effect of the lithium salt addition on the transport mechanisms, diffusion coefficients were measured for the pyrrolidinium cation and NTf_2^- anion as a function temperature. Cation diffusion coefficients for pure $P_{12}NTf_2$ were measured by the pulsed field gradient and fringe field gradient NMR techniques and the results are shown in Figure 4-6. The diffusion coefficients from the pulsed field gradient method were consistently reproduced by the fringe field gradient technique. The anion diffusion coefficients are also shown in Figure 4-6 and are similar to the cation coefficients. No diffusion was detected for either the cation or the anion below 343 and 363K respectively. This may be attributed to two factors: the diffusion coefficients are lower than the limitations of the equipment (approximately $10^{-15}m^2s^{-1}$); and/or the concentration of diffusing species is too small to be detected.

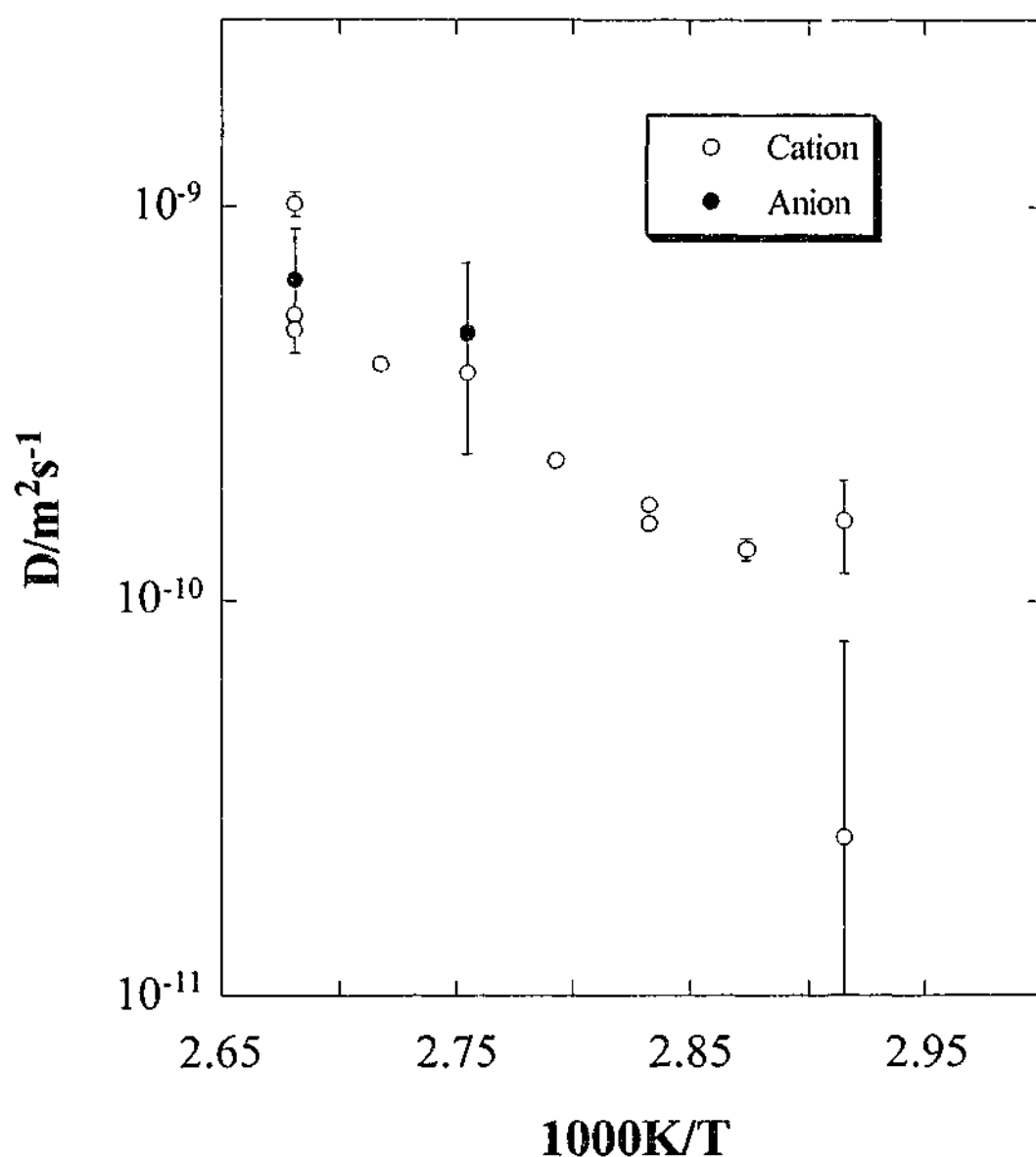


Figure 4-6 Ionic diffusion coefficients for pure $P_{12}NTf_2$ measured with the pulsed field gradient and fringe field gradient techniques.

The pyrrolidinium cation and amide anion diffusion coefficients in the 0.9mol% and 4.8mol% $LiNTf_2$ doped systems are shown in Figure 4-7 and Figure 4-8. Although proton diffusion in the 0.9mol% $LiNTf_2$ material was detected above 303K, anion diffusion was only observed above 363K due to interference effects from the T_2 relaxation time at the lower temperatures (see section 2.1.5.2 of Chapter 2). Similar diffusion coefficients were obtained for the two ions, suggesting a similar diffusion

process. It is possible, therefore, that the anion may have been measured at the lower temperatures if the T_2 interference had not affected the results. Both the proton and fluorine diffusion coefficients for the 4.8mol% LiNTf₂ system were observed over the entire temperature range. At the lower temperatures, the anion diffuses at a slower rate than the cation, but similar coefficients for both ions were observed at the higher temperatures.

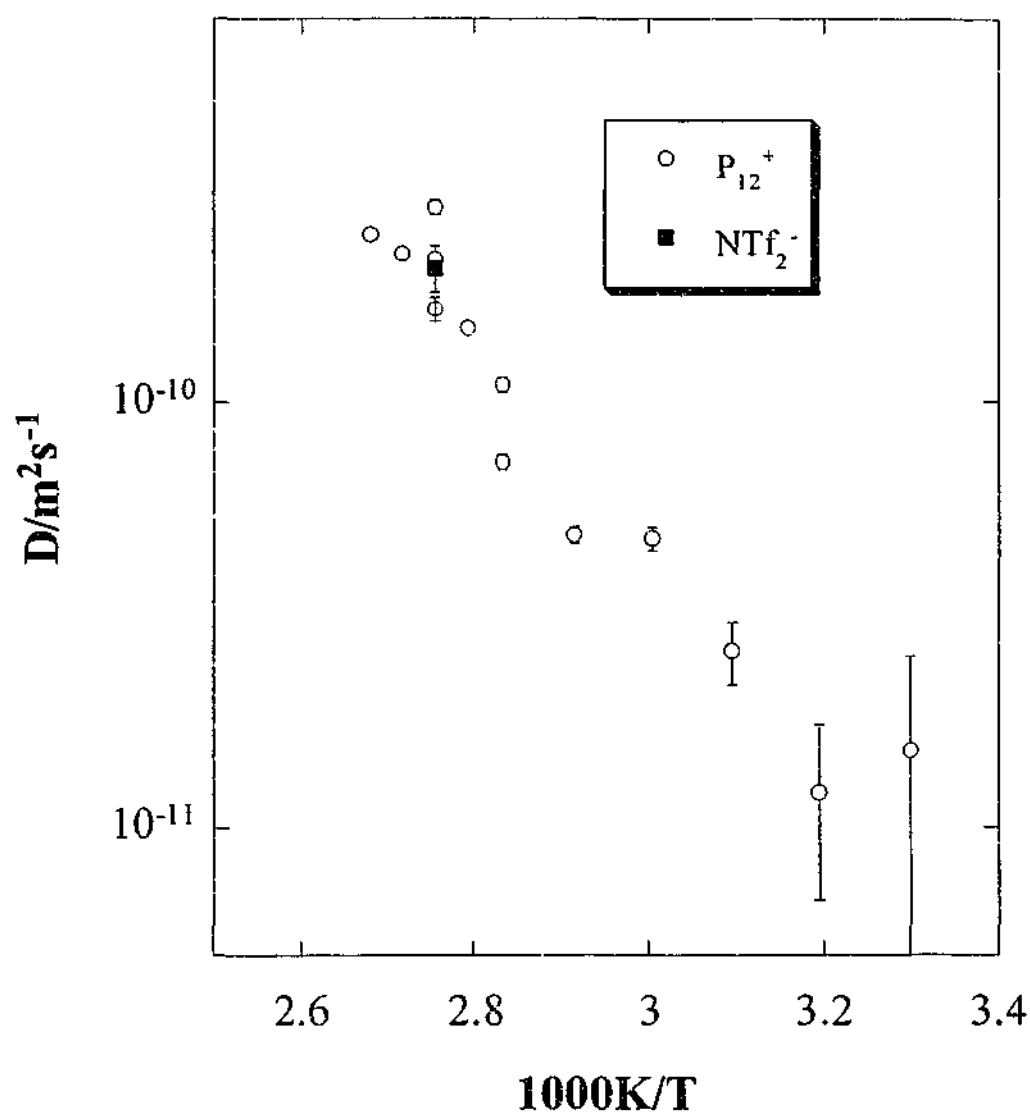


Figure 4-7 Diffusion coefficients for the pyrrolidinium cation and the amide anion as a function of temperature for the 0.9mol% LiNTf₂ doped system.

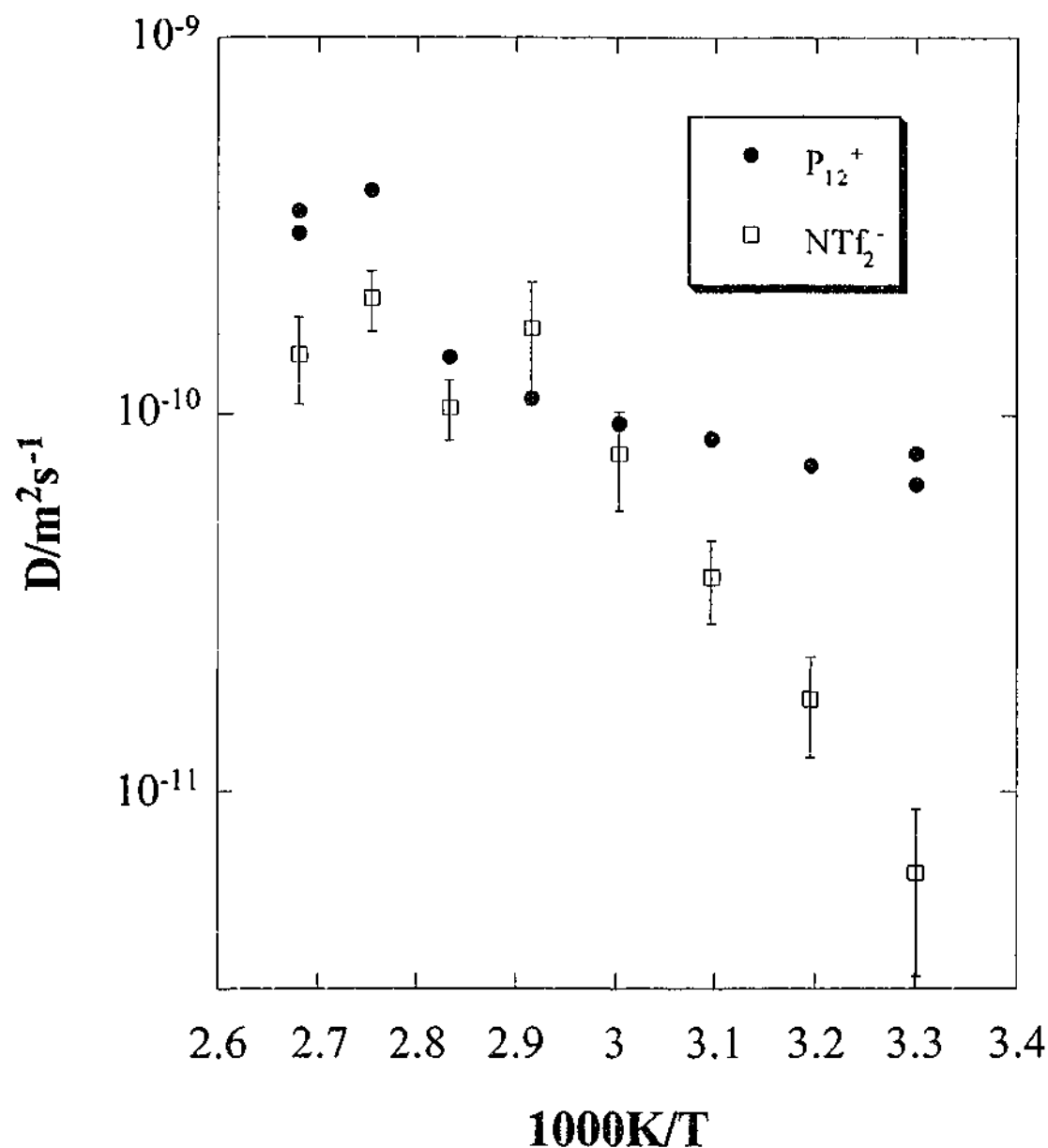


Figure 4-8 Diffusion coefficients for the pyrrolidinium cation and the amide anion as a function of temperature for the 4.8mol% LiNTf₂ doped system.

Figure 4-9 shows the pyrrolidinium cation and the amide anion diffusion coefficients upon adding 33mol% LiNTf₂ to pure P₁₂NTf₂. Similarly, the pyrrolidinium cation and amide anion diffusion coefficients for the 49.9mol% LiNTf₂/P₁₂NTf₂ system are shown in Figure 4-10. It was possible to measure the cation and anion diffusion coefficients for both systems over the entire temperature range studied. For the

33mol% system, the ionic diffusion coefficients are the same within error, whereas the cation diffusion coefficients are slightly higher than those for the anion for the 49.9mol% system.

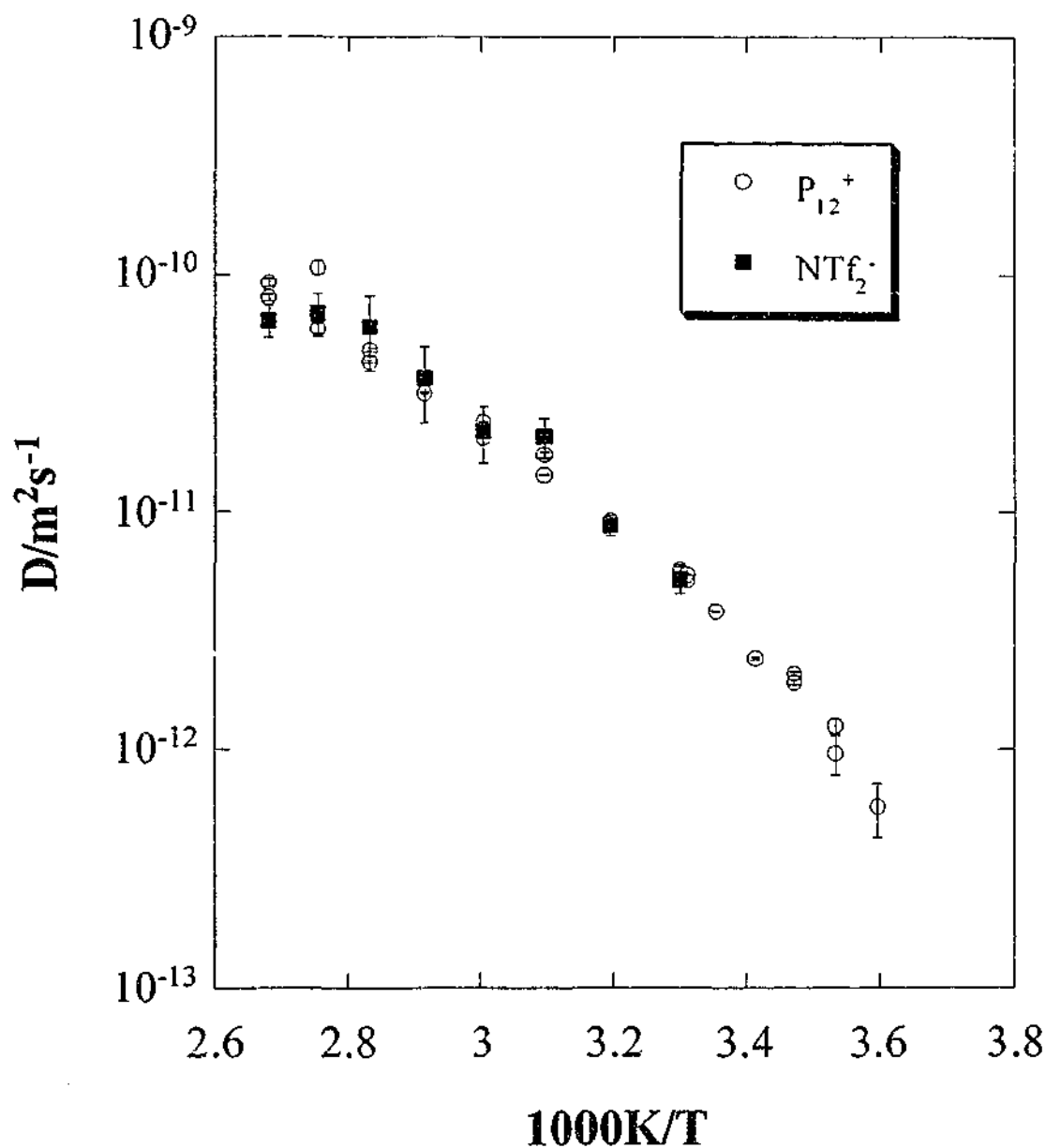


Figure 4-9 Diffusion coefficients for the pyrrolidinium cation and the amide anion as a function of temperature for the 33mol% LiNTf₂ binary system.

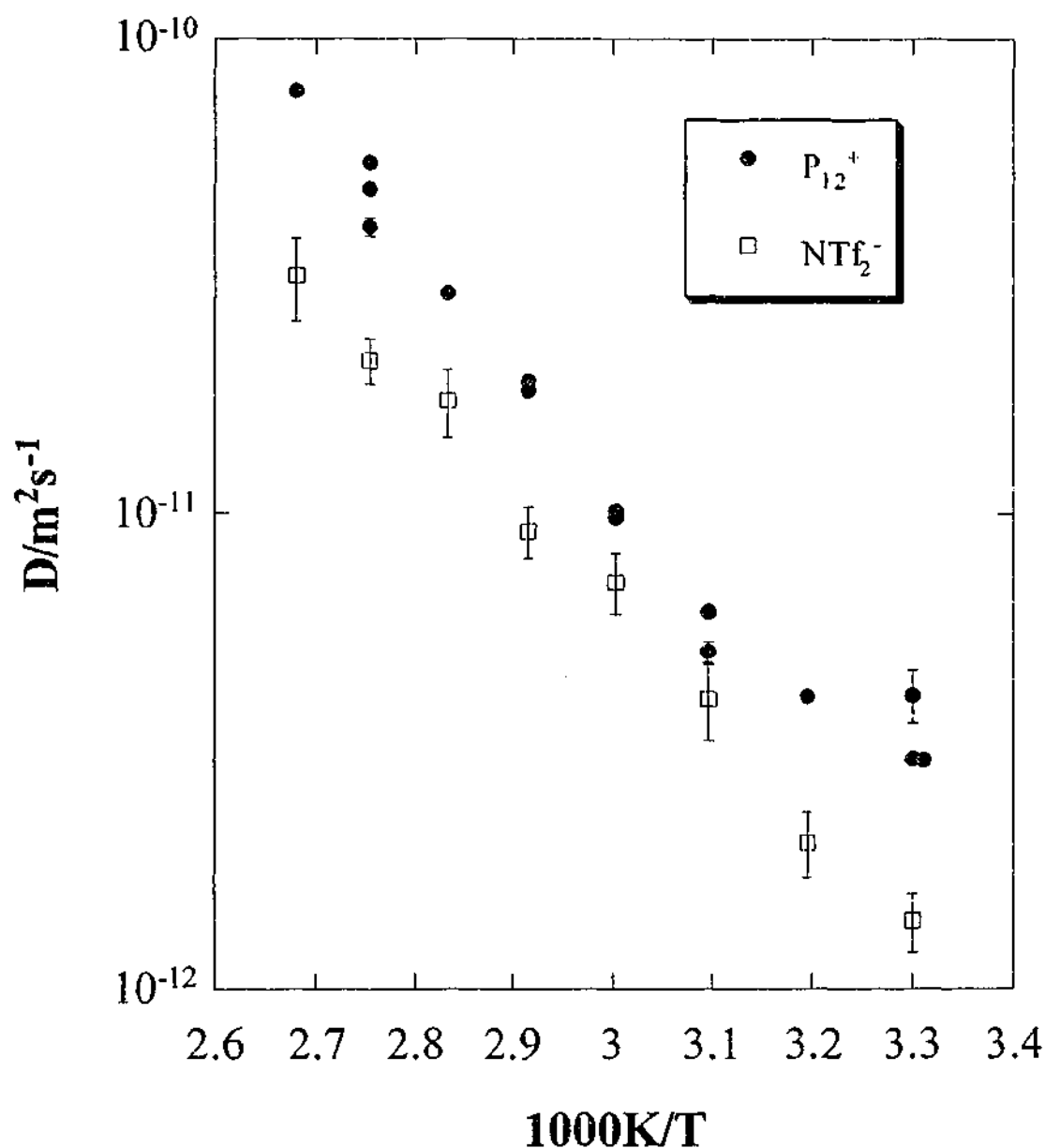


Figure 4-10 Diffusion coefficients for the pyrrolidinium cation and the amide anion as a function of temperature for the 49.9mol% LiNTf₂ binary system.

In the following discussion, the diffusion data will be analysed and compared to the previous work in our laboratories in order to elucidate the conduction mechanisms in these systems.

4.4 Discussion

4.4.1 Characterisation of the Diffusion Mechanisms

What seems quite extraordinary about these systems is how such a small amount of lithium salt can have such an impact on the ion mobility. The addition of 0.9mol% LiNTf₂ to pure P₁₂NTf₂ has a significant effect on the diffusion behaviour. A further increase in LiNTf₂ salt concentration results in a further change in ion mobility, as indicated by the 4.8mol%, 33mol% and 49.9mol% LiNTf₂ systems. Proton diffusion coefficients have been measured to monitor the mobility of the pyrrolidinium ring as a function of LiNTf₂ content. Figure 4-11 compares the pyrrolidinium cation diffusion coefficients of pure P₁₂NTf₂ with those of the LiNTf₂/P₁₂NTf₂ mixed systems. The overall trend indicates a decrease in pyrrolidinium diffusion coefficient with increasing lithium salt. A similar trend was also observed for the anion diffusion coefficients (Figure 4-12). Isothermal plots of the pyrrolidinium and amide diffusion coefficients highlight the effect of the lithium salt. At the lower temperatures, the initial addition of lithium salt actually results in an increase in the pyrrolidinium diffusion coefficient. A maximum is reached at approximately 4.8mol%, with subsequent LiNTf₂ salt addition resulting in a decrease in ion diffusion. At the highest temperatures, however, where all the materials should be molten, the addition of LiNTf₂ results in a decrease in both pyrrolidinium and amide diffusion.

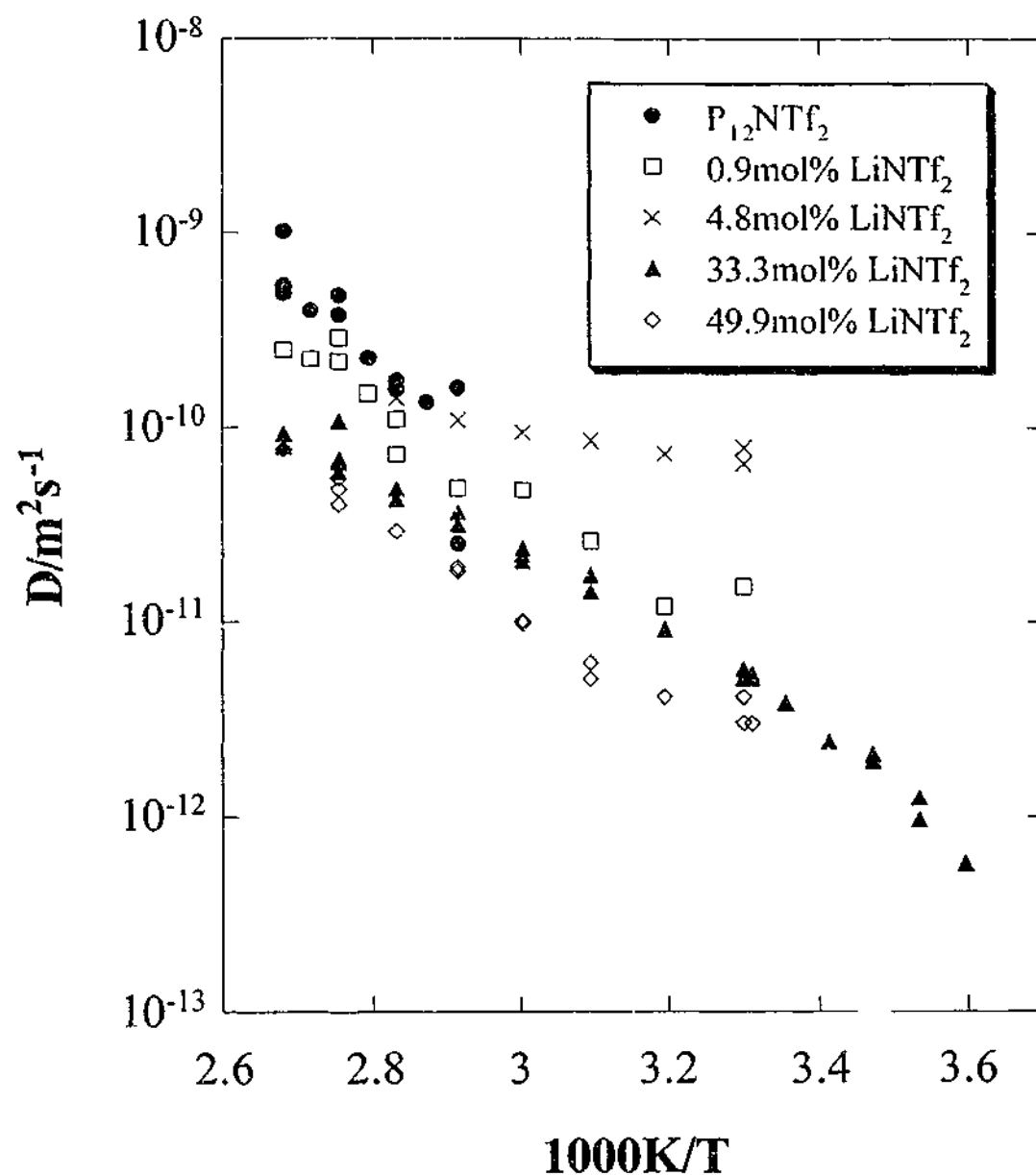


Figure 4-11 A comparison of the pyrrolidinium cation diffusion coefficients for the pure $P_{12}NTf_2$ and the $LiNTf_2/P_{12}NTf_2$ mixtures.

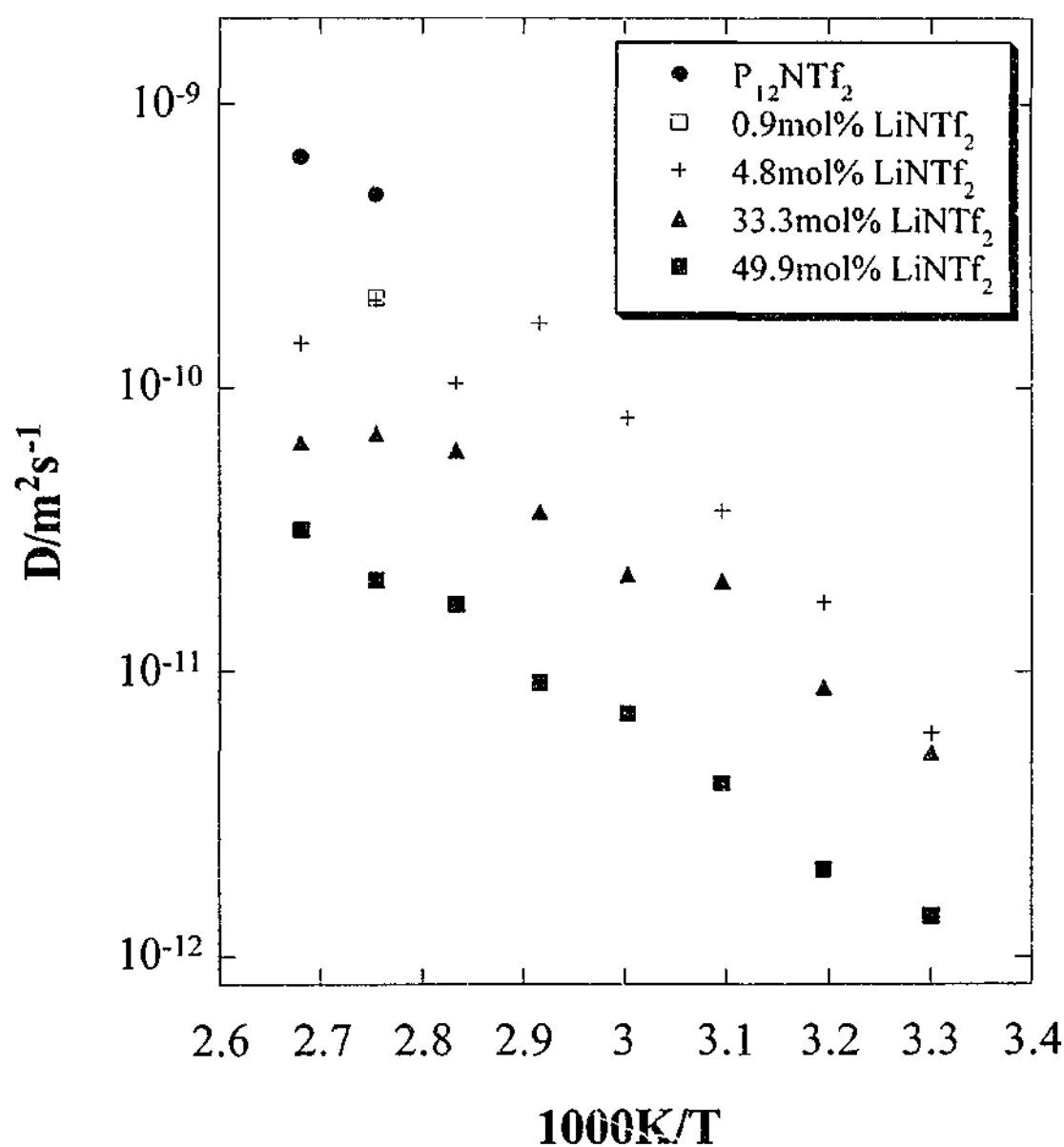


Figure 4-12 A comparison of the anion diffusion coefficients for the pure $P_{12}NTf_2$ and $LiNTf_2/P_{12}NTf_2$ mixtures.

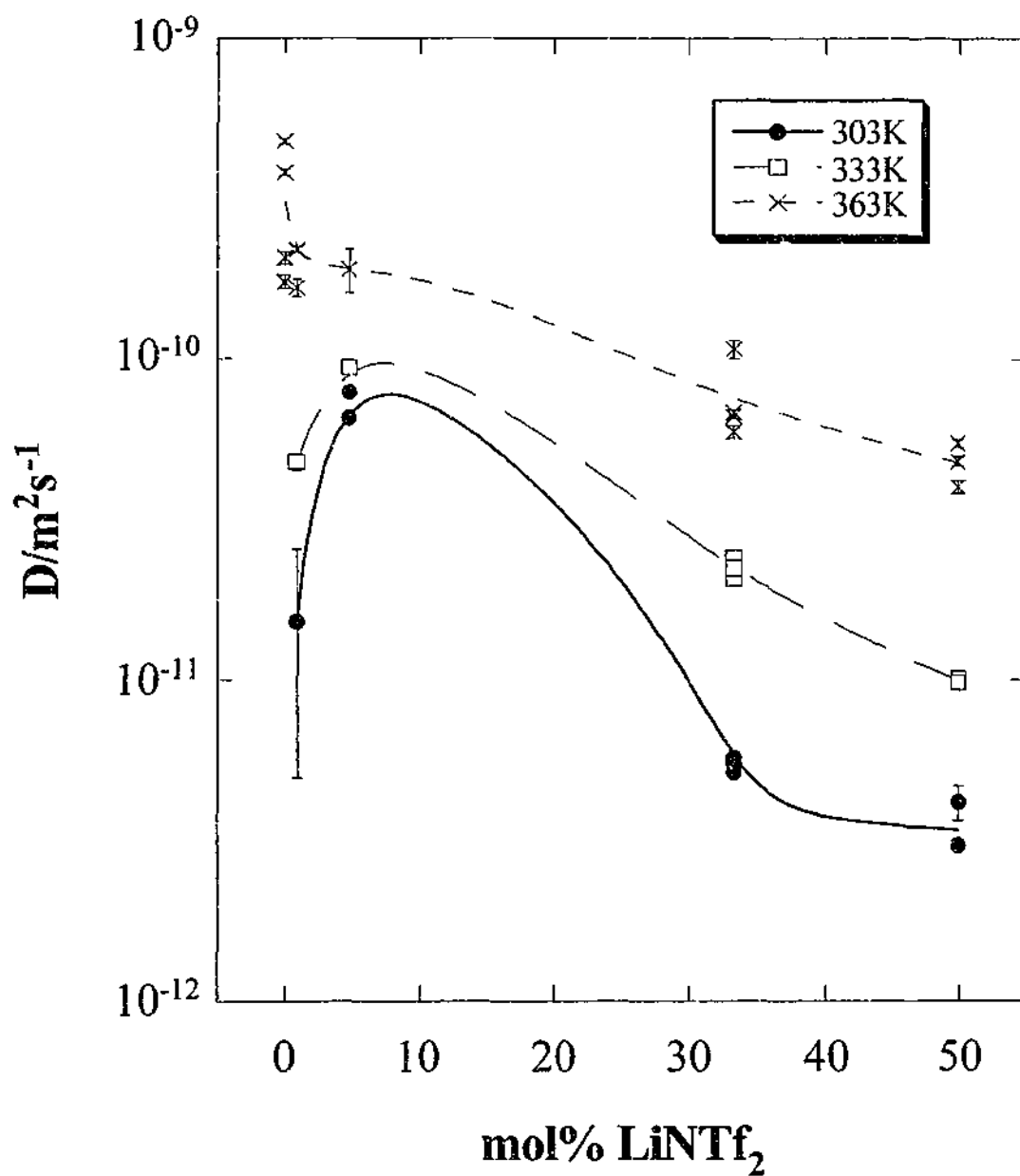


Figure 4-13 Pyrrolidinium diffusion coefficient isotherms as a function of LiNTf_2 concentration.

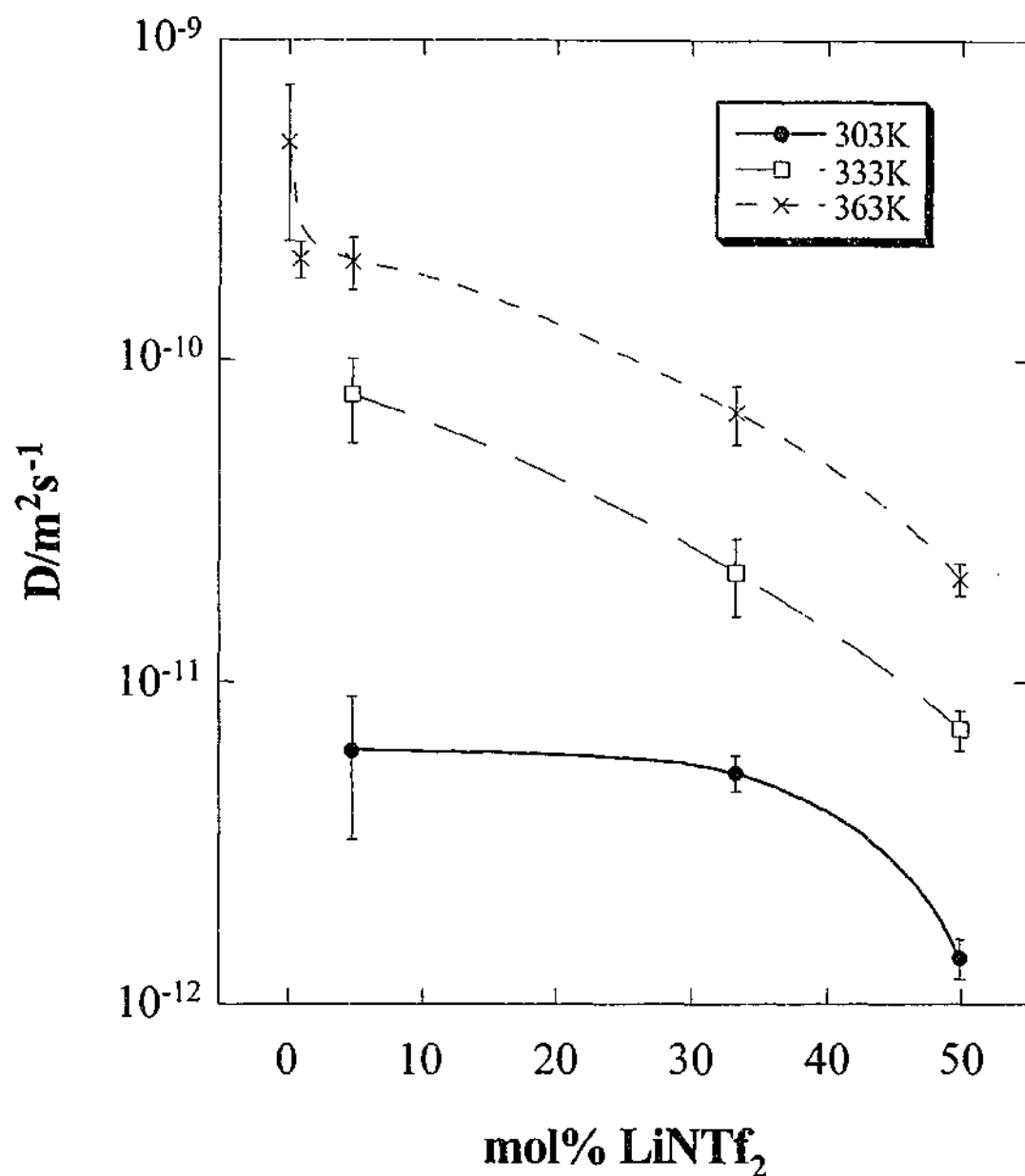


Figure 4-14 Amide anion diffusion coefficient isotherms as a function of LiNTf₂ concentration.

Presenting the isothermal diffusion data as a function of LiNTf₂ is actually somewhat ambiguous. As mentioned earlier, the LiNTf₂/P₁₂NTf₂ system exhibits complex phase behaviour, undergoing a number of solid-solid transitions with evidence of a eutectic transformation for some compositions. Therefore, for certain samples, solid and liquid phases will coexist at some temperatures. A partial binary phase diagram

was constructed based on these thermal transitions (see Figure 4-4 in section 4.1.2.3), from which it was concluded that the 33mol% LiNTf₂ composition is the eutectic composition. From this phase diagram, the solid solubility limit of LiNTf₂ in P₁₂NTf₂ was assumed to be 5mol% at 308K, which, accordingly, is the onset of the eutectic isotherm. Consequently, all samples, other than the pure material and the eutectic composition, will display two-phase behaviour at some temperature.

The proportion of liquid phase (W_L) at any given temperature can be calculated using the Lever rule:⁵⁶

$$W_L = \frac{C_0 - C_\alpha}{C_L - C_\alpha}$$

Equation 4-2

where C_0 is the mixture composition and C_L and C_α are the compositions of the liquid and solid phases respectively at the selected temperature. An example phase diagram indicating these compositions is shown in Figure 4-15. A similar two-phase region will also exist for LiNTf₂ contents greater than 33mol%, for which the proportion of liquid can also be calculated upon slight rearrangement of the above equation. However, as the thermal transitions for mixtures containing more than 50mol% LiNTf₂ have not been studied in any detail, no attempt has been made to calculate the proportion of liquid for the 49.9mol% LiNTf₂ system. It is highly likely, though, that a substantial amount of this system will be liquid at any given temperature above the eutectic isotherm.

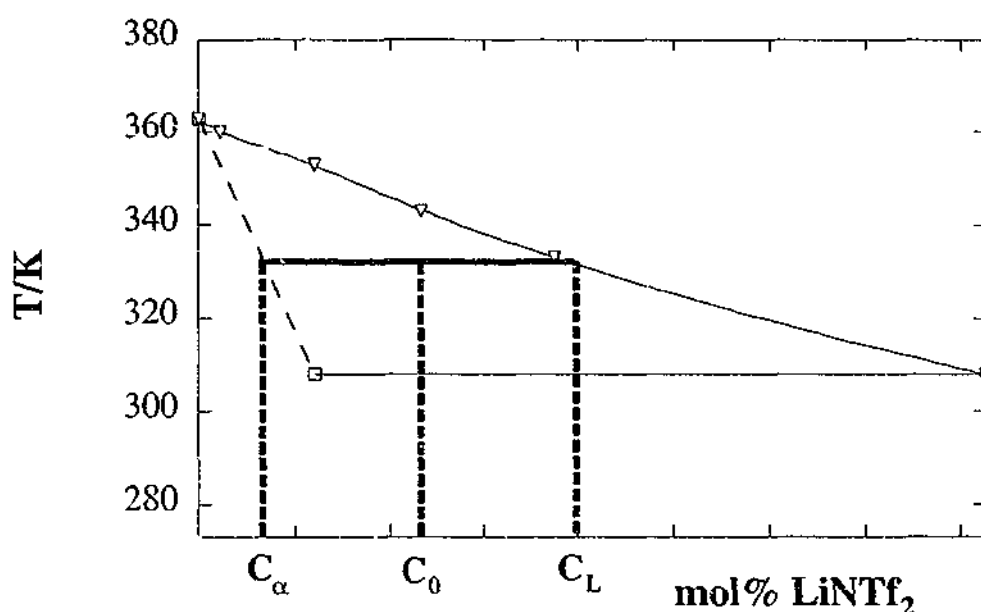


Figure 4-15 Lever rule quantities used to determine the proportion of liquid phase.

From the Lever rule calculations, the proportion of liquid phase as a function of temperature for the 0.9 and 4.8mol% $\text{LiNTf}_2/\text{P}_{12}\text{NTf}_2$ mixtures is shown in Figure 4-16. For both samples, the amount of liquid phase rapidly increases as the materials approach their melting points. This increase is more extreme in the case of the 0.9mol% LiNTf_2 sample due to the limited temperature range over which the two-phase region exists. At 310K, approximately 3% of the 4.8mol% LiNTf_2 system is liquid. Only at 350K does the proportion of liquid reach 50% before finally melting at 353K. From this data, it can be concluded that the 0.9mol% LiNTf_2 system is essentially solid while the 4.8mol% sample will coexist as two phases over the temperature range of interest.

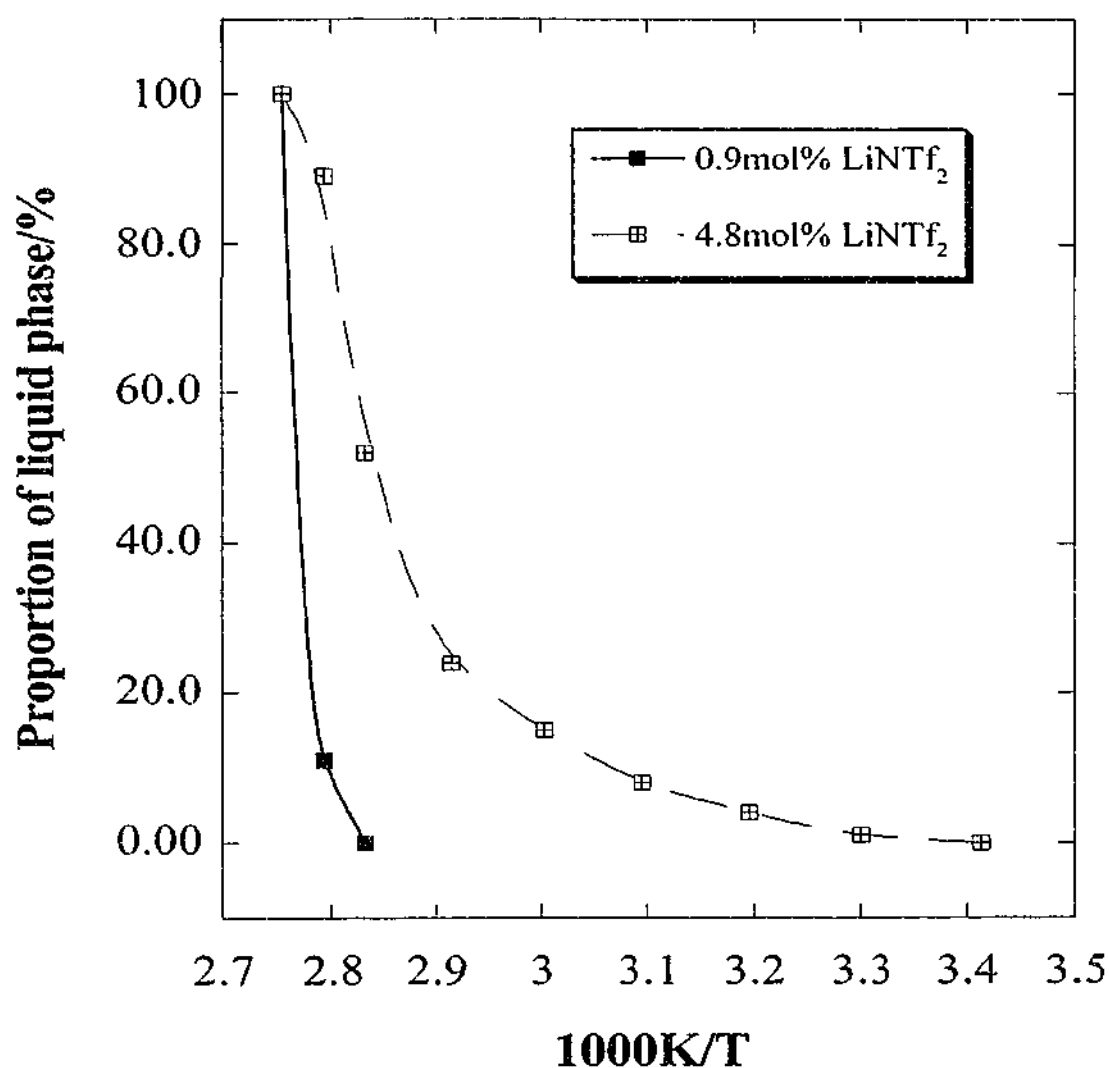


Figure 4-16 The proportion of liquid phase as a function of temperature for 0.9 and 4.8mol% LiNTf₂/P₁₂NTf₂ mixtures. Lines are to guide the eye.

Despite the coexistence of two phases in the 4.8mol% LiNTf₂ sample, there was no evidence of more than one diffusion coefficient. Based on this observation, two possible conclusions can be drawn: the measured diffusion coefficients are an average value for all the mobile species, regardless of whether they are diffusing in the solid or the liquid; or the measured diffusion coefficients are dominated by one of the two phases. As it was not possible to measure the diffusion coefficients for the liquid and solid state separately, it is difficult to say which of the above scenarios is more likely. At the lower temperature, where the sample is mostly solid, one would

expect the measured diffusion coefficient to reflect the behaviour in the solid state. However, as the amount of liquid phase increases, it seems likely that the diffusion in this phase will begin to dominate the measurement.

With regard to the other systems, the phase behaviour of these salts will surely have an effect on the resultant diffusion coefficients. For the solid imidazolium salts (MeEtImI and MeEtImBr), the solid state diffusion coefficients were found to be considerably higher than those for the supercooled liquid state (see section 3.4.4 in Chapter 3). The difference between the solid and liquid phase diffusion coefficients was attributed to a difference in the transport mechanism. In the solid state, diffusion will most likely occur via a vacancy mechanism where the ions move in discrete jumps through the crystalline matrix. In the liquid state, however, ion motion is more likely to involve the collective rearrangement of small sections of the material. The diffusion in the liquid is therefore limited by these rearrangements, whereas diffusion in the solid is only limited by the formation of vacancies. In the case of these pyrrolidinium salts, it would seem that the same behaviour is responsible for the differences in diffusion coefficients. The solid materials, being pure $P_{12}NTf_2$ and the 0.9mol% $LiNTf_2$ mixture, have higher diffusion coefficients than the 33mol% and 49.9mol% $LiNTf_2$ systems, which are mostly liquid. The 4.8mol% $LiNTf_2$ sample, however, exhibits similar behaviour to the 0.9mol% $LiNTf_2$ sample, despite the presence of both the solid and liquid phases. It should be noted, however, that pyrrolidinium diffusion coefficients were also measured in the solid state for 33mol% $LiNTf_2$, and found to be slightly lower than the other solid materials (see Figure 4-11 and Figure 4-13). In this case, diffusion is also expected to involve a vacancy type mechanism.

Anion diffusion was only observed at the higher temperatures for pure $P_{12}NTf_2$ and the 0.9mol% $LiNTf_2$ sample, but was measured over the entire temperature range for the remaining samples (see Figure 4-12). As mentioned earlier, the amide diffusion

coefficients were measured using the fringe field technique, which suffers from T_2 interference effects. Therefore, the inability to measure diffusion coefficients for the pure and 0.9mol% LiNTf₂ systems does not preclude the presence of anion diffusion. Solid state anion diffusion in pyrrolidinium perchlorate and hexafluorophosphate was studied by Ono *et al.*⁴⁷ through measurement of NMR second moments and relaxation times. In each case, both the anion and cation were mobile and thought to diffuse via a vacancy mechanism. In comparison to the amide anion, however, the perchlorate and hexafluorophosphate anions are relatively small, symmetrical ions (0.33nm radius for the amide ion compared to 0.24 and 0.25nm for the perchlorate and hexafluorophosphate ions respectively⁵⁷) and are therefore likely to undergo diffusion more readily. For the 4.8mol% and 49.9mol% LiNTf₂ sample, the diffusion coefficients for the pyrrolidinium cation are slightly higher than those for the anion, particularly at the lower temperatures. In the case of the 33mol% LiNTf₂ system, the diffusion coefficients are the same within error.

The ionic diffusion coefficients for these pyrrolidinium systems range from approximately 10^{-12} to $10^{-9}\text{m}^2.\text{s}^{-1}$ over the temperature range studied (see Figure 4-11 and Figure 4-12). By comparison, the ionic diffusion coefficients for pyrrolidinium and piperidinium hexafluorophosphate salts were of the order of $10^{-13}\text{m}^2.\text{s}^{-1}$ at the melting point.^{46,47} Ono and co-workers calculated these diffusion coefficients from the diffusional correlation times, τ_{diff} , using the following equation:

$$D = \frac{\langle r^2 \rangle}{6\tau_{\text{diff}}}$$

Equation 4-3

where $\langle r^2 \rangle$ is the mean-square jump distance. The diffusional correlation times used in this equation were determined from relaxation measurements, which is an indirect measurement of diffusion. Moreover, it is possible that such relaxation

measurements do not reflect the translational motion which is responsible for diffusion. For several plastic crystal materials,^{21,23,24,32,34} diffusion coefficients calculated from conductivity data have been compared with diffusion coefficients derived from relaxation measurements. From the conductivity data, calculated diffusion coefficients were typically of the order of $10^{-12} \text{m}^2 \cdot \text{s}^{-1}$ and found to be greater than those from the relaxation measurements. For some materials,^{23,34} the discrepancy was up to several orders of magnitude. For the pyrrolidinium systems studied here, the diffusion coefficients are measured by a direct method (fringe field or pulsed field gradient NMR) and are more likely to be representative of the ion transport involved in conduction. Consequently, it is assumed that the different measurement technique accounts for the slightly higher diffusion coefficients reported here, compared to previous studies.

Given the relationship between conductivity and diffusion, one might expect the addition of LiNTf_2 to have the same effect on both properties. Adding the lithium salt resulted in a decrease in diffusion coefficient, which has been attributed to a change in the transport mechanism from solid to liquid state diffusion. On the contrary, the addition of LiNTf_2 enhances the conductivity, which peaks with the 33mol% sample, as shown in Figure 4-3. Recall from the Nernst-Einstein relationship (see Equation 1-2 in Chapter 1) that the conductivity is also dependent on the number of charge carriers while the absolute diffusion coefficients are not. The difference in behaviour displayed by these two properties must therefore be attributed to a difference in the concentration of charge carriers. The effect of the charge carrier concentration is discussed below.

4.4.2 Analysis of the Charge Carrier Concentration

The concentration of mobile charge carriers is an important factor in the determination of conductivity, but also plays an important role in the measurement

of diffusion. Although diffusion was detected in most samples over the entire temperature range studied, no pyrrolidinium diffusion was observed below 343K for pure $P_{12}NTf_2$. The inability to measure diffusion coefficients below this temperature does not necessarily rule out diffusion of a small fraction of ions. Too few diffusing species will result in an immeasurable diffusion coefficient, regardless of the rate of diffusion. The concentration of mobile species can be determined from the NMR signal intensity data. As discussed in the previous chapter (see section 3.4.4), the NMR diffusion experiments only measure the mobile species that are moving on the time scale of the experiment. Immobile nuclei will not be detected and therefore will not contribute to the overall signal. The signal intensities for all samples taken from the pyrrolidinium diffusion measurements are shown in Figure 4-17. The data has been normalised with respect to the signal intensity in the melt, as it is assumed that all the pyrrolidinium cations will be mobile in this phase.

The very rapid increase in mobile cation concentration at 343K for pure $P_{12}NTf_2$ may suggest that there are mobile cations at lower temperatures but that the NMR technique lacks the sensitivity to detect such small concentrations. For the 0.9mol% $LiNTf_2$, approximately 3% of the cations are mobile at 303K. Upon increasing the temperature, a gradual change in mobile cation concentration is observed initially, with the change becoming more rapid as the melting point is approached. A steady increase in mobile pyrrolidinium concentration is observed for the 4.8mol% $LiNTf_2$ sample up to the melting point. At the lowest temperatures, however, only 10% of the cations are mobile. The same behaviour is also reflected in the 49.9mol% $LiNTf_2$ and can be attributed to the coexistence of both solid and liquid phases, whereby the solid phase limits the concentration of mobile species. The 33mol% $LiNTf_2$ sample exhibits the largest signal intensities of all the samples over the entire temperature range. The signal intensity increases very rapidly with increasing temperature below the eutectic isotherm (308K). Upon exceeding this temperature, however, the signal intensity is once again constant. As one might expect, this behaviour is similar to signal intensities observed for the pure $P_{12}NTf_2$.

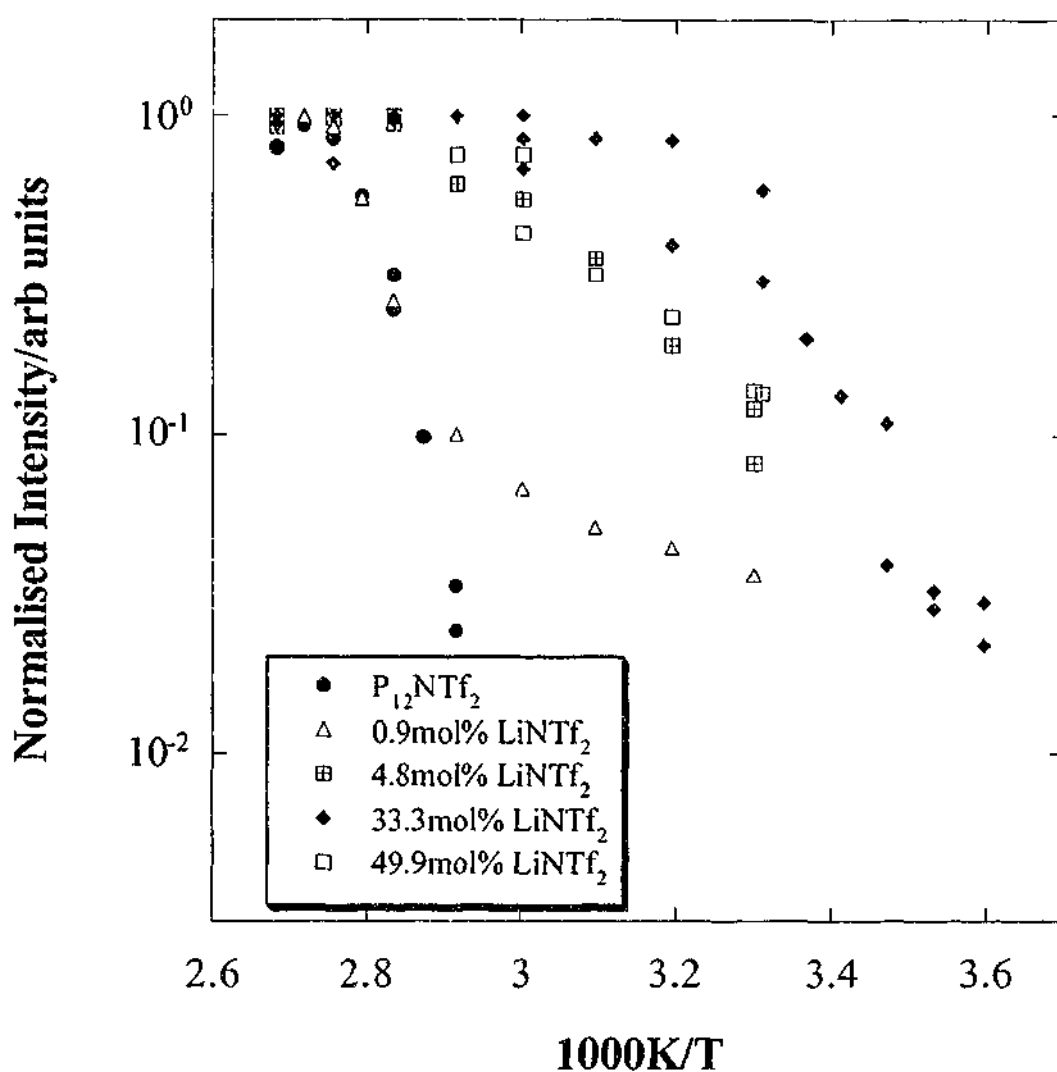


Figure 4-17 Normalised NMR signal intensities as a function of temperature for pure $P_{12}NTf_2$ and the $LiNTf_2/P_{12}NTf_2$ mixtures.

While the change in signal intensity for the pure salt and the 0.9mol% $LiNTf_2$ system is very similar, the signal intensity for the 4.8mol% $LiNTf_2$ sample is significantly greater at any given temperature. If it is assumed that the diffusion is governed by a solid state mechanism, it would seem that there are far more vacancies available in the 4.8mol% $LiNTf_2$ sample, enabling more ions to move. Alternatively, if diffusion in the liquid state dominates the measurement, then the signal intensity for 4.8mol% $LiNTf_2$ may reflect the proportion of liquid phase as determined by the Lever rule. Figure 4-18 and Figure 4-19 compare the NMR signal intensities with the proportion

of liquid phase for the 0.9 and 4.8mol% LiNTf_2 samples respectively and in both cases, the NMR signal is greater than the Lever rule values. The most likely conclusion from this observation is that both solid and liquid state diffusion is detected in these experiments.

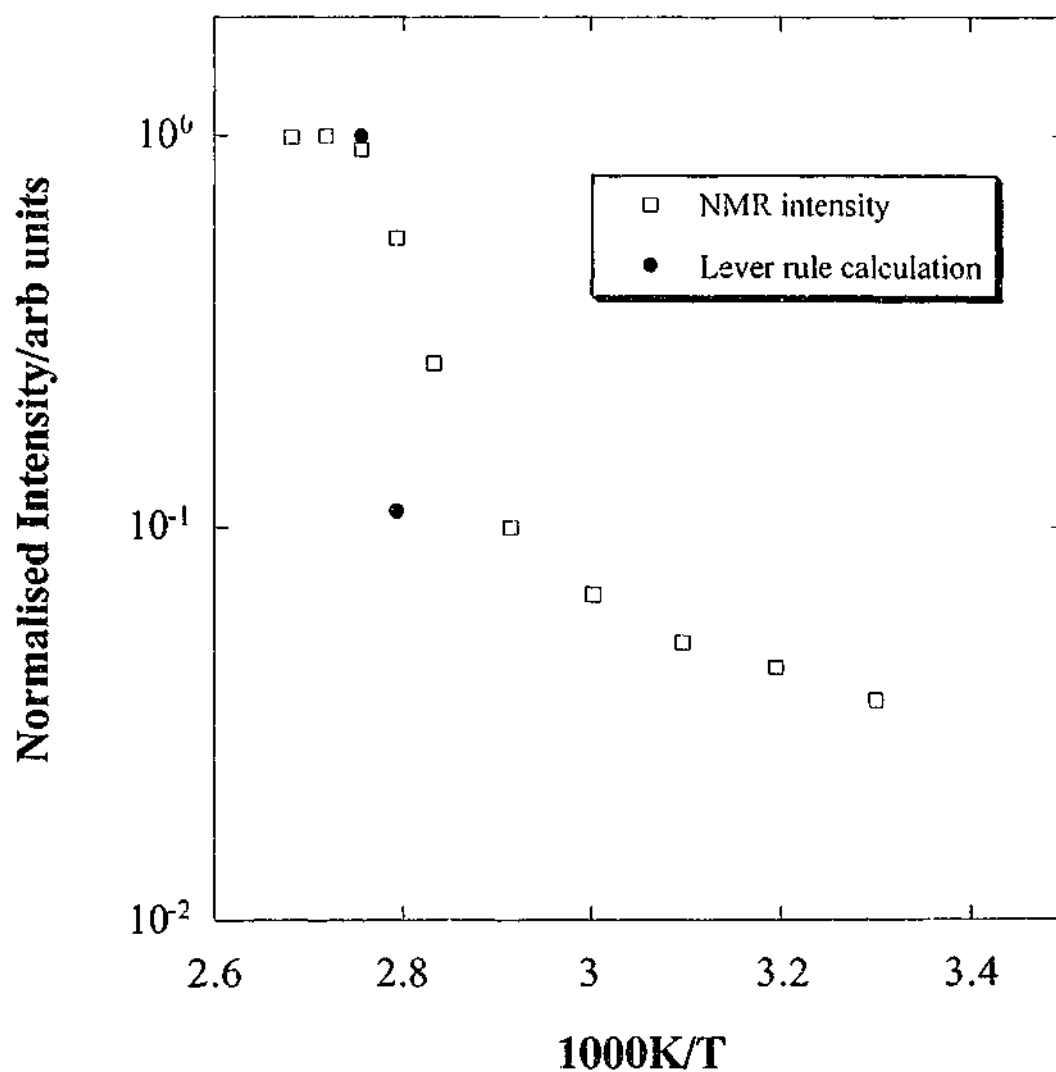


Figure 4-18 A comparison of the NMR signal intensities with the proportion of liquid phase calculated from the Lever rule for 0.9mol% $\text{LiNTf}_2/\text{P}_{12}\text{NTf}_2$.

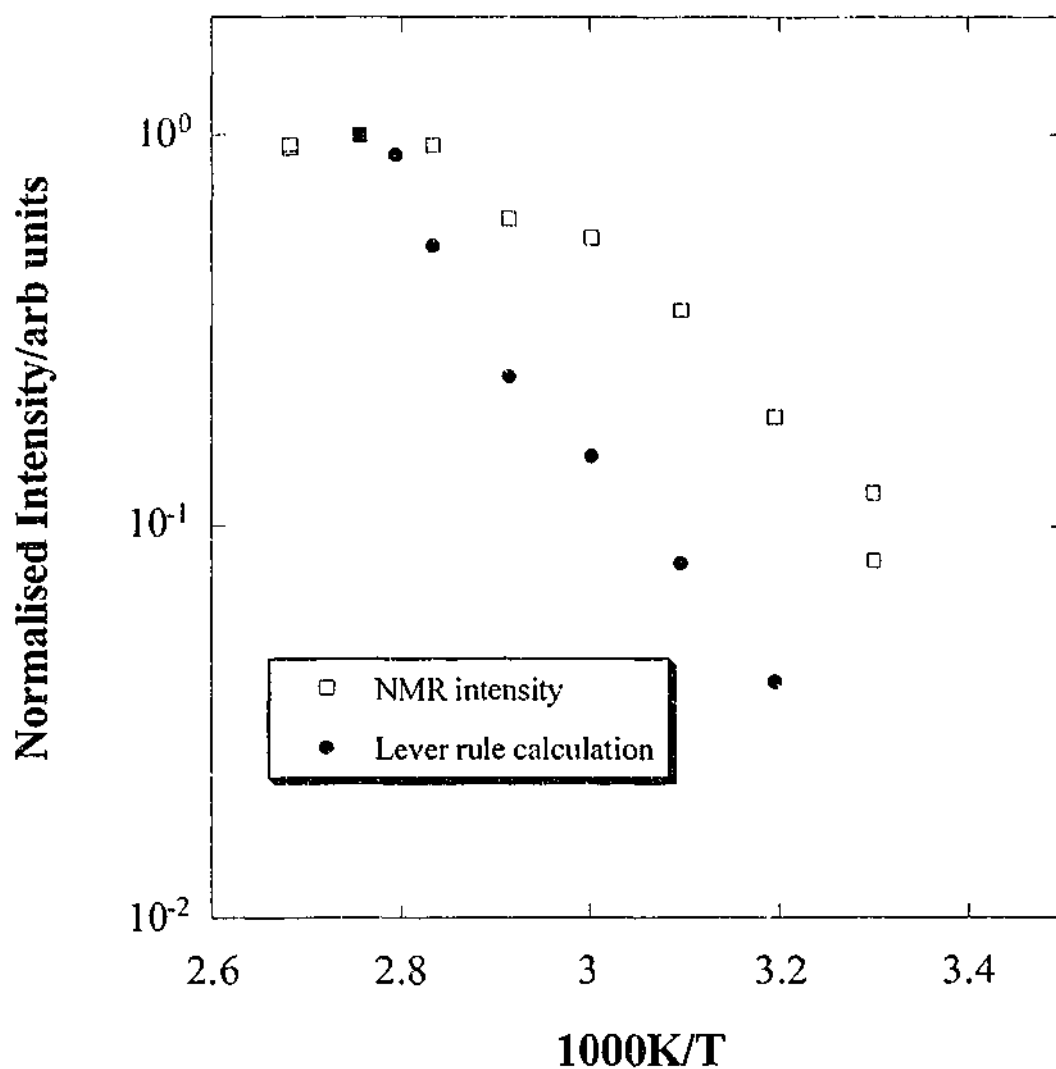


Figure 4-19 A comparison of the NMR signal intensities with the proportion of liquid phase calculated from the Lever rule for 4.8mol% LiNTf₂/P₁₂NTf₂.

It has been shown that the NMR diffusion measurements not only reveal the nature of ion transport but also provide information about the concentration of mobile species within the sample. From this information, it is possible to model the conductivity of these materials with use of the Nernst-Einstein equation. The following section outlines the use of this equation in calculating the conductivity and compares these values to those obtained experimentally.

4.4.3 Modelling Conductivity from Diffusion

As indicated by the Nernst-Einstein equation (Equation 4-4), ionic conductivity is dependent on the ionic diffusion coefficients (D being the sum of the anion and cation diffusion coefficients, D_- and D_+), the ionic charge, q , the concentration of charge carriers, c , and the temperature, T . In this equation, k is the Boltzmann constant.

$$\sigma = \frac{Dq^2c}{kT}$$

Equation 4-4

For the LiNTf₂/P₁₂NTf₂ mixtures, both the cations, the lithium and pyrrolidinium ions, and the anion will possibly contribute to the conductivity. While both the pyrrolidinium and amide diffusion coefficients have been observed in these systems, no lithium diffusion coefficients have been measured in this work due to the lack of appropriate equipment. It is expected, however, that the lithium ions will behave in one of three possible ways: 1. They are immobile: 2. They diffuse in a similar manner to the pyrrolidinium cations: 3. They diffuse faster than the pyrrolidinium cations. Given the size of the lithium ions with respect to the other ions in the system, lithium immobility is difficult to imagine. From lithium linewidth measurements, it appears that the lithium ions are mobile in these materials at temperatures as low as 238K.⁵¹ The extent to which they are mobile probably depends on the nature of the transport mechanism. In the solid state, a similar transport mechanism to the pyrrolidinium cations is expected if a vacancy mechanism is responsible for ion conduction. However, if the lithium ions occupy interstitial sites, then one might expect a slightly faster mode of transport. In the liquid state, the lithium and pyrrolidinium ions will probably exhibit the same diffusion coefficients.

In order to test this hypothesis, the conductivity was calculated from the diffusion coefficients using the Nernst-Einstein equation (Equation 4-4). In performing this

calculation, a number of conditions were imposed. The pyrrolidinium and lithium ions were assumed to diffuse at the same rate over the entire temperature range. Where no ^{19}F signal was detectable, it was assumed that the amide ions were either immobile or diffusing at a similar rate to the cations. The latter assumption, however, is probably an overestimate of the situation. The concentration of charge carriers was calculated from the density of the material, ρ , using the following equation

$$c = \frac{N_A \rho}{MW}$$

Equation 4-5

where N_A is Avogadro's number and MW is the molecular weight of the salt. As the melt densities for the homologous $\text{P}_{13}\text{NTf}_2$ and $\text{P}_{14}\text{NTf}_2$ are 1.45 and 1.41g.cm^{-3} respectively,⁴⁸ it was assumed that $\text{P}_{12}\text{NTf}_2$ would have a melt value of 1.5g.cm^{-3} . The density of LiNTf_2 was taken to be approximately 2g.cm^{-3} as a similar value had been reported for LiBF_4 elsewhere.¹⁸ The molecular weights of $\text{P}_{12}\text{NTf}_2$ and LiNTf_2 are 394.35 and 286.97g.mol^{-1} respectively. This concentration is not constant, however, as the proportion of mobile species will vary with temperature. The variation was assumed to follow either the NMR signal intensity or the proportion of liquid phase, as indicated by the Lever rule in the case of the 0.9 and $4.8\text{mol}\%$ samples.

The calculated and measured conductivities for pure $\text{P}_{12}\text{NTf}_2$ are compared in Figure 4-20. The two calculated curves represent two possible conduction mechanisms where the anion is either mobile or immobile. In both cases, the calculated conductivities are considerably higher than the measured values, although the discrepancy is smaller when the anion is immobile. Such behaviour suggests that there is a significant proportion of mobile ions (in terms of the NMR diffusion

experiment) that are not contributing to the conductivity. This is probably due to the motion of neutral ion pairs.^{47,58}

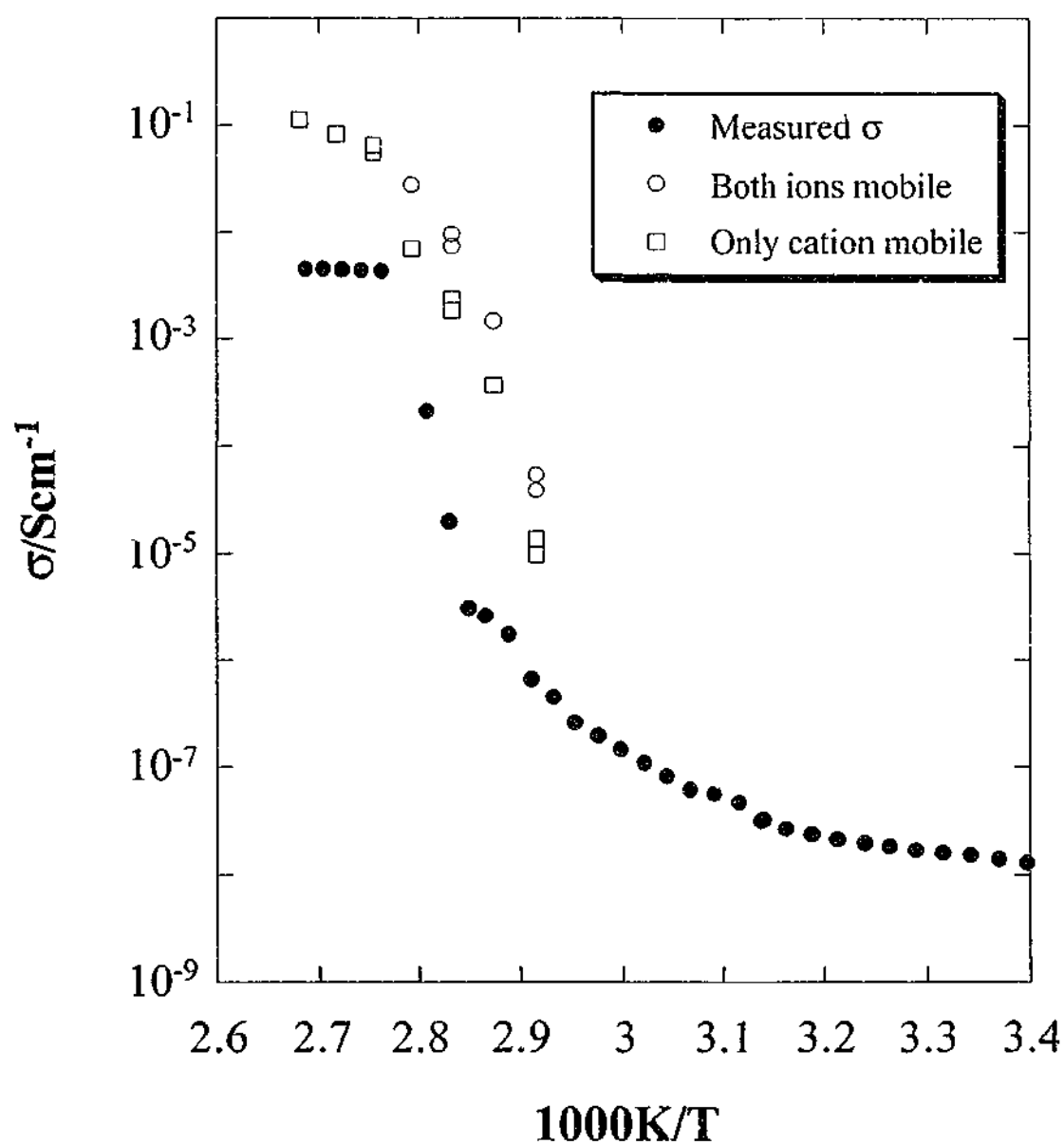


Figure 4-20 A comparison of the calculated and measured conductivities for pure $\text{P}_{12}\text{NTf}_2$.

Figure 4-21 displays the calculated and measured conductivities for 0.9mol% $\text{LiNTf}_2/\text{P}_{12}\text{NTf}_2$. Depending on the anion mobility (mobile or immobile) and the

charge carrier concentration (from the Lever rule or NMR signal intensity), four possible conduction mechanisms may occur as indicated by the four calculated curves. Once again, the calculated conductivities are higher than the measured values, albeit less so when the anion is assumed to be immobile. The calculation based on the Lever rule is also limited to temperatures above 353K, whereas the use of the NMR signal intensity in the calculation predicts the conductivity as low as 303K.

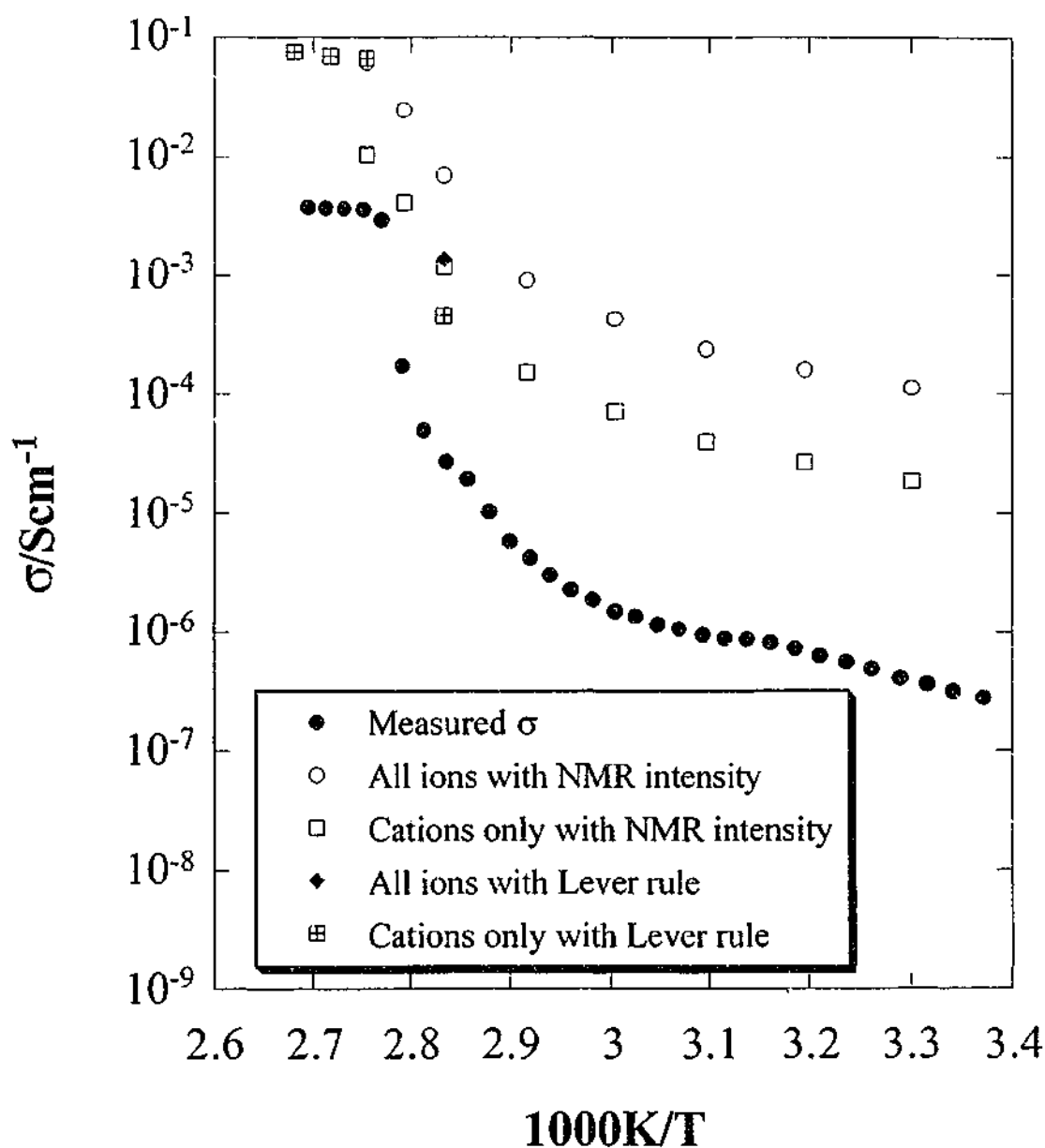


Figure 4-21 A comparison of the calculated and measured conductivities for 0.9mol% $\text{LiNTf}_2/\text{P}_{12}\text{NTf}_2$.

Two calculated conductivity curves are compared with the measured conductivities for the 4.8mol% LiNTf₂ sample in Figure 4-22. As both cations and the anion are assumed to contribute to the conductivity in this material, the calculated curves represent the different charge carrier concentrations (Lever rule or NMR intensity). For both curves, the resultant conductivity is significantly higher than the measured data. However, in using the Lever rule to predict the concentration of charge carriers, the difference is not as great. This observation may suggest that diffusion in the liquid phase is the dominant transport mechanism in the measured temperature range for this particular sample. However, given the large discrepancy between the calculated and measured conductivities, it is difficult to say which of the two mechanisms is more likely.

Figure 4-23 and Figure 4-24 compare the calculated and measured conductivities for 33mol% and 49.9mol% LiNTf₂/P₁₂NTf₂ respectively. In most cases, the calculated conductivities are considerably higher than the measured values. Again, this behaviour has been attributed to the presence of neutral ion pairs that are able to diffuse through the material but that makes no contribution to the conductivity. For the 33mol% sample, for which solid state diffusion has also been measured, the differences below the melting point are not so extreme. Based on this observation, it seems that all mobile ions contribute to the conductivity in the solid state and that the NMR signal intensity adequately predicts the change in charge carrier concentration.

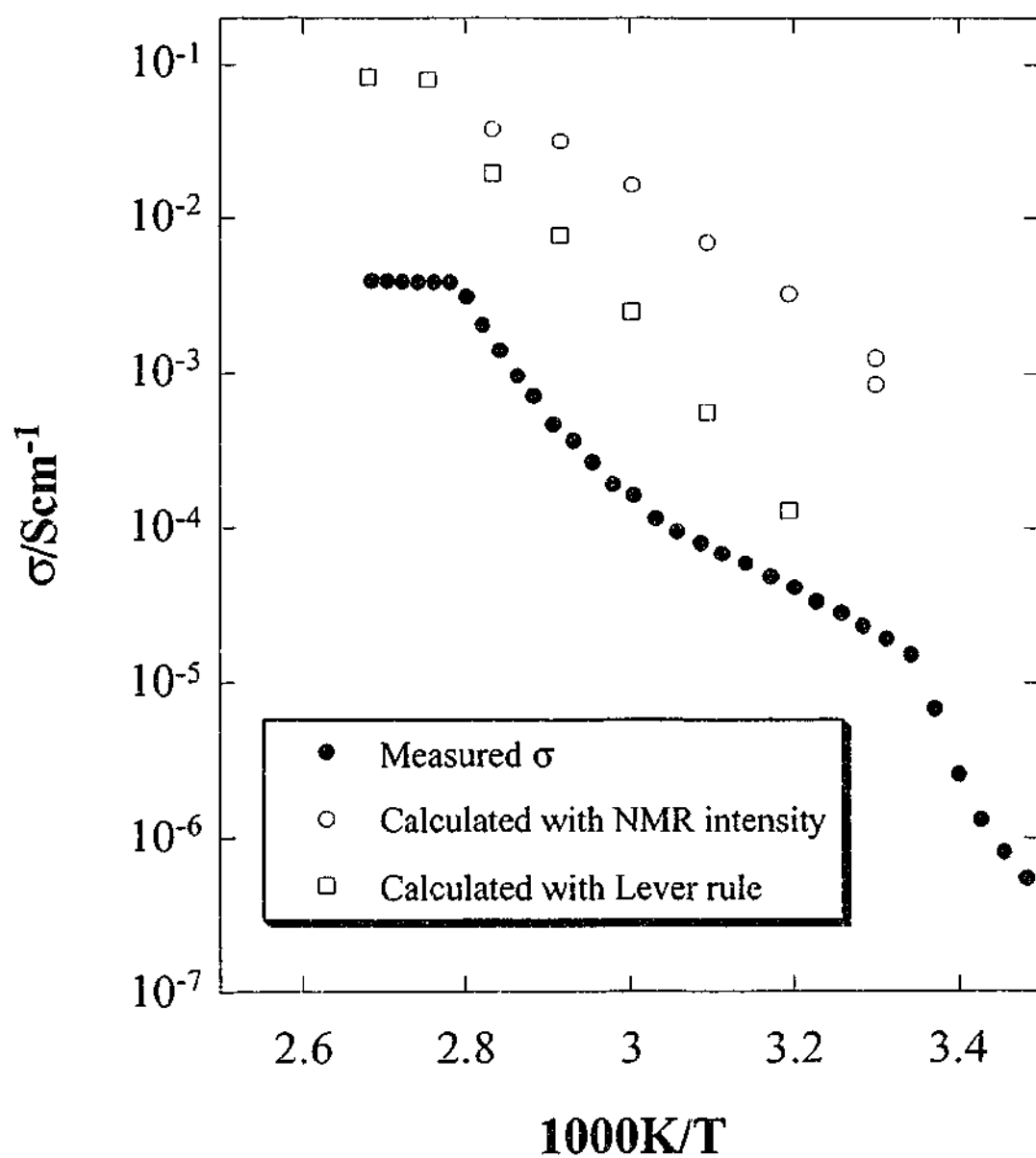


Figure 4-22 A comparison of the calculated and measured conductivities for 4.8mol% $\text{LiNTf}_2/\text{P}_{12}\text{NTf}_2$.

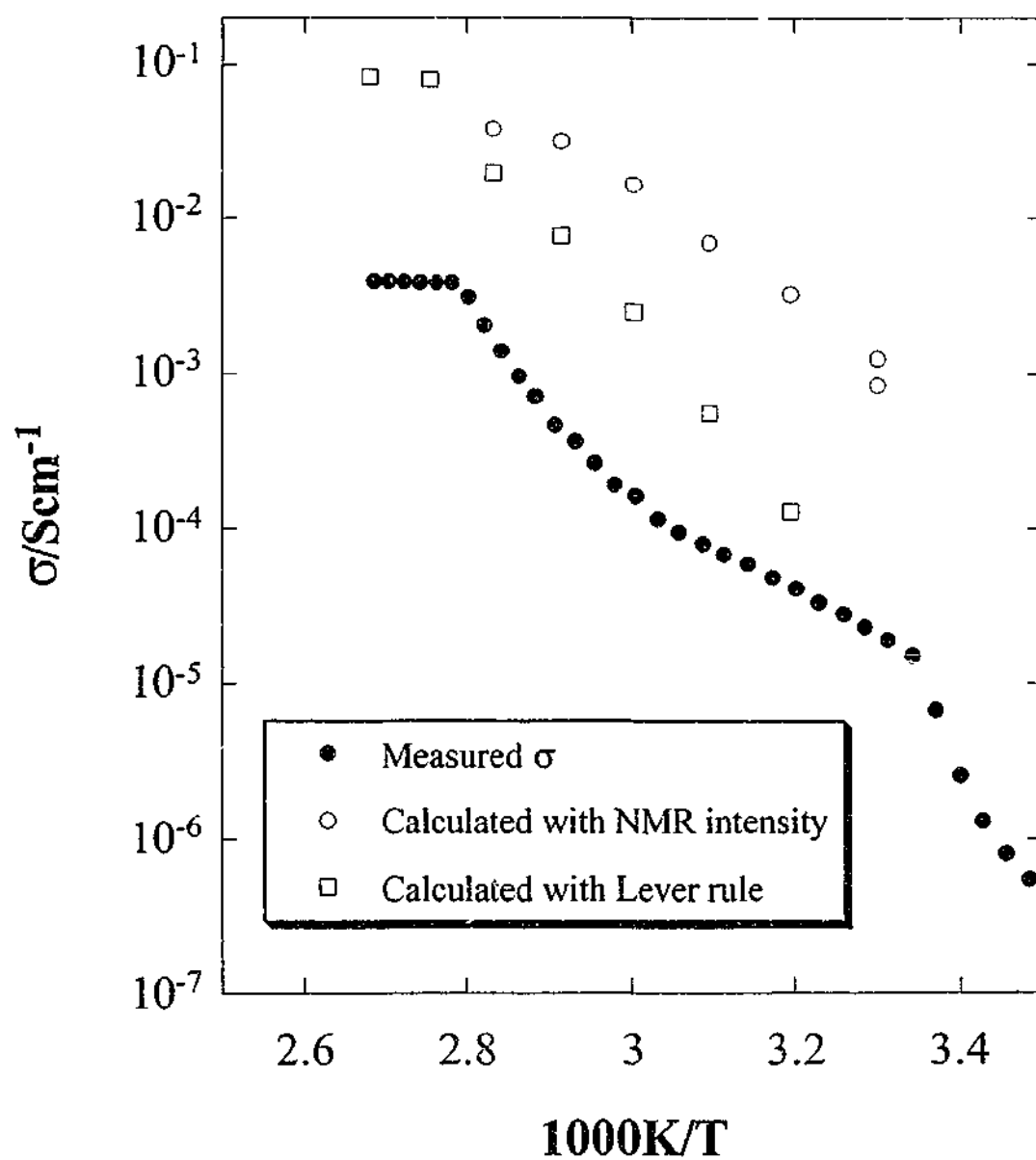


Figure 4-22 A comparison of the calculated and measured conductivities for 4.8mol% $\text{LiNTf}_2/\text{P}_{12}\text{NTf}_2$.

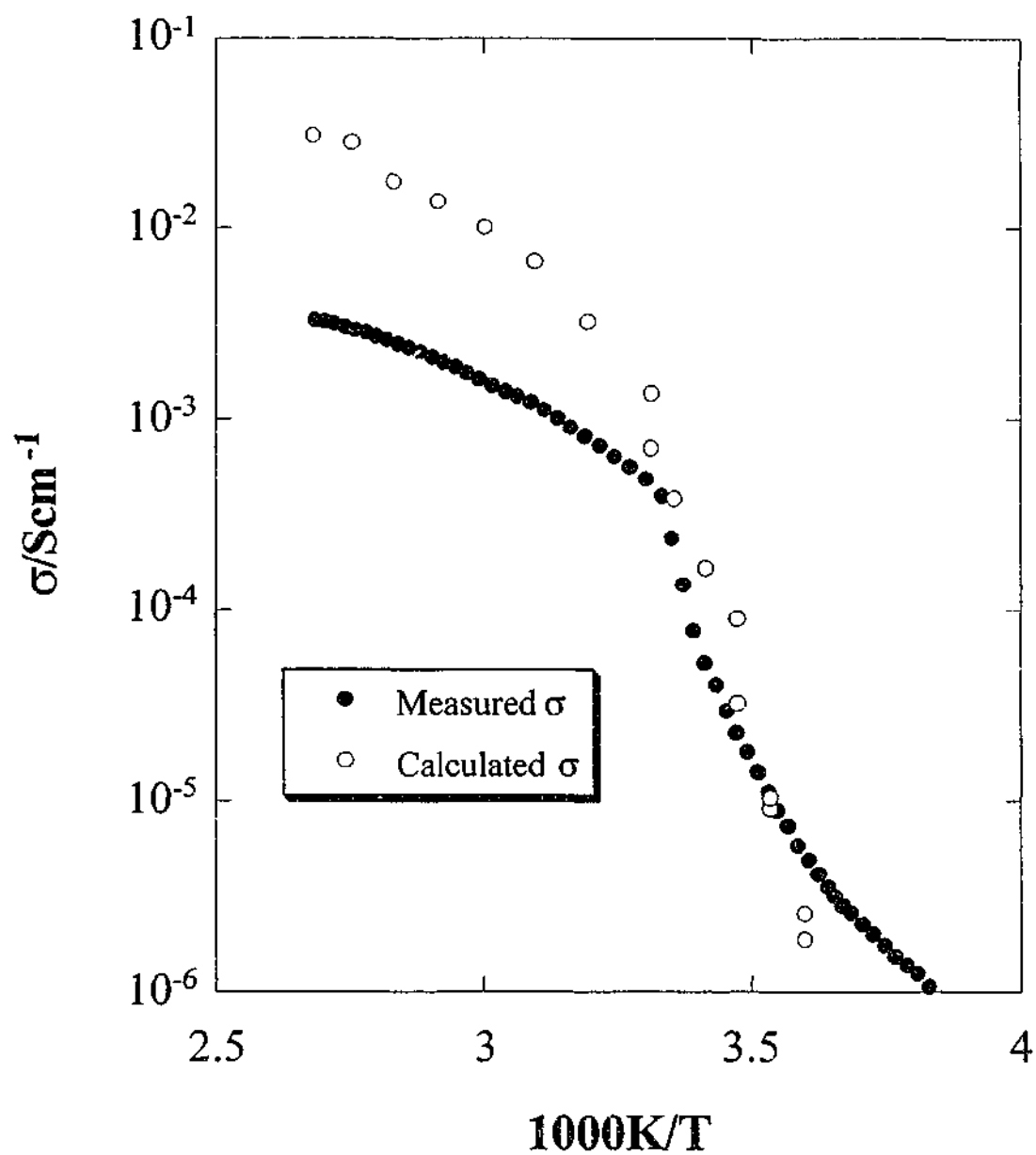


Figure 4-23 A comparison of the calculated and measured conductivities for 33mol% LiNTf₂/P₁₂NTf₂.

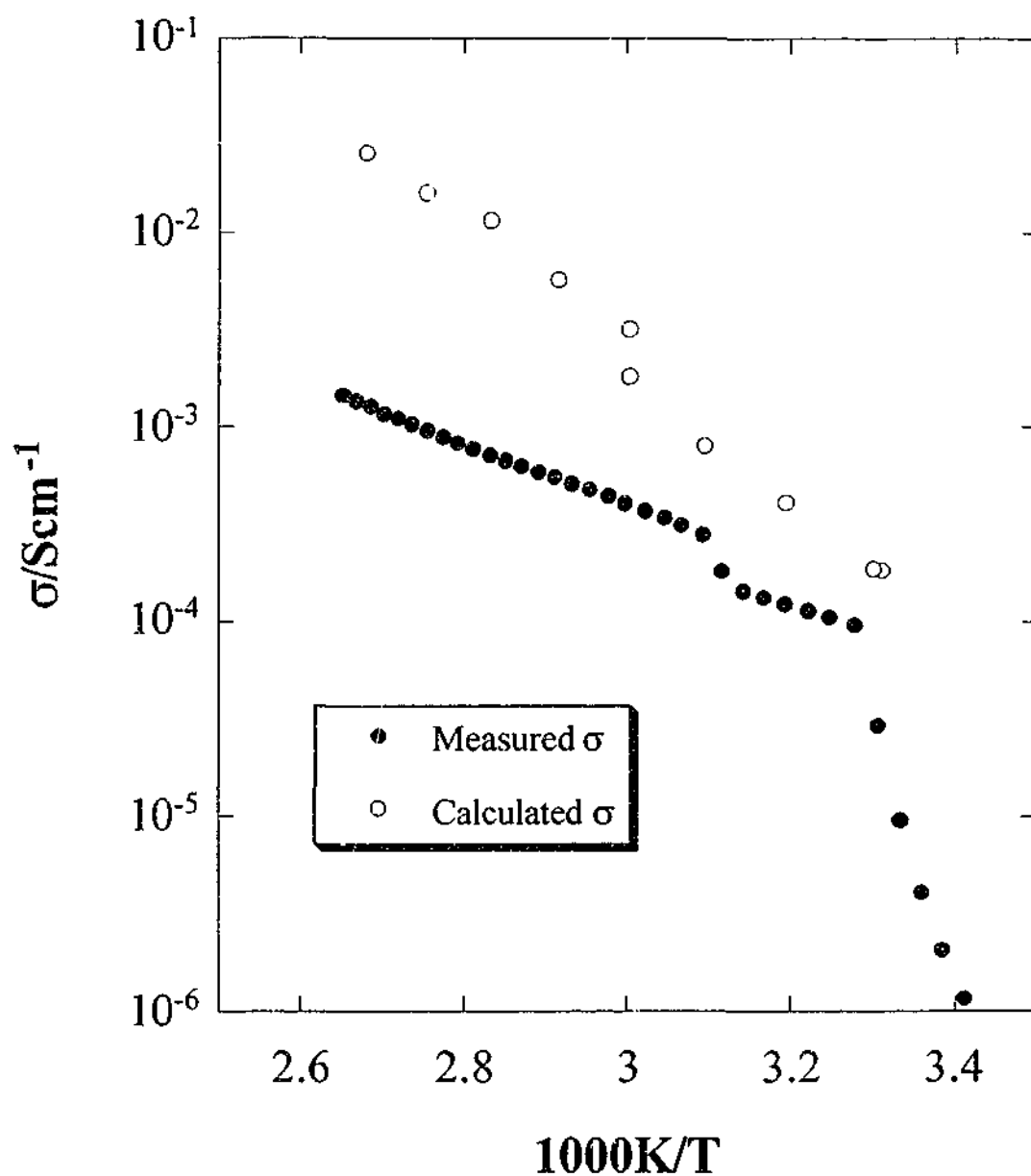


Figure 4-24 A comparison of the calculated and measured conductivities for 49.9mol% LiNTf₂/P₁₂NTf₂.

Although the discrepancy between the calculated and measured conductivities has been attributed to the diffusion of neutral ion pairs, some ions must exist for conduction to occur. The fraction of ions available for conduction, f , can be determined from the following ratio:

$$f = \frac{\sigma_{\text{meas}}}{\sigma_{\text{calc}}}$$

Equation 4-6

where σ_{meas} and σ_{calc} are the measured and calculated conductivities respectively. Figure 4-25, Figure 4-26 and Figure 4-27 show the fraction of free ions as a function of temperature for pure $\text{P}_{12}\text{NTf}_2$, 0.9mol% and 4.8mol% $\text{LiNTf}_2/\text{P}_{12}\text{NTf}_2$. Considering that a value of 1 indicates complete ionic dissociation, significant ion association is evident in all the samples, with less than 10% of the ions available for conduction. In the melt, there is generally a consistent decrease in the number of free ions with increasing temperature. This is most likely the result of increased ionic aggregation, which was also observed in the imidazolium ionic liquids (see the previous chapter, section 3.4.1.2). A slight decrease in free ion concentration was also observed in the solid state for pure $\text{P}_{12}\text{NTf}_2$ and the 4.8mol% LiNTf_2 sample when the Lever rule was used to calculate the concentration of charge carriers. For the remaining calculations, the free ion concentration in the solid state is relatively independent of temperature. An interesting feature of each data set is a slight increase in free ion concentration as the melting point is approached. Such behaviour is not unexpected, as one would assume that vacancy formation will increase rapidly just prior to melting.

The fact that so few ions are involved in the conduction mechanism in the solid state is somewhat difficult to explain. In the pyrrolidinium perchlorate and hexafluorophosphate systems studied by Ono *et al.*,⁴⁷ it was suggested that vacancy pairs and/or Schottky defects were responsible for the diffusion mechanism. Under such circumstances, it would be possible for the ions to diffuse as a neutral pair and therefore have no contribution to the conductivity. In this amide system, however, the anions may not be diffusing in the solid state, hence only the cations will

contribute to the conductivity. Based on this model, there should be no neutral pairs and therefore, all the cations should move as individual ions. It was noted earlier, however, that the inability to observe any anion diffusion in the solid state does not necessarily imply that the anion is immobile. The fringe field gradient technique used to measure the anion diffusion coefficients is often limited by T_2 interference effects. As it would appear that only a small fraction of the ions is mobile in the solid state, the larger fraction of immobile ions will result in the dominance of T_2 in the fringe field gradient measurement. Such behaviour can only be confirmed by a pulsed field gradient measurement for anion diffusion using ^{19}F NMR.

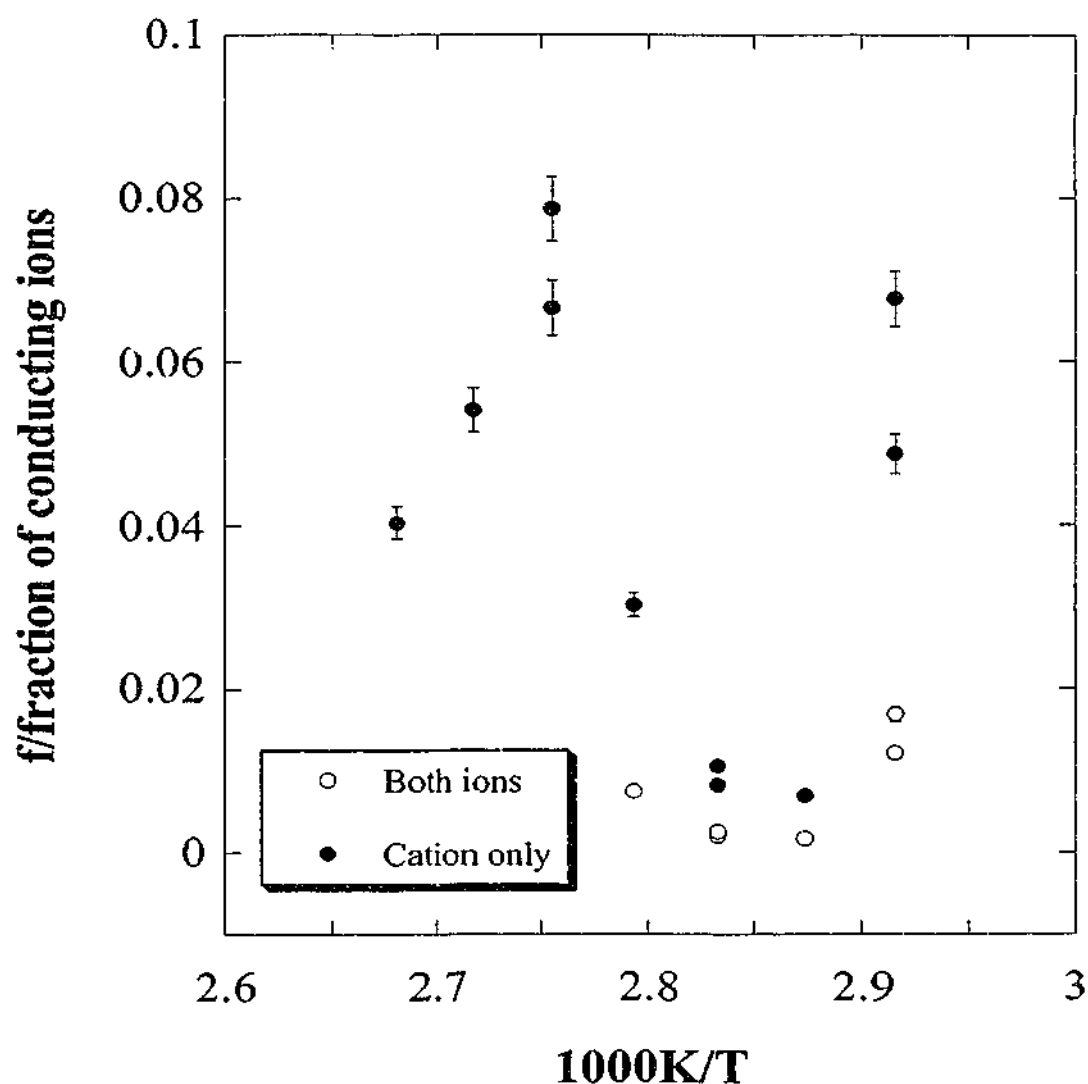


Figure 4-25 The free ion fraction as a function of temperature for pure $\text{P}_{12}\text{NTf}_2$.

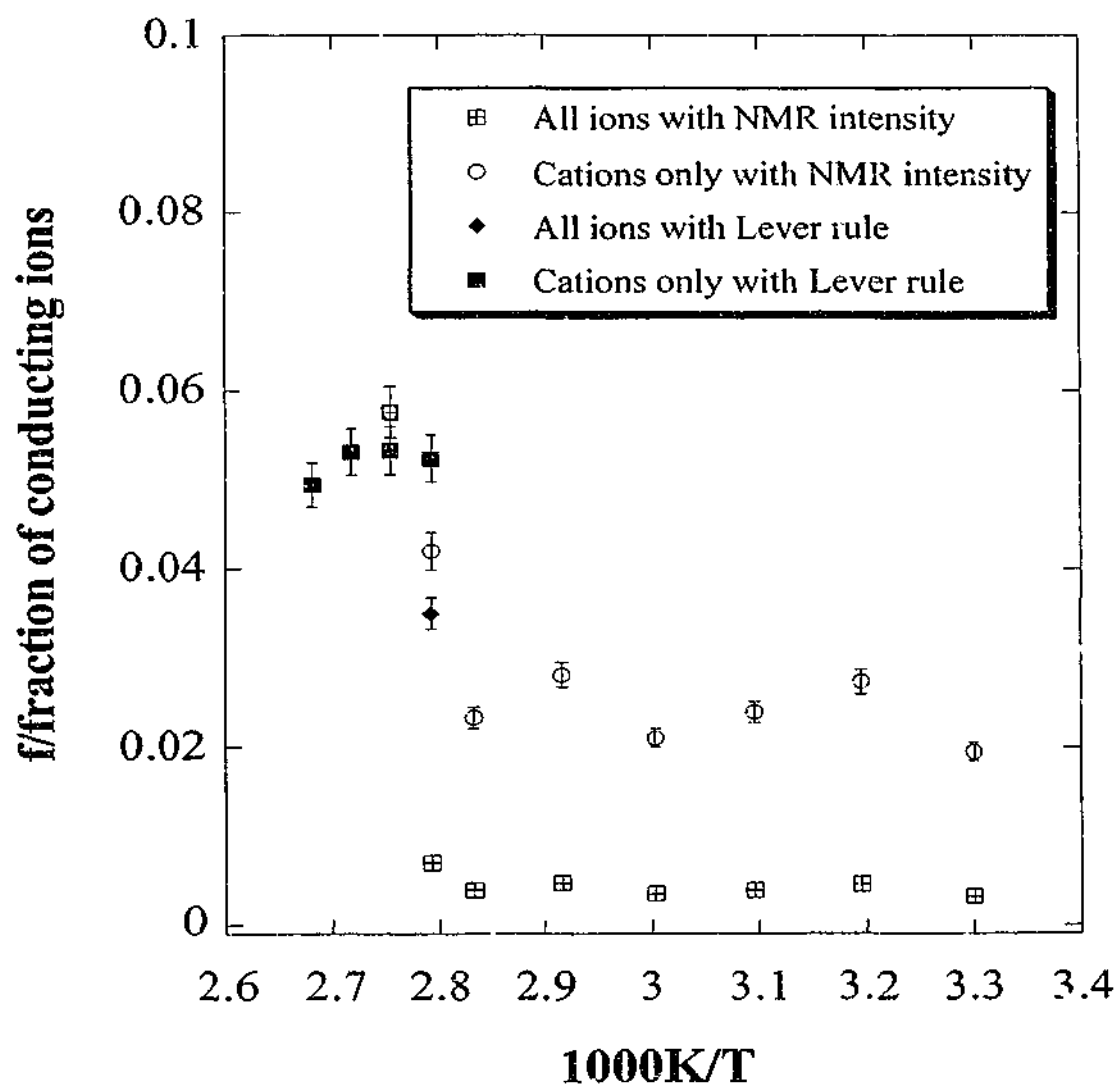


Figure 4-26 The free ion fraction as a function of temperature for the 0.9mol% LiNTf₂/P₁₂NTf₂ mixture.

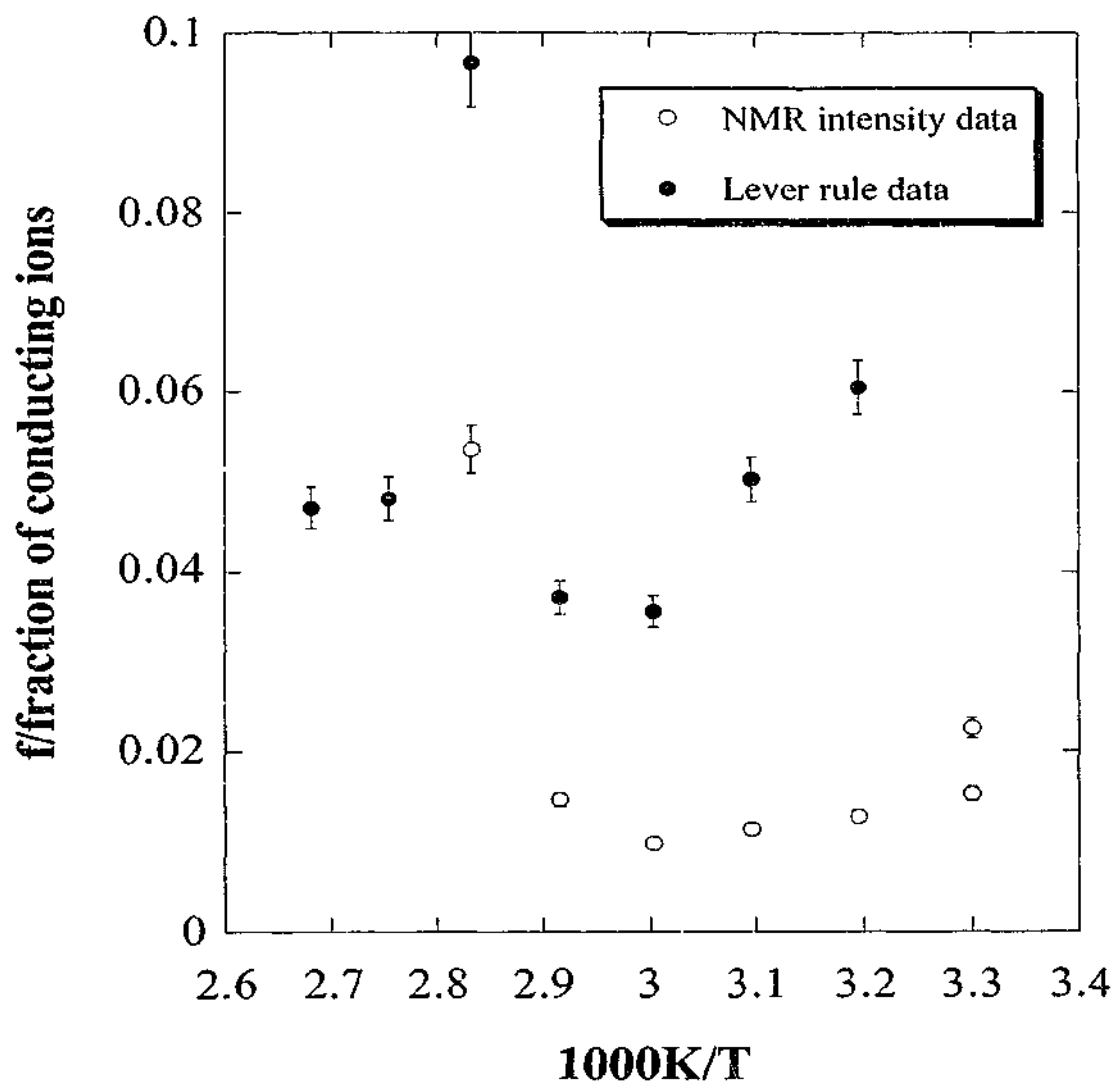


Figure 4-27 The free ion fraction as a function of temperature for 4.8mol% LiNTf₂/P₁₂NTf₂.

Figure 4-28 and Figure 4-29 show the fraction of free ions as a function of temperature for the 33mol% and 49.9mol% samples respectively. Both plots indicate a steady decrease in the fraction of free ions with increasing temperature and there is no jump around the melting points of each material (unlike the other systems). Although there is some scatter at the lower temperatures, the fraction of free ions is around 60 to 80%, which suggests that most of the mobile ions are available for conduction. As the temperature increases, however, this fraction decreases to about 10% as more neutral species form. Similar behaviour was

observed in the molten imidazolium salts (see section 3.4.1.2) and therefore appears to be characteristic of largely liquid materials.

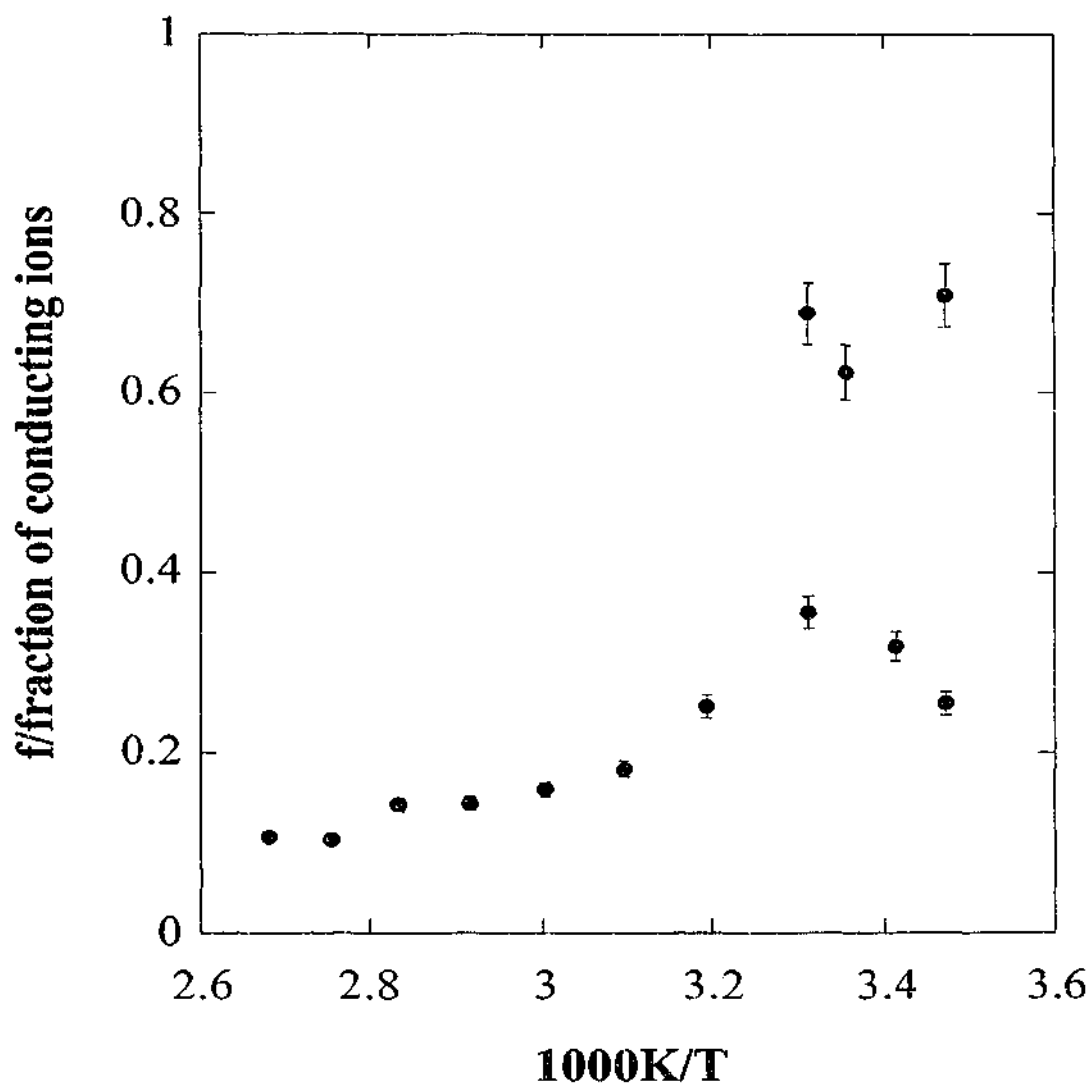


Figure 4-28 The free ion fraction as a function of temperature for 33mol% LiNTf₂/P₁₂NTf₂.

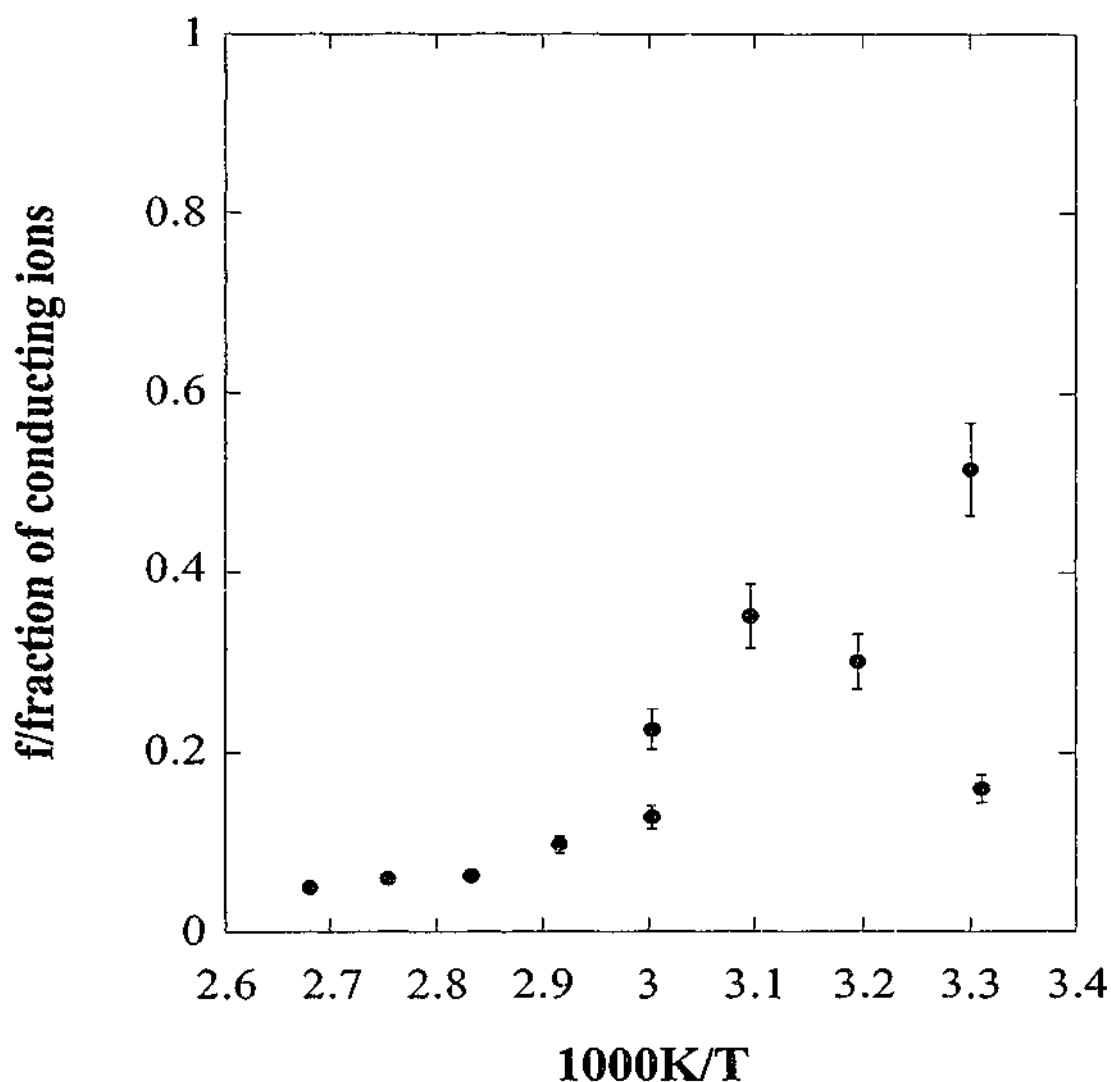


Figure 4-29 The free ion fraction as a function of temperature for 49.9mol% LiNTf₂/P₁₂NTf₂.

In summary, the addition of a small amount of lithium salt has a significant effect on the ion mobility in pyrrolidinium amide salt. The increase in conductivity upon adding 0.9mol% and 4.8mol% LiNTf₂ appears to be the result of an increase in the number of mobile cations. The inability to measure amide diffusion coefficients for pure P₁₂NTf₂ and the 0.9mol% LiNTf₂ sample, together with the modelling of conductivity using either all the ions or only the cations, suggests that the conduction mechanism does appear to be dominated by the cations, which move via a vacancy type mechanism. The concentration of charge carriers as a function of temperature is

reflected in the signal intensity from the NMR diffusion measurements. Less than 10% of the charge species actually contribute to the conductivity.

The addition of larger amounts of LiNTf_2 (33 and 49.9mol%) results in the lowering of the melting point. The pyrrolidinium and amide diffusion coefficients in these two materials decrease with increasing LiNTf_2 content. Although the conductivity also decreases as the LiNTf_2 content is increased from 33mol% to 49.9mol%, the change is far greater than what the diffusion measurements predict. The NMR signal intensity, which represents the concentration of mobile ions, can account for this behaviour. The fraction of free ions for both systems is quite high at 303K, but decreases with increasing temperature as a result of ionic aggregation.

4.4.4 The Nature of Ion Transport

Based on the information presented here, it appears that the nature of ion transport at any given temperature varies with the concentration of LiNTf_2 . Small amounts of LiNTf_2 added to pure $\text{P}_{12}\text{NTf}_2$ form a solid solution, therefore the mixture is expected to have the same crystal structure as the pure salt. This is confirmed by the thermal analysis data, where similar behaviour was observed for the pure and doped materials.⁵¹ Since the amide ions are so large, they will not fit into the interstitial sites and therefore must be incorporated into the crystal lattice. The lithium ions, however, are small enough to occupy interstitial sites (ionic radius of 0.07nm^{57}), which would create vacant cation sites for the pyrrolidinium cations to move into. Even if the lithium ions occupy lattice sites, there will be a significant size difference between the two cations (the pyrrolidinium ions are assumed to have an ionic radius of approximately 0.2 to 0.3nm^{51}). This mismatch may result in some structural instability in the environment surrounding the lithium ions, causing vacancy formation. Either way, the addition of the lithium salt is thought to generate more vacancies, thus enabling more parent ions to diffuse throughout the material in

addition to the lithium ions. The result is, of course, a higher conductivity. In the case of the 33 mol% LiNTf₂ sample, solid state behaviour was also observed below the eutectic isotherm. Although exhibiting slightly lower solid state diffusion coefficients than the other solid samples, this material displayed some of the highest solid state conductivities. A similar solid state mechanism is expected for this sample, where the larger LiNTf₂ content results in a further increase in the concentration of mobile ions.

Larger amounts of LiNTf₂ resulted in higher conductivities, which can largely be explained by the presence of a liquid phase. Transport in a liquid involves the collective rearrangement of small sections of the material, a mechanism that has been shown to result in a slightly slower diffusion than that observed in the solid state. Given that every ion is mobile in this transport mechanism, the concentration of charge carriers will be substantially greater in the liquid state. This increased charge carrier concentration offsets the slower diffusion mechanism resulting in an enhanced conductivity. These transport mechanisms are proposed to account for the observed behaviour in the LiNTf₂/P₁₂NTf₂ mixtures.

4.5 References

1. F. M. Gray, *Polymer Electrolytes*, (Royal Society of Chemistry, Cambridge, 1997).
2. W. J. Dunning, in *The Plastically Crystalline State*, edited by J. N. Sherwood (John Wiley and Sons, New York, 1979), pp. 1-37.
3. J. M. Chezeau and J. H. Strange, *Phys. Rep. Phys. Lett.* **53**, 1-92 (1979).
4. F. Simon and C. von Simson, *Z. Phys.* **21**, 168 (1924).
5. A. Müller, *Proc. Roy. Soc. London Ser. A* **138**, 514-530 (1932).

6. E. R. Andrew and R. G. Eades, *Proc. Roy. Soc. London Ser. A* **216**, 398-412 (1953).
7. E. R. Andrew, *J. Phys. Chem. Solids* **18**, 9-16 (1961).
8. J. Timmermans, *J. Phys. Chem. Solids* **18**, 1-8 (1961).
9. J. G. Powles, *J. Phys. Chem. Solids* **18**, 17-20 (1961).
10. J. E. Tanner, *J. Chem. Phys.* **56**, 3850-3852 (1972).
11. J. N. Sherwood, *Surface and Defect Properties of Solids* **2**, 250-268 (1973).
12. *The Plastically Crystalline State*, edited by J. N. Sherwood (John Wiley and Sons, New York, 1979).
13. S. M. Ross and J. H. Strange, *J. Chem. Phys.* **68**, 3078 (1978).
14. W. P. Rothwell and J. S. Waugh, *J. Chem. Phys.* **74**, 2721-2732 (1981).
15. A. V. Chadwick, in *Diffusion in Solids: Unsolved Problems*, Vol. 83, edited by G. E. Murch (Trans Tech Publications Ltd., 1992), pp. 235-258.
16. A. H. Fuchs, J. Virlet, D. Andre and H. Szwarc, *J. Chim. Phys.* **82**, 293-303 (1985).
17. J. Tsau and D. F. R. Gilson, *Can. J. Chem.* **51**, 1990-1994 (1973).
18. E. C. Reynhardt and J. A. J. Lourens, *J. Chem. Phys.* **80**, 6240-6244 (1984).
19. E. I. Cooper and C. A. Angell, *Solid State Ionics* **18-19**, 570-576 (1986).
20. C. A. Angell, *Solid State Ionics* **18-19**, 72-88 (1986).
21. H. Ishida, R. Ikeda and D. Nakamura, *Bull. Chem. Soc. Jpn.* **59**, 915-924 (1986).
22. S. Iwai, R. Ikeda and D. Nakamura, *Can. J. Chem.* **66**, 1961-1969 (1988).
23. M. Hattori, S.-I. Fukada, D. Nakamura and R. Ikeda, *J. Chem. Soc., Faraday Trans.* **86**, 3777-3783 (1990).
24. T. Tanabe, D. Nakamura and R. Ikeda, *J. Chem. Soc., Faraday Trans.* **87**, 987-990 (1991).

25. E. A. Secco, *J. Solid State Chem.* **96**, 366-375 (1992).
26. Y. Furukawa and R. Ikeda, *Ber. Bunsenges. Phys. Chem.* **97**, 1143-1146 (1993).
27. A. Lundén, *J. Solid State Chem.* **107**, 296-298 (1993).
28. M.-L. Saboungi, J. Fortner, W. S. Howells and D. L. Price, *Nature* **365**, 237-239 (1993).
29. M. Kenmotsu, H. Honda, H. Ohki, R. Ikeda, T. Erata, A. Tasaki and Y. Furukawa, *Z. Naturforsch. A* **49**, 247-252 (1994).
30. Z. Pajak and J. Zaleski, *Solid State Commun.* **91**, 821-823 (1994).
31. H. Ishida, Y. Kubozono, S. Kashino and R. Ikeda, *Z. Naturforsch. A* **49**, 723-726 (1994).
32. H. Ishida and Y. Furukawa, *Z. Naturforsch. A* **51**, 83-86 (1996).
33. Z. Pajak, *Solid State Commun.* **92**, 707-709 (1994).
34. R. Ikeda, S.-I. Ishimaru, T. Tanabe and D. Nakamura, *J. Mol. Struct.* **345**, 151-157 (1995).
35. Y. Furukawa, *J. Mol. Struct.* **345**, 119-122 (1995).
36. H. Honda, M. Kenmotsu, H. Ohki, R. Ikeda and Y. Furukawa, *Ber. Bunsenges. Phys. Chem.* **99**, 1009-1014 (1995).
37. H. Honda, S.-I. Ishimaru, N. Onoda-Yamamuro and R. Ikeda, *Z. Naturforsch. A* **50**, 871-875 (1995).
38. H. Ono, R. Seki, R. Ikeda and H. Ishida, *J. Mol. Struct.* **345**, 235-243 (1995).
39. H. Ishida, Y. Furukawa, S. Kashino, S. Sato and R. Ikeda, *Ber. Bunsenges. Phys. Chem.* **100**, 433-439 (1996).
40. H. Ono, S.-I. Ishimaru, R. Ikeda and H. Ishida, *Bull. Chem. Soc. Jpn.* **70**, 2963-2972 (1997).

41. H. Ishida, M. Kato, H. Ono and R. Ikeda, *Z. Naturforsch. A* **52**, 637-639 (1997).
42. H. Ono, S.-I. Ishimaru, R. Ikeda and H. Ishida, *Chem. Phys. Lett.* **275**, 485-490 (1997).
43. Z. Pajak, B. Szafranska, P. Czarnecki, J. Mayer and A. Kozak, *Chem. Phys. Lett.* **247**, 106-111 (1997).
44. S. Tanaka, N. Onoda-Yamamuro S.-I. Ishimaru and R. Ikeda, *Bull. Chem. Soc. Jpn.* **70**, 2981-2986 (1997).
45. T. Shimizu, S. Tanaka, N. Onoda-Yamamuro, S.-I. Ishimaru and R. Ikeda, *J. Chem. Soc., Faraday Trans.* **93**, 321-326 (1997).
46. H. Ono, S. Ishimaru, R. Ikeda and H. Ishida, *Ber. Bunsenges. Phys. Chem.* **102**, 650-655 (1998).
47. H. Ono, S.-I. Ishimaru, R. Ikeda and H. Ishida, *Bull. Chem. Soc. Jpn.* **72**, 2049-2054 (1999).
48. D. R. MacFarlane, P. Meakin, J. Sun, N. Amini and M. Forsyth, *J. Phys. Chem. B* **103**, 4164-4170 (1999).
49. D. R. MacFarlane, J. Huang and M. Forsyth, *Nature* **402**, 792-794 (1999).
50. H. Honda, S.-I. Ishimaru and R. Ikeda, *Z. Naturforsch. A.* **54**, 519-523 (1999).
51. M. Forsyth, J. Huang and D. R. MacFarlane, *J. Mater. Chem.* **10**, 2259-2265 (2000).
52. J. Huang, M. Forsyth and D. R. MacFarlane, *Solid State Ionics* **136**, 447-452 (2000).
53. N. Boden, in *The Plastically Crystalline State*, edited by J. N. Sherwood (John Wiley and Sons, New York, 1979), pp. 147-213.
54. M. Witschas, H. Eckert, D. Wilmer, R. D. Banhatti, K. Funke, J. Fitter, R. E. Lechner, G. Korus and M. Jansen, *Z. Phys. Chem.* **214**, 643-673 (2000).

55. D. Wilmer, K. Funke, M. Wischas, R. D. Banhatti, M. Jansen, G. Korus, J. Fitter and R. E. Lechner, *Physica B* **266**, 60-68 (1999).
56. W. D. Callister, *Materials Science and Engineering, an Introduction* (John Wiley and Sons, Inc., 1991).
57. M. Ue, *J. Electrochem. Soc.* **141**, 3336-3342 (1994).
58. H. Bloom and J. O. M. Bockris, in *Fused Salts*, edited by B. R. Sundheim (McGraw-Hill Book Company, New York, 1964), pp. 1-62.

Chapter Five

A Comparison of the Imidazolium and Pyrrolidinium Salt Systems

The focus of this thesis, thus far has been to understand the effect of chemical structure on the diffusion properties of the individual imidazolium and pyrrolidinium systems. However, given that both salts are based on a cyclic ammonium structure with alkyl substituents, it is also possible to contrast the transport mechanisms for these two materials. The two systems are intrinsically different - the imidazolium five membered ring is aromatic and planar; while the pyrrolidinium ring is essentially a quaternary ammonium salt, with a more globular shape. The following discussion compares the behaviour of the pure salts.

5.1 Comparing the Salts

Consider the two salts, 1,3-methylethylimidazolium amide (MeEtImNTf_2) and N,N-methylethylpyrrolidinium amide ($\text{P}_{12}\text{NTf}_2$) (where "amide" is the shortened form of bis(trifluoromethanesulfonyl amide)). The properties of these two salts have been summarised in Table 5-1. Both salts have the same alkyl substituents (a methyl and an ethyl group) and the same anion, and only differ in the actual ring structure. The ionic radius for the imidazolium cation has been reported to be 0.3nm^1 and the pyrrolidinium ring is thought to be quite similar.² Despite these similarities, the two salts are physically quite different. MeEtImNTf_2 is a liquid with melting and glass transitions at 255K and 180K respectively.³ $\text{P}_{12}\text{NTf}_2$ is a solid that exhibits a melting transition at 363K.² Although no glass transition was observed for this

material, a number of sub-melting solid-solid transitions have been reported,² implying plastic crystal behaviour.

Table 5-1 A comparison of the properties of MeEtImNTf₂ and P₁₂NTf₂.

Property	MeEtImNTf ₂	P ₁₂ NTf ₂
Molecular weight	391.20g.mol ⁻¹	394.35g.mol ⁻¹
Cationic radius/nm	0.3nm ⁽¹⁾	0.2 to 0.3nm ⁽²⁾
T _m , T _g	255K, 180K ⁽³⁾	363K, - ⁽²⁾
Density	1.52 to 1.55g.cm ⁻³ at 295K ^(3,4)	1.5g.cm ⁻³ † at 295K
D _{cation}	1.6e ⁻¹⁰ ± 1.5e ⁻¹¹ m ² .s ⁻¹ at 343K 4.3e ⁻¹⁰ ± 5.5e ⁻¹¹ m ² .s ⁻¹ at 383K	1.6e ⁻¹⁰ ± 4.2e ⁻¹¹ m ² .s ⁻¹ at 343K 5.3e ⁻¹⁰ ± 1.3e ⁻¹¹ m ² .s ⁻¹ at 373K
E _a for D _{cation}	24.6 ± 2.3kJ.mol ⁻¹	66.6 ± 17.5kJ.mol ⁻¹

† Estimated value

The cation diffusion coefficients for the two salts are quite similar, with coefficients of the order of 10⁻¹⁰m².s⁻¹ (Table 5-1 and Figure 5-1). An obvious difference in activation energy was observed, however, the pyrrolidinium diffusion coefficient increasing far more rapidly with temperature. The anion diffusion coefficients are shown in Figure 5-2 and indicate faster amide diffusion in the case of the P₁₂NTf₂. The main difference between the two salts is the temperature range over which diffusion was detected. Diffusion in P₁₂NTf₂ was only detected above 343 and 363K for the cation and anion respectively, while diffusion coefficients for both ions were measured above 243K for MeEtImNTf₂. As P₁₂NTf₂ exists as a solid below 363K, the measured diffusion behaviour reflects diffusion primarily in the liquid state; diffusion in the solid appears to be limited.

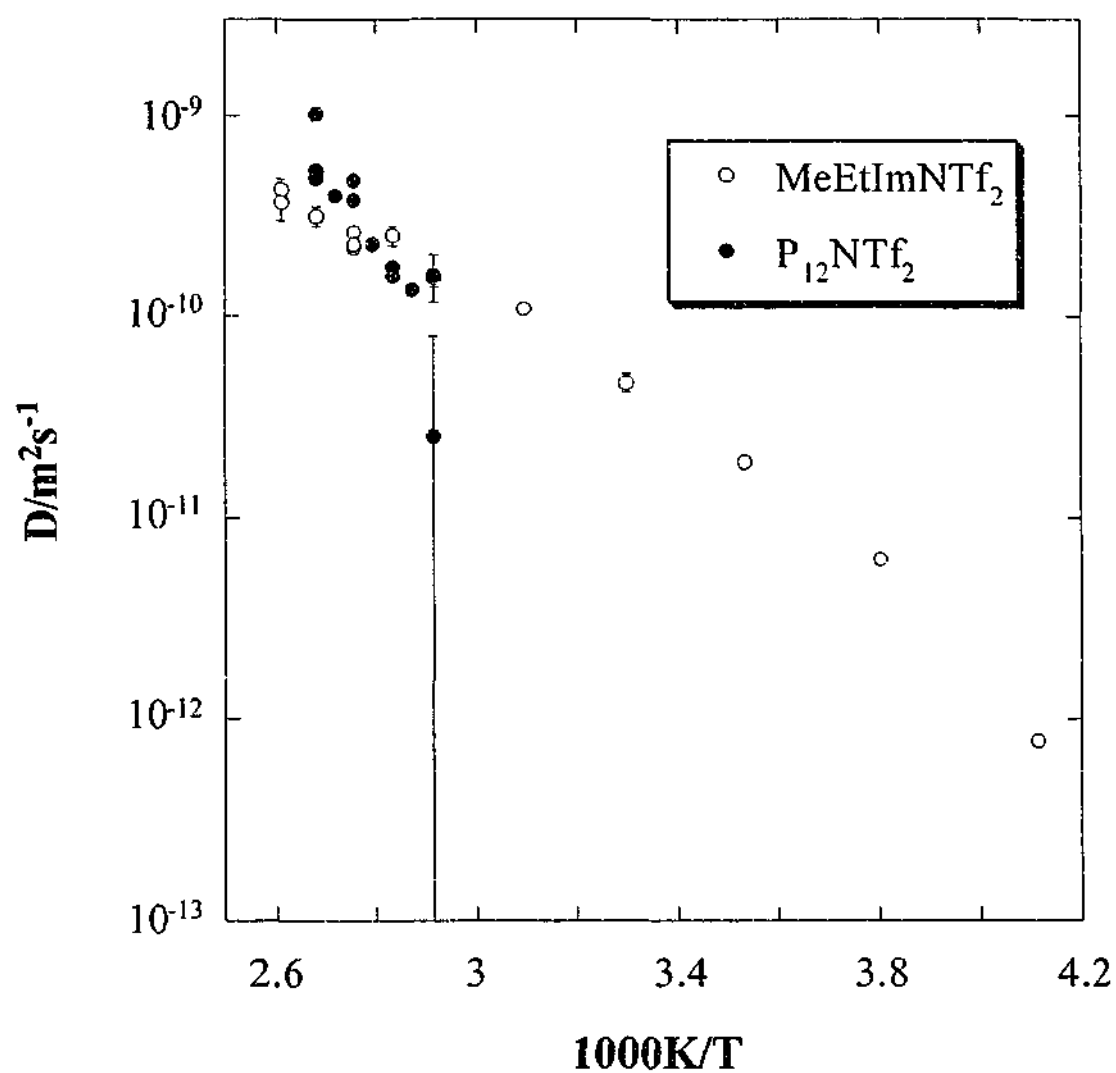


Figure 5-1 A comparison of the cation diffusion coefficients for MeEtImNTf_2 and $\text{P}_{12}\text{NTf}_2$.

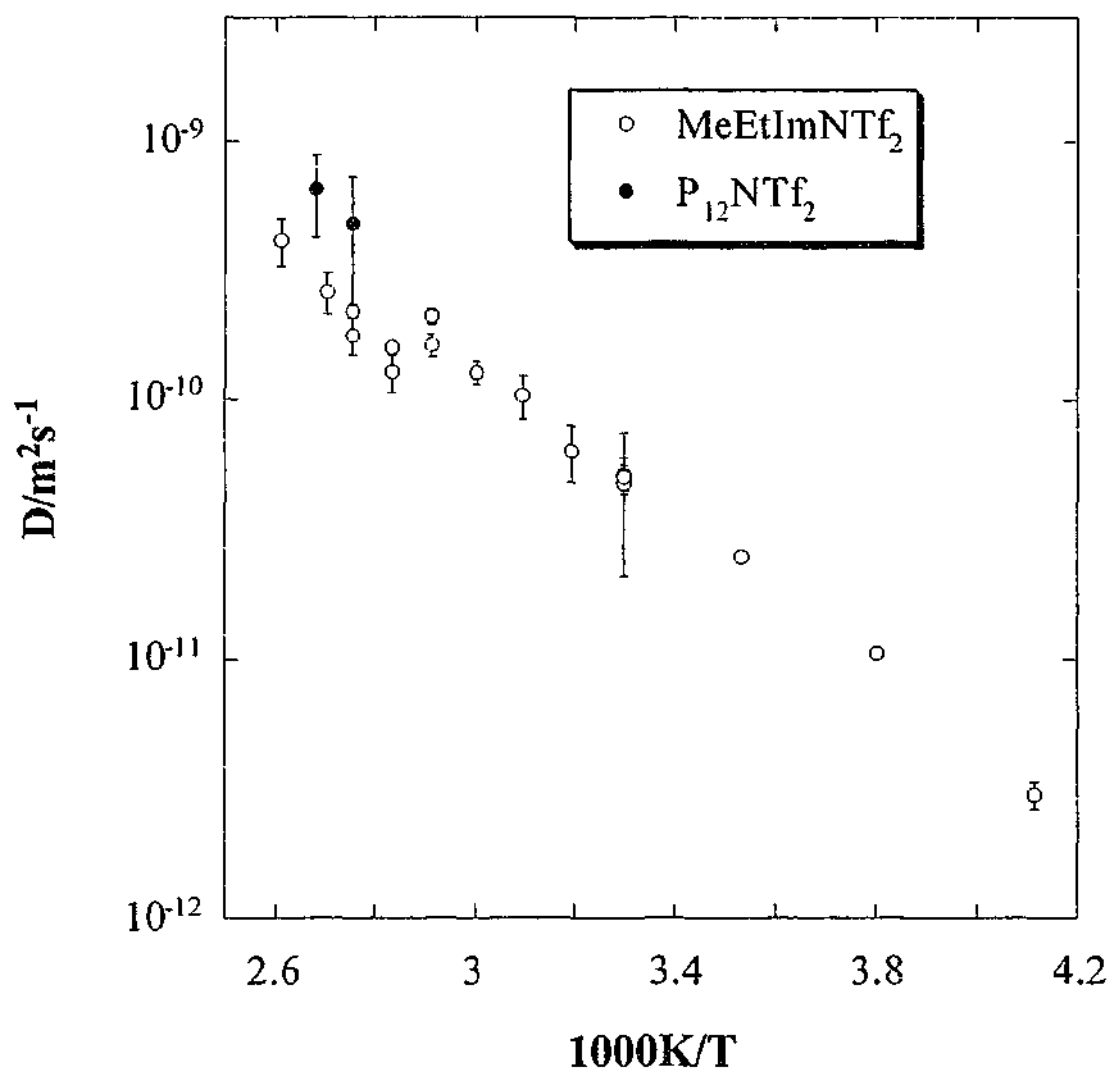


Figure 5-2 A comparison of the anion diffusion coefficients for MeEtImNTf₂ and P₁₂NTf₂.

The conductivities for these two salts are shown in Figure 5-3. In contrast to the diffusion coefficients, a difference in conductivity of five orders of magnitude is observed at room temperature, although it should be noted that P₁₂NTf₂ is a solid while MeEtImNTf₂ is a liquid at this temperature. Above the melting temperature of both salts (363K), the conductivity of MeEtImNTf₂ is still an order of magnitude greater than P₁₂NTf₂. The trends observed for the diffusion coefficients are not able to account for the differences in conductivity. Significant ion association has been reported for each salt (see sections 3.4.1.2 and 4.4.3), with the fraction of free ions

available for conduction shown in Figure 5-4. Both salts exhibit some degree of ionic association, although it is substantially greater for $P_{12}NTf_2$. Based on this observation, one might expect the cation diffusion coefficients of $P_{12}NTf_2$ to be significantly lower as the cation moves as a part of a cluster. It was shown in Chapter 3, section 3.4.1.2, however, that the degree of ion association seems to have very little impact on the diffusion behaviour, which may also be the case here. The results in Figure 5-4 suggest that there are considerably fewer ions contributing to the conductivity in $P_{12}NTf_2$.

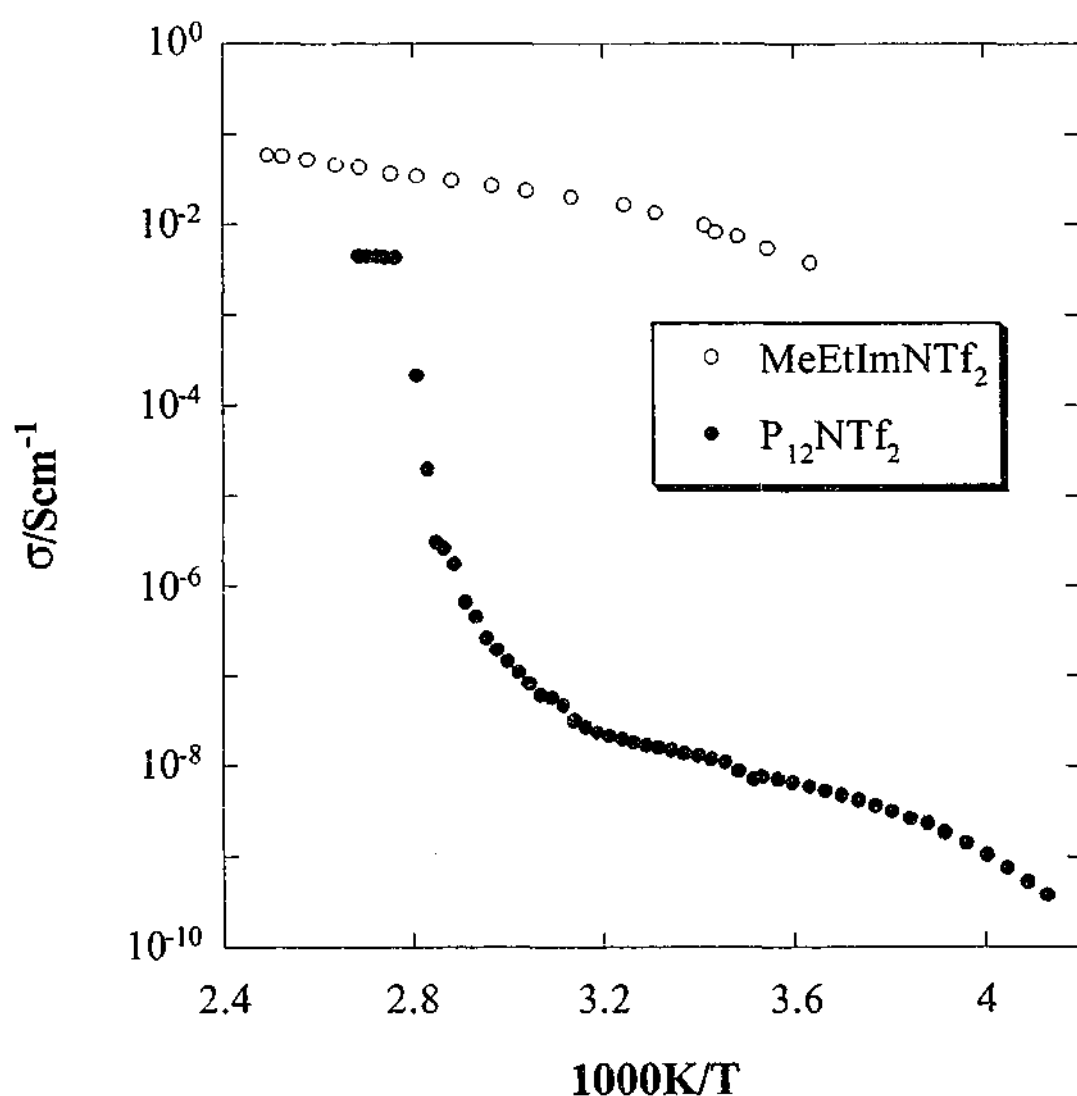


Figure 5-3 A comparison of the conductivities for MeEtImNTf₂ and P₁₂NTf₂.

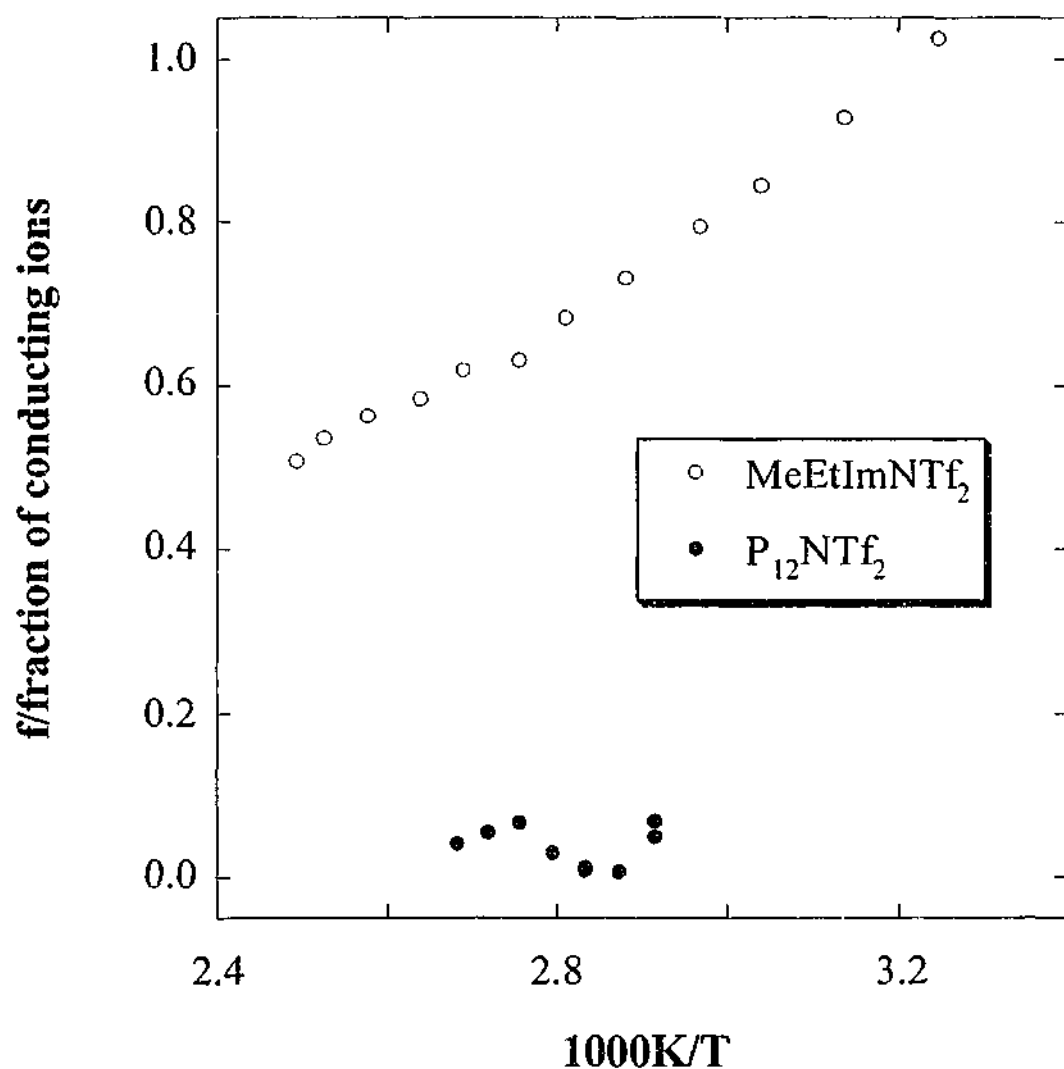


Figure 5-4 A comparison of the fraction of free ions for MeEtImNTf₂ and P₁₂NTf₂.

Given the similarities in structure and size between the two salts, how is it possible that the degree of ionic association differs so greatly? The answer probably lies in the distribution of the charge in each salt. The structure of the two salts is shown in Figure 5-5. It can be seen that the imidazolium cation consists of an aromatic ring structure with the charge delocalised between the two nitrogen atoms. The result is a more diffuse positive charge that is likely to result in weaker ionic interactions between the cation and anion. In the pyrrolidinium salt, however, there is no

aromaticity and therefore the charge is localised on the nitrogen atom. Acting effectively as a point charge, stronger ionic interactions are expected, which would account for the higher melting points and lower conductivities.

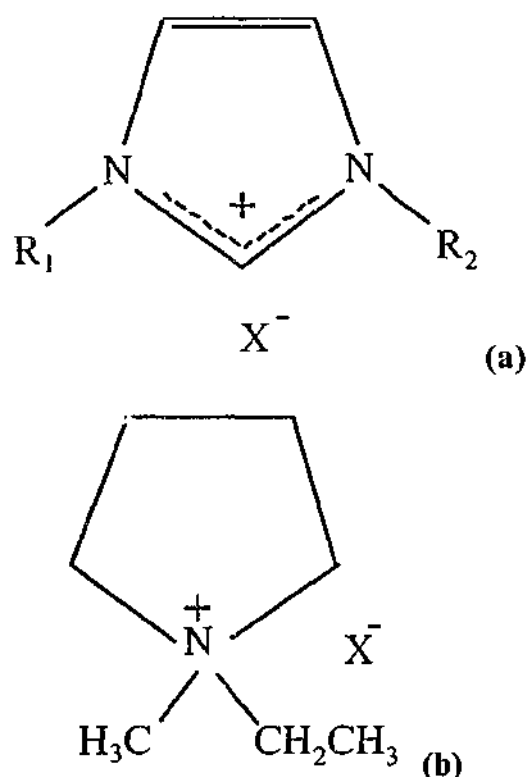


Figure 5-5 The structure of (a) MeEtImNTf₂ and (b) P₁₂NTf₂.

The difference in ionic interaction strength can also probably account for the differences in solid state behaviour observed for these two salt systems. As mentioned above, only limited diffusion was detected in the solid state for pure P₁₂NTf₂. For the imidazolium salts (MeEtImBr and MeEtImI), however, solid state diffusion seemed to occur far more readily and was detected at much lower temperatures. Figure 5-6 highlights the difference in diffusion coefficients for P₁₂NTf₂ and MeEtImBr. Cation diffusion in P₁₂NTf₂ could only be measured above 343K, which is very close to the melting point of 363K. For the imidazolium halides, however, solid state diffusion was detected at 273K, approximately 80K below the melting point.

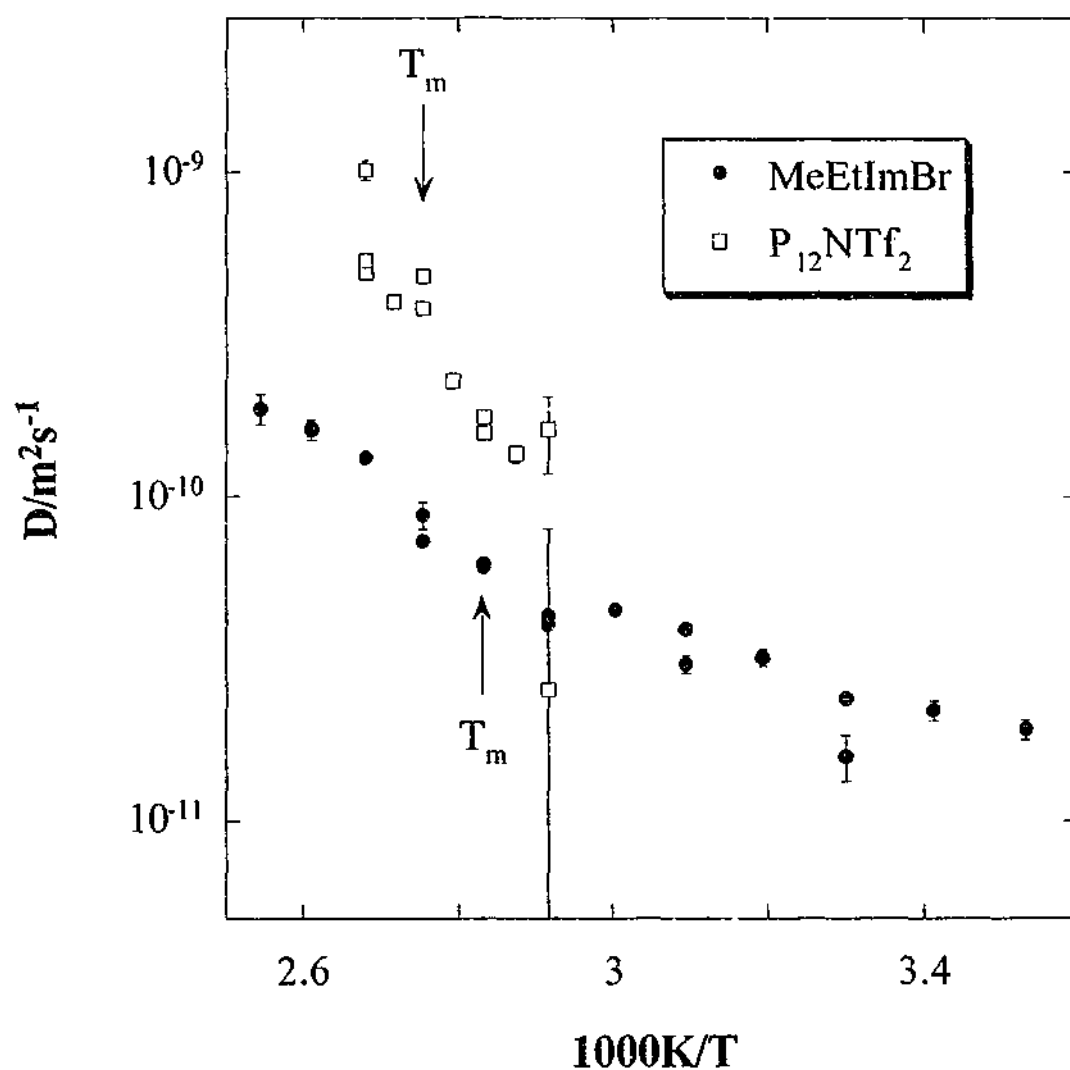


Figure 5-6 A comparison of the cation diffusion coefficients for $P_{12}NTf_2$ and MeEtImBr.

If stronger ionic interactions exist within a material, the onset of diffusion will require a greater activation energy and only occur at higher temperatures. The behaviour of $P_{12}NTf_2$ seems to support this theory. However, the concentration of charge carriers may also be a significant factor in the measurement of solid state diffusion. The presence of more vacancies will enable more ions to diffuse throughout the material. This effect appears to be confirmed by the doped $P_{12}NTf_2$ systems, where a small amount of lithium salt, $LiNTf_2$ (0.9mol%), resulted in the detection of increased cation diffusion in the solid state. In this case, the addition of the lithium salt is

thought to cause a slight structural instability as a result of the mismatch between the lithium and pyrrolidinium cations (see section 4.4.4 of Chapter 4). This instability will possibly generate more vacancies enabling more ions to diffuse. A comparison of the normalised signal intensities for $P_{12}NTf_2$ and MeEtImBr (Figure 5-7) indicates a greater concentration of mobile ions in the imidazolium salt. Vacancy formation is also an activated process such that higher temperatures result in an increase in vacancy concentration. The energy barrier to vacancy formation is also dependent on the strength of the ionic interactions, where stronger interactions will require more energy to displace the ion.⁵ Therefore, the difference in charge carrier concentration between these two materials is also likely to be the result of the difference in ionic interactions.

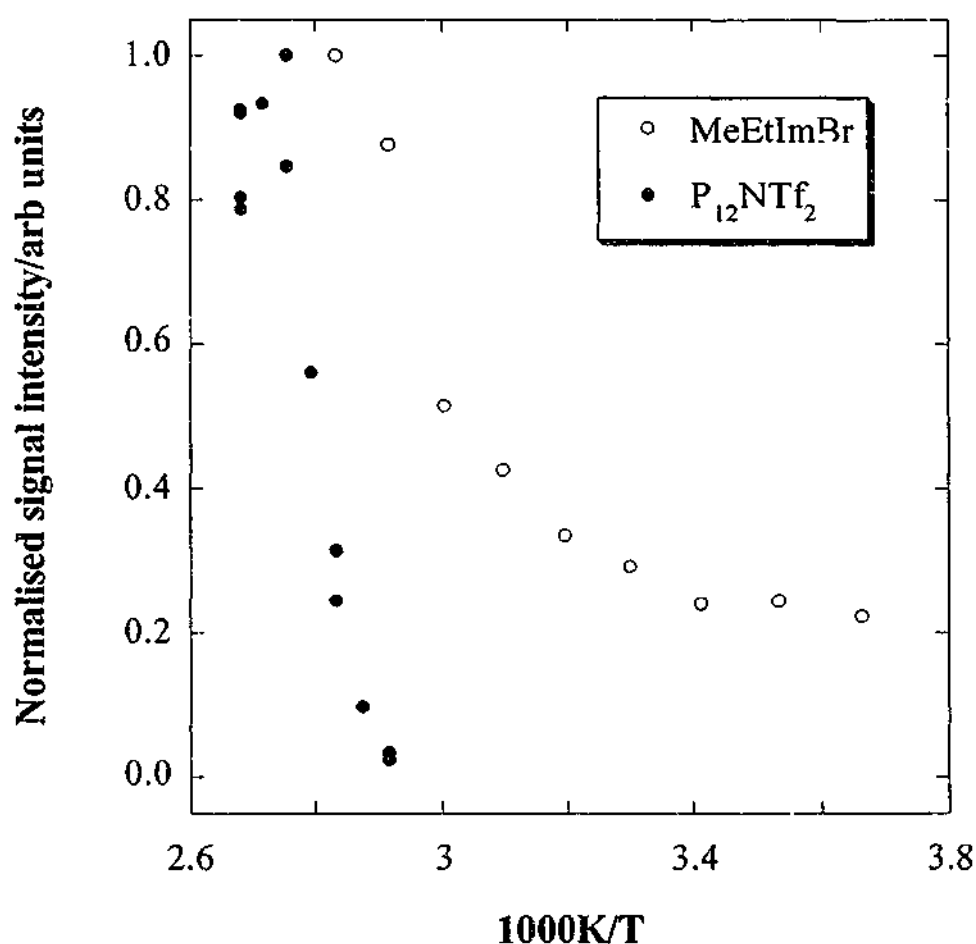


Figure 5-7 A comparison of the normalised NMR signal intensities for $P_{12}NTf_2$ and MeEtImBr.

Based on these observations, it appears that the properties of these salts are highly dependent on the interaction strength between the ions. Decreasing the ionic interactions decreases the melting point and the degree of ionic association but increases the solid state diffusion rate and conductivity. Diffusion in the liquid state, however, is similar for both materials, and, in some cases, greater for the $P_{12}NTf_2$ salt. While ionic interactions are still prevalent in the liquid state, the diffusion measurements are not affected by the charge of the ions, but are only dependent on the mobility of the species.

5.2 References

1. A. B. McEwen, H. L. Ngo, K. LeCompte and J. L. Goldman, *J. Electrochem. Soc.* **146**, 1687-1695 (1999).
2. M. Forsyth, J. Huang and D. R. MacFarlane, *J. Mater. Chem.* **10**, 2259-2265 (2000).
3. A. G. Bishop, Ph.D Thesis, Monash University, Melbourne, Australia, 1999.
4. P. Bonhôte, A.-P. Dias, N. Papageorgiou, K. Kalyanasundaram and M. Grätzel, *Inorg. Chem.* **35**, 1168-1178 (1996).
5. A. J. Walton, *Three Phases of Matter*, 2nd ed. (Oxford University Press, Oxford, 1983).

Chapter Six

Conclusions and Future Work

The main objective of this research was to study the transport mechanisms in two organic electrolyte systems, imidazolium and pyrrolidinium salts, with particular attention to the effect of chemical structure on the diffusion properties. Following is an outline of the main findings of this work.

6.1 Imidazolium Salts

6.1.1 The Anion Effect

The effect of the anion on the transport properties was investigated for MeEtImX, where X is the bromide, iodide, triflate or amide ion (Br^- , I^- , Tf^- or NTf_2^-). Previously reported thermal analysis for these salts indicates higher melting transitions for the halide salts (MeEtImBr and MeEtImI) compared to the fluorinated salts (MeEtImTf and MeEtImNTf₂). Despite the different melting points, the liquid state conductivities are very similar for all four salts. As a direct relationship exists between conductivity and diffusion, it was initially assumed that the cation diffusion coefficients would also be similar for all four salts. However, the coefficients were divided into two groups, with the halide salts displaying considerably lower coefficients than the fluorinated salts.

The differences in diffusion coefficient between the two groups were adequately described by differences in viscosity, where previously reported data indicated much higher viscosities for the halide salts. The discrepancy between the diffusion and

conductivity data, however, was accounted for by a difference in ionic concentration. The halide salts have more charge carriers per unit volume than do the fluorinated salts, although each salt experiences some degree of ionic association. In conclusion, the combination of high charge carrier concentration and low diffusion coefficients for the halide salts results in the same conductivity as the more diffusive but less concentrated fluorinated salts.

6.1.2 MeEtImTf and MeEtImNTf₂ Binary System

Individually, MeEtImTf and MeEtImNTf₂ are two of the most conductive materials in this family of salts. Combining these two salts to form binary mixtures results in an enhancement in conductivity. By contrast, analysis of the ionic diffusion coefficients for these binaries showed very little change compared to the pure materials. The increase in conductivity must therefore be attributed to a change in the extent of ion association.

In the pure materials, an equilibrium exists between dissociated and associated ions. Mixing these two salts will not affect the cation concentration, but the concentration of each anion will be halved. This decrease in anion concentration will shift the equilibria towards further dissociation, thereby increasing the number of ions available for conduction. As ion association occurs to a greater extent at higher temperatures, this shift in the equilibrium will have a more pronounced effect as the temperature increases. It is therefore this increase in ion concentration that accounts for the increase in conductivity.

6.1.3 The Alkyl Chain Length Effect

The substitution of longer alkyl chains on one of the nitrogens in the imidazolium ring was also found to affect the transport properties. MeMeImI and MeEtImI are both

solids, melting at 368 and 351K respectively. For longer alkyl substituents, crystallisation is suppressed, with only a glass transition detected around 203K. As previously reported, conductivities were found to decrease with increasing alkyl chain length. A similar trend was observed for the cation diffusion coefficients at 298K. At 358K, however, an initial increase in diffusion coefficient with increasing alkyl chain length was observed up to MePrImI, after which longer alkyl chains resulted in slower diffusion.

The conductivity and diffusion behaviour could be explained to some extent by the increase in viscosity with increasing alkyl chain length. The slight increase in diffusion up to MePrImI was attributed to a decrease in the viscosity of the salts, but longer alkyl chains actually increase the viscosity. However, the viscosity for MeHxImI is lower than MeEtImI, which would imply faster diffusion for MeHxImI. As this was not the case, the size of the cation must also influence the diffusion properties. An approximate radius for each cation was determined from the pre-exponential term in the VTF equation, used to model the temperature dependence of the diffusion coefficient. The results showed an increase in ionic radius up to MeBuImI, after which a further increase in alkyl chain resulted in a decrease in the cation radius. It is thought that this decrease in cation size may be due to increased intramolecular interactions between the imidazolium ring and the alkyl chain. What is apparent from this analysis is that both viscosity and ion size influence the transport properties in this series of salts.

6.1.4 Solid State Diffusion

Conductivity in the solid state was previously measured for MeEtImBr and MeEtImI and was found to be slightly lower than the corresponding liquid state values. Around the melting point, a jump in the conductivity was observed, where the material changed from solid to liquid. Cation diffusion coefficients were measured

in both the solid state and the supercooled liquid, the former being considerably higher at the lowest temperatures. Unlike the conductivity data, no jump in diffusion coefficient was detected as the material melted.

The faster diffusion in the solid state compared to the supercooled liquid is attributed to a difference in the diffusion mechanism. Solid state diffusion is thought to involve a vacancy mechanism whereas diffusion in the liquid state requires the cooperative rearrangement of small sections of the material. Despite fast diffusion, the solid state is less conductive due to fewer charge carriers. This was confirmed by the NMR signal intensities, which reflect the concentration of mobile ions. The results show a steady increase in the number of mobile ions as the temperature increases up to the melting point. The solid state conductivities were modelled using the diffusion and signal intensity data. The conductivity is overestimated if it is assumed that both ions are mobile. However, a reasonable agreement between the measured and calculated conductivities is obtained if only the cation is assumed to be diffusing. Therefore, the conduction mechanism in the solid state appears to involve only the cation, with the anion assisting in maintaining the crystal structure.

6.1.5 Future Work

As a number of assumptions were made regarding the behaviour of these imidazolium salts, possible future work should focus on clarifying these hypotheses. In studying the anion effect, no diffusion coefficients were measured for the bromide and iodide ions. Given the similarity in anion and cation diffusion coefficients for the fluorinated salts, liquid state ionic diffusion coefficients for the halide salts were also assumed to be the same. In the solid state, however, it was assumed that the anion is not mobile and that only the cation contributes to the conductivity. Anion diffusion measurements are necessary in order to confirm this. Furthermore, the fast solid state diffusion and conduction detected in these salts warrants further investigation.

With respect to the binary systems, the mixed anion system consisting of MeEtImTf and MeEtImNTf₂ was examined in this study. A number of alternative systems based on other mixed anions or mixed cations have been considered, with the thermal behaviour and conductivities reported elsewhere. While most binary mixtures showed an increase in conductivity over the pure materials, the enhancement was different for each system. Analysis of the diffusion behaviour in these alternative systems would also be of interest.

6.2 Pyrrolidinium Salts

6.2.1 Diffusion Mechanisms

From an earlier study, it was shown that pure P₁₂NTf₂ is conductive in the solid state, although a rapid increase in conductivity was observed near the melting point (363K). The addition of 0.9mol% LiNTf₂, however, was found to increase the conductivity by almost two orders of magnitude at room temperature. Higher LiNTf₂ salt concentrations resulted in further conductivity enhancement, which was accompanied by a decrease in melting point and evidence of eutectic behaviour. In this work, diffusion in the pure sample was limited to near the melting point and above. However, pyrrolidinium mobility was detected at room temperature upon addition of 0.9mol% and 4.8mol% LiNTf₂. Diffusion, albeit slower than in the other samples, was also detected at lower temperatures for the 33mol% and 49.9mol% LiNTf₂ systems.

For all samples other than pure P₁₂NTf₂ and the eutectic composition (33mol% LiNTf₂), both the solid and liquid phases coexist at some temperatures. From Lever rule calculations, 0.9mol% LiNTf₂ is mostly solid until just below the melting temperature while 4.8mol% LiNTf₂ exhibits two-phase behaviour over most of the temperature range. The 49.9mol% LiNTf₂ sample, however, is mostly liquid.

Despite this two-phase behaviour, there was no evidence of more than one diffusion coefficient. The diffusion coefficients for pure $P_{12}NTf_2$ and 0.9mol% were mostly representative of solid state motion, while diffusion in 33mol% and 49.9mol% was largely indicative of liquid state behaviour. However, some solid state diffusion was also observed for 33mol% $LiNTf_2$ below the melting temperature. Although both solid and liquid coexists for 4.8mol% $LiNTf_2$, the diffusion coefficients reflected the behaviour observed in the solid materials. The lower diffusion coefficients observed for 33mol% and 49.9mol% $LiNTf_2$ are a result of the differences in diffusion mechanism. Solid state diffusion is thought to involve a vacancy mechanism where ions move in discrete jumps. In contrast, diffusion in the liquid state requires the cooperative rearrangement of small sections of the material.

The predominantly liquid materials displayed higher conductivities, although they exhibited slower diffusion. This apparent contradiction can be explained by a difference in charge carrier concentration. The proportion of mobile ions was obtained from the NMR signal intensity. In the liquid state, all of the ions are mobile and may therefore contribute to the conductivity. In the solid state, however, only a fraction of the ions are mobile because a large number of ions are involved in maintaining the crystal structure.

The conductivities were modelled from the diffusion coefficients using the Nernst-Einstein equation. Although no lithium diffusion coefficients were measured, it was assumed that they would diffuse in a similar manner to the pyrrolidinium cations. In all cases, the calculated conductivities were greater than the measured values, suggesting some degree of ion association. For the solid materials (pure $P_{12}NTf_2$ and 0.9mol% $LiNTf_2$), the discrepancy was not as large when the anion was assumed to be immobile. When both solid and liquid phases coexist, a smaller difference between the calculated and measured conductivities resulted if it was assumed that diffusion in the liquid phase dominated the conduction mechanism.

Based on these observations, a conduction mechanism for these pyrrolidinium salts is proposed. The addition of a small amount of LiNTf_2 forms a solid solution such that the lithium and amide ions are incorporated into the $\text{P}_{12}\text{NTf}_2$ lattice. Since the lithium ions are considerably smaller than the pyrrolidinium ions, it is likely that the lattice is distorted, which generates vacancies. This increase in vacancy concentration enables more ions to move in the solid state, therefore increasing the conductivity. As the concentration of LiNTf_2 increases, a liquid phase forms. Although diffusion in this liquid phase is slower than in the solid, the concentration of mobile ions is considerably greater. The overall result is a further increase in conductivity.

6.2.2 Future Work

The transport mechanisms in $\text{LiNTf}_2/\text{P}_{12}\text{NTf}_2$ mixtures were studied through measurement of the pyrrolidinium and amide diffusion coefficients using the pulsed field gradient and fringe field gradient methods respectively. The fringe field method, however, frequently suffered from T_2 interference, inhibiting the measurement of amide diffusion coefficients in the solid state. The pulsed field gradient method does not experience the same limitation and therefore could be used to confirm amide diffusion in these systems. The lack of appropriate equipment also impeded the study of lithium diffusion. In modelling the conductivity behaviour, it was assumed that the lithium ions would diffuse in a similar manner to the pyrrolidinium ions. The validity of this assumption can only be confirmed through ^7Li diffusion measurements.

Conductivities calculated from the diffusion coefficients were much greater than the measured conductivities, with the discrepancy attributed to the presence of neutral ion pairs. The nature of these ion interactions can be revealed by Fourier Transform Infrared (FTIR) or Raman spectroscopy. Through these techniques, the effect of chemical composition and temperature on the degree of ion association could also be

examined. Such measurements could provide further support to the conclusions drawn in this work.

The addition of a small amount of LiNTf_2 was found to increase ion mobility considerably in the solid state. Based on the experimental data, it was assumed that the lithium salt generates more vacancies within the crystalline lattice, enabling more ions to diffuse. X-ray and neutron scattering experiments can provide information regarding both the crystal structure of these materials and the local ion behaviour. Combining the structural information with the ion dynamics will enable the model for ion transport in the solid state to be refined.

In this study of pyrrolidinium salts, only the addition of LiNTf_2 to pure $\text{P}_{12}\text{NTf}_2$ was examined. However, like the imidazolium salts a number of structural variations are possible. Substituting the anions or altering the length of the alkyl groups may increase the conductivity. Binaries from pyrrolidinium salt mixtures or the combination of a pyrrolidinium salt with an analogous lithium salt could also be considered. Research of such materials would provide a better understanding of the structure-property relationships in pyrrolidinium salts.

6.3 A Comparison of Imidazolium and Pyrrolidinium Salts

MeEtImNTf_2 and $\text{P}_{12}\text{NTf}_2$ are similar cyclic ammonium salts with the same alkyl substituents and anions. However, the thermal and transport properties of the two salts are remarkably different. MeEtImNTf_2 was found to exhibit a lower melting transition and higher conductivity than $\text{P}_{12}\text{NTf}_2$, although the liquid state diffusion coefficients were very similar for both materials. The difference in conductivity,

despite the similarity in diffusion coefficients, was attributed to greater ion association in $P_{12}NTf_2$ than in $MeEtImNTf_2$.

The solid state conductivities for $P_{12}NTf_2$ were also found to be substantially lower than either of the solid imidazolium salts ($MeEtImBr$ or $MeEtImI$). Solid state diffusion coefficients were limited to near the melting point for $P_{12}NTf_2$, whereas solid state diffusion was detected well below the melting point for the imidazolium salts. Fewer mobile ions were detected for $P_{12}NTf_2$, indicative of a lower vacancy concentration. This behaviour was again attributed to stronger ionic interactions inhibiting the formation of vacancies.

The difference in ion association between these two systems was related to the distribution of charge on the cations. $MeEtIm^+$ has an aromatic structure, with the charge delocalised between the nitrogen atoms in the imidazolium ring. The result is a diffuse charge that undergoes weak interactions with the anion. For P_{12}^+ , the charge is localised on the nitrogen group, leading to stronger ionic interactions. The differences in ionic interaction account for the different properties of these two cyclic ammonium salts.

6.4 The Merits of NMR Diffusion Techniques

The work presented in this thesis has highlighted how powerful NMR diffusion methods are in the characterisation of electrolyte transport mechanisms. The ability to reliably monitor the translational motion of a particular species, independent of the rest of the sample, is the major advantage of NMR diffusion techniques over other diffusion methods. Characterisation of ionic diffusion coefficients coupled with other properties, such as conductivity, can provide a detailed profile of the conduction mechanisms within an electrolyte. With reference to this work, the diffusion properties have been correlated with the chemical structure of organic salt. Similarly,

the role of chemical composition on transport properties can be considered in other ionic materials such as liquid electrolytes, fast ion solid state conductors and polymer electrolytes. Such systems may be pursued in future research at Monash University.

The availability of more advanced NMR diffusion equipment can only be beneficial for future studies of electrolyte diffusion. Higher gradients will allow slower diffusion to be detected, which will be of particular benefit in the analysis of solid state diffusion behaviour. The ability to conduct multinuclear NMR diffusion experiments will enable the characterisation of all mobile species, which will be of particular importance in studying the mobility of dopants in plastic crystals. NMR diffusion coupled with an electric field, as in electrophoretic NMR, will allow the mobility of charged species to be isolated from that of the uncharged species, enabling further refinement of models of conduction mechanisms in electrolytes. The anticipated introduction of such methods at Monash University will greatly assist in the research and development of novel electrolytes for alternative energy sources.

Appendix

Publications

1. H. A. Every, F. G. Zhou, M. Forsyth and D. R. MacFarlane, *Electrochim. Acta* **43**, 1465-1469 (1998).
2. M. Forsyth, H. A. Every, F. Zhou and D. R. MacFarlane, in *Structure and Properties of Glassy Polymers; ACS Symposium Series*, Vol. 710 (Oxford University Press, New York, 1998), pp. 367-382.
3. H. Every, A. G. Bishop, M. Forsyth and D. R. MacFarlane, *Electrochim. Acta* **45**, 1279-1284 (2000).

Papers are currently being prepared from Chapter 4 and parts of Chapter 3.



Lithium ion mobility in poly(vinyl alcohol) based polymer electrolytes as determined by ^7Li NMR spectroscopy

H. A. Every,^a F. Zhou,^b M. Forsyth^a and D. R. MacFarlane^{b*}

^aDepartment of Materials Engineering, Monash University Clayton, Victoria 3168, Australia

^bDepartment of Chemistry, Monash University Clayton, Victoria 3168, Australia

(Received 16 September 1996; accepted 2 May 1997)

Abstract—Solvent-free polymer electrolytes based on poly(vinyl alcohol) (PVA) and LiCF_3SO_3 have shown relatively high conductivities (10^{-8} – $10^{-4} \text{ S cm}^{-1}$), with Arrhenius temperature dependence below the differential scanning calorimeter (DSC) glass transition temperature (343 K). This behaviour is in stark contrast to traditional polymer electrolytes in which the conductivity reflects VTF behaviour. ^7Li nuclear magnetic resonance (NMR) spectroscopy has been employed to develop a better understanding of the conduction mechanism. Variable temperature NMR has indicated that, unlike traditional polymer electrolytes where the linewidth reaches a rigid lattice limit near T_g , the lithium linewidths show an exponential decrease with increasing temperature between 260 and 360 K. The rigid lattice limit appears to be below 260 K. Consequently, the mechanism for ion conduction appears to be decoupled from the main segmental motions of the PVA. Possible mechanisms include ion hopping, proton conduction or ionic motion assisted by secondary polymer relaxations. © 1998 Published by Elsevier Science Ltd. All rights reserved

Key words: poly(vinyl alcohol), conductivity, ^7Li NMR, electrolytes.

INTRODUCTION

Most studies of polymer electrolytes have investigated subambient glass transition temperature, amorphous polymer systems with alkali metal salts as the conducting species. In these systems, ion transport has mostly been associated with the segmental motions of the polymer, as significant conductivity is only observed above the glass transition temperature of the system [1]. Cation mobility is of particular interest in these systems with regard to polymer-based batteries.

Yamamoto *et al.* [2] have studied polymer electrolyte systems based on poly(vinyl alcohol)(PVA). The films obtained from PVA-lithium salt solutions exhibited relatively high conductivities (10^{-5} – $10^{-3.5} \text{ S cm}^{-1}$ at 293 K) for a polymer salt system, despite having glass transition temperatures well above room temperature (approximately 320 K). For such high conductivities to be observed below

the glass transition temperature, the mechanism for ion transport is likely to be decoupled from the segmental motions of the polymer.

Cation mobility in polymer electrolytes has previously been investigated by measuring the linewidth of solid state nuclear magnetic resonance (NMR) spectra [3–8]. The spectral linewidths are a result of quadrupolar or internuclear dipole-dipole interactions [9]. When the nuclei are fixed, these interactions are accentuated, which results in a broad linewidth, commonly referred to as the rigid lattice linewidth. As the mobility of the cation increases, the NMR linewidth decreases due to averaging of the interactions experienced by each nucleus.

Stallworth and co-workers [8] have used NMR spectroscopy to study lithium ion mobility in gel electrolytes based on poly(methyl methacrylate). At low temperatures, below the glass transition temperatures of the systems, the linewidths were broad. This suggests that the lithium ions are fixed and are therefore not able to conduct. Upon increasing the temperature, the central linewidths were motionally

*Author to whom correspondence should be addressed.

narrowed, with the onset of narrowing correlating with the glass transition temperatures of the systems. The NMR results also support the temperature dependent conductivity data, which shows increasing conductivity with increasing temperature. Chung *et al.* [6] have observed similar lithium ion behaviour for LiCF_3SO_3 in poly(propylene glycol). Other groups have reported the mobility of sodium as determined by NMR linewidth measurements [3–5, 7]. In all these cases, the linewidths were found to be broad below the glass transition temperature with the onset of line narrowing generally occurring near T_g . Consequently, the mobility of the cations in traditional polymer electrolytes appears to be closely associated with the relaxations of the polymer.

^7Li solid state NMR measurements, together with conductivity and thermal analysis, of LiCF_3SO_3 -based PVA systems are presented in this work in order to determine whether ^7Li mobility can account for conductivity in these systems and also to investigate the correlation between ^7Li mobility and polymer motion.

EXPERIMENTAL

The polymer electrolytes were based on lithium triflate, LiCF_3SO_3 (Aldrich), dissolved in poly(vinyl alcohol). Two polymers were studied with the molecular weight ranges of 31,000–50,000 (Aldrich) and 105,600–110,000, with degrees of hydrolysis being 88% and 99.8% respectively. The polymer films were prepared by dissolving the PVA and the LiCF_3SO_3 in dimethyl sulfoxide (DMSO), (17 g DMSO/1 g PVA) at 70°C for 1 hour. The solution was then cast onto a glass plate and the DMSO removed using a high vacuum pump over a period of 15 hours. The film was finally dried between two pieces of teflon in a vacuum oven at 50 to 70°C for approximately 20 hours. The polymer systems studied consisted of salt to polymer weight ratios of 0.5 and 1. The thickness of the films ranged from 0.1 to 0.6 mm.

The glass transition temperatures of the polymer systems were determined using a dry ice/ethanol cooled Perkin-Elmer differential scanning calorimeter (DSC 7). The DSC was calibrated using cyclohexane (mp 6.59°C) and 4-nitrotoluene (mp 56.2°C). The samples were placed in aluminium pans and quenched in liquid nitrogen. Measurements were made using heating rates of 30°C min⁻¹ and 40°C min⁻¹.

The conductivities of the polymer systems were obtained via *ac* impedance, using a Hewlett-Packard 4284A LCR meter. Gold electrodes (5 mm diameter) were sputter coated onto the polymer. Under nitrogen, the sample was then placed between two stainless-steel plates and loaded into a shielded, spring-loaded brass cell. Measurements were made from -20°C to 80°C.

The ^7Li NMR linewidth measurements were made using a modified Bruker CXP 300 NMR spectrometer operating at 116.6 MHz. The linewidths were taken to be the full width at half maximum (FWHM) of the peaks and measured as a function of temperature from -40°C to 80°C. The results were analysed using Bloembergen-Purcell-Pound (BPP) theory and the following equation [10]

$$(\Delta\nu)^2 = \left(\frac{2}{\pi}\right) \delta\omega_0^2 \tan^{-1}(\tau\Delta\nu) \quad (1)$$

where $\Delta\nu$ is the measured linewidth, $\delta\omega_0$ is the rigid lattice linewidth and τ is the correlation time. The temperature dependence of the correlation time is assumed to follow Arrhenius-type behaviour

$$\tau = \tau_0 \exp\left(\frac{E_a}{kT}\right) \quad (2)$$

from which activation energies for the mobility of the lithium ions were determined. The onset of narrowing temperature was obtained from an extrapolation of the linear region of the sigmoidal plot to the rigid lattice limit.

RESULTS AND DISCUSSION

Thermal analysis

Glass transition temperatures of approximately 333 K were observed for the pure PVA polymers. For the PVA/salt systems, the DSC traces show evidence of a thermal event at approximately 343 K. The transition appeared as a peak when using the 40°C min⁻¹ scanning rate but as a step, typical of a glass transition temperature, at a lower scanning rate (30°C min⁻¹). Therefore, the evidence suggests that this thermal event is likely to be a glass tran-

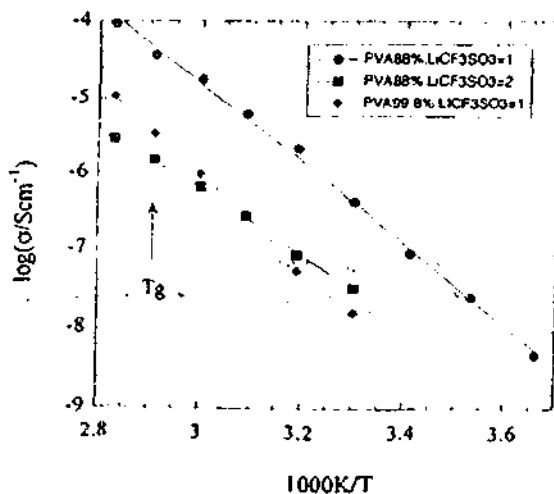


Fig. 1. Arrhenius plot of conductivity for PVA electrolytes.

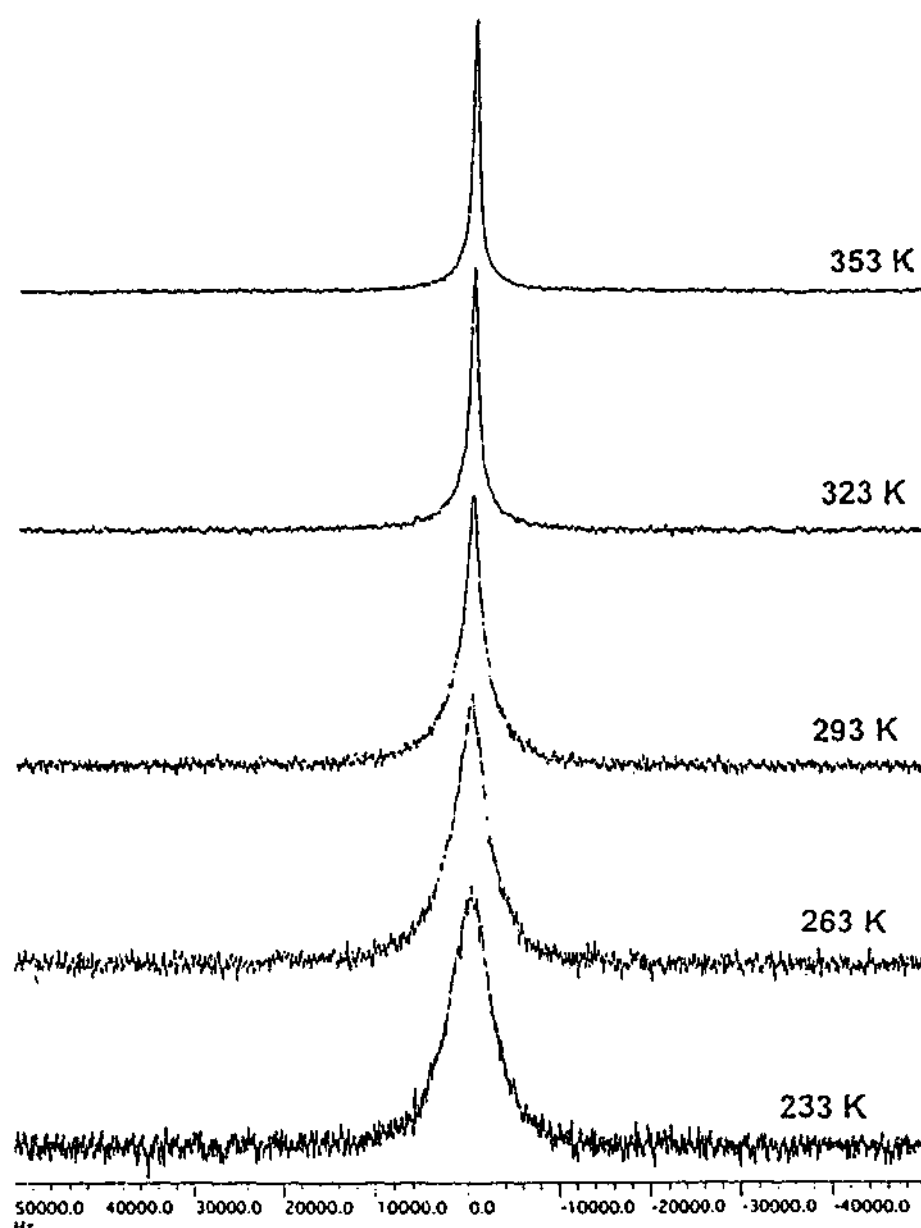


Fig. 2. ^7Li NMR spectra indicating the variation in linewidth as a function of temperature.

sition temperature, with its associated enthalpy overshoot observed at higher heating rates. In this case, T_g appears to be slightly increased by salt addition, in contrast to previous reports [2]. DSC scans between -100 and 20°C indicate that no further low temperature event occurs.

Effect of temperature on ion mobility

For many polymer electrolytes, the temperature dependence of the conductivity has been described by the Vogel-Tamman-Fulcher equation.

$$\sigma = \sigma_0 \exp\left[\frac{B}{(T - T_0)}\right] \quad (3)$$

This equation proposes that ionic conductivity is only prevalent above a temperature, T_0 , which is

often related to the glass transition temperature of the system ($\sim T_g = 220\text{ K}$). Consequently, polymer relaxations appear to influence the conductivity of the electrolyte. The PVA-based electrolytes studied here are conductive well below the glass transition temperature (Fig. 1) and the temperature dependence of their conductivities can be approximated by Arrhenius behaviour, with activation energies more than twice those measured for polyether-based electrolytes [11]. The PVA electrolytes studied by Yamamoto and co-workers showed similar conductivity behaviour [2]. This observation seems to indicate that the conduction mechanism is not entirely attributable to the segmental motions of the polymer and is more likely to involve ion hopping between static sites or limited motions of parts of

Table 1.
Experimental parameters obtained for $\text{LiCF}_3\text{SO}_3/\text{PVA}$ polymer electrolytes

Salt/PVA systems (degree of hydrolysis)	Onset of narrowing/K	Activation energy/ kJ mol^{-1} (NMR)	Activation energy/ kJ mol^{-1} (conductivity)
0.5 (88%)	-	-	79.2 ± 1.4
0.5 (99.8%)	244 ± 2	18.6 ± 1.2	-
1 (88%)	-	19.7 ± 0.7	99.1 ± 2.0
1 (99.8%)	260 ± 2	23.8 ± 1.1	115.6 ± 2.6

the polymer chain. Alternatively, conduction might be due to proton motion by a Grotthius-type mechanism involving the polymer hydroxy groups with some release of protons being generated by a lithium hydrolysis reaction.

The ^7Li NMR linewidth measurements as a function of temperature for the 99.8% hydrolysed $\text{PVA}:\text{LiCF}_3\text{SO}_3=0.5$ sample are shown in Fig. 2. At the lowest temperatures, the linewidths are very broad and are approaching the rigid lattice linewidth. These broad linewidths imply that the lithium ions are essentially immobile and therefore the linewidth observed is the result of increased quadrupolar or internuclear dipole-dipole interactions. As the temperature increases, the linewidth decreases as a result of increased lithium ion mobility and hence averaging of the internuclear interactions. The linewidths also reach a high temperature limit which is due to magnetic field inhomogeneities.

Table 1 presents the ^7Li linewidth parameters obtained for fitting equation (1 and 2). The onset of narrowing in these PVA materials is observed well below the glass transition temperature (343 K). The lithium ions are therefore mobile below the DSC glass transition temperature, which is consistent with the materials having a measurable conductivity at room temperature. This is in stark contrast to NMR behaviour observed in traditional polyether based polymer electrolytes [3, 5-7]. The decoupling of the onset of narrowing from the DSC glass tran-

sition temperature in these PVA systems implies that the main segmental motions of the polymer do not govern the overall lithium ion mobility.

Effect of salt concentration on ion mobility

At the concentrations investigated, there appears to be no effect on the temperature dependent linewidths for the 99% hydrolysed samples (Fig. 3). The conductivity results, however, indicate a significant increase in the conductivity with increasing salt concentration. Conductivity is related to the number of charge carriers (n_i) and their mobility (μ_i) according to the following equation

$$\sigma = \sum_i n_i q_i \mu_i \quad (4)$$

where q_i is the charge on each charge carrier. Therefore, it appears that the increase in the number of charge carriers is responsible for the increase in the conductivity in these 99% hydrolysed PVA electrolytes.

Table 1 also compares the onset of narrowing with activation energies from the ^7Li linewidths and the conductivity data. In using the BPP equation [equation (1 and 2)] to obtain activation energies for the NMR measurements, it was assumed that there was only one correlation time. As the salt concentration increases, there is a slight increase in the NMR activation energies and the temperature onset at which the narrowing occurs. The activation

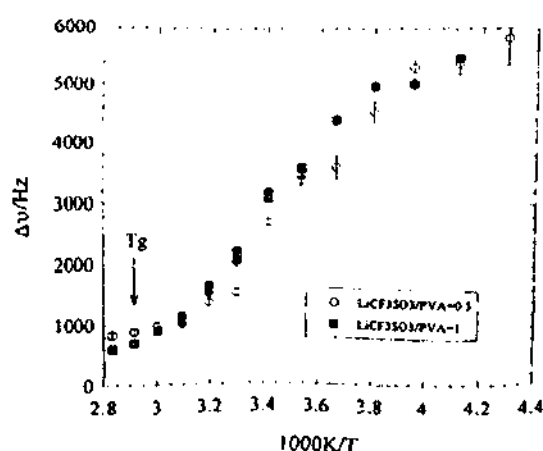


Fig. 3. A comparison of the ^7Li linewidths for 99.8% hydrolysed PVA electrolytes.

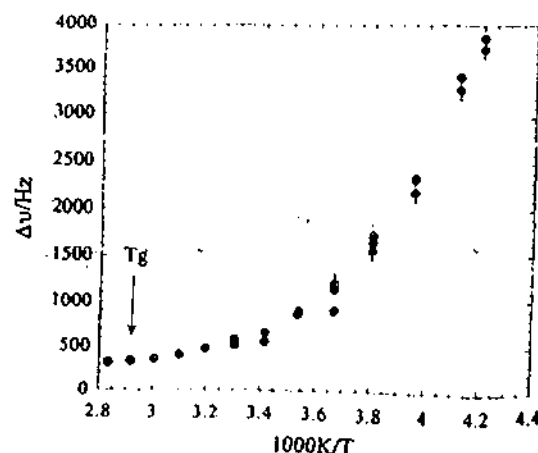


Fig. 4. ^7Li linewidths for 88% hydrolysed $\text{LiCF}_3\text{SO}_3/\text{PVA} = 1$ electrolyte.

energies from the conductivity data also show an increase upon increasing salt content.

The activation energies obtained from the conductivity data are approximately five times larger than those obtained from the linewidth measurements. Bishop and Bray [12] have also observed differences in NMR and conductivity activation energies in lithium borate glasses. They attributed this difference to the scale which each technique is probing. The NMR can detect ion motions on a local scale whereas the conductivity data represents motions on a more global scale. Consequently, the energy barrier for the lithium ions to exceed in order to undergo global, long-range motions is higher than that of local motions.

Effect of degree of hydrolysis

The ^7Li linewidth measurements for the 88% hydrolysed sample are shown in Fig. 4, and are narrower than the 99.8% hydrolysed system, over the temperature range studied. No rigid lattice linewidth was observed and consequently it is not clear where the onset of narrowing will occur in this case. A comparison of both the NMR and conductivity activation energies, for these two systems, shows that the 88% hydrolysed samples have lower activation energies (Table 1). The narrower linewidths indicate a higher lithium ion mobility, which is consistent with the conductivity data (Fig. 1). The inability to measure a narrowing onset implies that the lithium ions are mobile to much lower temperatures. The lower activation energies are also indicative of enhanced lithium ion motion.

CONCLUSION

The ^7Li NMR measurements of $\text{LiCF}_3\text{SO}_3\text{-PVA}$ systems have shown high lithium ion mobilities below their glass transition temperatures, which is also reflected in the conductivity behaviour. This

contrasts with traditional polyether-based polymer electrolytes, which only show motional narrowing of the ^7Li linewidth once the glass transition temperature is exceeded. These results, therefore, imply that cation motion in PVA electrolytes is decoupled from the polymer relaxations. That is, the main polymer relaxations (*ie* α relaxations) do not contribute in a major way to cation transport. Lithium ion motion is therefore likely to take place by an ion hopping mechanism. Alternatively, secondary polymer relaxations or even proton conduction may contribute to conductivity. This will be investigated in further work.

REFERENCES

1. F. M. Gray, *Solid Polymer Electrolytes*, VCH Publishers Inc., New York (1991).
2. T. Yamamoto, M. Inami and T. Kanbara, *Chem. Mater.* 6, 44 (1994).
3. M. Forsyth, M. E. Smith, P. Meakin and D. R. MacFarlane, *J. Polym. Sci. Polym. Phys.* 32, 2077 (1994).
4. S. G. Greenbaum, Y. S. Pak, M. C. Wintersgill and J. J. Fontanella, *Solid State Ionics* 31, 241 (1988).
5. S. G. Greenbaum, Y. S. Pak, C. Wintersgill, J. J. Fontanella, J. W. Schultz and C. G. Andren, *J. Electrochem. Soc.* 135, 235 (1988).
6. S. H. Chung, K. R. Jeffery and J. R. Stevens, *J. Chem. Phys.* 94, 1803 (1991).
7. S. H. Chung, K. Such, W. Wicczorek and J. R. Stevens, *J. Polym. Sci. Polym. Phys.* 32, 2733 (1994).
8. P. E. Stallworth, S. G. Greenbaum, F. Croce, S. Slane and M. Salomon, *Electrochim. Acta* 40, 2137 (1995).
9. J. A. Pople, W. G. Schneider and H. J. Bernstein, *High-resolution Nuclear Magnetic Resonance*, McGraw-Hill Book Company Inc., New York (1959).
10. N. Bloembergen, E. M. Purcell and R. V. Pound, *Phys. Rev.* 73, 679 (1948).
11. M. Forsyth, M. Garcia, D. R. MacFarlane, S. Ng, M. E. Smith and J. H. Strange, in *Solid State Ionics* (in press).
12. S. G. Bishop and P. J. Bray, *J. Chem. Phys.* 48, 1709 (1968).

Ionic Conductivity in Glassy PVOH-Lithium Salt Systems

M. Forsyth¹, H. A. Every¹, F. Zhou², and D. R. MacFarlane¹

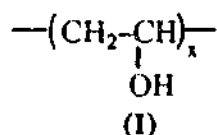
¹Departments of Materials Engineering and ²Chemistry, Monash University, Wellington Road, Clayton, Victoria 3168, Australia

Ionic conductivity (10^{-4} S/cm at 25°C) has been observed in glassy poly(vinyl alcohol)/lithium salt complexes. X-ray diffraction patterns indicate that, while the pure polymer is semi-crystalline, the addition of salt suppresses the extent of crystallinity. The glass transition temperatures of these systems are typically in the region of 50-70°C. The conductivity is dependent on the concentration and anion in the lithium salt; LiClO₄ producing the highest conductivities in this work. The presence of unhydrolyzed acetate groups in the polymer backbone causes T_g to be decreased, as compared to the homopolymer, and produces an order of magnitude increase in conductivity. ⁷Li solid state NMR spectroscopy suggests that lithium ion motion is present below T_g indicating that, at least in part, lithium ion motion is responsible for the ionic conductivity and that this motion is decoupled from the polymer segmental motions. ¹⁹F T_1 and T_2 NMR relaxation times were also measured for the anion, and the lack of correlation with the conductivity data suggests anion motion is unlikely to be a major contributor to the conductivity.

Polymer electrolytes have been under intense investigation (1) for the past two decades owing to their potential applications in a variety of new electrochemical devices, in particular lithium batteries. The most successful of these (ie. having high ionic conductivities with suitable mechanical properties) have been based on, or have contained segments of, the polyether unit. These have served to act as a good solvent, in particular for alkali metal cations which coordinate to the ether oxygen. In work carried out in our laboratories (2) and others (3) it has been shown that optimum conductivity in these electrolytes occurs at salt concentrations of the order of 1 mol/kg, with higher salt concentrations resulting in a decreasing conductivity. This fall off in conductivity occurs as a result of (i) an increasing degree of ion aggregation and therefore the availability of fewer small ions, and (ii) an increasing glass transition temperature, T_g , and hence a decrease in ionic mobility. These systems are

characterized by a T_g well below room temperature and are therefore soft elastomeric materials (4) or semi-crystalline materials at ambient temperatures.

Recently (5,6,7) solid electrolyte systems based on poly(vinyl alcohol), PVOH, (I)



have been investigated which contain a very substantial amount of salt (up to 75wt% salt). These electrolytes have been shown to have room temperature conductivities up to 10^{-4} S/cm (5), almost an order of magnitude higher than other known solvent-free polymer electrolytes. One of the unusual and interesting characteristics of these new PVOH systems is that higher salt concentrations result in higher conductivities, up to the current limit of miscibility. Further, the glass transition temperature is above room temperature (ca. 70°C) and shows little dependence on salt concentration, in contrast to the systems based on polyethers (8).

These solid electrolyte systems are of considerable scientific and technological significance since ionic conductivity appears to be decoupled from the polymer motions, as manifest in the DSC glass transition temperature. This characteristic probably qualifies these systems as the first polymeric members of the group of fast ion conductive materials (5). Fast ion conduction occurs when the diffusive/conductive modes of motion of one or more species in the material become decoupled from the main structural modes which determine T_g . Ion motion then takes place against a static background of sites between which the ions hop. Systems having conductivities in the range of 10^{-5} - 10^{-4} S/cm at room temperature, and having T_g above room temperature, are of interest in the electrochromic window device (9) being developed by a number of groups. Further improvement of the conductivity may open other applications, for example in photoelectrochemical solar cells and low power capacitors.

Poly(vinyl alcohol) is well known to be a semi-crystalline material ($T_m=220^\circ\text{C}$, $T_g=85^\circ\text{C}$) although it often degrades before melting (10). The polymer is made by a hydrolysis reaction of poly(vinyl acetate) which is typically 80-99% complete. The 99% hydrolyzed polymer can be viewed as a pure homopolymer, whereas the materials having a higher fraction of remaining acetate groups should be viewed as a random copolymer. The degree of hydrolysis influences the glass transition temperature of the amorphous fraction (T_g (99%) $\sim 68^\circ\text{C}$, T_g (88%) $\sim 55^\circ\text{C}$) in PVOH. The glass transition temperature of PVOH is relatively high for a vinyl polymer of this structure. This is the result of the strong hydrogen bonding interactions, both intra- and interchain. The effect of acetate groups is to disrupt this to some extent as seen in the decreased T_g .

One possible interpretation of the high ionic conductivities observed in these PVOH based electrolytes is that the conduction involves protons liberated from the hydroxy group. The mobility of such protons can be high as a result of small size and mass and may even be assisted by a mechanism similar to the Grotthius mechanism observed in aqueous systems. In this model, the alkali metal ions and the corresponding anion which are dissolved in the polymer may be relatively immobile and hence may not contribute to the conductivity. In our recent work (5) we have used ^7Li NMR experiments to probe cation mobility. These have shown significant

lithium ion mobility below T_g and this is enhanced at higher salt concentrations. Hence we hypothesize that the dissolved ions *are* a major conductive species.

Since the pure polymer is partly crystalline, the question arises as to the role of the crystal domains in the conduction process. This question also arose in the interpretation of conductivity in the polyether electrolytes (1) and it was shown that conduction occurs predominantly in the amorphous regions. In polyether systems containing a substantial degree of crystallinity, the conductivity is observed to increase by as much as an order of magnitude as the temperature is increased through the melting point. It has been concluded therefore that the presence of a mobile amorphous phase is necessary for conduction in these polyether systems. Ion mobility also rapidly diminishes as the temperature is decreased towards T_g (1). As with these polyether systems it is hypothesized that significant conduction occurs in the amorphous regions of the PVOH/salt mixtures.

In this paper we have investigated the influence of the degree of hydrolysis, salt content and the nature of the salt on conductivity in PVOH/lithium salt mixtures. These results, along with ^7Li and ^{19}F NMR relaxation measurements and X-ray diffraction data, are used to examine the hypotheses outlined above regarding the nature of the conduction mechanism.

Experimental method

Sample preparation. LiCF_3SO_3 (Aldrich), LiBF_4 , and LiClO_4 salts were dissolved in poly(vinyl alcohol), PVOH. Two polymers were studied with the molecular weight ranges of 31,000-50,000 g/mol (Aldrich) and 105,600-110,000 g/mol (Aldrich), with degrees of hydrolysis being 88% and 99.8% respectively. The polymer films were prepared by dissolving the PVOH and salt in dimethyl sulfoxide (DMSO), (17g DMSO/1g PVOH) at 70°C for one hour. The solution was then cast onto a glass plate and the DMSO removed using a high vacuum pump over a period of 15 hours. The film was finally dried between two pieces of teflon in a vacuum oven at 50 to 70°C for approximately 20 hours. The DMSO removal was monitored gravimetrically. The polymer systems studied consisted of salt to polymer weight ratios between 0.25 and 1.5.

Conductivity measurements. The conductivity of the electrolytes was measured using a Hewlett Packard 4284A LCR meter in the range 20Hz-1MHz. Disc shaped samples ~1.5cm in diameter and 0.2mm thick were sandwiched between a pair of blocking electrodes after coating each side with a circular gold electrode by sputtering. The brass conductivity cell was loaded with the sample in a nitrogen drybox and sealed to prevent moisture ingress during the measurements.

Thermal analysis. Differential scanning calorimeter thermograms were obtained using a Perkin Elmer DSC7. Samples were encased in Al sample pans and quenched to liquid nitrogen temperatures prior to heating in the DSC at rates between 10 and 30°C/min. Annealing experiments were carried out by holding the sample in the DSC at temperatures just below T_g for various periods of time. After this period of annealing the sample was cooled and rewarmed to observe the resultant shape of the glass transition region.

X-ray diffraction. Wide-angle x-ray diffraction (WAXD) patterns were obtained on a Scintag PAD5 instrument in reflection mode with filtered $\text{CuK}\alpha$ radiation. The data

was obtained from 10° through to 70° with a 0.05° step size at a scanning rate of 2°/min.

NMR Linewidth measurements. A home built permanent magnet spectrometer operating at 13.69 MHz was used to measure ^{19}F relaxation times for the PVOH electrolytes. T_1 and T_2 were obtained using the Inversion-Recovery and Spin-echo methods respectively at temperatures between -70°C to 20°C.

^7Li NMR linewidth measurements for the PVOH electrolytes were made using a modified Bruker CXP 300 NMR spectrometer operating at 116.6 MHz. A simple one pulse experiment was used with a pulse length of 1.5 μs . The linewidths were taken at full width at half maximum (FWHM) of the peaks between -40°C to 80°C. The onset of narrowing was determined from plotting the magnitude of the linewidth as a function of temperature.

Results and Discussion

Thermal Analysis and XRD. Figure 1(a) shows a typical thermogram for pure PVOH (99.8%). A weak step in the heat capacity is observed between 60°C and 70°C. To prove that this event is in fact a glass transition, the polymer was annealed at 60°C for 3 hours. Such annealing produces a characteristic enthalpy overshoot at the glass transition if some non-reversible relaxation process has taken place. This is often taken as clear indication that a thermal transition is in fact a glass transition. The second thermogram confirms this hypothesis by showing a substantial enthalpy overshoot peak after the annealing. In Figure 1(b) similar behaviour in a salt/copolymer (88%) system is seen, indicating a glass transition temperature around 55°C.

Heating to higher temperatures showed a broad endotherm around 190°C which may be the melting transition in the semi-crystalline pure polymer. This transition was not distinctly observed in the polymer/salt systems, indicating suppression of crystallinity by the salt. This behaviour is confirmed in Figure 2, which shows the wide angle X-ray diffraction pattern for the 88% hydrolyzed systems. The pure copolymer, which contains no salt but has otherwise been prepared in the same manner, by casting from DMSO solution, exhibits a clear crystalline diffraction peak at $2\theta = 20^\circ$. This peak corresponds to the 110 reflection arising from the planar zig-zag configuration of the backbone (11). Addition of salt to this polymer causes a marked decrease in the intensity of this peak relative to the broad amorphous peak. The degree of crystallinity in PVOH is well known to be strongly dependent on its thermal treatment (10,12-14). Sakurada has found that PVOH cast from solution is isotropic with a degree of crystallinity around 15% (10). Peppas and Hansen however show that solution cast PVOH is 20% crystalline (12), as does Molyneux (13). Annealed (180°C) isotropic PVOH, can have crystalline fractions as high as 75% (Kenny and Willcockson) (14). On the basis of these results, the extent of crystallinity in the pure copolymer sample in Figure 2 is likely to be of the order of 20%. The extent of crystallinity in the corresponding salt containing system appears to be lower than this, implying that the addition of salt to PVOH does indeed suppress crystallinity.

Conductivity. Conductivity data as a function of salt content in the PVOH/Li triflate system are presented in Figure 3. At all temperatures the conductivity increases sharply with added salt content up to the solubility limit. This behaviour is in marked contrast to the polyether based electrolyte systems where a conductivity maximum is

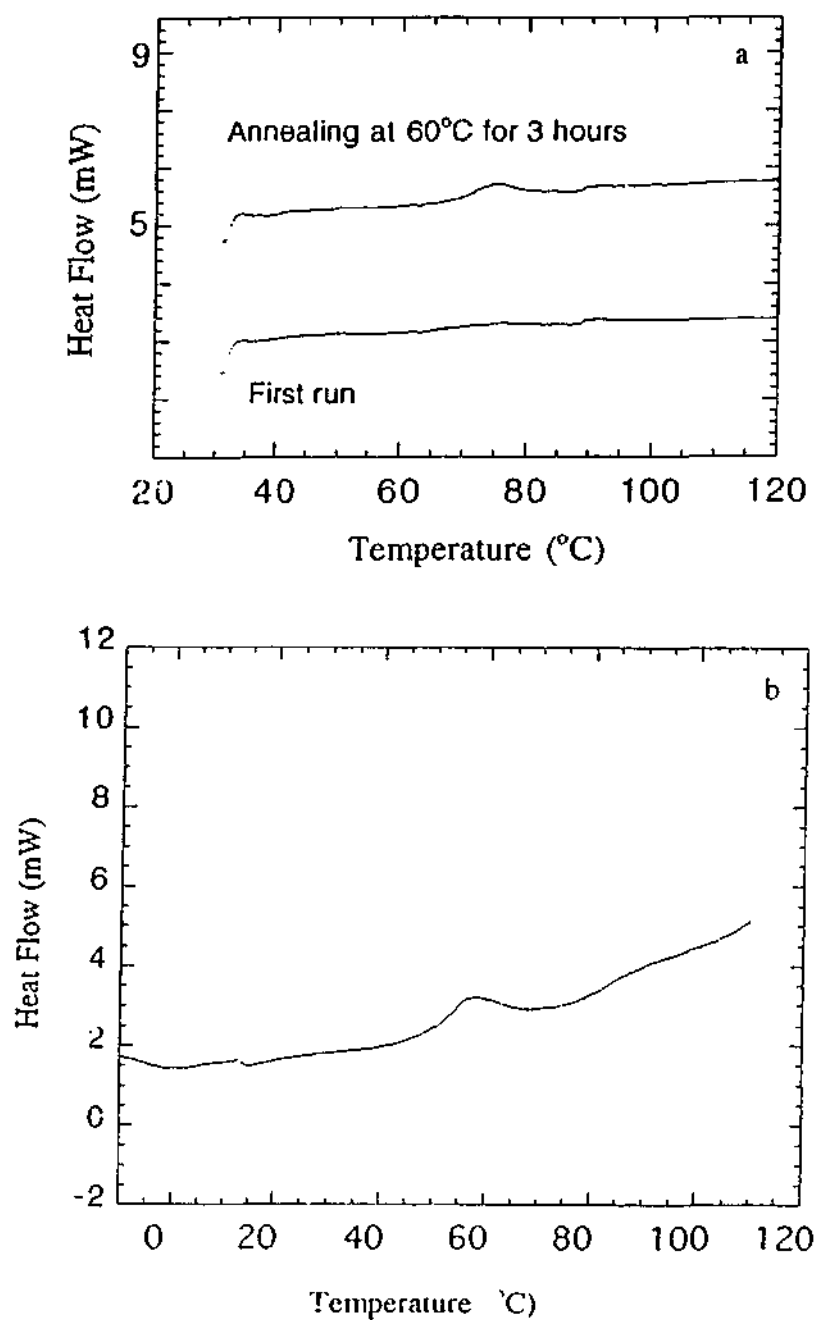


Figure 1. DSC thermograms of (a) PVOH (99.8% hydrolyzed) before and after annealing and (b) a PVOH (88% hydrolyzed) system containing 33% by weight Li triflate.

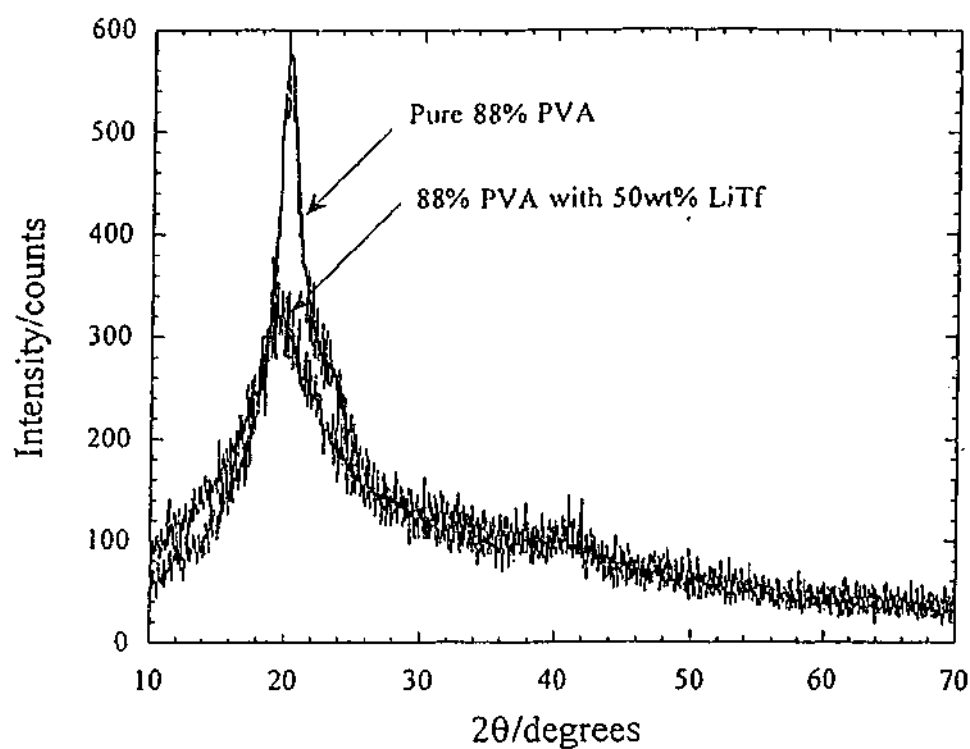


Figure 2. X-ray diffraction pattern of a PVOH (88% hydrolyzed) system containing 50 percent by weight Li triflate

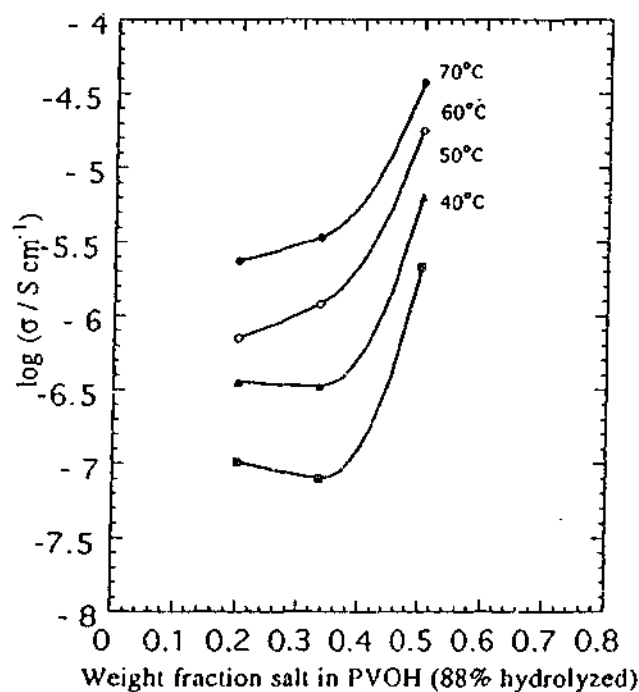


Figure 3. Conductivity as a function of salt content in the PVOH (88% hydrolyzed)/Li triflate system.

observed typically around 1 mol/kg ($\approx 10\%$ (w/w) in the case of LiClO_4). In fact, there is a suggestion in the low concentration data in Fig. 3 that the conductivity passes through a minimum. Since pure PVOH is not known to be ion conductive, the conductivity must therefore exhibit a maximum at yet lower concentrations. This data emphasizes the very much higher salt content of these electrolytes, as compared to the traditional polyether systems, and the likelihood of a molten salt like conduction mechanism.

In Figure 4(a) conductivity data for selected systems are presented as a function of inverse temperature. Comparison of these results with those in the literature for the 88% hydrolyzed PVOH systems reveal some significant differences. The Li triflate and LiBF_4 data are significantly lower than the measurements of Yamamoto *et al.* (6) while the LiClO_4 measurements from the present work are quite similar to the LiBF_4 results of Yamamoto *et al.* One possible cause of such variations is the extent of residual DMSO in the sample. Yamamoto *et al.* quote a value of residual DMSO of 3.5% (w/w) as obtained by GLC. In our work accurate weight loss measurements have shown that typical residual DMSO content is between 5 and 10%, the higher DMSO contents being recorded for the higher salt content samples. A determination of the effect of DMSO content on conductivity shows that the conductivity changes by approximately one order of magnitude as the DMSO content is reduced from 25% to $\sim 5\%$. Hence the presence of small amounts of residual DMSO cannot obviously explain the above discrepancy. The thermal analysis traces of the materials prepared in this work are also significantly different from those of Yamamoto *et al.*, who observed melting transitions around 100°C . The lack of this transition in our samples suggests morphological differences between samples prepared in this work, which are possibly the result of i) the molecular weights used, ii) the tacticity of the PVOH samples, and iii) the precise details of the thermal history of the samples in the final stages of preparation.

Figure 4(b) compares Li triflate systems based on the homopolymer with those of the copolymer. At both salt concentrations the copolymer systems are at least an order of magnitude more conductive than the corresponding homopolymer systems. This correlates with the higher T_g for the homopolymer systems and the ^7Li NMR data, as will be discussed further below.

The data in Figure 4 exhibit Arrhenius behaviour in the lower temperature region well below T_g . Near T_g , all data sets become curved and exhibit decreasing activation energy. Table I summarizes the activation energies obtained from linear fits to the lower temperature regions, as indicated by the lines drawn in the Figure. These activation energies are notably higher by at least a factor of 2 than polyether electrolytes of similar conductivity. However, these activation energies correspond to a sub- T_g process. Under similar conditions (ie. below their T_g) polyether electrolytes are not conductive. A more useful comparative system for these PVOH electrolytes is the family of lithium ion conductive ceramics in which facile lithium motion takes place within a rigid inorganic oxide framework (15). The mechanism in the latter case is thought to be ion hopping between vacant isoenergetic sites. In these systems the activation energy is typically $\sim 10^2$ kJ/mol and corresponds to the energy required to break the Li^+ - lattice oxygen bond. In the PVOH electrolyte systems described in this work, given that the activation energies are obtained below T_g , there must exist a rigid framework of some sort and E_a probably corresponds to the breaking of a bond between the mobile ion and this rigid framework.

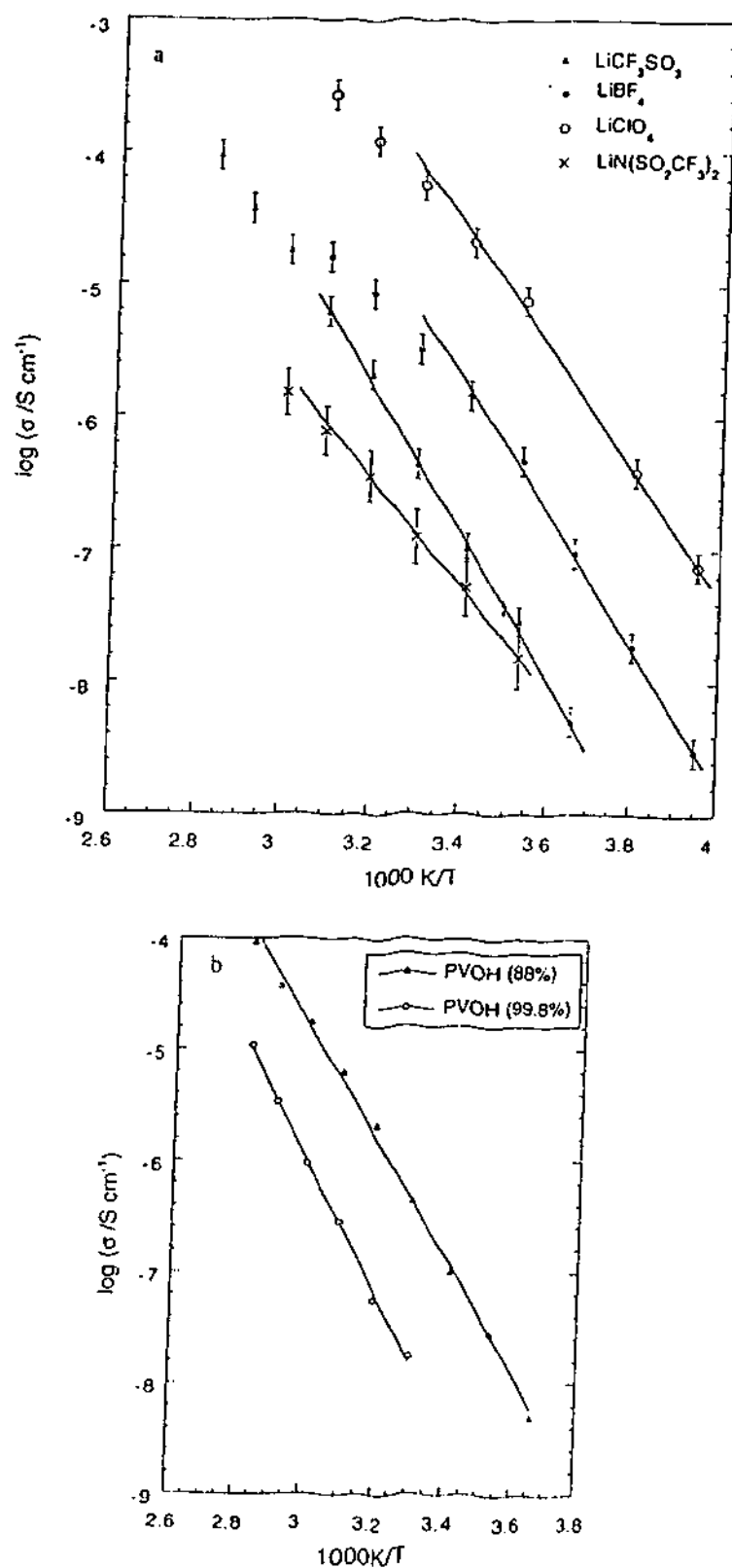


Figure 4. Conductivity as a function of inverse temperature, showing the effect of (a) different anions at fixed composition (50% salt by weight) and degree of hydrolysis (88%) and of (b) polymer degree of hydrolysis (salt=Li triflate)

Table I. Activation energies for ion conduction in PVOH based polymer electrolytes

Salt	Polymer	Weight ratio of salt/PVOH	E_a (kJ/mol)
LiCF ₃ SO ₃	PVOH(88%)	1:2	118 ± 5
LiBF ₄	PVOH(88%)	1:2	87 ± 2
LiClO ₄	PVOH(88%)	1:2	72 ± 2
LiClO ₄	PVOH(99.8%)	1:2	130 ± 6
LiClO ₄	PVOH(88%)	1:2	72 ± 1
LiClO ₄	PVOH(88%)	1:1	67 ± 2
LiCF ₃ SO ₃	PVOH(88%)	1:1	99 ± 2
LiCF ₃ SO ₃	PVOH(88%)	1:2	94 ± 3
LiCF ₃ SO ₃	PVOH(88%)	1:4	118 ± 5

The activation energy is almost independent of salt content but is higher for the homopolymer than for the copolymer in the case of the perchlorate systems. This is consistent with the higher T_g observed for the homopolymer based electrolytes and also their lower room temperature conductivity. The activation energies decrease in the order $\text{CF}_3\text{SO}_3^- > \text{BF}_4^- > \text{ClO}_4^-$ observed (under similar conditions of hydrolysis and concentration), concomitant with the increase in conductivity as a function of the anion.

NMR.

Anion mobility by ^{19}F NMR

Figure 5 presents the ^{19}F temperature dependent T_1 relaxation times for various PVOH/triflate samples. A comparison of polymer type and salt concentration can be made here. All data pass through a minimum. The position of this minimum, in temperature, relates to the correlation time of the motion responsible for the ^{19}F relaxation, whilst the magnitude of T_1 at the minimum is indicative of the strength of the interaction governing the relaxation process. As illustrated in Figure 5 at a fixed salt concentration, ^{19}F relaxation is independent of the degree of hydrolysis of the polymer. This suggests the fluorines are unlikely to be relaxing as a result of polymer-anion interactions. The decrease in T_1 at the minimum with increasing salt confirms that the relaxation is either Li-F or F-F dominated. The shift of the T_1 minimum to lower temperatures suggests an increase in mobility (probably anion tumbling) with increasing salt concentration.

The T_2 measurements (Figure 6) support the behaviour observed in the T_1 data. Upon the addition of salt, the T_2 relaxation times increase suggesting enhanced ion mobility. For the electrolytes with the same salt concentration, but differing degrees of hydrolysis, the T_2 relaxation times are very similar. If the anion was diffusing in these systems, then it might be expected that the T_2 would approach T_1 at high temperatures. According to simple BPP theory, the relaxation times are dependent on the correlation time, τ_c , and the Larmor frequency, ω_l , (16) as shown for example in the following equations:

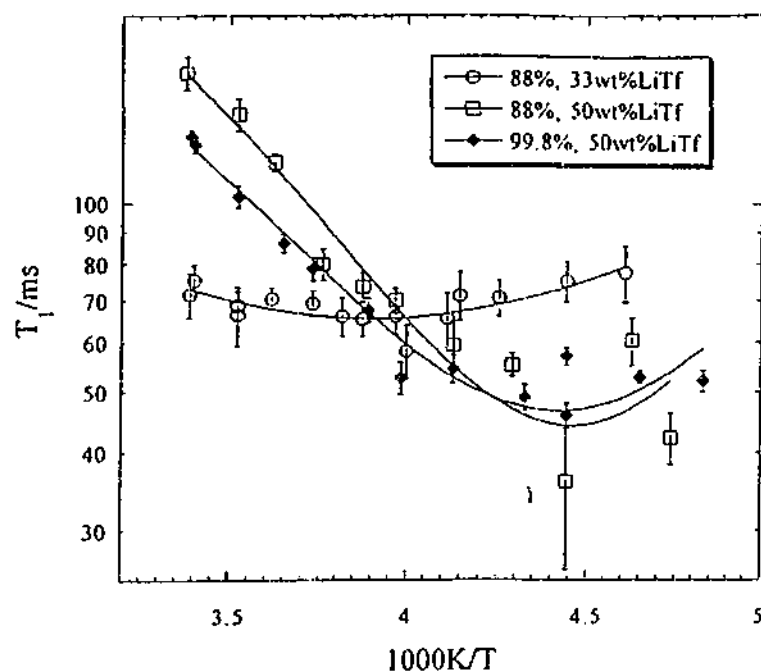


Figure 5. ^{19}F Spin-lattice relaxation measurements (T_1) for PVOH/Li triflate systems as a function of inverse temperature. Lines drawn are a guide to the eye only.

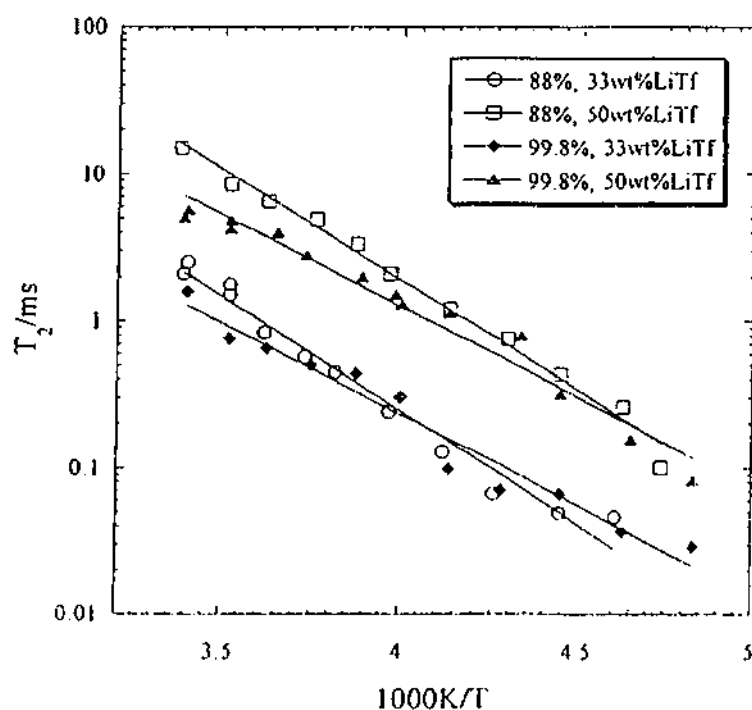


Figure 6. ^{19}F Spin-spin relaxation (T_2) measurements as a function of inverse temperature in PVOH/Li triflate systems. Lines are Arrhenius fits to the data with activation energies indicated in Table II.

$$\frac{1}{T_1} \propto \left[\frac{\tau_c}{1 + \omega_L^2 \tau_c^2} + \frac{4\tau_c}{1 + 4\omega_L^2 \tau_c^2} \right]$$

$$\frac{1}{T_2} \propto \left[3\tau_c + \frac{5\tau_c}{1 + \omega_L^2 \tau_c^2} + \frac{2\tau_c}{1 + 4\omega_L^2 \tau_c^2} \right]$$

These equations show that field components which contribute to the relaxation in T_1 also affect T_2 , but T_2 is also sensitive to static fields. It is this static field component which dominates when T_2 is considerably smaller than T_1 . The T_2 relaxation times for these samples are approximately an order of magnitude lower than the T_1 relaxation times at corresponding temperatures. Combining this observation with the lack of any correlation between the ^{19}F T_1 and T_2 trends and conductivity trends with salt and polymer type, it is suggested that the anion is unlikely to be diffusing in these systems. Future NMR diffusion measurements will test this hypothesis.

This conclusion is not inconsistent with the dependence of conductivity on anion type as seen in Figure 4. The influence of an immobile anion on conductivity may be due to the strength of its interaction with the Li^+ ion. This is also observed in the conductivity activation energy data in Table I. The lack of contribution of the anion to conductivity in these systems is also indicated by the very low conductivity observed by Yamamoto *et al.* for PVOH systems containing $\text{Bu}_4\text{N}^+ \text{ClO}_4^-$ (Bu = butyl); the Bu_4N^+ is known to be a large weakly interacting cation. Therefore the conductivity in these systems does not appear to be due to anion motion. Comparison with the Bu_4N^+ based system suggests that Li^+ ion mobility is chiefly responsible for the observed conductivity in the Li^+ based systems of this work. Further evidence for this is found in the ^7Li NMR linewidth measurements discussed below.

Cation mobility by ^7Li NMR

The ^7Li NMR linewidth measurements as a function of temperature for the 99.8% hydrolysed $\text{PVOH}:\text{LiCF}_3\text{SO}_3 = 1$ sample are shown in Figure 7. At the lowest temperatures, the linewidths are broad (~5500 Hz) and the shape of the curve appears to be approaching a Gaussian line shape. As the temperature increases, the linewidth decreases and, at the highest temperature, the lineshape becomes increasingly Lorentzian.

In Figure 8 the linewidth (FWHM) data are plotted for several systems as a function of temperature. The two systems based on 99.8% hydrolyzed PVOH show little dependence of the ^7Li linewidth on salt content. The shape of the curve as a function of temperature is characteristic of a system passing out of its low temperature state in which the Li^+ ions are effectively immobile. This low temperature behaviour is termed the rigid lattice limit. With increasing temperature the line begins to narrow as a result of increased ion mobility. The high temperature (motionally narrowed) limit is set by the resolution of the spectrometer. In the case of the 88% hydrolyzed sample with salt to polymer ratio of 0.5, a rigid lattice limit is not reached over the temperature range studied. In addition, over this entire temperature range, the lithium linewidth is always smaller for the copolymer; this also therefore indicating higher lithium ion mobility.

The linewidth data can be well fitted by the following equation (19,20):

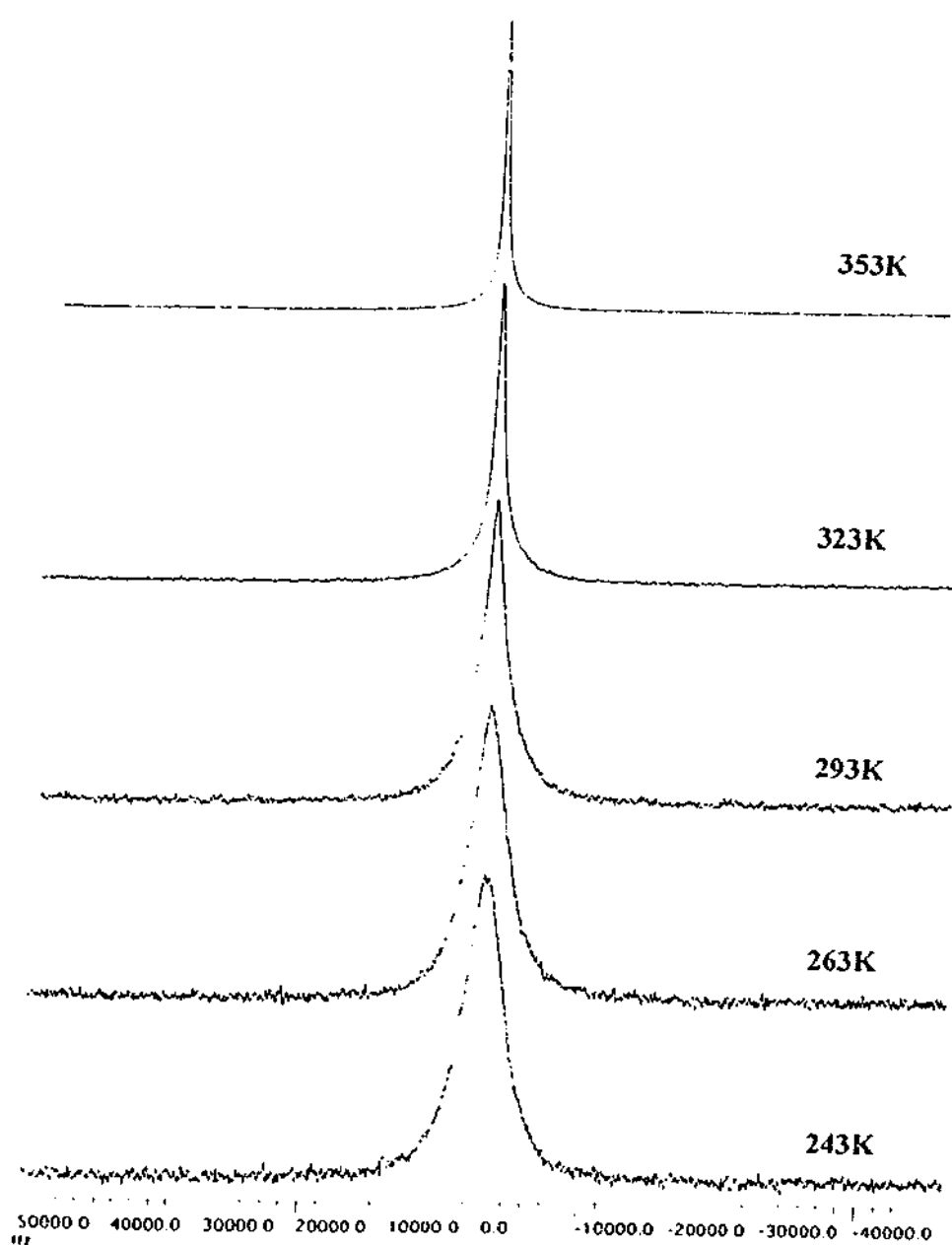


Figure 7. ^7Li NMR spectra for $\text{LiCF}_3\text{SO}_3:\text{PVOH} = 1:1$ by weight as a function of temperature.

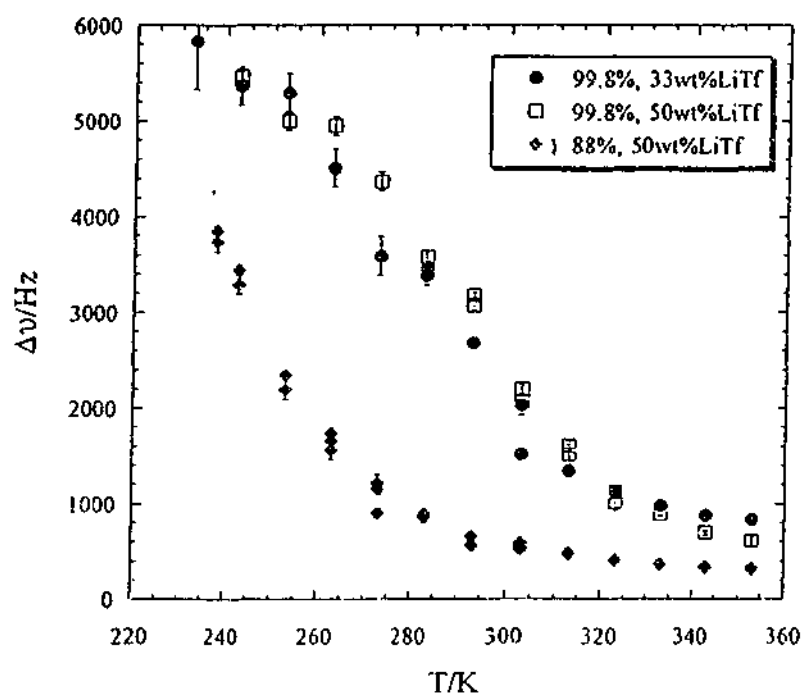


Figure 8. ^7Li NMR linewidths as a function of temperature for 99.8% and 88% hydrolyzed PVOH/Li triflate electrolytes. The temperature of onset of motional narrowing is estimated by extrapolating the linear portion of the curve to the rigid lattice estimate.

$$(\delta\omega)^2 = \left(\frac{2}{\pi}\right) \delta\omega_0^2 \tan^{-1}(\tau_c \delta\omega)$$

where $\delta\omega$ is the narrowed linewidth, $\delta\omega_0$ is the rigid lattice linewidth and τ_c is the correlation time related to diffusional motion. The correlation time is assumed to show an Arrhenius temperature dependence

$$\tau_c = \tau_0 \exp\left(\frac{E_a}{kT}\right)$$

The activation energies obtained from these fits are also shown in Table II.

Table II. NMR ion mobility parameters

<i>Salt/PVOH systems</i> (degree of hydrolysis)	<i>Onset of</i> <i>Narrowing/K</i>	$\tau_c(^7\text{Li})$ Activation energy/kJ mol ⁻¹	$^{19}\text{F}, T_2$ Activation energy /kJ mol ⁻¹
1:1 (88%)	214±2	19.7±0.7	28.7 ± 0.1
1:2 (99.8%)	244±2	18.6±1.2	23.8 ± 0.1
1:1 (99.8%)	260±2	23.8±1.1	23.8 ± 0.1
1:2 (88%)	-	-	29.7 ± 0.1

For the same salt concentration, the activation energy for lithium ion mobility (as given by τ_c) is lower in the case of 88% hydrolyzed PVOH.

The onset of line narrowing can be estimated from these linewidth curves (see Table II). The higher salt content, higher degree of hydrolysis samples give the highest onset temperature. Given that the rigid lattice limit has not been reached in the case of the copolymer sample, an approximate onset temperature has been determined by assuming the rigid lattice is approximately 6000Hz. This data clearly shows the higher lithium ion mobility in the case of the copolymer. It is interesting to note that the onset of motional narrowing occurs at temperatures at least 70°C below T_g as determined from thermal analysis. This is in stark contrast to polyether and other polymer electrolytes where motional narrowing appears closely linked to T_g (17,18). It is also of interest to observe that higher conductivities are measured in samples based on the 88% hydrolyzed PVOH polymer, consistent with the higher lithium ion mobility indicated by ^7Li NMR (in contrast to the ^{19}F relaxation data). However, in comparing the temperature dependence of the linewidths for the 99.8% hydrolyzed PVOH with different salt concentrations, it appears that the higher salt content results in a slightly decreased lithium ion mobility. This is in contrast to the increased ionic conductivity. Since conductivity is related to the number of charge carriers (n_i) and their mobility (μ_i) by the equation $\sigma = \sum n_i q_i \mu_i$ (where q_i =charge),

the increased conductivity for the higher salt content is apparently the result chiefly of an increase in the number of charge carriers. The contributions of H^+ , Li^+ and anion to conductivity will be clarified in the near future by diffusion measurements.

Conclusions

The work reported here on poly(vinyl alcohol) electrolytes shows that the materials are mainly amorphous with T_g around 50-70°C and conductivity at room temperature as high as 10^{-4} S/cm. ^{19}F NMR relaxation measurements are consistent with the hypothesis that the anion, or at least the triflate anion, is not significantly mobile below T_g . ^7Li NMR linewidth measurements indicate, however, that the lithium ion only approaches its rigid lattice linewidth at ca. 250K. Above this temperature the ^7Li line is motionally narrowed, consistent with either mobile ^7Li ions or motion of some other species in the vicinity of the Li ion. This NMR evidence, plus the observation that tetrabutylammonium analogues of these systems show only very low conductivity, are all consistent with the hypothesis that the lithium ion is the chief conducting species in these systems below T_g . The observation of high ionic mobility below T_g is a common phenomenon in the so called fast ion conducting glasses and ceramics. To our knowledge this is the first observation of such fast ion conducting behaviour in a polymeric system. The observation of fast ion conduction in this polymer system may reflect the high solubility of the lithium salts in the systems due to the hydroxy groups in the polymer chain. This high solubility results in a medium which has more in common with a molten salt system than traditional polyether based electrolytes. The fact that the 88% PVOH has a higher conductivity than the 99% hydrolysed PVOH suggests that the polymer is not irrelevant in the conduction process. The room temperature activation energies for conduction in these systems is high compared to other polymer electrolytes and is a strong function of the anion, suggesting an anion-cation bond breaking step in the overall conduction.

Literature Cited

1. Gray, F.M. *Solid Polymer Electrolytes*, VCH Publishers Inc. New York (1991).
2. (a) Bishop, A.G.; MacFarlane, D.R.; McNaughton, D.; Forsyth, M. *J. Phys. Chem.* **1996**, *100*, 2237.
(b) Bishop, A.G.; MacFarlane, D.R.; Forsyth, submitted to *Electrochimica Acta*.
3. Watanabe, M.; Ohashi, S.; Sanui, K.; Ogata, N.; Kobayashi, T. and Ohtaki, Z., *Macromolecules* **1985**, *18*, 1945.
4. Sun, J.; MacFarlane, D.R.; Forsyth, M. *Solid State Ionics* **1996**, *85*, 137.
5. Every, H.A.; Zhou, F.; Forsyth, M.; MacFarlane, D.R. submitted to *Electrochimica Acta*.
6. Yamamoto, T.; Inami, M.; Kanbara, T. *Chem. Mater.* **1994**, *6*, 44.
7. Kanbara, T.; Inami, M.; Yamamoto, T.; Nishikata, A.; Tsuru, T.; Watanabe, M.; Ogata, N. *Chem. Lett.* **1989**, 1913.
8. MacFarlane, D.R.; Sun, J.; Meakin, P.; Fasoulopoulos, P.; Hey, J.; Forsyth, M.; Rosalie, J.M. *Electrochimica Acta* **1995**, *40*, 2131-2136.
9. MacFarlane, D.R.; Sun, J.; Forsyth, M.; Bell, J.M.; Evans, L.A.; Skyrabin, I.I. *Solid State Ionics* **1996**, *86-88*, 959-964.
10. Sakurada, I. "Polyvinyl Alcohol Fibres, International fibre science and technology series, 6" New York, Marcel Dekker, Inc. (1985).
11. Hodge, R.M.; Edward, G.H.; Simon, G.P. *Polymer* **1996**, *8*, 1371.
12. Peppas, N.A.; Hansen, P.J. *J. Appl. Polym. Sci.* **1982**, *27*, 9787.
13. Molyneux, P. "Nonionic polymers - The vinyl group" Chapter 4 in "Water-soluble synthetic polymers" Vol. 1 CRC Press, Florida USA, p.110-131 (1983).
14. Kenney, J.F.; Wilcockson, G.W. *J. Polym. Sci. A-1* **1966**, *4*, 679.

15. (a) H. Aono, E. Sugimoto, Y. Sadaoka, N. Imanaka and G.-Y. Adachi, *J. Electrochem. Soc.* **1990**, *137*, 1023. (b) H. Aono, E. Sugimoto, Y. Sadaoka, N. Imanaka and G.-Y. Adachi, *J. Electrochem. Soc.* **1989**, *136*, 590.
16. Fukushima, E.; Roeder, S.B.W. "Experimental Pulse NMR: A nuts and bolts approach" Addison-Wesley Publishing Co., Inc. Reading, Massachusetts (1981).
17. Chung, S.H.; Jeffrey, K.R.; Stevens, J.R. *J. Chem. Phys.* **1991**, *97*, 1803.
18. Stallworth, P.E.; Greenbaum, S.G.; Croce, F.; Slane, S.; Solomon, M. *Electrochim. Acta* **1995**, *40*, 2137.
19. Bloembergen, N.; Purcell, E.M.; Pound, R.V. *Phys. Rev.* **1948**, *73*, 679.
20. A. Abragam, "The Principles of Nuclear Magnetism" Oxford University Press (1961), p.456.

Note added in Proof:

One of the referees points out that the degree of hydrolysis of polyvinylacetate directly influences the free volume as measured by PALS. This is consistent with a lower T_g for the 88% hydrolysed polymer and the corresponding higher conductivities measured in this copolymer.

(R.M. Hodge, T.J. Bastow and A.J. Hill, , roceedings of 10th IAPRI conference on Packaging, Melbourne, March 24-27, 1997)



PERGAMON

Electrochimica Acta 45 (2000) 1279–1284

ELECTROCHIMICA
Acta

www.elsevier.nl/locate/electacta

Ion diffusion in molten salt mixtures

H. Every^a, A.G. Bishop^b, M. Forsyth^a, D.R. MacFarlane^{b,*}^a Department of Materials Engineering, Monash University, Wellington Road, Clayton, Vic. 3168, Australia^b Department of Chemistry, Monash University, Wellington Road, Clayton, Vic. 3168, Australia

Received 5 November 1998

Abstract

The molten salts, 1-methyl,3-ethylimidazolium trifluoromethanesulfonate (triflate salt, MeEtImTf) and 1-methyl,3-ethylimidazolium bis(trifluoromethanesulfonimide) (imide salt, MeEtImNTf₂) are colourless ionic liquids with conductivities of the order of 10^{-2} S cm⁻¹ at room temperature. DSC measurements revealed subambient melting and glass transition temperatures. Analysis of the anion and cation diffusion coefficients suggested that the cation was the dominant charge carrier and that the motion was largely independent of the anion. Haven ratios (H_{RS}) of 1 and 1.6 were determined for the imide and triflate salts, respectively, at 30°C (303 K). Values greater than one imply some degree of ionic association, suggesting that aggregation is present in the triflate salt. Mixing of the salts to form binary systems resulted in enhanced conductivities which deviated from a simple law of mixtures. Thermal analysis showed no evidence of a melting point with only a glass transition observed. Corresponding diffusion measurements for the binaries appeared to show a weighted average of the diffusion coefficients of the pure components. The increased conductivity can be attributed to an increase in the number of charge carriers as a result of decreased ion association in the binary. © 2000 Elsevier Science Ltd. All rights reserved.

Keywords: Dialkylimidazolium molten salts; Ionic conductivity; Diffusion; Binary systems; Transport mechanisms

1. Introduction

Molten salts are the most concentrated electrolytic fluids, possessing a high number of charge carriers per unit volume. When these charge carriers are mobile, very high conductivities are possible. Interest in this field of research has increased since the discovery by Wilkes et al. in 1982 [1] of a molten salt which was liquid over a wide range of compositions and to temperatures as low as -95°C. Ionic liquids are being investigated for many applications including electroplating, batteries, electrochemical capacitors and photoelectrochemical (PEC) cells. In PEC cell applications,

molten salts could be utilised as the electrolyte solvent only or also be involved in the redox mediation processes. The physical properties which make the systems attractive in such roles are their large electrochemical windows and high conductivities, excellent thermal and chemical stability, negligible vapour pressure at elevated temperatures and miscibility in a diverse range of solvents [2–5].

The haloaluminate 1,3-dialkylimidazolium binary molten salt systems have been extensively studied for many applications due to their relative ease of preparation, wide electrochemical windows, high conductivities and interesting acid/base properties [1–3,6–9]. The sensitivity of dialkylimidazolium tetrahaloaluminates to water has precluded them from use in PEC cells. The ability of MeEtIm⁺ to form ambient molten salts with AlCl₃ [1–3,6,7], AlBr₃ [8,9] and CuCl₂ [10] is due to the anion/cation interactions. Thus, anion substitution

* Corresponding author. Tel.: +61-3-9905-4599; fax: +61-3-9905-4597.

E-mail address: [redacted]
(D.R. MacFarlane)

may lead to ambient temperature molten salts with no metal component.

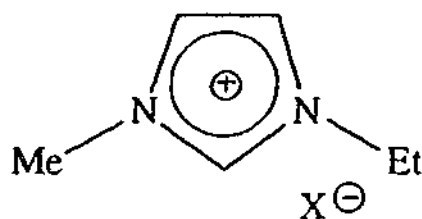
Melting points in ionic liquids are determined by ionic shapes and interactions. The energy change associated with melting is dominated by the entropy change from the ordered lattice to ionic liquid. Accordingly, room temperature (r.t.) molten salts often contain soft, unsymmetrical ions which ideally possess internal degrees of rotational freedom which can become active in the liquid state.

This study reports the conductivity, diffusion and thermal behaviour of two hydrophobic dialkylimidazolium salts and their binary mixtures. Enhanced conductivities were observed upon mixing the two salts. However, analysis of the diffusion coefficients in the binary systems did not show any increase in the ionic mobility. The influence of charge carrier concentration on the binary conductivities was therefore investigated through the calculation of the Haven ratio (H_R).

2. Experimental

2.1. Sample preparation

The preparation of 1-methyl-3-ethylimidazolium trifluoromethanesulfonate (triflate salt, MeEtImTf) and 1-methyl-3-ethylimidazolium bis(trifluoromethanesulfonimide) (imide salt, MeEtImNTf₂) was based on the method reported by Wilkes et al. [1,8]. Salted ice water was pumped through the reflux condenser to facilitate these reactions at atmospheric pressure. Binary systems of the MeEtImTf and MeEtImNTf₂ were prepared stoichiometrically and reported here as mole fractions of the triflate salt. The structure of the salts is shown below, where X is either CF₃SO₃⁻ or N(CF₃SO₂)₂⁻.



2.2. Thermal analysis

Thermal transitions were measured using a Perkin Elmer differential scanning calorimeter (DSC-7). The head was cooled with liquid nitrogen and the measurements scanned at 20°C min⁻¹ over a temperature range of -120 to 100°C (153–373 K). Calibration was performed with a cyclohexane standard. The values reported are reproducible within ±1°C.

2.3. Conductivity measurements

A micro-conductivity probe was constructed with 0.7 mm diameter platinum wire electrodes encased in a 50 × 10 mm glass tube. The wires were blackened by bulk electrolysis in a 50 mM solution of chloroplatinic acid in 2 M HCl. Electrolysis was performed at a current density ca. 200 mA cm⁻² against a platinum wire anode, until the electrodes were visibly blackened (5–10 min per electrode). The cell constant was determined in aqueous KCl to be ca. 500 m⁻¹. Conductivity was measured between 0 and 130°C (273–403 K) for the pure salts and at 90°C (363 K) for the binary systems via AC impedance. Impedance measurements were performed in the frequency range 20 Hz to 1 MHz using a Hewlett-Packard 4284 Precision LCR meter, and in the frequency range 100 kHz to 13 MHz using a Hewlett-Packard 4199A LF impedance analyser. The conductivity data was fitted with the Arrhenius equation, as described by

$$\sigma = \sigma_0 \exp\left(\frac{-E_a}{RT}\right) \quad (1)$$

where σ_0 is the limiting conductivity, E_a is the activation energy and R is the gas constant.

2.4. Density measurements

Density measurements were performed in a nitrogen filled dry box by weighing 2.00 ml aliquots on a four-figure balance. The densities of the pure salts were determined at r.t. and used to calculate the molar volumes and equivalent conductivities for the ionic liquids.

2.5. Diffusion measurements

Temperature dependent diffusion coefficients for the cation (¹H) and the anion (¹⁹F) were characterised using the fringe field NMR technique on a modified Bruker CXP300. The probe was positioned 24.5 cm from the centre of the magnet which corresponds to a field strength of 2.72 T (116 MHz for protons and 109.13 MHz for fluorine). The magnetic field gradient (G) of 46.8 T m⁻¹ was calibrated with H₂O ($D = 2.919 \times 10^{-9}$ m² s⁻¹ at 35°C [11]). A spin-echo pulse sequence ($\pi/2 - \tau - \pi - \tau$) was used with a $\pi/2$ pulse length of 2.1 and 2.2 μ s for protons and fluorine, respectively. The echo attenuation was fitted with the following equation [12]

$$\frac{A(2\tau)}{A(0)} = \exp\left(-\frac{2}{3}\gamma^2 G^2 D \tau^3\right) \quad (2)$$

where A is the echo amplitude, γ is the gyromagnetic ratio, G is the strength of the magnetic field gradient, D is the diffusion coefficient and τ is the variable delay

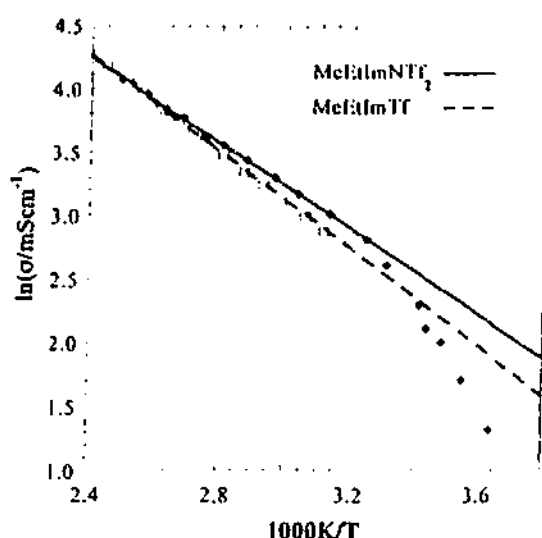


Fig. 1. Conductivity for MeEtImNTf₂ and MeEtImTf fitted with the Arrhenius equation (Eq. (1)).

Table 1

Activation energies (E_a) from Arrhenius fits of the conductivity and diffusion data

Salt	E_{σ} (kJ mol ⁻¹)	E_{ad} (kJ mol ⁻¹)
MeEtImTf	15.9 ± 1.0 ($R = 0.9984$)	Cation 23.8 ± 0.4 ($R = 0.9980$) Anion 24.9 ± 0.9 ($R = 0.9977$)
MeEtImNTf ₂	14.0 ± 1.0 ($R = 0.9996$)	Cation 24.9 ± 1.1 ($R = 0.9960$) Anion 22.2 ± 1.7 ($R = 0.9747$)

time in the spin-echo sequence. It is important to note

that the fringe field diffusion technique only gives an average diffusion coefficient for all protons or fluorines within the sample and can not distinguish charged from uncharged species. The diffusion coefficients were measured over a temperature range 30–130°C (303–403 K) and fitted with the Arrhenius equation below

$$D = D_0 \exp\left(\frac{-E_a}{RT}\right) \quad (3)$$

where, in this case, D_0 is the limiting diffusion.

3. Results and discussion

3.1. Pure molten salts

The imide and the triflate salts are both colourless liquids at r.t. DSC measurements revealed two thermal transitions for each salt; glass transitions at -98 and -93°C and melting transitions at -15 and -18°C for MeEtImTf and MeEtImNTf₂, respectively. The conductivities of the two salts are almost identical over the temperature range studied (Fig. 1). The temperature dependence of conductivity for the imide and triflate salts obeyed the Arrhenius equation (Eq. (1)) above 40 and 45°C, respectively. However, the observed curved nature of the conductivity in the triflate salt could also reflect Vogel–Tamman–Fulcher behaviour [13]. The conductivity activation energies determined from the Arrhenius fits are presented in Table 1. Comparison with the conductivity activation energies (E_a) determined for other MeEtIm⁺ salts [14], showed that E_a for the ionic liquids lie within two standard deviations of each other. This, along with the fact that conductivity depends strongly on cation size [5] suggests that the cation may dominate conduction in these systems.

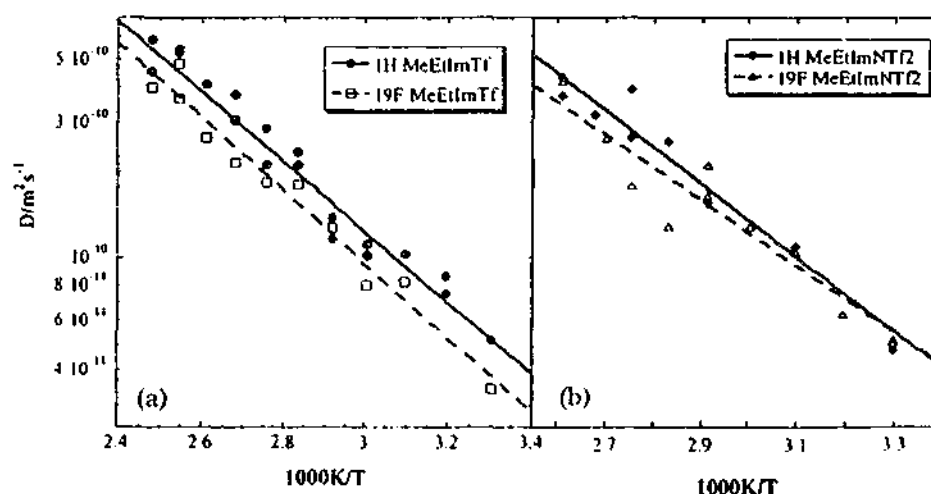


Fig. 2. Arrhenius fits (Eq. (3)) of the diffusion temperature dependence for (a) MeEtImTf and (b) MeEtImNTf₂.

Ionic diffusion coefficients were measured to characterise the conduction mechanism in these salts above 30°C. Fig. 2 shows temperature dependence of the anion and cation diffusion coefficients. The data have also been fitted with the Arrhenius equation (Eq. (3)) for comparison to the conductivity data. The activation energies observed for the diffusion coefficients are considerably different to the activation energies for conductivity (Table 1). This is somewhat unexpected since NMR based measurements usually result in lower activation energies [15].

For the MeEtImTf salt (Fig. 2(a)), the cation diffusion coefficients are about 50% greater than those of the anion. The activation energies, however, are almost the same within error (Table 1). In the MeEtImNTf₂ salt, both ions have similar diffusion coefficients (Fig. 2(b)) at lower temperatures, but the anion has a slightly lower activation energy (Table 1). The transport mechanisms for the cation would appear to be rather similar in both of the salts. It would also seem that this motion is largely independent of the anion. This concurs with the conductivity data and is also strong evidence for the cation being the more dominant conducting species.

A crude transport number can be calculated from the diffusion data using the following equation [16].

$$t^+ = D_{\text{cation}} / (D_{\text{cation}} + D_{\text{anion}}) \quad (4)$$

This equation assumes that only the ionic species contribute to the measured diffusion coefficients. It must be recalled, however, the fringe field method for measuring diffusion cannot distinguish between charged and uncharged species and it is an average diffusion coefficient for all species which is obtained. If one assumes that these systems are fully dissociated, the transport number for the cation in the triflate salt was approximately 0.6 over the whole temperature range. For the imide salt, the cationic transport numbers increased from 0.5 to 0.6 over the temperature range studied. This analysis suggests that the anion and cation contribute to charge transport to a similar extent in both salts, although the cation is slightly more dominant in the triflate salt.

A comparison of the diffusion data to the conductivity data can be made using the H_R [16].

$$H_R = D_{\text{NMR}} / D_a \quad (5)$$

The D_a term is calculated from the Nernst–Einstein equation

$$D_a = \frac{kT \cdot \lambda_m}{e^2 N_A} \quad (6)$$

where k is the Boltzmann constant, T is temperature, λ_m is the equivalent conductivity, e is the electron charge and N_A is the Avogadro constant. For a completely dissociated system where all the ions are involved in conductivity, the H_R will be 1. Any value greater than one implies that there is some degree of

ionic association. H_R s of 1.6 and 1.0 were calculated at 30°C (303 K) for MeEtImTf and MeEtImNTf₂, respectively. It can be concluded that there are only weak ionic interactions in the imide salt (equivalent to ionic dissociation), but stronger interactions, resulting in ionic aggregation, in the triflate salt. Since the negative charge on the imide anion is more diffuse in comparison with the triflate anion [17], weaker interactions could be expected.

3.2. Binary systems of MeEtImTf and MeEtImNTf₂

Binary solutions of MeEtImTf and MeEtImNTf₂ were analysed for various mole fractions of MeEtImTf. Whereas the pure components showed a glass transition and a melting transition, only a glass transition was observed for the binary mixtures. Single glass transition temperatures were observed for all the binary mixtures and were a weighted average of the glass transition temperatures for the pure components. The presence of only one glass transition is indicative of an intimately mixed solution.

The conductivity data for the binary systems is shown in Fig. 3(a). All measurements were made at 90°C (363 K). In comparison to the pure components, the binary mixtures show a substantially higher conductivity. This behaviour deviates considerably from what would be expected from the law of mixtures, which is indicated by the dashed line. For such conductivity enhancement to occur, there must be an increase in the ion mobility and/or the number of charge carriers, as implied by the following equation

$$\sigma = \sum n_i q_i \mu_i \quad (7)$$

where n is the number of charge carriers of type i , q is the charge and μ is the mobility of each species. Analysis of the diffusion coefficients in these binary systems however (Fig. 3(b)), shows that there is no appreciable deviation from a simple law of mixing and the cation exhibits higher diffusion coefficients, regardless of the binary composition. Consequently, it would appear that enhancement of ionic mobility is not responsible for the increase in conductivity observed upon the formation of a binary system.

The improvement of the absolute conductivity may therefore be due to an increase in charge carrier concentration. In the case of fully dissociated molten salts, this would have to involve a volume contraction upon mixing, which could be confirmed by measuring the density. However, density measurements for the binary samples indicate that this does not occur and a linear relationship due to additivity was observed [14].

Alternatively, we can consider the effect of mixing on the association equilibria that may exist in a 50 mol% mixture of the salts.

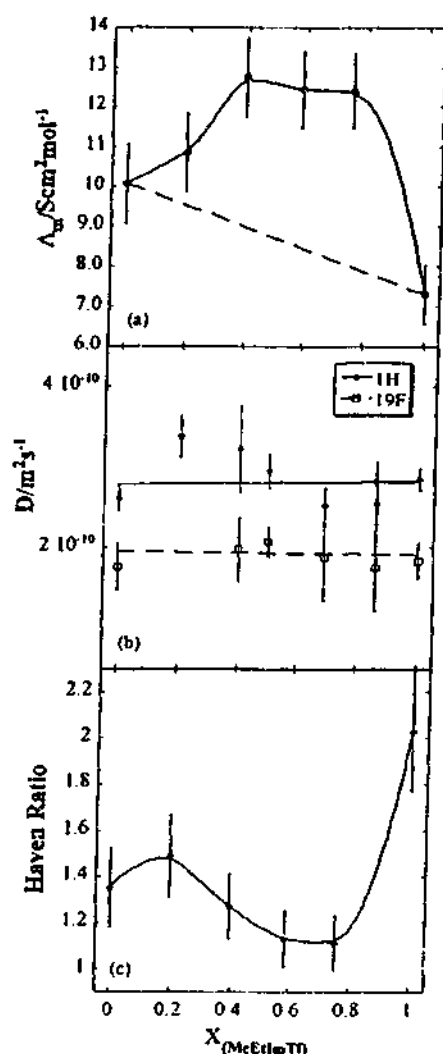
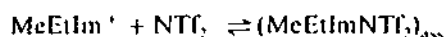
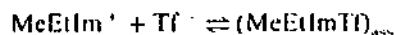


Fig. 3. (a) Conductivity, (b) diffusion and (c) H_R at 90°C as a function of binary composition. The dashed line in (a) shows the conductivity behaviour expected from a simple law of mixtures.



where $(\text{MeEtImTf})_{\text{ass}}$ indicates an associated species in the mixture, and note that the cation concentration is unchanged, while that of each anion is halved at this concentration. This decrease in anion concentration will shift the equilibria from association towards dissociation, thereby increasing the overall number of ions within the system. The degree of association in the binary systems is reflected in the H_R and therefore can be illustrated by calculating the value of H_R for the binary compositions. In order to calculate D_o (Eq. (6)), it was assumed that the density of the salt at 90°C would decrease by ca. 3% from the r.t. values [18] and that the law of mixing applies to the density values at

90°C, as it does at 30°C. The relationship between the H_R thus obtained and composition (Fig. 3(c)) shows clearly that association in the binary systems has been suppressed, relative to the pure components. Notably, the highest aggregation occurs in the pure triflate salt; the addition of even a small mole fraction of the imide component results in a marked decrease in ion associations. Whether this is solely the consequence of triflate salt equilibrium being highly concentration dependent or an effect specific to the imide ion will require further investigation. It is clear however, the effective increase in the number of conductive species can account for the rise in conductivity observed in the binary mixtures.

4. Conclusion

The characterisation of transport properties for the molten salts MeEtImTf and MeEtImNTf₂ has been reported here. The pure salts exhibited almost identical subambient melting and glass transition temperatures, along with similar conductivities over a wide temperature range. The conductivity behaviour was adequately modelled using the Arrhenius equation over most of the temperature range studied. Measurement of the ionic diffusion coefficients showed similar diffusive behaviour for the cations with slightly slower anionic diffusion. Calculation of the cationic transport numbers suggested that the cation contributed to a greater extent to conduction in MeEtImTf. Comparison of the conductivity data and the diffusion data through the H_R suggested that the imide salt was fully dissociated ($H_R = 1$), but that stronger ionic interactions are present in the triflate salt ($H_R = 1.6$).

In the binary systems, the melting point was suppressed with T_p being a weighted average of those for the pure salts. The conductivities were found to have a positive deviation from additivity. Analysis of the diffusion coefficients in the binary systems however, showed no such enhancement in the mobility. From the calculation of the H_R at 90°C, it is concluded that the increased conductivity in the binary mixtures is the result of decreased ion association.

References

- [1] J.S. Wilkes, J.A. Levisky, R.A. Wilson, C.L. Hussey, *Inorg. Chem.* 21 (1982) 1263.
- [2] C.L. Hussey, *Pure Appl. Chem.* 60 (1988) 1763.
- [3] A.A. Farnin, L.A. King, J.A. Levisky, J.S. Wilkes, *J. Phys. Chem.* 88 (1984) 2609.
- [4] N. Papageorgiou, Y. Athanassov, M. Armand, P. Bonhôte, H. Pettersson, A. Azam, M. Grätzel, *J. Electrochem. Soc.* 143 (1996) 3009.
- [5] P. Bonhôte, A.-P. Dias, N. Papageorgiou, K. Kalyanasundaram, M. Grätzel, *Inorg. Chem.* 35 (1996) 1168.

- [6] J.R. Sanders, E.H. Ward, C.L. Hussey, *J. Electrochem. Soc.* 133 (1986) 325.
- [7] C.J. Dymek, L.A. King, *J. Electrochem. Soc.* 132 (1985) 1375.
- [8] J.A. Boon, J.S. Wilkes, J.A. Lanning, *J. Electrochem. Soc.* 138 (1991) 465.
- [9] C.L. Hussey, J.R. Sanders, *J. Electrochem. Soc.* 134 (1977) 1987.
- [10] S.A. Bolkan, J.T. Yoke, *J. Chem. Eng. Data* 31 (1986) 194.
- [11] R. Mills, *J. Phys. Chem.* 77 (1973) 685.
- [12] A. Johansson, A. Gogoll, J. Tegenfeldt, *Polymer* 37 (1996) 1387.
- [13] F.M. Gray, *Polymer Electrolytes*, Royal Society of Chemistry, Cambridge, UK, 1997.
- [14] A.G. Bishop, 1998, unpublished results.
- [15] S.G. Bishop, P.J. Bray, *J. Chem. Phys.* 48 (1968) 1709.
- [16] A. Reiche, T. Cramer, G. Fleischer, R. Sandner, B. Sandner, F. Kremer, J. Kärger, *J. Phys. Chem. B* 102 (1998) 1998.
- [17] J.J. Golding, D.R. MacFarlane, L. Spiccia, M. Forsyth, B.W. Skelton, A.H. White, *Chem. Commun.* 15 (1998) 1593.
- [18] M. Spiro, F. King, in: D. Inman, D.G. Lovering (Eds.), *Ionic Liquids*, Plenum Press, New York, 1981, p. 57.

ADDENDUM

p 4, para 3: Comment: In comparing Equation 1-1 and Equation 1-2, n is equal to c , q is the same for both equations and μ is equal to Dq/kT .

p 42, Equation 2-29: Comment: In this equation, n indicates the quantum coherence. If n equals 1, then this implies single quantum coherence.

p 90: Comment: T_0 was taken to be T_g-50K . The glass transition temperatures for these salts were either determined directly from DSC analysis or calculated from the DSC melting points (where T_g is 2/3 of the melting temperature).

p 110, para 1: Comment: According to either the free volume or configurational entropy theories (refer to p88-89), as a sample is cooled down to the ideal glass transition temperature (T_0 taken to be T_g-50K), the free volume or configurational entropy of the system tends towards zero. Given the relationship between viscosity and/or diffusion and the free volume (or configurational entropy), it is expected that these properties will also tend towards zero as T_0 is approached.

p 160, para 1: Comment: Although it was assumed that the liquid state diffusion would dominate the diffusion measurement, it is apparent that high diffusion can also occur in the solid state. Changing the echo time in the PFG experiment may have allowed us to distinguish between the solid and liquid state diffusion process. In this work, however, the availability of the PFG instrumentation was limited while the FFG method does not enable such differentiation. Future work with PFG will address this issue.

p 163, para 2: Comment: The increase in intensity for 33.3mol% $LiNTf_2/P_{12}NTf_2$ is reasonably rapid, but not as sudden as for pure $P_{12}NTf_2$. The other three compositions (0.9, 4.7 and 45.5mol% $LiNTf_2$), however, show a reasonably gradual increase in intensity. For these materials, over a certain temperature range, both solid and liquid coexist in equilibrium, which is thought to lead to the gradual increase in signal intensity and can possibly be explained by the Lever rule. For the pure $P_{12}NTf_2$ and 33.3mol% $LiNTf_2$ samples, there is no temperature range where both the solid and liquid phases coexist. Thus a gradual increase in intensity as a result of the increasing proportion of the liquid component is not necessarily expected.

In response to examiner's comment: The salts analysed in this work were used as obtained from colleagues in the Department of Chemistry at Monash University. Salt purity was checked by solution NMR, Electrospray Mass Spectroscopy and, in some

instances, chemical analysis. $P_{12}NTf_2$ was separated from the solvent as a solid before being filtered and washed with water and rigorously dried under vacuum. Solid MeRImX salts were recrystallised from ethanol (or another suitable organic solvent). Molten MeRImX salts were washed with water or an organic solvent (depending on the degree of hydrophobicity of the salt) followed by rigorous drying under vacuum for at least 24 hours. The preparation and purification were generally performed as discussed in Wilkes J.S. *et al*, Inorg. Chem. 1982, 21, 1263-1264 and Boon J.A. *et al*, J. Electrochem. Soc. 1991, 138 465-469.

In response to examiner's comment: The following graph is an example of fringe field diffusion data fitted with Equation 2-32.

